공학박사학위논문

# Strut-and-Tie Model for Efficient Design of Bridge Pier Cap

## 효율적인 교각 피어캡 설계를 위한 스트럿-타이 모델

**2020 년 8 월**

서울대학교 대학원

건설환경공학부

박 재 현

# Strut-and-Tie Model for Efficient Design of Bridge Pier Cap

효율적인 교각 피어캡 설계를 위한
스트럿-타이 모델

지도 교수 조 재 열

이 논문을 공학박사 학위논문으로 제출함
**2020 년 7 월**

서울대학교 대학원
건설환경공학부
박 재 현

박재현의 공학박사 학위논문을 인준함
**2020 년 7 월**

위 원 장 김호경 (인)

부위원장 趙在悅 (인)

위 원 신현묵 (인)

위 원 이재훈 (인)

위 원 박홍근 (인)

# ABSTRACT

# Strut-and-Tie Model for Efficient Design of Bridge Pier Cap

Park, Jae Hyun
Department of Civil & Environmental Engineering
The Graduate School
Seoul National University

Bridge pier cap is one of the most important members transmitting the loads from superstructures to the column of the bridge. Due to this structurally critical role of members, pier caps, conventionally, have often been over-reinforced with conservative designs. Over-reinforcement in pier cap, however, considerably degrades the constructability and economic efficiency considering the bad working environment with high location in the top of pier and interference with the column reinforcement.

Pier cap, which belongs to discontinuity region due to loading and geometric conditions, is designed with Strut-and-Tie Model (STM) presented in design codes in accordance with the design method transition from ultimate strength design to limit state design. In the design of STM in bridge pier cap, strut-and-tie models can be selected by designers' discretion. This versatility of STM design, however, leads potential to select inefficient models resulting in the conservative designs with over-reinforcement. To avoid such ineffective

pier cap design, specific guidelines need to be proposed, and it can be achieved through analysis of the current design status and evaluation of structural safety in suggested guidelines.

In this study, to provide efficient guidelines for pier caps preventing conservative designs due to excessive reinforcement, following procedures were conducted: analytical studies such as contemplation of pier cap design status in current design codes, static loading test of the scaled models, verification of the test results and parametric studies with FE model analysis.

The analysis of the current design status of bridge pier cap was established by comparing and analyzing the design rules presented in various design codes and contemplating the existing STM design cases of pier cap. With the basis, STM design guidelines for bridge pier cap allowing more reasonable reinforcement designs were proposed.

To evaluate the structural safety of the proposed design guidelines, static loading test were conducted with specimens for the scaled model of pier cap. The results were analyzed and verified by nonlinear finite element analysis. Experimental program was conducted with total 3 specimens, which satisfy the proposed guidelines, with the various loading distributions in consideration of superstructure and horizontal shear reinforcement. Structural behavior such as loading, deflection, strains of the concrete and rebar, crack propagation were measured. As a result of the test, the pier caps designed with the proposed guidelines show load resistance capacities exceeding ultimate limit state (ULS), which is verifying the structural validity of the guidelines. Though, due to the

load distribution and sectional size, limitations such as cracks in serviceability limit state (SLS) and inconsistent design safety factor occurred in the test.

To observe structural behaviors, including shear, in various sectional depths overcoming the limitations of variable range in the experiment, additional parametric studies were conducted with FE analysis. As a result, it was confirmed that the proper sectional size can be determined using the shear strength prediction in design code before the STM design. In addition, underestimation of pier cap strength due to the vertical tie in the determinant STM could be complemented by placing the shear strength prediction in design code as a minimum value. This resulted in improved design guidelines complementing the limitations of previous design guidelines.

By the evaluation of the structural safety and serviceability in the current design of bridge pier caps, improved guidelines were proposed for the more efficient bridge pier cap design in STM. As a result, it is expected to enhance the constructability and economic feasibility of social infra-structures by preventing excessive reinforcement and conservative sectional size due to inefficient design of bridge pier caps in the design practice.

***Keywords:*** Pier cap, Strut-and-tie model, Shear reinforcement ratio, Scaled model test, Limit state design, Design code, Nonlinear finite element analysis

***Student Number:*** 2015-31057

# TABLE OF CONTENTS

# LIST OF TABLES

# LIST OF FIGURES

# NOTATIONS

| Symbol | | Definition and description |
|---|---|---|
| $A$ | = | Coefficient reflecting the influence of amount and orientation of transverse tensile reinforcement |
| $A_c$ | = | Area of concrete section |
| $A_p$ | = | Area of prestressing tendons |
| $A_{ps}$ | = | Nominal cross sectional area of prestressing reinforcement |
| $A_{st}$ | = | Nominal cross sectional area of reinforcement |
| $A_{s,min}$ | = | Minimum area of flexural reinforcement |
| $A_v$ | = | Area of shear reinforcement |
| $A_1$ | = | Loaded area |
| $A_2$ | = | Area of the lower base of the largest frustum of a pyramid, cone, or tapered wedge contained wholly within the support, having for its upper base the loaded area and having side slopes of 1 vertical to 2 horizontal |
| $C$ | = | Coefficient for sectional configuration |
| $F_{nt}$ | = | Nominal strength of a tie |
| $F_u$ | = | Factored tensile force in a tie |
| $M_{act}$ | = | Flexural strength with actual strengths of materials |
| $M_{cr}$ | = | Cracking moment |
| $M_d$ | = | Flexural strength with design strengths of materials |
| $M_n$ | = | Nominal flexural strength |
| $P$ | = | Total load |

| | | |
|---|---|---|
| $P_d$ | = | Design load |
| $P_{\max}$ | = | Maximum load |
| $P_{SA}$ | = | Total load capacity obtained from sectional analysis |
| $P_{Strut}$ | = | Total load capacity of strut |
| $P_{SLS}$ | = | Total load at Serviceability Limit State |
| $P_{Tensile\ Tie}$ | = | Total load capacity of tensile tie |
| $P_{ULS}$ | = | Total load at Ultimate Limit State |
| $P_{Vertical\ Tie}$ | = | Total load capacity of vertical tie |
| $V_c$ | = | Contribution of concrete in shear strength |
| $V_n$ | = | Nominal shear strength |
| $V_s$ | = | Contribution of reinforcement in shear strength |
| $b_w$ | = | Width of pier cap |
| $d$ | = | Effective depth of pier cap |
| $f_{cd}$ | = | Design strength for a concrete strut or nodal regions |
| $f_{ck}$ | = | Specified compressive strength of concrete |
| $f_c^{'}$ | = | Specified compressive strength of concrete |
| $f_{c,act}$ | = | Actual compressive strength of concrete from test |
| $f_y$ | = | Specified yield strength for non-prestressed reinforcement |
| $f_{yd}$ | = | Design strength for a tie with non-prestressed reinforcement |
| $f_{yk}$ | = | Characteristic yield strength of reinforcement |
| $f_{y,act}$ | = | Actual yield strength of reinforcement from test |
| $f_n$ | = | Axial force |
| $f_{pe}$ | = | Compressive stress in concrete due only to effective prestress forces, after allowance for all prestress losses, at |

| | | |
|---|---|---|
| | | extreme fiber of section if tensile stress is caused by externally applied loads |
| $f_{po}$ | = | Stress in prestressing tendons when strain in the surrounding concrete is zero |
| $f_{py}$ | = | Specified yield strength of prestressing reinforcement |
| $f_{pyd}$ | = | Design strength for a tie with prestressing reinforcement |
| $f_{p0.1k}$ | = | Characteristic 0.1% proof-stress of prestressing steel |
| $f_r$ | = | Modulus of rupture |
| $f_{vy}$ | = | Specified yield strength for vertical shear reinforcement |
| $h$ | = | Depth of pier cap |
| $m$ | = | Confinement factor |
| $n$ | = | The number of reinforcing steel bar |
| $s$ | = | Spacing of stirrups |
| $s_{req}$ | = | Required spacing of stirrups |
| $w_{eff}$ | = | Maximum effective width of tie |
| $z$ | = | Section modulus |
| $\Delta f_p$ | = | Increase in stress in prestressing reinforcement due to factored loads |
| $\alpha_{cc}$ | = | Coefficient taking account of long term effects on the compressive strength and of unfavourable effects resulting from the way the load is applied |
| $\beta_n$ | = | Factor used to account for the effect of the anchorage of ties on the effective compressive strength of a nodal zone |
| $\gamma$ | = | Partial factor |
| $\gamma_c$ | = | Partial factor for concrete |
| $\gamma_s$ | = | Partial factor for reinforcing or prestressing steel |

| | | |
|---|---|---|
| $\eta_{req}$ | = | The number of row for stirrups required to resist force in vertical shear tie |
| $\phi$ | = | Strength reduction factor |
| $\phi_c$ | = | Resistance factor for concrete |
| $\phi_p$ | = | Resistance factor for prestressing tendons |
| $\phi_s$ | = | Resistance factor for non-prestressed reinforcing bars |
| $\rho$ | = | Reinforcement ratio for flexural reinforcement |
| $\rho_h$ | = | Reinforcement ratio for horizontal shear reinforcement |
| $\rho_{\max}$ | = | Upper limit of required flexural reinforcement ratio in STM |
| $\rho_{\min}$ | = | Minimum flexural reinforcement ratio |
| $\rho_{req}$ | = | Required flexural reinforcement ratio in STM |
| $\rho_v$ | = | Reinforcement ratio for vertical shear reinforcement |
| $\rho_{v,req}$ | = | Required vertical shear reinforcement ratio |
| $\sigma_{XX}$ | = | X-directional stress |
| $\psi_p$ | = | Load reduction factor |

# I. Introduction

## 1.1. Research Background

Currently, the design of bridges has been changed from the design based on ultimate strength design, which focuses on the destruction of the section of structure, to the design based on limit state design, which covers the failure of entire structural systems. Prior to the implementation of limit state design, flexural and shear reinforcement were arranged in pier cap with the basis of sectional analysis where design moment and shear strength at the critical section shall exceed the factored moment and shear force. Pier cap, however, is a member with a relatively small shear span, which belongs to a discontinuity region (deep component) due to the local effects of the load in the geometry. In the discontinuity region, the distribution of strain in the section is nonlinear because Bernoulli assumption in the sectional design is not satisfied. The design method of discontinuity region is the design of strut-and-tie model that was settled after the implementation of the limit state design. STM is a design method for determining rebar details by truss analysis, considering the structures as a truss member consisting of struts, ties, and nodal regions. With the STM, safety of the design is secured because the STM satisfies lower-bound solution. In addition, it is possible to set up a model for arbitrary distribution of stress and geometry, allowing for various designs according to the various STM at the structures.

However, the versatility of such a diverse strut-and-tie models in the structure means that there is no ‘correct’ design in the structure, causing the

uncertainty in the design itself. Thus, STM design that ensures various options depending on the discretion of designers may result in too conservative design more than required, with excessive amount of rebar. Meanwhile, pier caps are located at top of the pier, which has lack of constructability: dangerous working space and interference between the shear rebar and column reinforcement. Though, as a member that serves to transmit the load of superstructures structurally to the substructures, role of pier cap is important and a conservative design with more than the required amount of rebar in the strut-tie model is customary conducted. Therefore, it is necessary to select a reasonable STM in the design of bridge pier cap and thereby prevent excessive amount of rebar from being assigned, resulting in improvement of economical and constructional feasibilities.

## 1.2. Scope and Objectives of the Thesis

In this study, efficient pier cap design guidelines to prevent conservative design according to excessive reinforcement are going to be presented. For the objectives, the scope of the study was set up as follows.

First, current design status of bridge pier cap is determined by comparing and analyzing the design rules of bridge pier cap in design codes and by examining the STM design cases of bridge pier caps in existing bridges. In the design of pier caps based on STM, the cause of over-reinforcement of shear rebars is analyzed. With this bases, STM design guidelines inducing efficient reinforcement arrangement in bridge pier caps are proposed.

And then, to evaluate the structural safety of the design guidelines presented, a scaled-model test is conducted and the results are verified by nonlinear finite element analyses. The experiment identifies structural behaviors of pier caps under SLS and ULS, and further identifies the behaviors of the members up to failures. Based on the experimental results, the structural feasibility and limitations of the proposed STM design guidelines are presented.

Lastly, the parametric studies with FE analysis are carried out to see the further structural behaviors which could not be captured in the experimental studies. The influence of the sectional depths in pier caps on the reinforcement ratios for flexural and shear rebars at the proposed STM guidelines is captured. And the corresponding changes in the behaviors of the member are determined. Based on the analyses, revised design guidelines improving the limitations of the prior guidelines are proposed.

In summary, the main research objectives of this study are as follows.

1. The status and limitations of bridge pier cap design based on the strut-and-tie model in design codes are analyzed.

2. Design guidelines for STM of bridge pier cap that enable rational placement of steel reinforcement are established, based on the analysis of the change in reinforcement of pier cap with the configuration of STM and the analysis of the validity of the layout of reinforcing steel bars arranged by STM.

3. To evaluate the structural safety of the proposed design guidelines for pier caps, a scaled-model test is conducted and the structural feasibility and limitations of the proposed guidelines are presented.

4. The improved design guidelines for pier caps overcoming limitations are proposed based on the parametric studies of the influence of sectional depths through FE analyses.

## 1.3. Organization of the Thesis

Chapter 1 shows an introduction to this thesis. It includes general descriptions on the background, objectives, scope, and outline of the research.

Chapter 2 provides a brief review of the current state of pier cap designs. Overview of strut-and-tie model design and pier cap design in current design codes were reviewed. With the studies, limitations of current pier cap design were captured.

Chapter 3 performs a comparison and analysis of the design cases of bridge pier cap in order to present an efficient method of designing bridge pier caps with STM. Based on the design data of various pier caps, design features such as dimensional properties, load characteristics, amount of reinforcement for flexural and shear rebar are identified and analyzed. Design characteristics of various STM layouts for T-type pier cap are also analyzed and STM design guidelines for bridge pier caps with more efficient reinforcement are proposed.

Chapter 4 presents the scaled model test in detailed. Totally, in order to not only verify the safety and serviceability of the proposed design guidelines but also investigate the influence of horizontal shear reinforcement and loading position on the structural behavior, 3 specimens were fabricated and tested in the static loading test. Included were: target structures, a scaled factor, specimens, material properties, procedures of fabrication and test. The structural behaviors of pier cap such as deflection of the pier cap, and crack propagation are discussed. In addition, the strains of concrete and longitudinal

rebar are examined using the measurement of strain gauges attached on the surface of the concrete beam and rebar.

The details of the analytical study are discussed in chapter 5. The parametric study that investigated the effect of the sectional depth in STM design was conducted by finite element analysis. First, a finite element model was suggested and the results of analysis were compared with that of the experiment for verifying its validity. Then, parametric study was conducted analytically using the FE model over a wider range of sectional depth that have not been performed in the experiment. Consequently, revised design guidelines considering the proper sectional depth were suggested and verified.

Finally, conclusions of this study are summarized in Chapter 6.

In Appendix A, detailed procedures of STM design to get the required reinforcement ratio for all specimens were contained. For brevity, in Appendix B and C, all experimental data, some of which are not mentioned in the chapters, are included. Appendix B is for concrete cylinder test data and Appendix C is for rebar and concrete strain data of the test.

# II. Literature Review

## 2.1. Introduction

Reasonable strut-and-tie model with rational design is considerably important in the design of bridge pier caps. The main context of STM design is the design of member by truss analysis with the elements of struts, ties, and nodal regions, and the versatile settings of STM models at the designer's discretion is one of the key features of the design. There exists, therefore, no one correct solution for the structure, but designs with various STM are possible. It is important to establish a strut-and-tie model appropriate for the structure. This requires identifying the concepts and procedures of STM design and applying them properly according to the structure.

Chapter 2.2 understands the strut-and-tie model (STM) for the design of discontinuity region based on design criteria and various research data and describes the design procedures. Chapter 2.3 compares the design codes to identify the design status of bridge pier caps and further identifies the limitations of current bridge pier cap designs based on STM.

## 2.2. Strut-and-Tie Model Design

### 2.2.1. Introduction

This chapter describes a series of processes to understand the design concepts and methods of STM used in the design of structures including various discontinuity regions. First, the local effects of geometric discontinuities and loads on the behavior of structures and the concept of discontinuity region (D-region) are described. Next, designing D-region by STM are presented.

### 2.2.2. Discontinuity Regions

Typically, strut-and-tie models are used primarily in the design of discontinuity regions (D-region). Discontinuity region (D-region) means the area where a nonlinear stress distribution occurs due to loads or geometrical discontinuities in the structures. Areas near the applied load and the support reaction are D-region because the local forces disturb surrounding areas. In addition, the structures such as corners of frame, openings, and corbels are the areas that create stress disturbances geometrically.

In Bernoulli region (B-region), Bernoulli assumption, where the section assumed to maintain plane remains plane after deformation, is satisfied. Therefore, linear strain distribution through the sectional depth is assumed in the B-region. In this assumption, the member is dominated by sectional behavior and the design is also accomplished through the sectional analysis. In flexural design of B-region, it is considered that compressive stress is mainly assumed as a rectangular compression block.

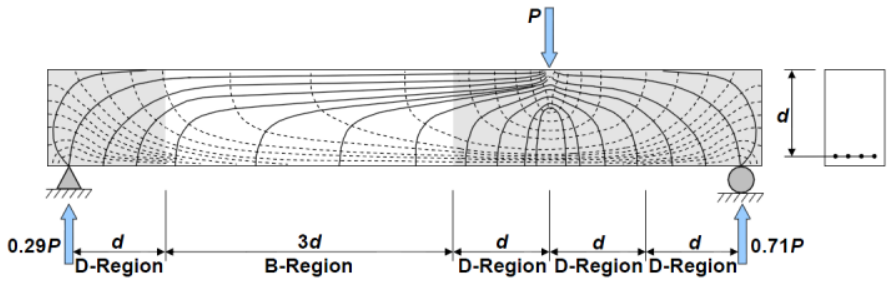


Figure 2.1 Stress distribution for B and D region (Birrcher et al. 2009)

On the other hand, the distribution of strain in D-region is nonlinear and the assumption for sectional analysis is not satisfied in that region. According to the principle of St. Venant, stress analysis based on linear strain distribution is possible where the area beyond the distance of sectional depth at the load or the geometric discontinuities is located. This means that there is a nonlinear stress distribution in the D-region within the distance of sectional depth from the load or the geometric discontinuities. Therefore, as shown in Figure 2.1, D-region is as far as $d$ from the points of loads and support reactions.

In general, if the shear span is $a < 2d$ to $2.5d$, the structural member is considered to be dominated by nonlinear behavior. In Figure 2.1, entire right side of the loading point is D-region because the member has a shear span of $2d$. On the other hand, since the left side of the loading point has a shear span of $5d$, it can be designed by a sectional analysis because it is dominated by sectional behavior even if it contains D-region on the left side. In reality, the transition of the region from B to D is gradual, but the principle of St. Venant can be applicable rationally to the design of the structure.

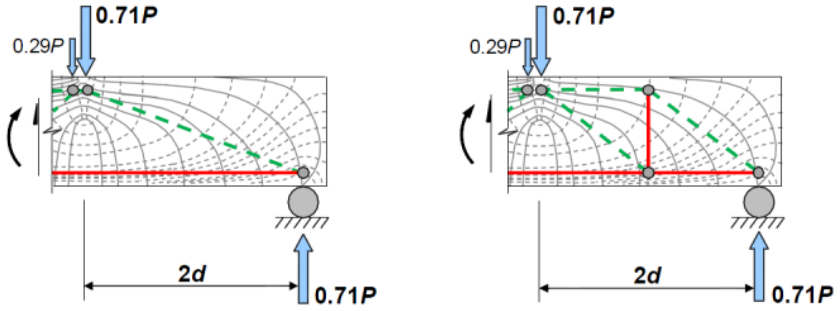


(a) (b)

Figure 2.2 Strut-and-tie models for deep component: (a) One-Panel(Arch action); (b) Two-Panels(Truss action) (Birrcher et al. 2009)

Behaviors of deep components can be explained by the transfer mechanism of forces between the applied loads and supports. The behavior of deep beam in Figure 2.2 is governed by the arch and truss action between the loads and the supports. In STM, either arch action or direct load transfer can be represented by diagonal concrete struts as shown in Figure 2.2 (a). Tensile members (ties) to meet the equilibrium with diagonal struts is able to be applied along the bottom of the beam. Deep component behavior between the load P and supports, also, can be represented by a two-panel truss model, which includes additional vertical ties as shown in Figure 2.2 (b), with an indirect load transfer effect of truss action.

### 2.2.3. Fundamentals of Strut-and-Tie Model

Fundamental principle of strut-and-tie model is lower-bound design, which makes the results of structural design using STM conservative. In the satisfaction of lower-bound solution, the truss model shall be balanced with the external force and have sufficient deformation margin for the assumed force distribution. Thus, reinforcing steel bar shall be sufficiently developed in the concrete. In addition, compressive force of concrete in STM analysis shall be less than the effective concrete strength, and the tensile force at STM shall also be less than the effective tie strength. If all of the above conditions mentioned are met, the application of STM turns to lower-bound design.

All STMs are represented by three elements: strut, tie, and nodal region. A simple STM considering a load flow in a simply supported beam is described in Figure 2.3. In this model, member forces can be obtained by truss analysis when the reaction of member and the STM shape are determined. Compressive and tensile member can be analyzed by strut and tie, respectively. Nodal region is area where struts, ties, loads, and supports intersect. Nodal region is the area where the largest stress occurs in STM because of the concentrating of truss forces.

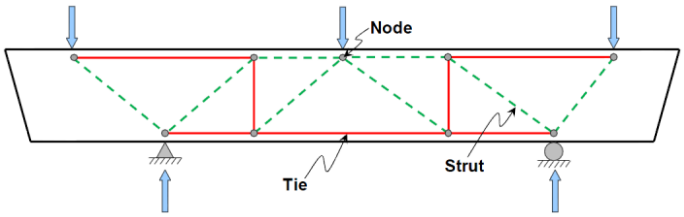


Figure 2.3 Examples of strut, tie, and nodal region (Williams et al. 2012)

When setting STM configurations, the positions of struts and ties shall be based on the stress flow with elastic analysis. If struts and ties are positioned in line with the elastic flow of the force, conservative designs where minimal cracks occur under SLS located in elastic zone are possible.

STM has the advantage of being applicable to arbitrary geometry and stress distribution in the design of D-region. This versatility of STM, however, can be both advantages and disadvantages. This means that there is no ‘correct’ STM design in structures because of allowance of various STM designs, resulting in uncertainty about the model. If the conditions for the lower-bound solution are satisfied in the design, the STM can be at least safe design.

Struts can often be distinguished as either prismatic or bottle-shaped strut depending on the uniformity of the stress field. In Figure 2.4, the prismatic strut can be used where constant compressive stress area. Bottled-shaped strut, on the other hand, is available if the compressive stress is spreading laterally. Diagonal struts in beams are usually bottle-shaped struts. As the compressive stress spreads laterally, tensile stress occurs in a direction perpendicular to the strut, which creates diagonal tension cracks in the member. These tensile stresses reduce the efficiency of concrete struts. Therefore, orthogonal rebars are placed near the bottle-shaped struts to cover the tensile forces, reinforce struts, and control cracks.

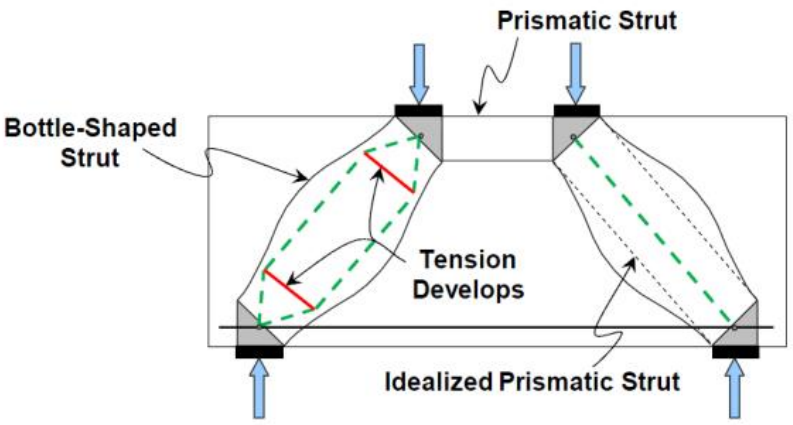


Figure 2.4 Prismatic and bottle-shaped strut (Birrcher et al. 2009)

In general, the procedure for designing STM for deep components is as follows.

1. Division of B-region and D-region: Predictions are made where exhibit deep member behavior. Whether the entire member can be designed with STM or not is also determined.

2. Determination of loading type: The factored loads acting on the structural members are calculated and simple alternations of loads to be used in STM are conducted.

3. Analysis of structural members: Assuming the elastic behavior of the member, support reactions are obtained.

4. Formation of strut-and-tie model: Struts and ties are positioned to reflect the flow of forces acting on structural members. Also, element forces acting on struts and ties are obtained.

5. Details of tie reinforcement: The amount and spacing of reinforcement required for ties are determined.

6. Strength check of nodal region: First, the geometry of nodal region is determined. And then, strengths at each face of nodal region shall be checked whether they resist the element forces obtained from STM analysis.

7. Crack-controlled reinforcement: Details for crack control reinforcement required for controlling the cracks in diagonal tension cracks due to the lateral tensile stress of the bottle-shaped struts shall be determined.

8. Bond of ties: Reinforcement shall be bonded in concrete nodal regions.

*2.2.3.1 B-regions and D-regions*

The first procedure in STM design process is to separate the structure into B and D-regions according to the principles of St. Venant. If the structure consists of all D-region, entire area shall be designed with STM. If the structure contains both B and D-region, portion of the structure expected to have deep component behavior is designed with STM, and the part of the structure expected to be dominated by sectional behavior is designed with the sectional design method. Designers may design the entire structure by STM if B-region is limited to local area.

*2.2.3.2 Definition of load case*

The next step after distinguishing between B and D-regions is to define the loads which act on the area of the nodal regions of the STM. Designers first define the type of load that creates a critical section. Each type of load applies a force corresponding to the type to struts and ties, thus the position of critical section and the magnitude of the force vary depending on the type of load. Therefore, STM analysis shall be conducted for each load combination. In the factored loads and moments with the certain load combination, designer shall determine whether an appropriate STM is established for this load combination. It is necessary to properly transit the loads fitting to STM. Several examples are shown below.

1. Since no moment can be applied to the truss model, the moment acting on the structure shall be replaced by a couple forces or an equivalent set of forces.

2. The nodal loads close to each other can be simply summed up in STM. This is at the discretion of the designer.

3. Since distribution loads cannot be applied to the truss model, the distribution loads applied to the structure shall be expressed as a series of point loads acting on the nodal regions in the STM. It is assumed that the self-weight of the structure also works in the same way.

*2.2.3.3 Analysis of structural member*

The forces acting on the interface of the D-region shall be determined. These boundary forces are used to determine the shape of the STM and are applied to STM to obtain the force acting on each strut and tie. For each load combination, an elastic analysis is conducted on the structures to obtain the reaction forces. If the structural member contains both B and D-region, so that only part of the member is designed as a strut-and-tie model, the internal force and moment of B-region shall be applied to the boundary of D-region. At the interface of B and D-regions, elastic linear stress distributions are assumed as shown in Figure 2.5. These stress distributions are used to determine the force acting on STM at the boundary. The position of the boundary is determined by the principle of St. Venant. With factored loads and interface forces acting on D-region, the strut-and-tie model can be established and analyzed.

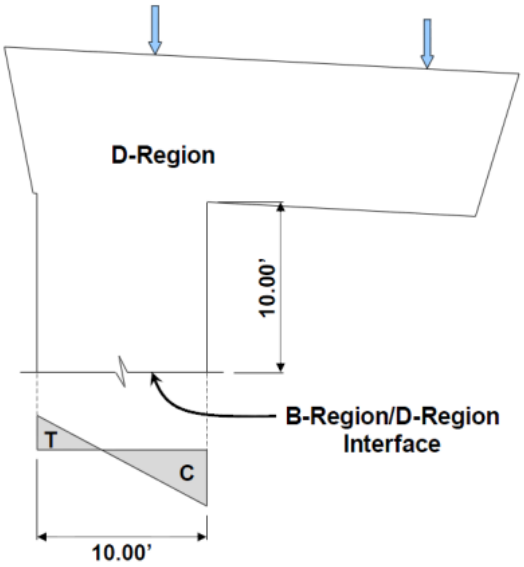


Figure 2.5 Linear stress distribution at the interface of B and D region (Williams et al. 2012)

*2.2.3.4 Development of strut-and-tie model*

The establishment of strut-and-tie model is usually carried out in two stages: First, determine the shape of the STM according to the applied load and the position of the boundary forces. Second, interpret STM to obtain the forces acting on struts and ties.

When establishing the shape of the strut-tie model, struts and ties shall be positioned to indicate the elastic flow of forces in the structural member. Designers usually determine the proper location of struts and ties in the following ways. Preferred struts and ties can be arranged according to the load path by the applied force and the reaction force. Also, struts and ties can be placed using the crack pattern of the structure. Depending on the stress flow

through linear elastic finite element analysis, strut and tie elements can also be positioned. The tie member shall be located in the center of the reinforcement assigned. For example, as shown in Figure 2.6, a tie indicating a longitudinal rebar placed at the bottom of the beam shall be placed in the centroid of the rebar, considering the cover thickness at the bottom of the beam.

In addition, the prismatic strut, such as the horizontal strut at the top of the beam in Figure 2.6, can be positioned according to the depth of the rectangular compression stress block in flexural analysis or the optimum depth of the STM. In the first case, place the strut in the center of the rectangular compression stress block. In the second case, position the strut at a height such that it becomes a larger moment arm. After positioning the longitudinal rebar tie and the prismatic strut, place the remaining STM elements considering the elastic flow of the structural resistance.

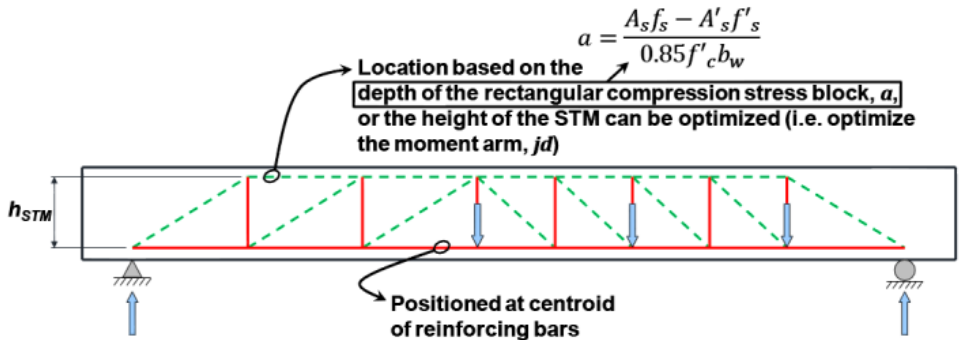


Figure 2.6 Placement of the longitudinal ties and prismatic struts within a strut-and-tie model (Williams et al. 2012)

In STM design, the angle between struts and ties located in the same nodal region shall not be less than 25 degrees. This is because smaller angles between struts and ties result in unexpected scenarios with tension and compression in same space. This minimum angle, therefore, prevent the occurrence of excessive strain on the rebars and alleviate the crack width.

Schlaich et al. (1987) said that there is no single optimal solution for the STM. And this means that there are several directions based on subjective decisions. Designers must recognize that if the STM has sufficient deformation capability to allow distribution of forces in equilibrium with the external force, the design of STM shows 'lower bound solution'. Though it is not necessary to configure the strut-and-tie model to accurately match the flow of resistance, the STM which best represents this stress distribution minimizes the occurrence of cracks under SLS load. STMs deviating from the elastic stress flow increase the risk of cracking at SLS.

Meanwhile, in the same structure, a STM consisting of the fewest ties is typically considered the most efficient model. Loads flow along a path that minimizes deformation. In RC structures, concrete struts delivering compression forces are accompanied by less deformation than the ties under tensile forces. STM in Figure 2.7 (a) is positioned to match the flow of resistant forces relative to STM in Figure 2.7 (b), and the forces will naturally move to the path of STM as shown in Figure 2.7 (a) since fewer ties are placed. (MacGregor and Light, 2005)

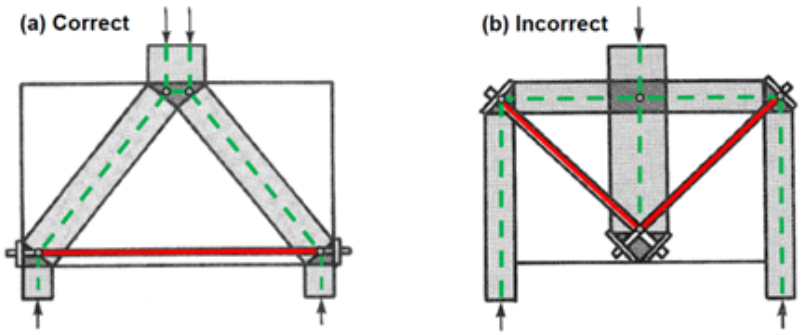


(a) (b)

Figure 2.7 Optimal strut-and-tie model based on number and length of ties: (a) Correct STM; (b) Incorrect STM (MacGregor and Wight, 2005)

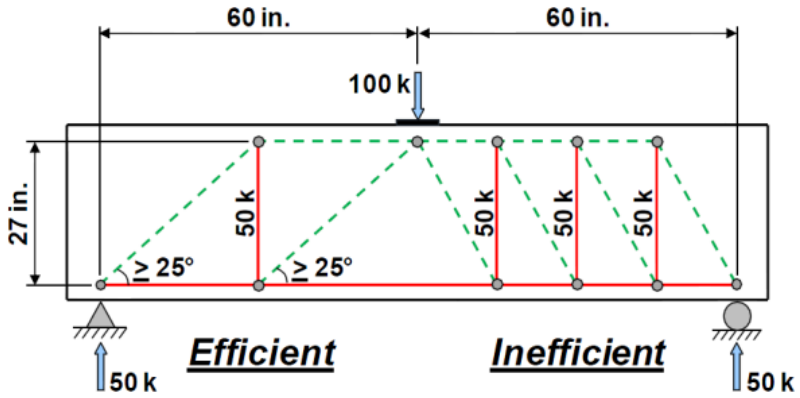


Figure 2.8 Examples of least number of vertical ties (Williams et al. 2012)

Similarly, when modeling beams, the least vertical ties should be used. In other words, STM must be designed to meet the minimum 25 degrees angle limit between struts and ties and having a minimum truss panel. STM with the least truss panel is on the left, and STM with more truss panels is on the right (in Figure 2.8). The STM on the left with fewer amount of vertical rebar is more efficient design because both designs satisfy the safety margin.

*2.2.3.5 Proportion of ties for rebar arrangement*

After positioning the strut-and-tie model, the next design step is the placement of rebars in the tie. The amount of rebars placed on each tie in STM shall be so placed that the rebars do not exceed the yield strength and resist the external forces applied to the ties. Typically, the amount of rebar required for ties in a reinforced concrete structure can be obtained by Equation (2.1):

$$A_{st} = \frac{F_u}{\phi f_y} \tag{2.1}$$

The centroid of the reinforcement layout shall coincide with the position of the tie in STM.

## 2.3. Pier Cap Design in Current Design Codes

### 2.3.1. Introduction

In current, the design of bridge pier caps for domestic highway bridges is based on Korean Highway Bridge Design Code (Limit State Design) and Korea Structural Concrete Design Code 2012. In the design codes, it is stipulated that discontinuity region, such as bridge pier cap, shall be designed by strut-and-tie model. The design of discontinuity regions, which was designed by ultimate strength design, began to transform the design method to the strut-and-tie model after the presentation of STM in Schlaich et al. (1987), starting from ACI 318: Building Code Requirements for Structural Concrete and Eurocode 2: Design of Concrete Structure. STM design in discontinuity region was first introduced in 2007 revision of KCI in accordance with international trends, and KHBDC suggested the design of STM in 2010 revision.

This chapter analyzes the design method of the bridge pier cap presented in the current design codes to identify the design status and limitations of bridge pier caps.

### 2.3.2. Design of Discontinuity Regions

Bridge pier caps belong to discontinuity regions where the Bernoulli assumption is not satisfied, and the design method is presented for these discontinuity regions at each design code. The design methods of discontinuity regions in design codes are summarized in Table 2.1. Under the current major design standards, the strut-and-tie model design method is used to design components belonging to discontinuity regions where the Bernoulli assumption is not valid.

Table 2.1 Comparison of a design method in a stress discontinuity region

| Design Code | Clause | Contents |
|---|---|---|
| KHBDC (2015) | 5.6.1 (2) | For stress discontinuity regions, additional local anlaysis such as strut-tie model in 5.6.4.4 is needed. |
| KCI (2017) | I.2.1 (1) | Structural concrete members or D-regions shall be permitted to be designed by using an idealized truss model. |
| ACI 318 (2019) | 6.2.4.4 | A member or region shall be permitted to be analyzed and designed using the strut-and-tie method in accordance with Chapter 23. |
| AASHTO LRFD (2017) | 5.8.1 | Refined analysis methods or strut-and-tie method may be used to determine internal force effects in disturbed regions such as those near supports and the points of application of concentrated loads at strength and extreme event limit states |
| CSA A23.3 (2014) | 11.1.2 | Regions of members in which the plane sections assumption of flexural theory is not applicable shall be proportioned for shear and torsion using the strut-and-tie model. |
| Eurocode 2 (2004) | 6.5.1 (1) | Where a non-linear strain distribution exists (e.g. supports, near concentrated loads or plain stress) strut-and-tie models may be used (see also 5.6.4). |

### 2.3.3. Design of Deep Components

Typical T-type pier caps can be classified as cantilever beams in their structural form. Bridge bearings carrying the load of the superstructure depends on the type of girders, and usually 2 to 5 bridge bearings are located on the top of the pier caps. Thus, the bridge pier cap can be treated as a deep component with a short shear span: a greater depth than the span. The design methods of deep beams in various design codes, applicable to pier caps, are compared and summarized.

*2.3.3.1 Definition of deep component*

The pier cap can be considered a cantilever beam, which is defined as a deep beam due to the characteristics of the member shape with a deep member depth relative to the span. For these deep components, definitions are given in each design code and are summarized in Table 2.2 below.

According to the principle of St. Venant, stress analysis based on the linear strain distribution is possible where far from the distance of the depth of the member from the loads or from the geometric discontinuities is located. In other words, there is a nonlinear stress distribution in the area of discontinuity regions where within the distance of the depth of the member from the loads or from the geometric discontinuities is located. In accordance with St. Venant's principle, most design standards generally use the ratio of span and member depth to define a deep component corresponding to discontinuity region.

KHBDC (2015), KCI (2017), and ACI 318 (2019) define deep components in two ways based on the principle of St. Venant: Clear span does not exceed

four times the overall member depth $h$; Concentrated loads exist within a distance $2h$ from the face of the support. Meanwhile, Eurocode 2 (2004) defines a member whose net span is less than three times the depth of the member as a deep member, in a narrower range than that of other 3 design codes mentioned. CSA A23.3 (2014) defines a deep component, most conservative among all design criteria, with a net span less than twice the depth of the member. Unlike other design codes, AASHTO LRFD (2017) defines deep members using shear force and effective depth, $d$, of members rather than net span and member depth, $h$.

Typical pier caps can be treated as deep members because the provisions given in Table 2.2 are satisfied, depending on their geometry and load distribution. Therefore, under current design standards, the bridge pier cap shall be designed with considered as a deep member.

Table 2.2 Comparison of a definition of deep beam in design codes

| Design Code | Clause | Contents | Note |
|---|---|---|---|
| KHBDC (2015) | 5.2<br>5.6.2.1 | 1. Bemas with a clear span, $l_n$, not exceeding **four times** the member depth<br>2. Beams where the concentrated force is applied within **two times** the member depth from the face of the support | Defines deep beam:<br>**1. clear span**<br>**2. distance from support to load** |
| KCI (2017) | 1.4<br>6.3.4 | 1. Members with a clear span, $l_n$, not exceeding **four times** the member depth<br>2. Region between concentrated load and support, where the concentrated force is applied within **two times** the member depth from the face of the support | |
| ACI 318 (2019) | 9.9.1.1 | 1. Clear span does not exceed **four times** the overall member depth ***h***<br>2. Concentrated loads exist within a distance **2*h*** from the face of the support | |
| AASHTO LRFD (2017) | 5.2 | 1. The distance from **the point of 0.0 shear** to the face of the support is less than **2*d***<br>2. Load causing more than **1/3 of the shear** at a support is closer than **2*d*** from the face of the support. | Defines deep beam:<br>**shear force and *d*** |
| CSA A23.3 (2014) | 10.7.1 | 1. Clear span to overall depth ratios less than **2** | Defines deep beam:<br>**clear span** |
| Eurocode 2 (2004) | 5.3.1 | 1. The span is less than **3 times** the overall section depth | |

*2.3.3.2 Design of distributed rebar in deep component*

In the design of strut-and-tie models of deep members, rebars are placed to satisfy the effective design strength of each element after establishing a strut-and-tie model appropriate for the stress distribution of deep members. In other words, reinforcement is placed so that the strength of the tie element can be exerted to ensure structural safety of the member through truss analysis. Meanwhile, in order to control cracks caused by loading such as temperature and dry shrinkage not considered in the strut-and-tie model, the design codes propose the distributed rebar mesh design provisions for deep members to satisfy serviceability. Distributed rebar mesh design provisions of deep members are compared and summarized in Table 2.3.

KHBDC (2015), Eurocode 2 (2004), and CSA A23.3 (2014) require least 0.1% of vertical and horizontal reinforcement ratio to be placed on each side of the member (0.2% in both directions). However, the reinforcement cannot be evenly distributed through the thickness because of the rule of placing the reinforcement on both surfaces of the member. KCI (2017), ACI 318 (2019), and AASHTO LRFD (2017) permit even distribution of rebars in deep members with thickness, and each design code assigns the amount of rebars in each direction corresponding to 0.15 to 0.3 percent of the effective section of concrete. According to Hsuing (1985) and Anderson (1989), the shear strength of slender beam is not significantly affected by the distribution of stirrup to the thickness direction. In Tuchscher (2011), distribution to the thickness direction of the rebar mesh is independent of member behavior because, as with slender beams, the shear strength and the width of the diagonal crack under SLS in deep

beam are not significantly affected by the distribution to the thickness direction of the stirrup.

In a typical strut-tie model of pier cap, the vertical shear reinforcement is arranged so that the vertical tie can exert its strength to secure structural safety. Whereas, horizontal shear reinforcement is not considered in the design of strut-and-tie models for typical pier caps, and the distributed rebar mesh provision shown in Table 2.3 is the only provision for the horizontal shear reinforcement. Rogowosky (1986) said that the horizontal shear reinforcement in deep members does not affect the shear strength of the member relative to the vertical shear reinforcement. According to Birrcher (2013), for ACI 318, 0.25% of horizontal and 0.15% of vertical rebar ratio was required prior to Rogowosky (1986), and this was turned to the distribution of a minimum rebar ratio of 0.15% horizontally and 0.25% vertically after Rogowosky (1986) revealed that the vertical rebar is more effective in shear strength of deep beams. Since the revision in 2011, ACI 318 requires a 0.25% rebar mesh in both directions to control the diagonal crack propagation and the crack width in serviceability, not strength, but in KCI (2017), the minimum distributed rebar mesh regulation is still used as suggested before ACI 318-11. Meanwhile, AASHTO LRFD (2017) stipulates 0.3% of rebar mesh layout in accordance with Bircher (2013) who insists that minimum 0.3% of reinforcement ratio is required to control the maximum diagonal crack width at the first crack or SLS. Therefore, it is deemed that the design of strut-and-tie models in the pier cap determines the vertical shear reinforcement in terms of strength, and the horizontal shear reinforcement in distributed rebar mesh rules is for the satisfaction of its serviceability.

Table 2.3 Comparison of distributed rebar design in a deep component

| Design Code | Vertical reinforcement | Horizontal reinforcement | Rebar spacing | $b_w$ |
|---|---|---|---|---|
| KHBDC (2015) | Near each face: $0.001A_c$ | Near each face: $0.001A_c$ | Lesser of $2b$ or 300 *mm* | **Not considered** |
| KCI (2017) | Perpendicular to longitudinal axis: $0.0025b_ws$ | Parallel to longitudinal axis: $0.0015b_ws$ | Lesser of $d$ / 5 or 300 *mm* | Consider |
| ACI 318 (2019) | Perpendicular to longitudinal axis: $0.0025b_ws$ | Parallel to longitudinal axis: $0.0025b_ws_2$ | Lesser of $d$ / 5 or 300 *mm* | Consider |
| AASHTO LRFD (2017) | In vertical: $0.003b_ws_v$ | In horizontal: $0.003b_ws_h$ | Lesser of $d$ / 4 or 12 *in.* | Consider |
| CSA A23.3 (2014) | In each direction: $0.002A_c$ | In each direction: $0.002A_c$ | Less than 300 *mm* | **Not considered** |
| Eurocode 2 (2004) | Near each face: $0.001A_c$ | Near each face: $0.001A_c$ | Lesser of $2b$ or 300 *mm* | **Not considered** |

### 2.3.4. Strut-and-Tie Model Design

The overall strut-and-tie model design calculates the force on the struts, ties, and nodal regions at the load equilibrium conditions, and the required cross-sectional area at the force received by each element according to the effective strength and geometry of the components is determined. If each of the configured STM elements is not resistant to component forces, the trial-and-error designs are performed with varying model configurations.

However, current design standards do not define design procedures for strut-and-tie models. Only the effective design strengths of STM components are specified in the design codes, with a different strength for each design code. Since the differences in these strengths can affect the reinforcement arrangement in STM, it is necessary to compare and analyze the effective design strengths for design codes.

*2.3.4.1 Strength design of strut*

After determining the shape of the strut-and-tie model for the target pier cap structure, the strengths of the struts are checked considering the effective design strength of the strut. The strength designs of struts in design codes are compared and the details are summarized in Table 2.4 as follows. Depending on the condition of the member, the strength of strut is defined differently in each case by dividing the strut into the cases whether the lateral tensile force perpendicular to the direction of the strut exists or not.

Table 2.4 Comparison of a design method in a strut-strength

| Design Code | Reduction factor | Design strength of strut without lateral tension | Amount and orientation of lateral rebar | Brittleness of high strength concrete | Reinforced struts |
|---|---|---|---|---|---|
| KHBDC (2015) | $\phi_c = 0.65$ | $0.85\phi_c f_c'$ | Consider $A_s$ & direction | $\left(1-\frac{f_c'}{250}\right)$ | **Not enhanced** |
| KCI (2017) | $\phi = 0.75$ | $0.85\phi f_c'$ | Considered with $\beta_c$ | **Not considered** | $1.13A_s' f_s'$ |
| ACI 318 (2019) | $\phi = 0.75$ | $0.85\phi f_c'$ | Considered with $\beta_c$ and $\beta_s$ | **Not considered** | $A_s' f_s'$ |
| AASHTO LRFD (2017) | Strength of strut is not presented (Strength of nodal region is presented) | | | | |
| CSA A23.3 (2014) | $\phi_c = 0.65$ | $0.85\phi_c f_c'$ | Considered with $\varepsilon_1$ | **Not considered** | $f_y A_{ss}$ |
| Eurocode 2 (2004) | $\gamma_c = 1.5$ | $\alpha_{cc} f_c' / \gamma_c$ | Consider only existence | $\left(1-\frac{f_c'}{250}\right)$ | **Not enhanced** |

Struts without lateral tension show the same strength expression as in Equation (2.2), and the difference of strengths from each design code is governed by the reduction factor. Figure 2.9 shows the comparison of effective design strengths of struts according to the specified compressive strength of concrete. The strengths of struts increase linearly in proportion to the specified compressive strength. Though the strength of strut is assessed most conservatively in KHBDC and CSA A23.3, the difference in effective design strength in normal strength concrete is not significant.

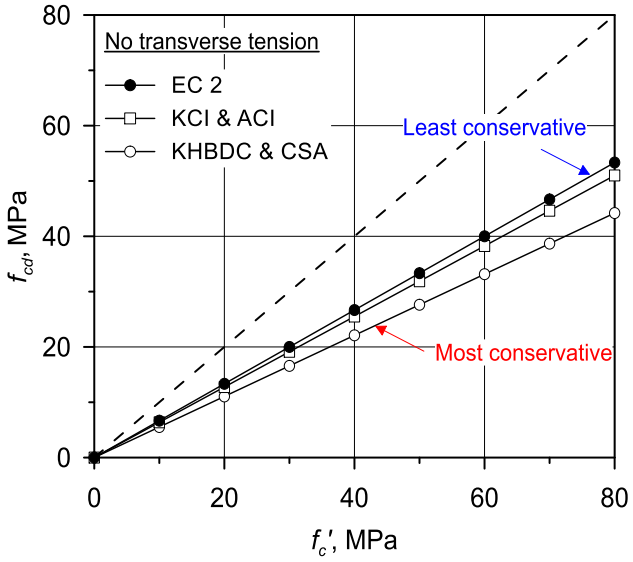


Figure 2.9 Effective design compressive strength of strut with no tension

Struts with lateral tension exhibit the same strength expression as Equation (2.2) or Equation (2.3), and the difference in strength for each design code is governed by the reduction factor and the specified compressive strength of concrete. The examples of effective design strengths of struts according to the specified compressive strength of concrete are shown in Figure 2.10 and Figure 2.11, depending on the amount of lateral tensile reinforcement.

$$f_{cd} = A \cdot \phi \cdot f_c' \tag{2.2}$$

$$f_{cd} = A \cdot \phi \cdot \left(1 - f_c' / 250\right) \cdot f_c' \tag{2.3}$$

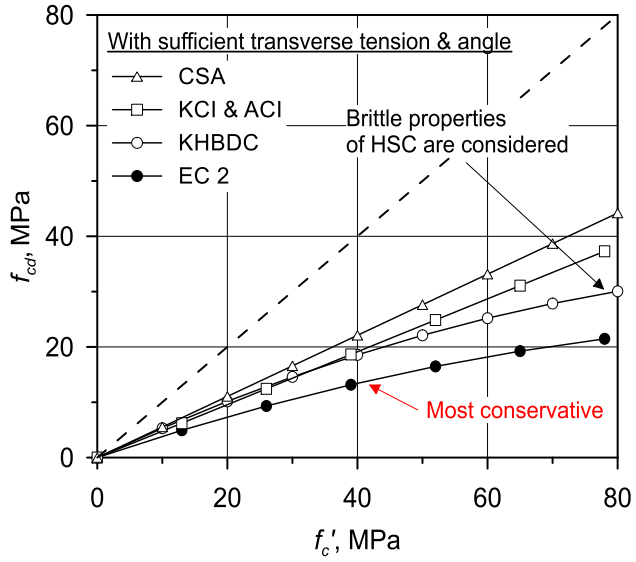


Figure 2.10 Effective design compressive strength of strut with over-reinforced lateral tensile rebar

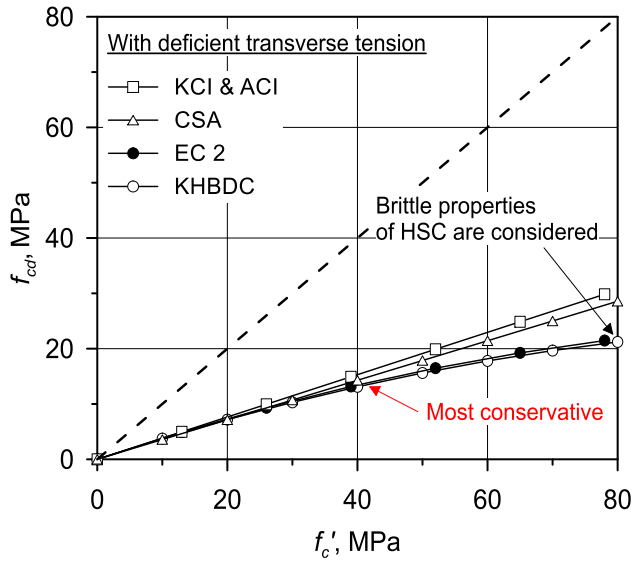


Figure 2.11 Effective design compressive strength of strut with under-reinforced lateral tensile rebar

KHBDC and Eurocode 2 reflect the brittleness of high-strength concrete in the formulas with the parabolic, and it is confirmed that the higher-strength concrete becomes, the lower the increase rate of the design strength for the increase in specified compressive strength. Consequently, the effective design strengths of struts in KHBDC and Eurocode 2 are evaluated conservatively compared to other design codes.

In the case that the lateral tensile reinforcement is less arranged, the deviation between the design codes is relatively small, and the strength deviation between the design codes tends to increase where high strength concrete exceeding 40 MPa is used. In general, normal strength concrete which has 40 MPa or less of compressive strength is used for the design and construction of the current bridge pier caps, so no significant difference in the effective design strength between the design codes occurs.

*2.3.4.2 Strength design of tie*

Table 2.5 Comparison of a design method in a tie-strength

| Design Code | Reduction factor | Design strength of tie with rebar | Design strength of tie with PS strands | Bonded or Unbonded |
|---|---|---|---|---|
| KHBDC (2015) | $\phi_s = 0.90$ | $f_{yd} = \phi_s f_y$ | $f_{pyd} = \phi_s f_{py}$ | **Not considered** |
| KCI (2017) | $\phi = 0.85$ | $\phi F_{nt} = \phi A_{st} f_y$ | $\phi F_{nt} = \phi A_{ps}\left(f_{pe} + \Delta f_p\right)$<br>$\Delta f_p = 420$ or 70 MPa | Bonded: 420<br>Unbonded: 70 |
| ACI 318 (2019) | $\phi = 0.75$ | $\phi F_{nt} = \phi A_{st} f_y$ | $\phi F_{nt} = \phi A_{ps}\left(f_{pe} + \Delta f_p\right)$<br>$\Delta f_p = 420$ or 70 MPa | Bonded: 420<br>Unbonded: 70 |
| AASHTO LRFD (2017) | $\phi = 0.90$ | $\phi P_n = \phi A_{st} f_y$ | $\phi P_n = \phi A_{ps}\left(f_{pe} + f_y\right)$ | **Not considered** |
| CSA A23.3 (2014) | $\phi_s = 0.85$ | $\phi_s A_{st} f_y$ | $\phi_p A_p\left(f_{po} + 400\right)$ | **Not considered** |
| Eurocode 2 (2004) | $\gamma_s = 1.15$ | $f_{yd} = f_{yk} / \gamma_s$ | $f_{pd} = f_{p0.1k} / \gamma_s$ | **Not considered** |

After determining the shape of the STM for the member corresponding to the target pier cap, the strengths of ties are checked to form a suitable strut-and-tie model. Comparing the effective design strengths of ties in design codes, the details are summarized in Table 2.5.

The effective design strengths of ties where no PS strand is assigned are defined as the yield strength of the rebar in all design codes. The reduction factor of ties for each design code is different. In the case of member with

prestressing strands, KCI and AASHTO LRFD consider whether the ties are bonded or not when determining the effective design strengths of ties. The effective design strength of tie with only reinforcing steel bar in ACI 318 is most conservative as shown in Figure 2.12.

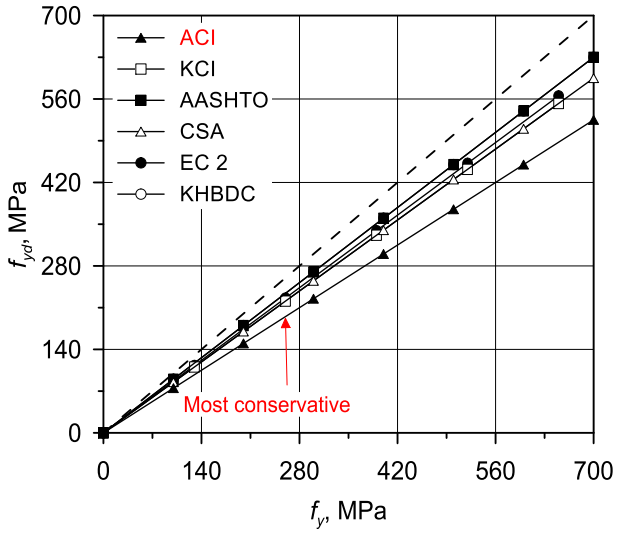


Figure 2.12 Effective design tensile strength of tie with reinforcing steel bar

*2.3.4.3 Strength design of nodal region*

Nodal region refers to the concrete area where struts and ties are connected in STM, and nodal region is typically the area where the greatest stress is applied by superimposed forces by load, reactions, the compressive forces of struts, and the tensile forces of ties. Therefore, it is important to check the effective design strength of nodal region in the design of strut-and-tie model. The strength designs of nodal region by design codes are compared and summarized in Table 2.6.

Table 2.6 Comparison of a design method in a nodal region

| Design Code | Reduction factor | Design strength for CCC node | Design strength for CCT node | Design strength for CTT node |
|---|---|---|---|---|
| KHBDC (2015) | $\phi_c = 0.65$ | $\left(1-\frac{f_{ck}}{250}\right)\phi_c f_c'$ | $0.85\left(1-\frac{f_{ck}}{250}\right)\phi_c f_c'$ | $0.75\left(1-\frac{f_{ck}}{250}\right)\phi_c f_c'$ |
| KCI (2017) | $\phi = 0.75$ | $0.85\phi\beta_n f_c'$<br>$\beta_n = 1.0$ | $0.85\phi\beta_n f_c'$<br>$\beta_n = 0.8$ | $0.85\phi\beta_n f_c'$<br>$\beta_n = 0.6$ |
| ACI 318 (2019) | $\phi = 0.75$ | $0.85\phi\beta_c\beta_n f_c'$<br>$\beta_n = 1.0$<br>$\beta_c = \sqrt{A_2/A_1} \le 2$ | $0.85\phi\beta_c\beta_n f_c'$<br>$\beta_n = 0.8$<br>$\beta_c = \sqrt{A_2/A_1} \le 2$ | $0.85\phi\beta_c\beta_n f_c'$<br>$\beta_n = 0.6$<br>$\beta_c = \sqrt{A_2/A_1} \le 2$ |
| AASHTO LRFD (2017) | $\phi = 0.70$ | $\phi \cdot mvf_c'$<br>$m = \sqrt{A_2/A_1} \le 2$<br>$v = 0.85 - \frac{f_c'}{20\ (\text{ksi})}$ | $\phi \cdot mvf_c'$<br>$m = \sqrt{A_2/A_1} \le 2$<br>$v = 0.85 - \frac{f_c'}{20\ (\text{ksi})}$ | $\phi \cdot mvf_c'$<br>$m = \sqrt{A_2/A_1} \le 2$<br>$v = 0.85 - \frac{f_c'}{20\ (\text{ksi})}$ |
| CSA A23.3 (2014) | $\phi_c = 0.65$ | $0.85\phi_c m f_c'$<br>$m = \sqrt{A_2/A_1} \le 2$ | $0.75\phi_c m f_c'$<br>$m = \sqrt{A_2/A_1} \le 2$ | $0.65\phi_c m f_c'$<br>$m = \sqrt{A_2/A_1} \le 2$ |
| Eurocode 2 (2004) | $\gamma_c = 1.5$ | $\left(1-\frac{f_{ck}}{250}\right) f_c'/\gamma_c$ | $0.85\left(1-\frac{f_{ck}}{250}\right) f_c'/\gamma_c$ | $0.75\left(1-\frac{f_{ck}}{250}\right) f_c'/\gamma_c$ |

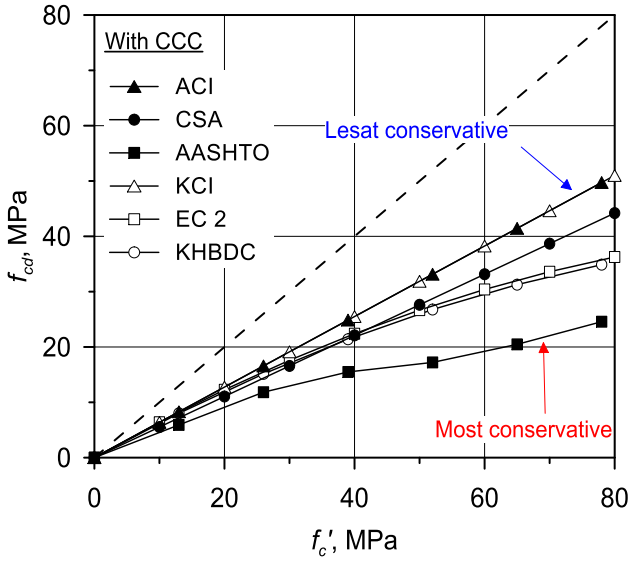


Figure 2.13 Effective design compressive strength of CCC nodal region

Depending on the condition of the member, the effective design strength of nodal region is defined differently whether the tensile ties are developed in nodal region or not. For compressive areas (CCC node) where tensile ties are not developed and are subject to purely compressive stress, the same effective design strength expressions as in equation (2.2) and equation (2.3) of the strut are presented. The differences in strength of each design code are governed by the reduction factor, additional reduction except tie's influence, and increase factor with concrete confinement. The effective design strengths of the CCC node with increase of the compressive strength is shown in Figure 2.13.

As with the effective design strength of struts, Eurocode 2 and KHBDC reflect the brittleness of high-strength concrete, so the higher strength concrete is used, the greater the difference in the strengths of nodal regions for design codes. Meanwhile, in AASHTO LRFD, ACI 318, and CSA A23.3, an increase

factor, $m$ or $\beta_c$, of concrete confinement effect is reflected in the strength formula, and it may enlarge effective design strength at bearing supports. At the most vulnerable part without increase factor, there is little difference in the effective design strength between the design codes in normal strength concrete of 40 MPa or less. And in high-strength concrete, AASHTO LRFD is the most conservative design for CCC node.

In the case of one developed tie in nodal region (CCT node) and two or more tie in nodal region (CTT node), the effective design strength expressions are also same as in Equation (2.2) or Equation (2.3). At the most vulnerable part without increase factor, the differences in strength of design codes are governed by the reduction factor, additional reduction except tie's influence. The effective design strengths of CCT and CTT node are plotted in Figure 2.14 and Figure 2.15, respectively. The trends of graphs are similar to that of Figure 2.13. The more ties are developed, the weaker effective design strength in nodal region, reflecting the properties of concrete that is vulnerable to tension. For node-to strut in AASHTO LRFD, however, the effect of tie is not considered because the reduction factor, $\nu$, is same for all node types.

In the case of pier caps with normal strength concrete of 40 MPa or less, there are similar effective design strengths at the vulnerable strut part regardless of design codes in all nodal regions.

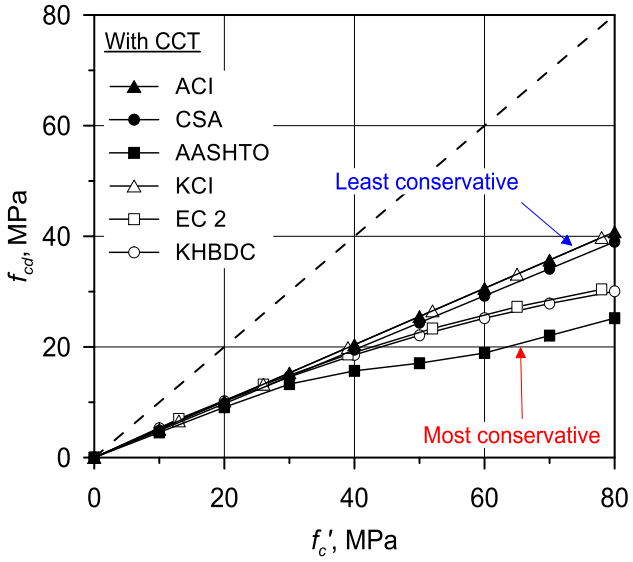


Figure 2.14 Effective design compressive strength of CCT nodal region

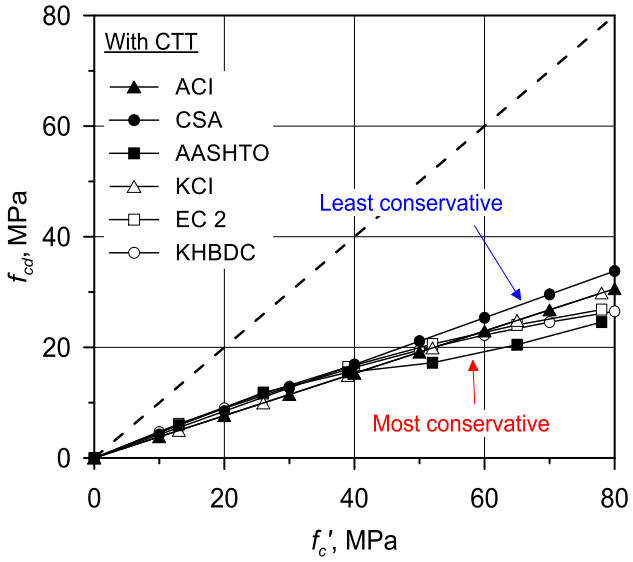


Figure 2.15 Effective design compressive strength of CTT nodal region

### 2.3.5. Concluding remarks

The design methods of bridge pier cap, which are currently stipulated in design codes, were summarized and compared. The analysis of pier cap designs revealed that KHBDC is based on Eurocode 2 and KCI follows ACI 318. Although the overall design procedures are similar for all design codes, it differs from the details of each item.

With the change of the design method from ultimate strength design to limit state design, in all design codes, structures which belong to discontinuity regions such as pier caps are specified or recommended to be designed with STM. Pier caps are also classified to deep beams and designed following the deep beam designs. The definition of deep beams differs by design codes, and for cantilever beams such as pier cap, there is uncertainty in the application of deep beam definitions. In distributed rebar mesh designs for deep beams, KHBDC and Eurocode 2 do not consider the thick width of deep components in the disposition of rebar. However, in some studies, distribution through the thickness little affect the shear strength of the member.

The overall design scheme of strut-and-tie model is similar to all design standards. However, the effective design strengths of strut, tie, and nodal region vary according to design codes, and the deviation of effective design strengths between design codes for strut and nodal region are shown to be greater when using high-strength concrete exceeding 40 MPa of compression strength. Although there is difference in the strengths for high-strength concrete, it was confirmed that the strengths of struts and nodal regions are similar in all design

criteria for concrete structures with normal strength under 40 MPa. Therefore, it is deemed that the current STM designs of bridge pier cap, which usually uses normal-strength concrete, show similar design results regardless of design code. It is necessary to verify the validity of the effective design strength by design codes in case of pier caps where high strength concrete is used.

# III. STM for Efficient Bridge Pier Cap Design

## 3.1. Introduction

There is no standard section in bridge pier cap in Korea, and details such as dimensions of geometry and reinforcement are determined at designer's discretion. This flexibility in design of pier caps leads to the design of pier caps in a variety of geometrical and structural environments, enabling various designs according to the design environment and the capability of the designer. However, in the absence of direction for efficient STM designs, this versatility may violate the consistency in designs and cause confusion such as excessive designs. Therefore, it is necessary to identify limitations in the STM design of pier caps by investigating and comparing the design status of the current bridge pier cap, and further to present the design direction that should be considered for the design of the bridge pier cap through an analysis on the reinforcement arrangement following the STM layout.

In this chapter, a comparison and analysis of the design cases of existing bridge pier caps are conducted to provide direction for the efficient STM design of pier caps. Chapter 3.2 identifies and analyzes design features such as specifications of pier caps, load characteristics, the amount of flexural and shear reinforcement based on the existing design data of various pier caps. Chapter 3.3 investigates the design characteristics in different STM layouts for the T-type pier caps. Chapter 3.4 presents the design guidelines for strut-and-tie models of pier caps for more efficient layout of rebars based on the previous analyses.

## 3.2. Study on Design Examples of Pier Caps

To compare the design characteristics of the pier caps, various design examples of bridge pier caps were collected, and a total of 20 cases were obtained. However, some of the data were excluded because it was not possible to calculate the rebar ratio of the pier caps. Other types of piers except both T-type piers, which are the main type of bridge pier, and Π-type piers were excluded. As a result, a total of 11 design examples for the T and Π-type bridge pier caps (seven for domestic and four for overseas data) were collected, and properties of design examples of bridge pier cap were summarized in Table 3.1.

As shown in Table 3.1, of the total 11 design data for bridge pier caps, the bridges except bridge number 9 are highway bridges. According to the type of bridge, there are seven T-type piers, two Π-type piers, and one Bent Cap and Cap Beam, respectively. The length of pier cap and the load distribution applied to pier cap are primarily determined by the support bearings corresponding to the superstructure. On the other hand, sectional depth of pier cap was found to vary from 1,500 mm to 3,200 mm. Unlike normal beam members, pier cap has a large width corresponding to the sectional depth, which is affected by the width of the support bearings. The current designs of pier caps do not use high-strength materials until now, but mainly uses normal-strength concrete and rebars.

The amount of reinforcement for a total of 11 design data of pier caps was organized in Table 3.2. Reinforcement ratios of tensile reinforcement, compressive reinforcement, vertical shear reinforcement, and horizontal shear

reinforcement were derived with reference to drawings and structural calculations. Distribution of shear reinforcement ratio is shown in Figure 3.1. In the graph, x-axis indicates horizontal shear reinforcement ratio and y-axis presents vertical shear reinforcement ratio.

As shown in Figure 3.1, it was confirmed that most shear rebar ratios of the pier caps designed based on the current strut-and-tie model are distributed within 0.6%. Though, some of the design cases for the pier caps in Korea (bridge number 3, 4 and 6) showed excessive shear rebar ratio of the vicinity of 1%. In most design cases, horizontal shear reinforcement was less than the vertical shear reinforcement, but horizontal rebar was accompanied by a somewhat corresponding amount to vertical rebars. All members with excessive shear reinforcement ratio were designed based on STM. And bridge number 3 and bridge number 5 with similar design load and dimensions were found to show different amount of shear reinforcement even though they were designed with STM.

Table 3.1 Properties of existing design cases of bridge pier cap

| Bridge number | | 1 | 2 | 3 | 4 | 5 | 6 | 7 | 8 | 9 | 10 | 11 |
|---|---|---|---|---|---|---|---|---|---|---|---|---|
| Nation | | Domestic | | | | | | | Abroad | | | |
| Bridge type | | Highway | | | | | | | | | Railway | Highway |
| Pier cap type | | T | Π | T | Π | T | T | T | T | T | Bent cap | Cap Beam |
| Design method | | Ultimate Strength Design | | Limit State Design (STM) | | | | | Ultimate Strength Design | | Limit State Design (STM) | |
| Dimension (mm) | Length | 12,000 | 24,000 | 12,400 | 24,500 | 12,400 | 11,800 | 10,500 | 4,100 | 10,000 | 6,500 | 14,350 |
| | Depth | 3,100 | 3,200 | 3,200 | 3,000 | 3,200 | 3,200 | 2,700 | 1,500 | 2,700 | 1,700 | 1,800 |
| | Width | 2,500 | 3,000 | 2,500 | 2,500 | 3,000 | 2,900 | 2,700 | 1,500 | 2,500 | 2,100 | 2,000 |
| Design load | | DB-24 DL-24 | DB-24 DL-24 | KL-510 | KL-510 | KL-510 | KL-510 | KL-510 | HS-20 | BD 21/01 Table 4.1 | No data | No data |
| Load distribution | | 5-point | 9-point | 5-point | 9-point | 4-point | 5-point | 2-point | 2-point | 5-point | 8-point | 14-point |
| Strength (MPa) | Concrete | 40 | 40 | 40 | 40 | 40 | 40 | 40 | 38 | 30 | 34 | 50 |
| | Rebar | 400 | 400 | 400 | 400 | 400 | 400 | 400 | 413 | 460 | 412 | 460 |

Table 3.2 Reinforcement details of design cases of bridge pier cap

| Num. | Type | Design method | Role of rebar | Diameter of rebar | $s$ (mm) | $n$ (EA) | $b_w$ (mm) | $d$ (mm) | Rebar ratio |
|---|---|---|---|---|---|---|---|---|---|
| 1 | T | Ultimate Strength Design | Tensile | H29, H25 | - | 42, 11 | 2,500 | 2,652 | 0.0049 |
| | | | Compressive | - | - | - | | - | - |
| | | | Vertical shear | H22 | 250 | 6 | | - | 0.0037 |
| | | | Horizontal shear | H22 | 250 | 6 | | - | 0.0045 |
| 2 | Π | Ultimate Strength Design | Tensile | H32 | - | 46 | 3,000 | 2,650 | 0.0040 |
| | | | Compressive | H29 | - | 23 | | 2,420 | 0.0020 |
| | | | Vertical shear | H25 | 200 | 6 | | - | 0.0051 |
| | | | Horizontal shear | H25 | 250 | 6 | | - | 0.0041 |
| 3 | T | Limit State Design | Tensile | H32 | - | 72 | 2,500 | 2,849 | 0.0080 |
| | | | Compressive | - | - | - | | - | - |
| | | | Vertical shear | H32 | 150 | 6 | | - | 0.0127 |
| | | | Horizontal shear | H32 | 200 | 6 | | - | 0.0095 |
| 4 | Π | Limit State Design | Tensile | H32 | - | 63 | 2,500 | 3,012 | 0.0066 |
| | | | Compressive | H29 | - | 21 | | 3,012 | 0.0018 |
| | | | Vertical shear | H29 | 150 | 6 | | - | 0.0103 |
| | | | Horizontal shear | H29 | 200 | 6 | | - | 0.0077 |
| 5 | T | Limit State Design | Tensile | H32, H25 | - | 23, 12 | 3,000 | 2,889 | 0.0028 |
| | | | Compressive | - | - | - | | - | - |
| | | | Vertical shear | H22 | 250 | 6 | | - | 0.0031 |
| | | | Horizontal shear | H19 | 250 | 6 | | - | 0.0023 |
| 6 | T | Limit State Design | Tensile | H32, H29 | - | 23, 23 | 2,900 | 2,895 | 0.0039 |
| | | | Compressive | - | - | - | | - | - |
| | | | Vertical shear | H25 | 300 | 6 | | - | 0.0084 |
| | | | Horizontal shear | H22 | 250 | 6 | | - | 0.0032 |
| 7 | T | Limit State Design | Tensile | H32, H29 | - | 25, 50 | 2,700 | 2,530 | 0.0076 |
| | | | Compressive | - | - | - | | - | - |
| | | | Vertical shear | H22 | 250 | 6 | | - | 0.0034 |
| | | | Horizontal shear | H19 | 250 | 6 | | - | 0.0026 |
| 8 | T | Ultimate Strength Design | Tensile | H32 | - | 10 | 1,500 | 1,500 | 0.0035 |
| | | | Compressive | - | - | - | | - | - |
| | | | Vertical shear | H16 | 250 | 4 | | - | 0.0021 |
| | | | Horizontal shear | H18 | 200 | 4 | | - | 0.0034 |
| 9 | T | Ultimate Strength Design | Tensile | H25, H20 | - | 42, 21 | 2,500 | 2,520 | 0.0043 |
| | | | Compressive | - | - | - | | - | - |
| | | | Vertical shear | H16 | 200 | 6 | | - | 0.0024 |
| | | | Horizontal shear | H20 | 250 | 6 | | - | 0.0030 |
| 10 | π | Limit State Design | Tensile | H32 | - | 14 | 2,133 | 1,700 | 0.0031 |
| | | | Compressive | H35 | - | 14 | | 1,700 | 0.0037 |
| | | | Vertical shear | H19 | 200 | 4 | | - | 0.0027 |
| | | | Horizontal shear | H13 | 178 | 2 | | - | 0.0007 |
| 11 | π | Limit State Design | Tensile | H32 | - | 39 | 2,000 | 1,664 | 0.0094 |
| | | | Compressive | H32 | - | 39 | | 1,664 | 0.0094 |
| | | | Vertical shear | H20 | 125 | 4 | | - | 0.0050 |
| | | | Horizontal shear | H20 | 125 | 2 | | - | 0.0025 |

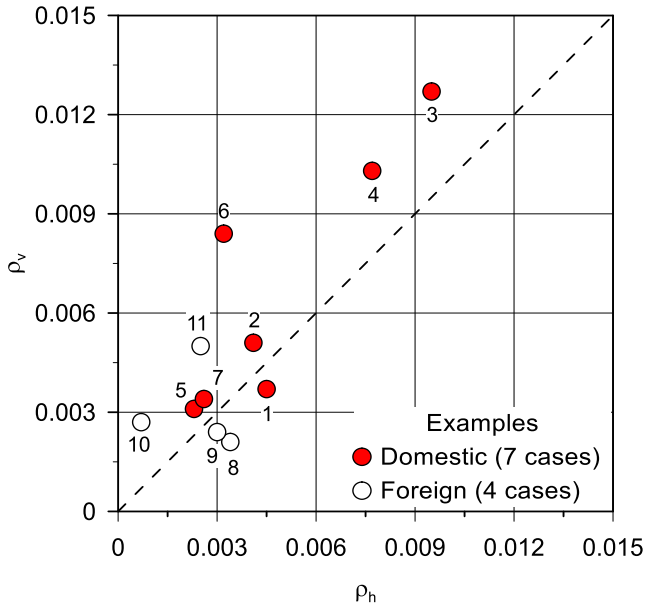


Figure 3.1 Comparison of shear rebar ratio in design cases of pier cap

In order to determine the cause of excessive arrangement of shear rebar in STM design of pier caps, the required bar spacings were derived according to Equation 3.1 and 3.2 for a total of 7 bridge pier caps designed with STMs, depending on the maximum member force acting on the vertical shear tie at the design load. The required bar spacings are compared to the actual spacings (shown in Table 3.3). $\phi_s$ is a reduction factor for the shear reinforcement, $n$ is the number of vertical shear rebar through the thickness of the pier cap, and $A_{st}$ is a nominal cross-sectional area of the steel. $f_{vy}$ is yield strength of vertical shear reinforcement. $b_w$ is a thickness of pier cap, and $F_u$ is a maximum force of vertical tie in STM. $w_{\text{eff}}$ is a maximum effective width of the vertical tie which has a maximum force. $s_{\text{req}}$ is a required spacing of

vertical shear reinforcement, and $\rho_{v,\,\mathrm{req}}$ is a required vertical shear reinforcement ratio based on the $s_{\mathrm{req}}$.

$$s \le s_{req} = \frac{w_{\mathrm{eff}}}{F_u}\left(\phi_s \cdot n \cdot A_{st} \cdot f_{vy}\right) \tag{3.1}$$

$$\rho_{v,\,\mathrm{req}} = \frac{\left(n \cdot A_{st}\right)}{\left(b_w \cdot s_{req}\right)} \tag{3.2}$$

According to Table 3.3, the spacings of vertical shear reinforcement for bridge number 3, 4 and 6 with excessive arrangement are not designed to be excessively conservative compared to the required rebar spacing required in STM. In other words, the required amount of rebars in STM itself is designed to be large, which depends on the magnitude of the maximum member force acting on the vertical tie, so it is necessary to analyze the cause of the difference in the maximum member force of each bridge.

Table 3.3 Spacing of vertical shear reinforcement with maximum tie force

| Bridge Num. | $\phi_s$ | $n$ | $A_{st}$ (mm$^2$) | $f_{vy}$ (MPa) | $b_w$ (mm) | $F_u$ (kN) | $w_{\text{eff}}$ (mm) | $s_{\text{req}}$ (mm) | $s$ (mm) | $\rho_{v,\text{ req}}$ (%) | $\rho_v$ (%) |
|---|---|---|---|---|---|---|---|---|---|---|---|
| 3 | 0.90 | 6 | 794.2 | 400 | 2,500 | 8,776 | 790 | 154 | 150 | 1.24 | 1.27 |
| 4 | 0.90 | 6 | 642.4 | 400 | 2,500 | 5,582 | 754 | 187 | 150 | 0.82 | 1.03 |
| 5 | 0.90 | 6 | 387.1 | 400 | 3,000 | 3,206 | 1,600 | 417 | 250 | 0.19 | 0.31 |
| 6 | 0.90 | 6 | 506.7 | 400 | 2,900 | 6,200 | 792 | 140 | 125 | 0.75 | 0.84 |
| 7 | 0.90 | 6 | 387.1 | 400 | 2,700 | 5,937 | 1,885 | 265 | 250 | 0.32 | 0.34 |
| 10 | 0.90 | 4 | 286.5 | 412 | 2,100 | 2,337 | 1,677 | 305 | 200 | 0.18 | 0.27 |
| 11 | 0.90 | 4 | 314.0 | 460 | 2,000 | 5,045 | 6,384 | 658 | 125 | 0.10 | 0.50 |

## 3.3. Reinforcement in accordance with STM

Chapter 3.2 considered the design characteristics of the pier caps by identifying the specifications, material properties, design load, and rebar ratio of the pier caps in various design examples. Some of the pier caps designed with STM have excessive shear reinforcement, and the direct cause of over-reinforcement was not due to a more conservative design than the amount of rebars required in the design, but due to the large member forces acting on vertical shear ties of STMs applied in the pier caps. Therefore, it is necessary to identify the effect of STM placement on the rebar ratio of the members.

Chapter 3.3 analyzes the validity of STM configuration through bridge number 3 and bridge number 5, which show great difference in shear reinforcement ratio despite of similar specifications and load characteristics. And the effect of shear tie arrangement on shear reinforcement ratio is analyzed. Furthermore, the change in the amount of rebar with the various STM configuration is determined. Through this, a strut-and-tie model with efficient rebar arrangement of bridge pier cap is proposed.

### 3.3.1. Stress Distribution in accordance with Elastic Analysis

In order to establish a strut-and-tie model properly on the bridge pier cap, it is recommended to identify the stress flow of the structure under loading and position struts and ties to fit in the flow of tensile, compressive and shear stress. A two-dimensional linear elastic finite element analysis was performed to identify the validity of strut-and-tie models in bridge numbers 3 and 5 with similar structural environment among the existing design cases of pier caps. From the elastic analysis results, the stress distributions were identified, and STM elements were arranged in accordance with the stress flow.

*3.3.1.1 Bridge number 3*

A linear analysis of the two-dimensional elastic finite element model was conducted using the commercial finite element analysis program, DIANA, to identify the stress flow for the load distribution of bridge number 3. Though Figure 3.2 shows the altitude difference due to the curvature of the roadway, the vertical elevation at the top of pier cap was ignored in the analysis. In addition, only a portion of the column was simulated, with a hinge on one end of the column and a roller point on the other. A five-point load, due to the superstructure consisting of 5 I-type girders, at SLS was applied to the structure.

The results of an elastic analysis are shown in Figure 3.3. The flow of stress distribution shows that principal tensile stress is applied to the top of the member shown in Figure 3.3 (a), since the pier cap is kind of cantilever beam. For principal compressive stresses, the tendency of the compression stress to transfer from the load point to the column is shown in Figure 3.3 (c). Stress

concentration occurred at the load point and at the interface between the column and the bottom of the pier cap. In the case of shear stress, it is shown that the shear stress occurs in the area between the outer part of the column and the inner and outer load points, and the largest shear stress occurs in the area between the outer part of the column and the inner load point, as shown in Figure 3.3 (f). It is easy to predict where the greatest shear force occurs at the pier caps, corresponding to the fact that vicinity of the support of cantilever beam is the critical section for shear stress.

Afterwards, each element of the STM is placed to reflect the stress flow acting on the member obtained through the elastic analysis.

As shown in Figure 3.3 (b), the tensile tie is located at the top of the member and the tensile tie is placed in the corresponding position considering the arrangement of longitudinal reinforcement.

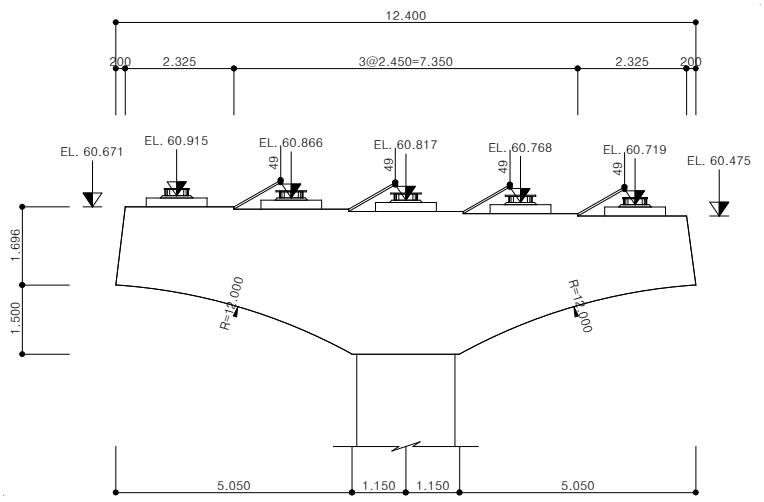


Figure 3.2 Dimensions and load distribution of pier cap (Bridge number 3)

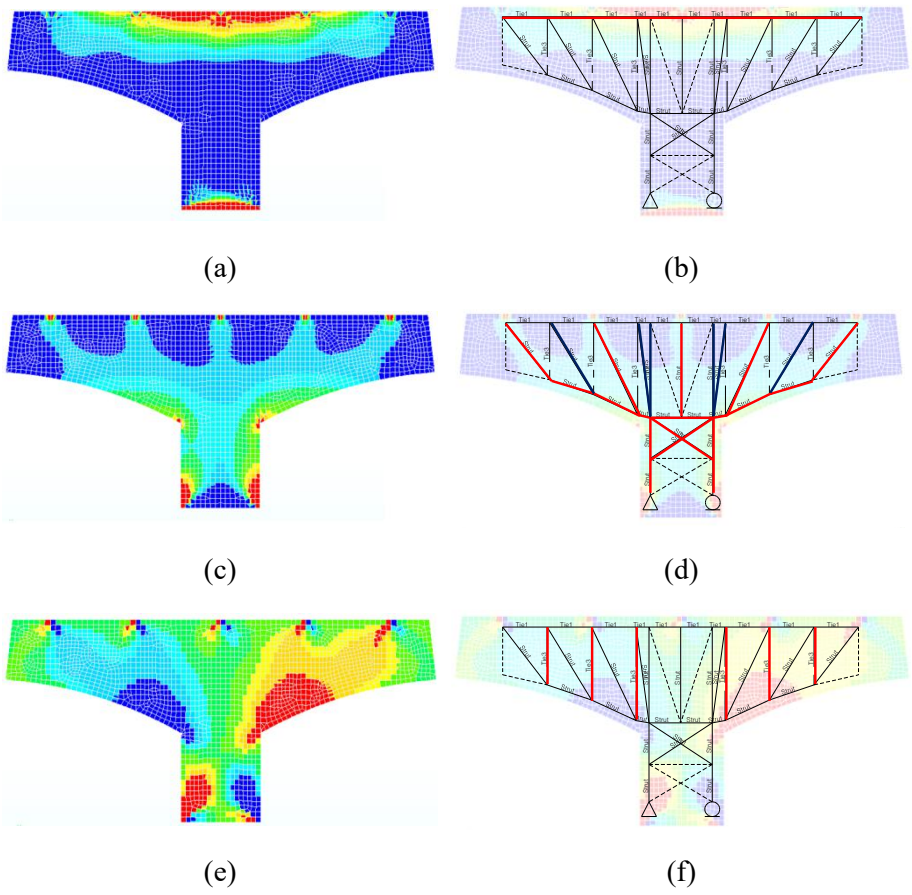

Figure 3.3 Cauchy total stresses for elastic analysis and corresponding STM elements (Bridge number 3): (a) S1: Tensile principal stress; (b) Tension ties; (c) S2: Compressive principal stress; (d) Compressive strut; (e) $S_{XY}$: Shear stress; (f) Shear ties

For compressive struts, it is reasonable to position strut elements as shown in the red line in Figure 3.3 (d), since the principal compressive stress flows to the column at the 5 load points. The blue line is the dummy elements caused by placing a vertical shear tie regardless of the stress flow.

The vertical shear ties are positioned in the area of shear stress as the shear stress occurs between the outer part of the column and the outer load point as shown in Figure 3.3 (e). When looking at the actual layout patterns of the shear ties used to design bridge number 3, as shown in Figure 3.3 (f), additional vertical shear ties were placed in the position expected to be the shear critical section between the outer part of the column and the inner load point, together with the vertical ties between the outer load point and the inner load point.

*3.3.1.2 Bridge number 5*

Linear analysis of the 2-D elastic finite element model was also performed to identify the stress flow acting on bridge number 5. As shown in Figure 3.4, the actual pier cap receives the load through the support bearings at the top of the pier cap. Since the presence of a support bearings does not significantly affect the flow of stress, the stress flow was analyzed for the model where the point loads were applied. Similarly, the elevation in the pier cap was ignored.

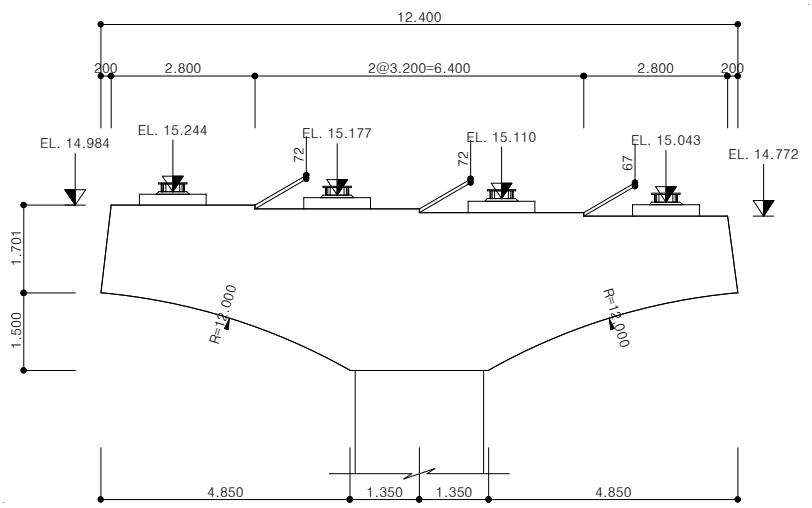


Figure 3.4 Dimensions and load distribution of pier cap (Bridge number 5)

In addition, only a portion of the column was modeled with a hinge on one end of the column and a roller point on the other. A four-point load, due to the superstructure consisting of 4 I-type girders, at SLS was applied to the structure.

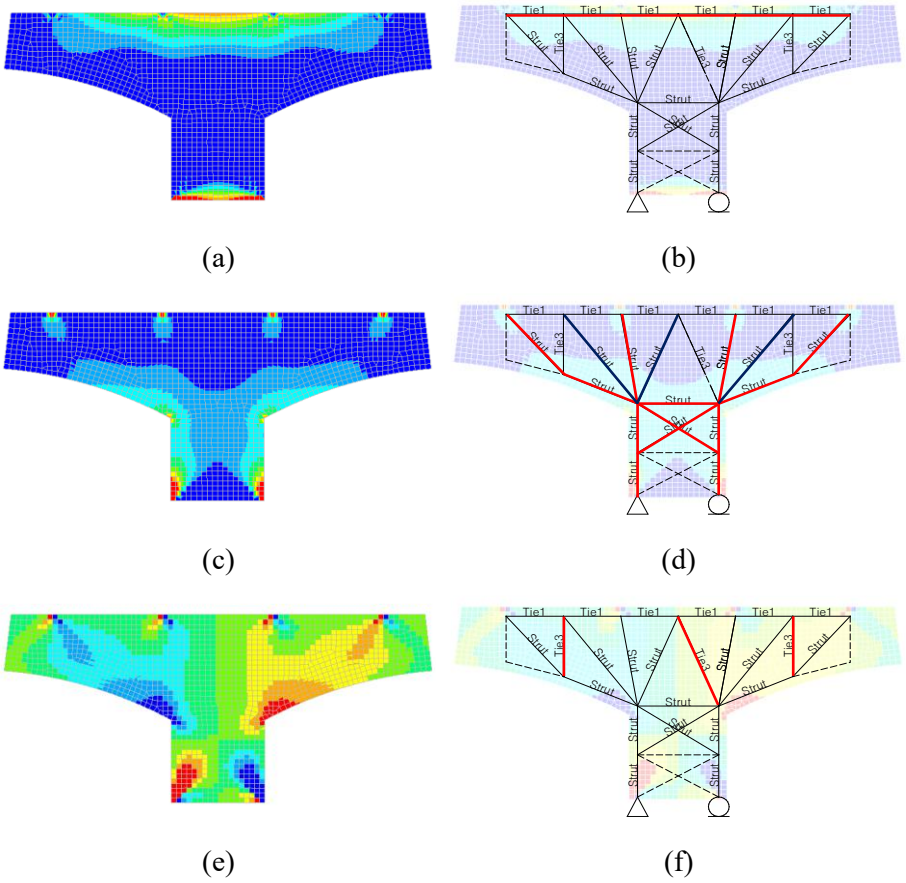


Figure 3.5 Cauchy total stresses for elastic analysis and corresponding STM elements (Bridge number 5): (a) S1: Tensile principal stress; (b) Tension ties; (c) S2: Compressive principal stress; (d) Compressive strut; (e) $S_{XY}$: Shear stress; (f) Shear ties

The stress distribution in Figure 3.5 confirmed that tensile stress is on the top of the pier cap because the member is type of the cantilever beam same as bridge number 3. Principal compressive stress is shown to be transmitted from the load points to the column. Shear stress occurs in the area between the outer part of the column and the outer load point, and it is maximum at the region between the outer part of the column and the inner load point.

The layout of strut-and-tie model in the actual design reflecting the stress flow of the pier cap is shown in Figure 3.5 (b), (d), and (f). The tensile tie is located at the top of the member and the tensile tie is placed in the corresponding position considering the arrangement of flexural reinforcement.

For compressive struts, strut elements were positioned as shown in the red line in Figure 3.5 (d), since the principal compressive stress flows to the column at the 4 load points. The blue line is the dummy elements caused by placing a vertical shear tie regardless of the stress flow.

For shear ties, the vertical shear ties are positioned in the area where the shear stress occurs as shown in Figure 3.5 (f). In contrast with the actual layout patterns of the shear ties used to design bridge number 3 shown in Figure 3.3 (f), no additional vertical shear ties were placed in the position expected to be the shear critical section between the outer part of the column and the inner load point.

### 3.3.2. Rebar Ratio in accordance with Vertical-Tie-Arrangement

As discussed in 3.3.1, the vertical shear ties in the strut-and-tie model of a typical T-type pier caps are determined at the discretion of the designer. Shear stress flow shows that the largest shear stress acts in the area between the column and the inner load point, and some designers thereby place additional vertical ties in the area expected to be shear critical section. According to researchers such as Schlaich et al. (1987), MacGregor and Wight (2005), and Williams et al. (2012), however, vertical ties as less as possible are considered to be more efficient designs. From this point of view, additional vertical tie arrangement may cause more shear reinforcement than is necessary. To examine the effect of vertical ties on the design of rebars, the reinforcement ratios required for various vertical tie layouts in the STM design examples of pier cap such as bridge number 3 and bridge number 5 were derived.

*3.3.2.1 Bridge number 3*

In the STM used in the design example, additional vertical shear ties, element C and D, are placed between the column and the inner load points, as shown in Figure 3.6 (a). In order to identify the effects of these additional ties, STM without element C and D are selected (shown in Figure 3.6 (b)). For STMs denoted by Type 1 and Type 2, respectively, the truss analyses at the ULS loads were conducted to identify the member forces acting on the vertical tie elements, shown in Table 3.4.

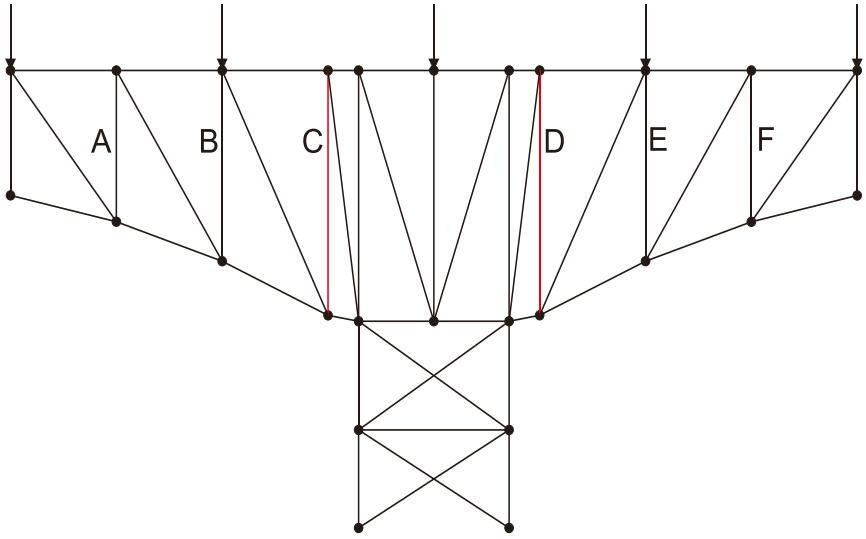


(a)

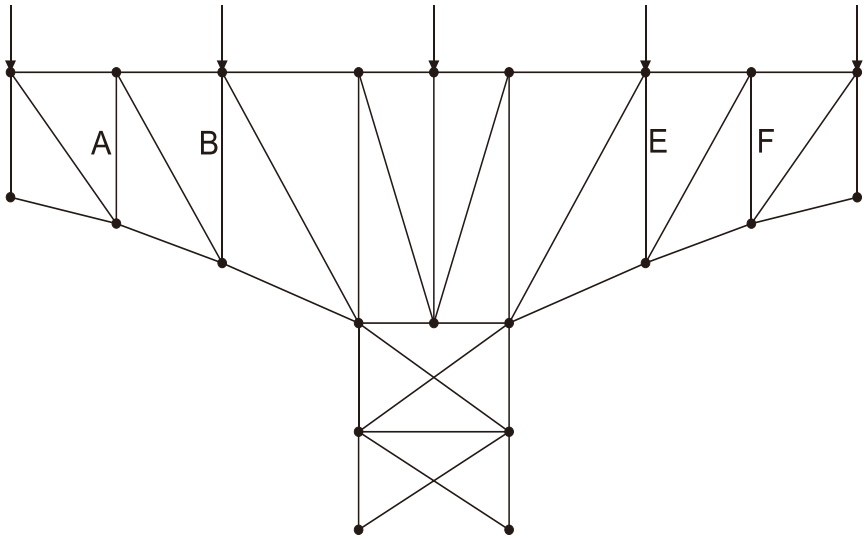


(b)

Figure 3.6 Type of STM applied with different vertical shear tie arrangement and corresponding elements (Bridge number 3): (a) Type 1: Existing STM; (b) Type 2: STM with additional ties at the location of inner load point

Table 3.4 Forces of vertical ties with various disposition (Bridge number 3)

| Element / Type of STM | A | B | C | D | E | F |
|---|---|---|---|---|---|---|
| | Forces of vertical ties (kN) | | | | | |
| Type 1 | 3,683 | 2,154 | **8,452** | **8,776** | 2,371 | 4,049 |
| Type 2 | 3,683 | 2,550 | - | - | 2,801 | 4,049 |

Table 3.5 Required vertical shear rebar ratio (Bridge number 3)

| Type | $\phi_s$ | $n$ | $A_{st}$ ($mm^2$) | $f_{vy}$ (MPa) | $b_w$ (mm) | $F_u$ (kN) | $w_{eff}$ (mm) | $s_{req}$ (mm) | $\rho_{v,\,req}$ (%) |
|---|---|---|---|---|---|---|---|---|---|
| 1 | 0.90 | 6 | 794.2 | 400 | 2,500 | 8,776 | 790 | 154 | 1.24 |
| 2 | | | | | | 4,049 | 1,225 | 519 | 0.37 |

The required vertical shear reinforcement ratios of STMs calculated with Equation 3.1 and Equation 3.2 at the given member forces of vertical shear ties are shown in Table 3.5.

If unnecessary vertical ties are placed between the column and the inner load points like Type 1, the vertical tie will have a large member force and the maximum effective width which the vertical tie covers will also be reduced, resulting in a large vertical shear reinforcement ratio. If vertical ties are not placed, such as Type 2, the required rebar ratio is reduced by about a third compared to Type 1.

*3.3.2.2 Bridge number 5*

In the STM used in the actual design, no vertical shear ties were placed in the area expected to be the shear critical section between the column and the inner load points, as shown in Figure 3.7 (a). To identify the effect of additional vertical ties on reinforcement ratio, STM expressed in Type 2, 3 and 4 were selected as follows. For each STM, a truss analysis was performed at the ULS load and the resulting member force acting on the vertical tie element is shown in Table 3.6.

In Type 2, where additional vertical shear ties B and G are placed at the inner loading point, the member forces act on the additional vertical shear ties as shown in Table 3.6, but there is no change in the magnitude of maximum member forces in vertical ties.

In Type 3, where the addition of vertical shear ties B and G at the location of the inner loading point and the addition of vertical shear ties D and E at the location of the column occur, there is also no change in the magnitude of maximum member forces because the loads do not transfer to the vertical ties D and E.

In Type 4, where the additional vertical shear ties C and F are placed in the center of the area between the outer part of the column and the inner loading point, the load transfer path changed, resulting in a large member force for the ties C and F of about 7,000 kN. Same as bridge number 3, placing unnecessary vertical ties between the column and the inner loading points in bridge number 5 also causes excessive reinforcement in the STM design.

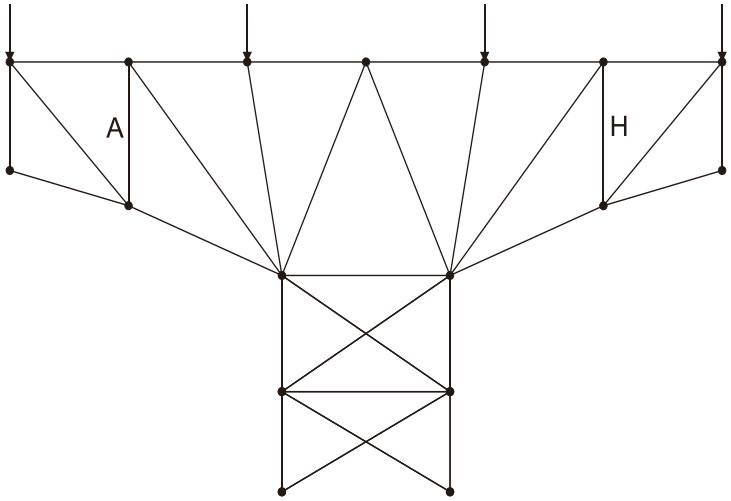


(a)

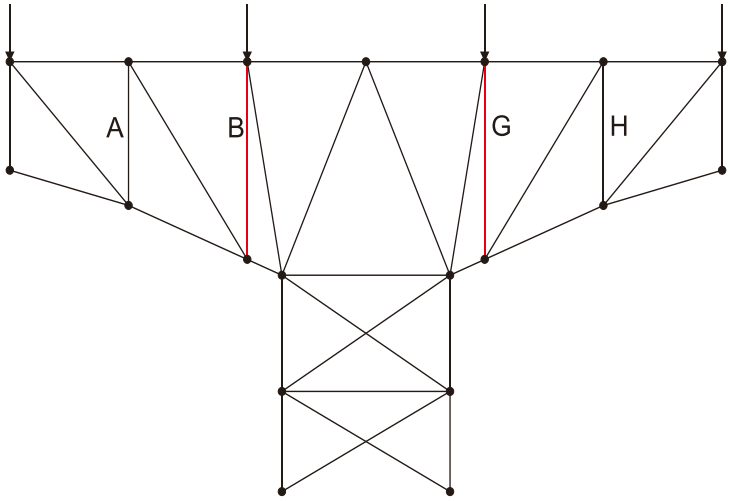


(b)

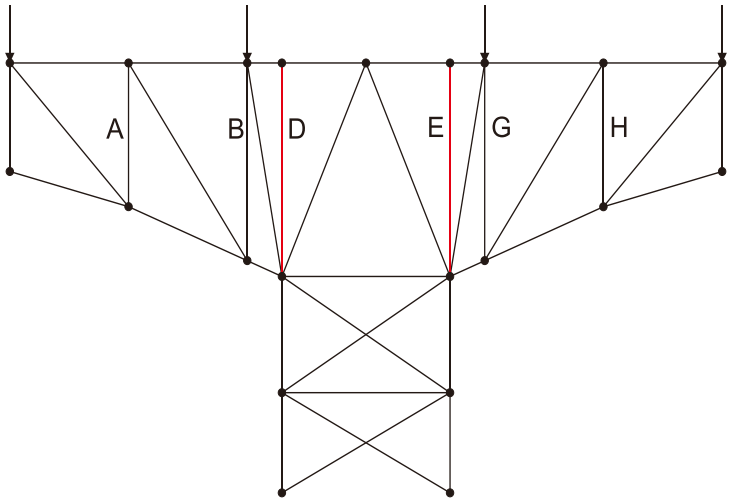


(c)

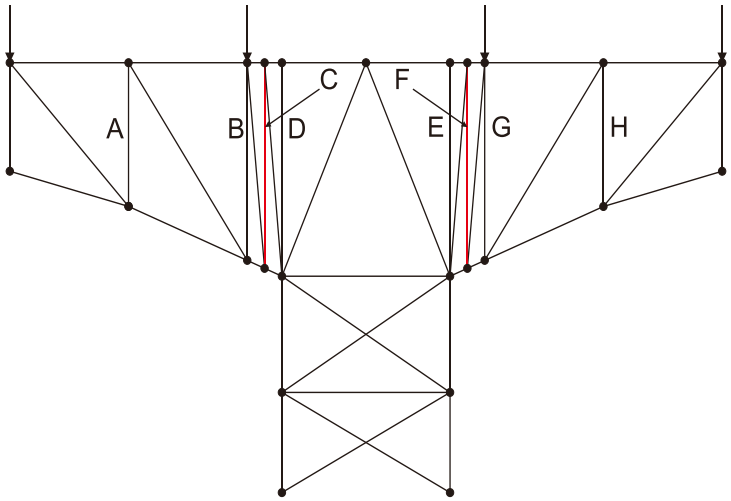


(d)

Figure 3.7 Type of STM applied with different vertical shear tie arrangement and corresponding elements (Bridge number 5): (a) Type 1: Existing STM; (b) Type 2: STM with additional ties at the location of inner load point; (c) Type 3: STM with additional ties at the location of column; (d) Type 4: STM with ties between location of inner load point and column

Table 3.6 Forces of vertical ties with various disposition (Bridge number 5)

| Element / Type of STM | A | B | C | D | E | F | G | H |
|---|---|---|---|---|---|---|---|---|
| | Forces of vertical ties (kN) | | | | | | | |
| Type 1 | 3,206 | - | - | - | - | - | - | 3,124 |
| Type 2 | 3,209 | 2,311 | - | - | - | - | 2,250 | 3,128 |
| Type 3 | 3,209 | 2,311 | - | 0 | 0 | - | 2,250 | 3,128 |
| Type 4 | 3,209 | 2,282 | **7,370** | 0 | 0 | **7,271** | 2,222 | 3,128 |

Table 3.7 Required vertical shear rebar ratio (Bridge number 5)

| Type | $\phi_s$ | $n$ | $A_{st}$ ($mm^2$) | $f_{vy}$ (MPa) | $b_w$ (mm) | $F_u$ (kN) | $w_{eff}$ (mm) | $s_{req}$ (mm) | $\rho_{v,\,req}$ (%) |
|---|---|---|---|---|---|---|---|---|---|
| 1 | 0.90 | 6 | 387.1 | 400 | 3,000 | 3,206 | 1,600 | 417 | 0.19 |
| 2 | | | | | | 3,209 | 1,600 | 417 | 0.19 |
| 3 | | | | | | 3,209 | 1,600 | 417 | 0.19 |
| 4 | | | | | | 7,370 | 800 | 91 | 0.85 |

The required vertical shear reinforcement ratios in STMs with the member forces of given vertical shear ties are shown in Table 3.7.

If unnecessary vertical ties are placed between the column and the inner loading points, such as Type 4, the additional vertical tie will have a large member force and the maximum effective width of the vertical tie will also be reduced, resulting in a large vertical shear reinforcement ratio. Unnecessary vertical ties placed in STM design of Type 4 lead to excessive design of shear

reinforcement, with the vertical shear rebar ratio increased by about 4.5 times compared to Type 1.

Through the contemplation of the rebar ratio with various vertical shear tie arrangement in STMs for the design cases of bridge pier caps, it is confirmed that unnecessary vertical tie arrangement can result in excessive shear reinforcement. Therefore, it is necessary to avoid unnecessary vertical ties in order to reasonably assign shear rebars in the STM design of pier caps.

### 3.3.3. Vertical-Tie-Arrangement in Design Examples

In the strut-and-tie model of pier caps, it was confirmed that unnecessary vertical ties between the column and the inner load points considered as a shear critical section cause excessive design of shear reinforcement. The bridge pier caps with large shear reinforcement shown in Figure 3.1 spring from the unnecessary vertical shear ties in the STM. To verify this, the layouts of STM in design examples of pier caps are shown in the following Figure 3.8.

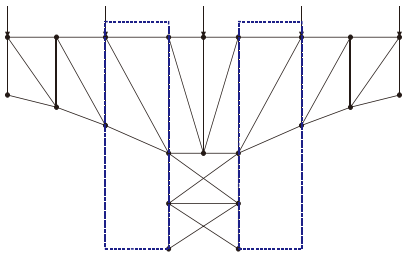

(a)

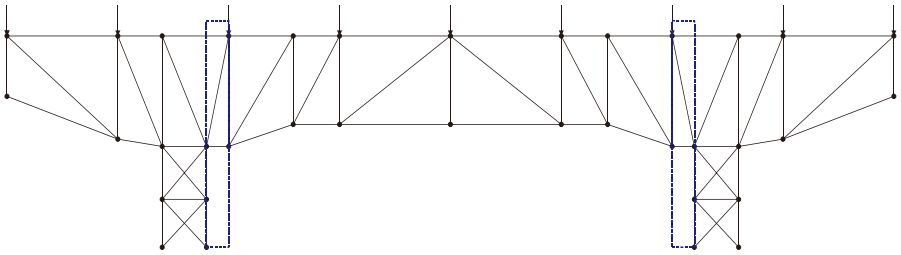

(b)

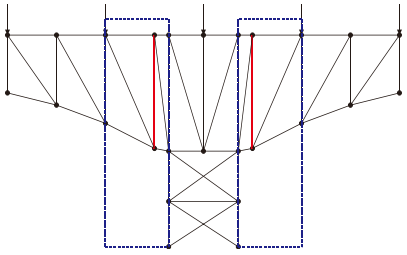

(c)

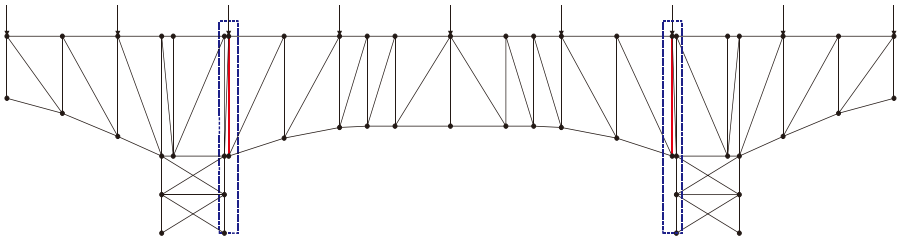

(d)

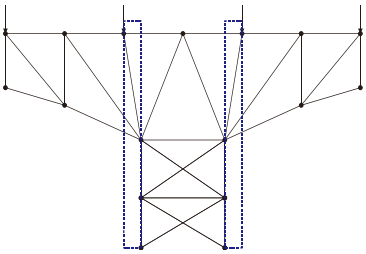

(e)

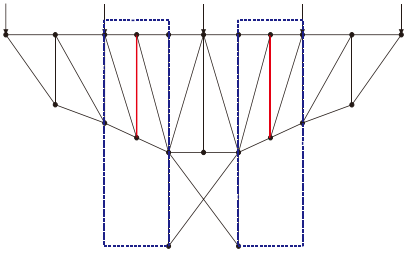

(f)

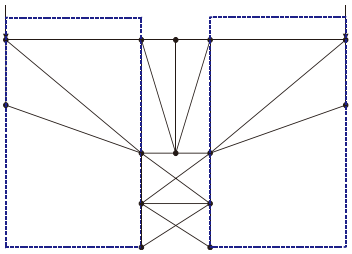

(g)

Figure 3.8 Elements of STM applied in the bridge pier cap designs: (a) Bridge number 1; (b) Bridge number 2; (c) Bridge number 3; (d) Bridge number 4; (e) Bridge number 5; (f) Bridge number 6; (g) Bridge number 7

As shown in Figure 3.7, bridge number 3, 4, and 6 with relatively excessive shear reinforcement placed the vertical shear ties in the areas between the column and the inner load points, marked with dashed lines, considered to be shear critical sections. In that, it is an inefficient design case in which shear rebars are over-reinforced due to the deployment of unnecessary vertical ties.

As shown in Figure 3.9, the shear critical sections of the pier caps generally occur in the area adjacent to the column. Due to these distributions of shear stresses, some designs place vertical shear ties at shear critical section, but these tie arrangements are a cause of over-reinforcement of vertical shear rebars. Thus, it is necessary to select STMs reasonably for efficient rebar designs.

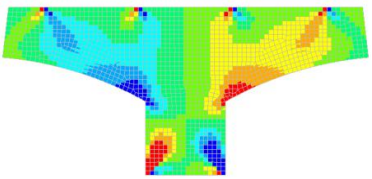

(a)

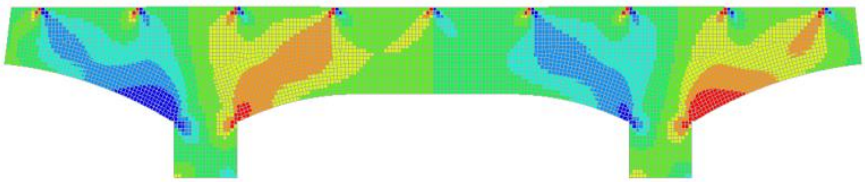

(b)

Figure 3.9 Examples of shear stress distribution of bridge pier caps: (a) T-type pier cap; (b) π-type pier cap

### 3.3.4. Forces in STM with Various STM Configurations

In addition to the placement of vertical shear ties, generally determined at the discretion of the designer, details of the STM arrangement, such as the distance from the top and bottom of the structure to the tensile ties and compression struts, and the width of the column compression struts, are determined at the discretion of the designer. In order to understand the change in member forces of the truss models with these detailed STM layout, the following is considered for more efficient STM layout, using bridge number 5 as an example.

*3.3.4.1 Disposition of tensile tie and strut considering stress distribution*

In the STM model, tensile ties are placed where flexural rebars are arranged in the member because only rebar is assumed to play all the roles of tension. In the STM of bridge number 5, the tensile ties are placed 125 mm from the upper end of the section.

The compressive strut at the bottom is located considering the distribution of sectional stress based on the elastic analysis of the pier cap. Figure 3.10 shows the distribution of the compressive stress on a section at center of the pier cap. The compressive struts are located at the position of line of action for the distribution of the stress. For bridge number 5, the compressive struts shall be located at the location 570mm above from the bottom of the section.

In the existing STM design of bridge number 5, tensile ties were placed at the position of arranged rebars, but the compressive struts were placed at 410mm above from the bottom of the section. In other words, the compressive

struts at the bottom are located 160mm lower than the STM design based on the stress distribution.

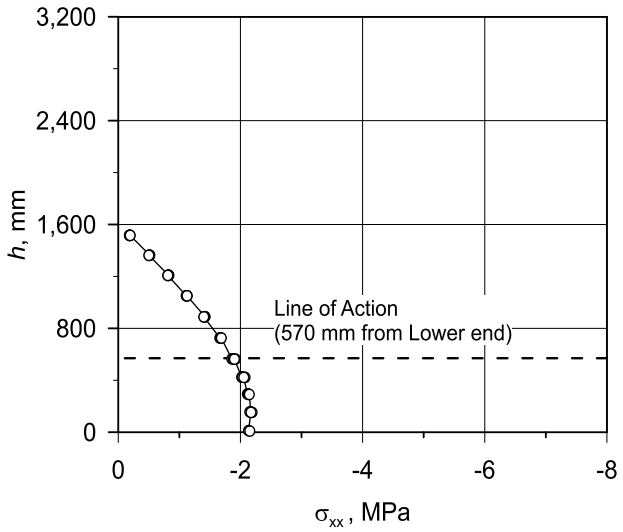


Figure 3.10 Compressive stress distribution at center of bridge number 5

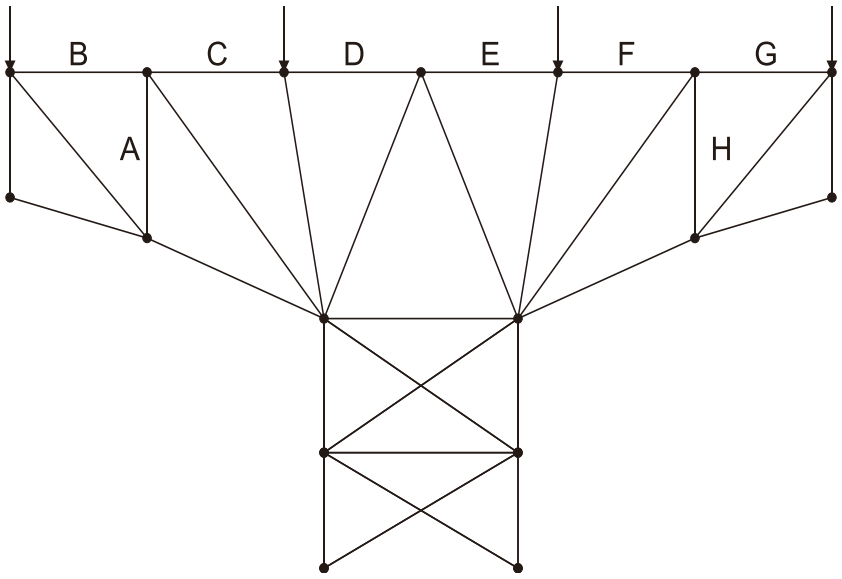


Figure 3.11 Element designation of bridge number 5

The truss model of STM, which positioned the upper tie and bottom struts considering the line of action of stress distribution in the pier cap, was analyzed. The analysis results of the member force acting on the vertical ties are shown in Table 3.8. Each element is designated in Figure 3.11.

The forces of the member acting on the vertical ties were reduced about 6% by positioning the compression struts at the location of the net compressive force acting in the elastic stress distribution.

Table 3.8 Vertical tie's force in STM considering section stress of pier cap

| Element / Type of STM | A | H |
|---|---|---|
| | Force of vertical ties (kN) | |
| Existing STM | 3,205 | 3,124 |
| Redesigned STM considering section stress | 3,017 | 2,941 |
| Ratio (%) | 94% | 94% |

Table 3.9 Tension tie's force in STM considering section stress of pier cap

| Element / Type of STM | B | C | D | E | F | G |
|---|---|---|---|---|---|---|
| | Force of tension ties (kN) | | | | | |
| Existing STM | 4,584 | 7,070 | 8,003 | 7,810 | 6,884 | 4,460 |
| Redesigned STM considering section stress | 5,030 | 7,519 | 8,511 | 8,305 | 7,321 | 4,894 |
| Ratio (%) | 110% | 106% | 106% | 106% | 106% | 110% |

Meanwhile, the member forces acting on the tensile ties tended to increase as shown in Table 3.9, increasing the maximum member force which determines the amount of flexural reinforcement by about 6%. Reducing the distance between the upper tensile tie and the lower horizontal compression strut makes the moment arm decrease, and the member forces acting on the top and bottom of the STM elements shall be increase to resist the same moment.

It is recommended that the pier cap is designed to reduce the amount of shear reinforcement where interference with the column reinforcement occurs significantly, by reducing the member force acting on the vertical tie with the STM arrangement corresponding to the elastic stress distribution.

*3.3.4.2 Forces in accordance with position of column strut*

Stress distribution of the cross section of the column in contact with the pier cap is shown in Figure 3.12. In the existing STM design, the compressive struts of the column were placed 216 mm from the column cover, without positioning them at the line of action of the stress distribution. The location of column strut is adjusted to 500 mm away from the cover corresponding to the stress distribution.

Truss analysis of the STM reflecting stress distribution of the column was performed, and the results were compared to those of existing STM. The member forces for vertical ties are compared in Table 3.10, and the member forces for tensile ties are shown in Table 3.11.

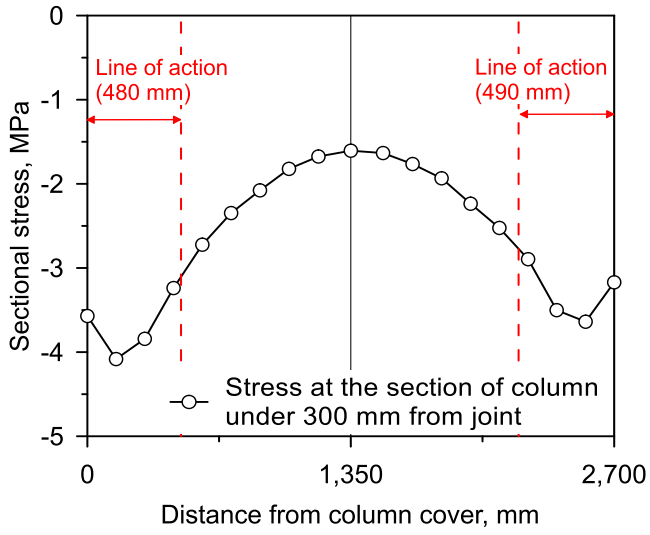


Figure 3.12 Compressive stress distribution at column section of bridge number 5

Table 3.10 Vertical tie's force in STM considering section stress of column

| Element / Type of STM | A | H |
|---|---|---|
| | Force of vertical ties (kN) | |
| Existing STM | 3,205 | 3,124 |
| Redesigned STM considering section stress | 2,899 | 2,826 |
| Ratio (%) | 90% | 90% |

Table 3.11 Tension tie's force in STM considering section stress of column

| Element / Type of STM | B | C | D | E | F | G |
|---|---|---|---|---|---|---|
| | Force of tension ties (kN) | | | | | |
| Existing STM | 4,584 | 7,070 | 8,003 | 7,810 | 6,884 | 4,460 |
| Redesigned STM considering section stress | 4,988 | 7,288 | 8,721 | 8,518 | 7,096 | 4,853 |
| Ratio (%) | 109% | 103% | 109% | 109% | 103% | 109% |

As the width of the column struts was narrowed, the diagonal struts in the pier cap were laid out more horizontally. And the force of the tensile tie was increased by about 9% to meet the equilibrium, and the member force of the vertical tie decreased by about 10%. From the results, it is confirmed that setting the width of the column to fit in the stress distribution of the column requires less vertical shear reinforcement.

## 3.4. Proposal of STM Design Guidelines for Pier Caps with Efficient Reinforcement Arrangements

Through the analyses on the design status of strut-and-tie model and the amount of shear reinforcement with STM layout of bridge pier caps, the following STM design guidelines for pier caps with efficient reinforcement arrangement were proposed.

1. Avoid vertical ties between column and adjacent load point to prevent excessive design of vertical shear reinforcement.

2. Reinforcement required in STM is structurally enough because STM design is kind of lower-bound solution.

3. It is enough for horizontal shear rebar to follow the rules of minimum distributed rebar mesh in deep components.

4. Design the strut-and-tie model of pier caps considering the elastic stress distribution.

The STM design of pier caps, based on the analyses in 3.3.2 and 3.3.3, shall prevent the over-reinforcement of vertical shear rebar by not placing additional vertical shear ties at the location of shear critical section, an area adjacent to the column.

STM-based design is a lower-bound solution as mentioned in 2.2.3 and produces conservative design results when properly designed. However, many of pier cap designs are unnecessarily conservative with more reinforcement

than required in STM. It is not necessary to assign excessive amount of rebars than the required amount in STM.

Horizontal shear reinforcement is not considered in the typical STM designs of pier cap. In other words, there is no need to include horizontal shear reinforcement in truss behavior and in tied-arch behavior. However, as discussed in 3.2, the amount of horizontal shear reinforcement is similar with that of vertical shear reinforcement without any basis. This may result in more horizontal shear reinforcement than is required. Therefore, as shown in 2.3.3.2, excessive placement of horizontal shear reinforcement might be mitigated by just following the minimum mesh rules required for serviceability in deep beams.

When forming a strut-and-tie model, it is recommended that each element be positioned according to the stress distribution acting on the member. The analyses in 3.3.4 confirmed a slight increase in the amount of vertical shear reinforcement when the distances between the bottom strut and upper ties and between the column strut and the column cover are not correspond to the line of action in the stress distributions.

# IV. Experimental Verification

## 4.1. Introduction

Through a discussion and analysis on the design of strut-and-tie models of pier caps, the STM design guidelines for pier caps with more efficient reinforcement were proposed. To ensure the validity of the proposed design guidelines, an evaluation of structural safety and serviceability of bridge pier caps designed based on the guidelines is required. To this end, a scaled model test was conducted to simulate the structural behavior of the bridge pier caps designed with the proposed design guidelines as load increases.

This chapter covered the details of a scaled model test of highway bridge pier caps. Scaled model test is generally performed to simulate the structural behavior of a real structure where assessment limitations exist. This study tried to eliminate the size effects as much as possible by testing with specimens of a similar size to the size of real structures. Accordingly, the test was carried out using a strong wall and floor system and static hydraulic actuators at the Hybrid Structural Testing Center. In addition to evaluating the structural safety and serviceability of the proposed design guidelines, identifying the effect of horizontal shear rebar and loading positions on the behavior of the structure is also needed. To achieve these goals, a total of three cases of scaled models for the T-type pier caps was constructed. This chapter describes target structures, scale factor, specimens, material properties, fabrication, test load, equipment, measurement, and test procedures. In addition, the evaluation was performed by measuring deflections, cracks, and rebars and concrete strains.

## 4.2. Test Program

### 4.2.1. Target Structure

Korean highway bridge pier caps were selected as the target structures for the experiment. In order to determine the effect of loading position (the number of support bearing) on the behavior of the pier cap, bridge number 5 under 4-point load and bridge number 7 under 2-point load, with similar specifications, were selected as target structures. The dimensions of the selected target structures are shown in Figure 4.1 and Figure 4.2. In general, 2 to 5 support bearings are used in the T-type highway bridge pier caps depending on the superstructure. The equivalent load shall be applied at each loading position in order to simulate the load from the superstructure. Accordingly, the pier caps under 5-point load were excluded from the target structure, considering the constraints of hydraulic actuators, dimension of specimens and frames, and capacity of the equipment.

The existing STM designs for the target structures are relatively efficient designs designed without unnecessary vertical tie arrangement. Details of rebars in existing designs are shown in Table 4.1 as Case A and Case B. According to the proposed STM design guidelines of bridge pier cap, three experimental cases were selected by redesigning bridge number 5 and 7. Case 1 and Case 2 are designed satisfying the design guidelines. Horizontal shear reinforcement in Case 1 was only assigned as much as necessary for the fabrication by excluding the effects of horizontal shear reinforcement as possible. Case 2 is based on 0.2% horizontal shear reinforcement in the

minimum distributed mesh rule of deep beams provided by KHBDC (2015). Case 3 is the design of bridge number 7 according to the guidelines. The required reinforcement ratio in STM for each member is given in Appendix A.

Table 4.1 Reinforcement detail of experimental cases

| Case | Rebar ratio (%) | | | Note |
|---|---|---|---|---|
| | $\rho$ | $\rho_v$ | $\rho_h$ | |
| A | 0.28 | 0.31 | 0.23 | Existing reinforcement detail of bridge # 5 (4-point load) |
| B | 0.76 | 0.34 | 0.26 | Existing reinforcement detail of bridge # 7 (2-point load) |
| 1 | 0.26 | 0.19 | 0.06 | Satisfying proposed STM design guidelines for bridge # 5 (No horizontal shear reinforcement) |
| 2 | 0.26 | 0.20 | 0.20 | Satisfying proposed STM design guidelines for bridge # 5 (Minimum horizontal shear rebar for serviceability) |
| 3 | 0.67 | 0.32 | 0.20 | Satisfying proposed STM design guidelines for bridge # 7 (Minimum horizontal shear rebar for serviceability) |

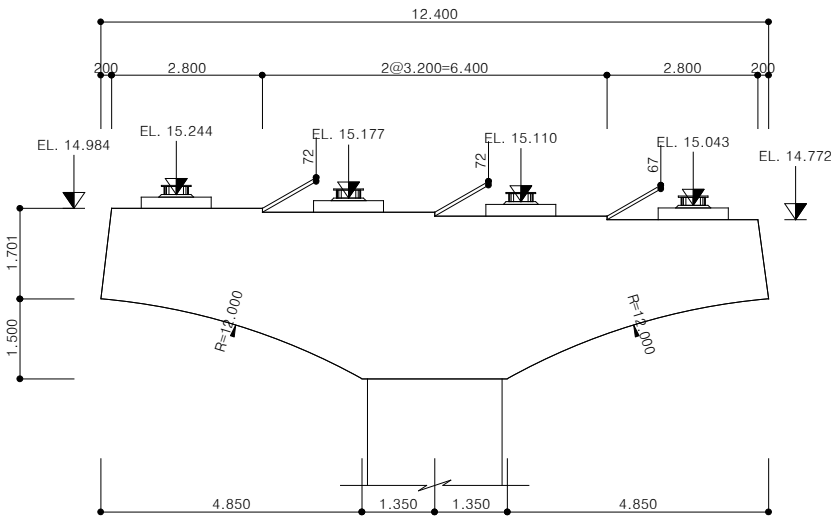


(a)

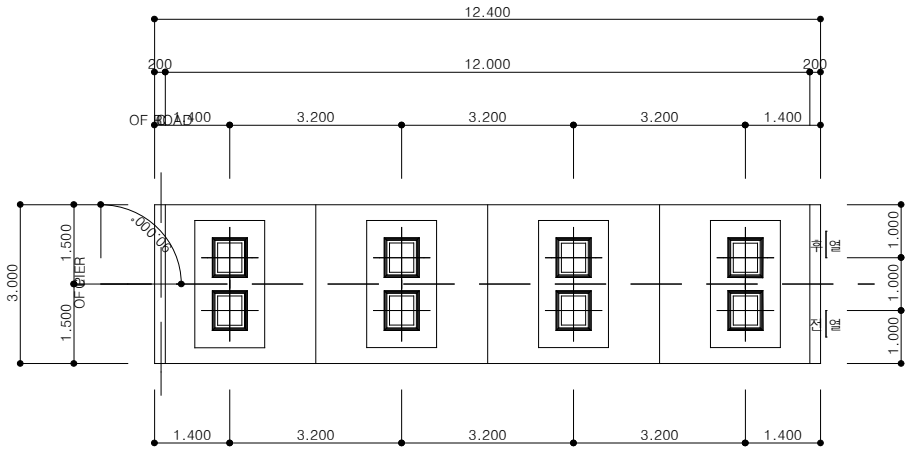


(b)

Figure 4.1 Design drawing of bridge number 5: (a) A front view; (b) A plane view

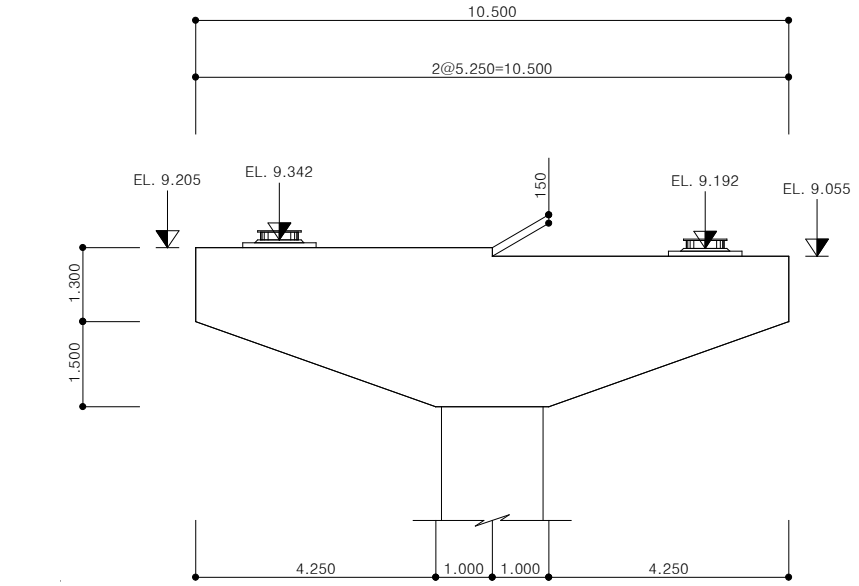


(a)

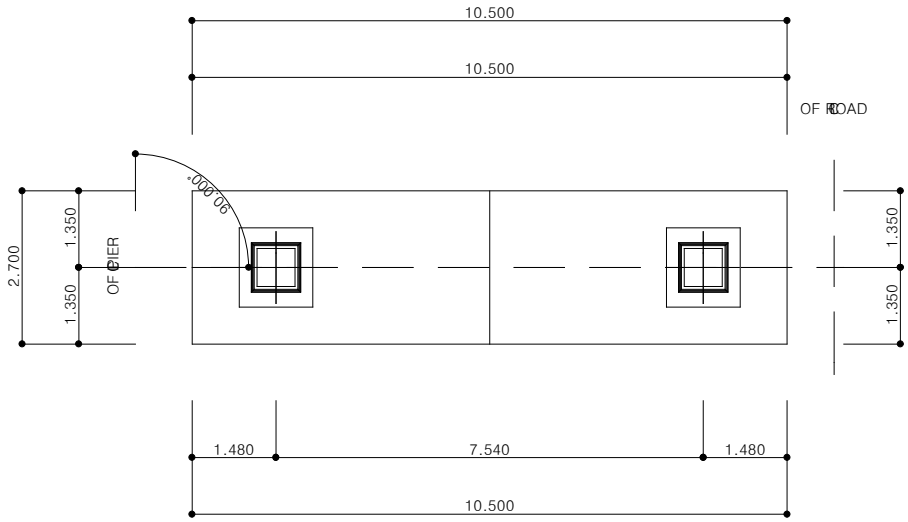


(b)

Figure 4.2 Design drawing of bridge number 7: (a) A front view; (b) A plane view

### 4.2.2. Model-to-prototype Scale

Due to the constraints of experimental facilities in Korea, there are considerable difficulties in the test of real-size bridge pier caps. This requires scaled model tests of the target structures in order to conduct a static loading test. The target structure was scaled down to be as large as possible with the scale factor of length so that to exclude as much as possible the size effect. Applying similitude law to the target structure, the specifications of the test specimens, the rebar cross section and the volume, total load size, and the position of loading were established. The scale factor of length was derived taking the following limitations into account:

1. Ease of on-site fabrication of specimens and transportability at test facility
2. Suitability with rebar products and down-scaled rebar dimensions
3. Size and capacity of load and hydraulic equipment acting on specimens
4. Constraints of experimental facility

The maximum total loads of the prototypes were expected through a commercial nonlinear finite element analysis program (DIANA), and the maximum total loads of three experimental cases of scaled models were obtained with scale factor of length. Those are presented in Table 4.2.

Table 4.2 Expected load resistance capacities of scaled models

| Scale | Case | Total load (kN) | Load for support (kN) | | | |
|---|---|---|---|---|---|---|
| | | | Outer left | Inner left | Inner right | Outer right |
| Prototype | 1 | 41,552 | 10,388 | 10,388 | 10,388 | 10,388 |
| | 2 | 45,600 | 11,400 | 11,400 | 11,400 | 11,400 |
| | 3 | 35,872 | 17,936 | | 17,936 | |
| 50% | 1 | 10,388 | 2,597 | 2,597 | 2,597 | 2,597 |
| | 2 | 11,400 | 2,850 | 2,850 | 2,850 | 2,850 |
| | 3 | 8,968 | 4,484 | | 4,484 | |
| 45% | 1 | 8,416 | 2,104 | 2,104 | 2,104 | 2,104 |
| | 2 | 9,236 | 2,309 | 2,309 | 2,309 | 2,309 |
| | 3 | 7,264 | 3,632 | | 3,632 | |
| 40% | 1 | 6,648 | 1,662 | 1,662 | 1,662 | 1,662 |
| | 2 | 7,296 | 1,824 | 1,824 | 1,824 | 1,824 |
| | 3 | 5,740 | 2,870 | | 2,870 | |

The number of hydraulic actuators that can be installed in the cross beam of frames is up to three, considering the specifications of the cross beam and the hydraulic actuators. In these limitations, for 4-point loads, as shown in Case 1 and Case 2, the loads acting on the both inner sides shall be applied to one hydraulic actuator. Since the maximum capacity of the hydraulic actuator is 5,000 kN, it is not possible to apply 50% of the scale factor. Also, 45% of the scale factor is not applicable due to the maximum capacity of the cross beam of 8,000 kN.

Table 4.3 Spacing between actuators for scaled models

| Scale | Case | Length of pier cap (mm) | Space of support (mm) | Space of actuator (mm) | Minimum space (mm) | Satisfaction |
|---|---|---|---|---|---|---|
| 50% | 1, 2 | 6,200 | 1,625 | 2,437 | 1,500 | Satisfied |
| | 3 | 5,250 | 3,770 | 3,770 | | Satisfied |
| 45% | 1, 2 | 5,580 | 1,462 | 2,193 | | Satisfied |
| | 3 | 4,725 | 3,393 | 3,393 | | Satisfied |
| 40% | 1, 2 | 4,960 | 1,300 | 1,950 | | Satisfied |
| | 3 | 4,200 | 3,016 | 3,016 | | Satisfied |

The width of the 5,000 kN hydraulic actuator is 900 mm and the minimum distance between the hydraulic actuators to prevent interference between them is 1,500 mm. Therefore, when installing the hydraulic actuators, it shall be determined whether proper distances between the hydraulic actuators are secured as shown in Table 4.3.

Depending on the capacity and specifications of the test equipment, the maximum scale factor of length, 2/5, was applied to the scaled models.

### 4.2.3. Dimension of Specimens

Applying the scale factor of 2/5, the specifications of the scaled model on the target structures shown in Figure 4.1 and Figure 4.2 are shown in Figure 4.3 and Figure 4.4. It is assumed that there is no elevation in the top of pier caps for ease of test. In addition, only part of the total length of the column was simulated, considering the height of the specimens and the hydraulic actuator. The specifications of each component of the specimens in test cases are summarized in Table 4.4. A total weight per specimen, including the pier cap, the column, and the basement, is up to approximately 25 Ton.

Table 4.4 Properties of member's dimension for experimental cases

| Class | Case | Dimension (m) | | | Volume ($m^3$) | Weight (Ton) |
|---|---|---|---|---|---|---|
| | | Length | Width | Depth | | |
| Pier cap | 1 | 4.96 | 1.20 | 1.20 | 5.57 | 13.93 |
| | 2 | | | | | |
| | 3 | 4.20 | 1.08 | 1.06 | 3.71 | 9.28 |
| Column | 1 | 1.00 (Diameter) | | 0.80 | 0.63 | 1.58 |
| | 2 | | | | | |
| | 3 | 0.72 (Diameter) | | 0.80 | 0.33 | 0.83 |
| Basement | 1 | 2.00 | 2.00 | 1.00 | 4.00 | 10.00 |
| | 2 | | | | | |
| | 3 | | | | | |

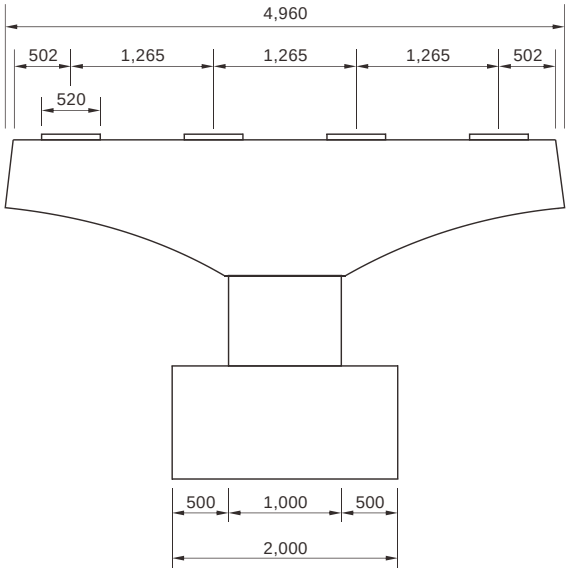


(a)

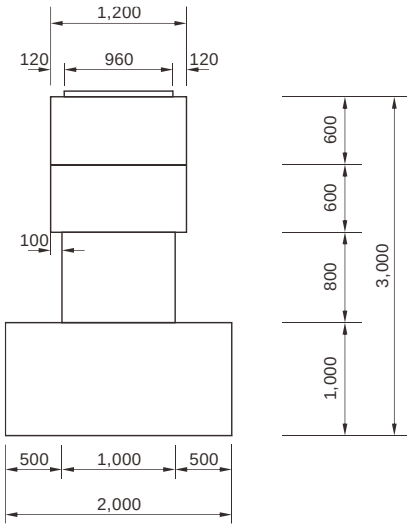


(b)

Figure 4.3 Design drawing of specimens for Case 1 and Case 2: (a) A front view; (b) A sectional view (unit: mm)

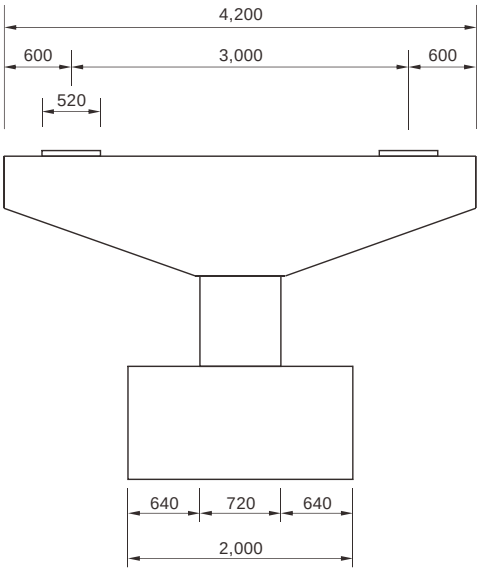


(a)

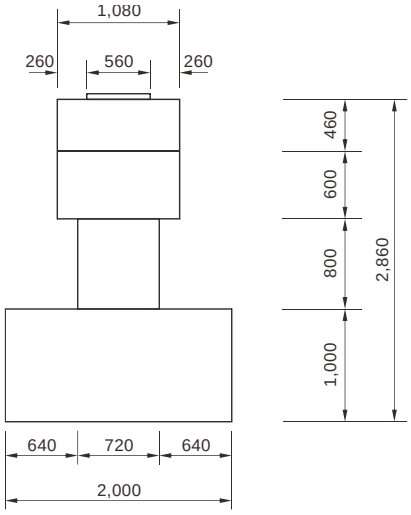


(b)

Figure 4.4 Design drawing of specimen for Case 3: (a) A front view; (b) A sectional view (unit: mm)

### 4.2.4. Material Properties

Table 4.5 Material properties of target structure

| Design strength (MPa) | | Pier cap | Column | Basement |
|---|---|---|---|---|
| Concrete | $f_c'$ | 40 | 40 | 27 |
| Longitudinal reinforcement | $f_y$ | 400 | 500 | 500 |
| Shear reinforcement | $f_{vy}$ | 400 | 400 | 400 |

The specified compressive strength of concrete and the specified yield strength of reinforcing steel bar used in the scaled models were set to have the material properties applied to the target structure. The design strength of each material in the target structure is as shown in Table 4.5. The specified compressive strength of concrete at the basement, not the member of interest, was increased to 40 MPa to prevent the basement from being failed during the test.

*4.2.4.1 Concrete*

The specimens were fabricated with the sequence of construction by step, in three stages: basement part, column part, and pier cap part, as in the stage of the general pier cap construction. Since the maximum capacity of a single concrete batch was 6 $m^3$, it was not possible to place basements or pier caps for all three cases with a single concrete batch. Therefore, the basements or the pier caps were inevitably placed using one concrete batch per case, and the concrete

mix proportion for each member was set to be same. The column was relatively small in volume, so the columns for all three cases were covered by a single batch of concrete. As shown in Table 4.6, a total of seven batches of concrete were used, using three types of concrete mix proportions. For all types of concrete mix proportions, a typical Type I Portland cement was used and the maximum aggregate size was 25mm. Target slump was 150mm and high-range water-reducer (HRWR) was used for the fluidity of concrete.

Concrete cylinders with a size of 150 x 300 mm for each batch were placed with the specimens in the same place to be cured on site in the same condition. The compressive strength test of three cylinders for each batch was performed using the Universal Testing Machine (UTM) in the Seoul National University, and the results were shown in Table 4.7. Elastic modulus was averaged by obtaining the secant elastic modulus at $0.4 f_{cu}$ in each cylinder.

Table 4.6 Concrete mix proportion of each batch for tests

| Batch | $f_c^{'}$ (MPa) | Unit weight (kg/m$^3$) | | | | | Note |
|---|---|---|---|---|---|---|---|
| | | Water | Cement | Fine aggregate | Coarse aggregate | Admixture | |
| 1 | 40 | 170 | 480 | 730 | 993 | 4.80 | Basement (Case 1) |
| 2 | | | | | | | Basement (Case 2) |
| 3 | | | | | | | Basement (Case 3) |
| 4 | 40 | 166 | 480 | 720 | 993 | 4.32 | Column (All Case) |
| 5 | 40 | 149 | 490 | 725 | 1,010 | 4.90 | Pier cap (Case 1) |
| 6 | | | | | | | Pier cap (Case 2) |
| 7 | | | | | | | Pier cap (Case 3) |

As a result of the compressive strength test, the average compressive strength of concrete on the pier cap was less than 40 MPa, the specified compressive strength. However, there is not much difference in the strength of the pier cap in each test case, and the results for that strength are available as conservative metrics for the structural safety assessment for the specified compressive strength, so it is not an issue for the performance evaluation of the specimens.

Figure 4.5 Setting of unconfined compression test of cylinder with UTM

Table 4.7 Unconfined compression test results for cylinder specimens

| Class | Case | $t$ (days) | $f_c^{'}$ (MPa) | $f_{cu}$ (MPa) | $E_c$ (MPa) |
|---|---|---|---|---|---|
| Pier cap | 1 | 41 | 40 | 35 | 25,542 |
| | 2 | 33 | 40 | 32 | 25,176 |
| | 3 | 41 | 40 | 36 | 24,991 |
| Basement | 1 | 55 | 40 | 54 | 34,679 |
| | 2 | 55 | 40 | 57 | 35,708 |
| | 3 | 55 | 40 | 57 | 36,117 |
| Column | all | 51 | 40 | 53 | 35,613 |

Details of the test results by cylinder of the compressive strength test are given in Appendix B. Since the 7-day compressive strength was obtained for the prediction of 28-day compressive strength, no strain measurement by Linear Variable Differential Transformer (LVDT) was performed, separately. There was no need to derive stress-strain curve and the secant elastic modulus at the 7-day compressive strength tests.

*4.2.4.2 Reinforcing steel bars*

The sectional areas of rebar in 2/5 scaled specimens are reduced to the square of the scale factor of length. However, since rebars are produced as standard products, rebar specifications with the most approximate values were used for the reduced sectional areas. Errors in the amount of rebars that appear due to the manufactured reinforcement were minimized by adjusting the spacing of rebar.

The standard products of rebar used in the test were three types of SD400 (D10, D13, D16) and one type of SD500 (D10). Uniaxial tension test of reinforcing steel bar was performed for all types of rebar specimens used in the fabrication. The test was carried out, as shown in Figure 4.6, using UTM at the Seoul National University. The test results of the specimens are summarized and presented in Table 4.8 and Figure 4.7. As a result of the test, all specimens have a yield strength exceeding their design yield strengths.

Table 4.8 Details of reinforcing bar properties

| Type | Diameter | $\varepsilon_y$ (x10$^{-3}$) | $f_y$ (MPa) | $\varepsilon_{sh}$ (x10$^{-3}$) | $\varepsilon_u$ (x10$^{-3}$) | $f_u$ (MPa) | $E_s$ (MPa) |
|---|---|---|---|---|---|---|---|
| SD400 | D10 | 4.16 | 436 | 34.29 | 188.46 | 548 | 200,000 |
| | D13 | 4.17 | 436 | 20.83 | 154.17 | 610 | 200,000 |
| | D16 | 4.14 | 425 | 15.24 | 132.69 | 620 | 200,000 |
| SD500 | D10 | 4.83 | 558 | 17.31 | 115.38 | 677 | 200,000 |


Figure 4.6 Setting of uniaxial tension test of deformed rebar with UTM

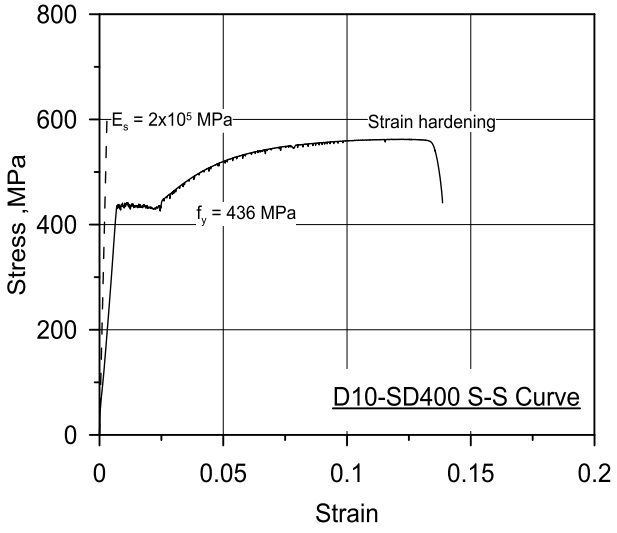
800
600
400
200
0
Stress ,MPa
$E_s$ = 2x10$^5$ MPa
Strain hardening
$f_y$ = 436 MPa
D10-SD400 S-S Curve
0
0.05
0.1
0.15
0.2
Strain

(a)

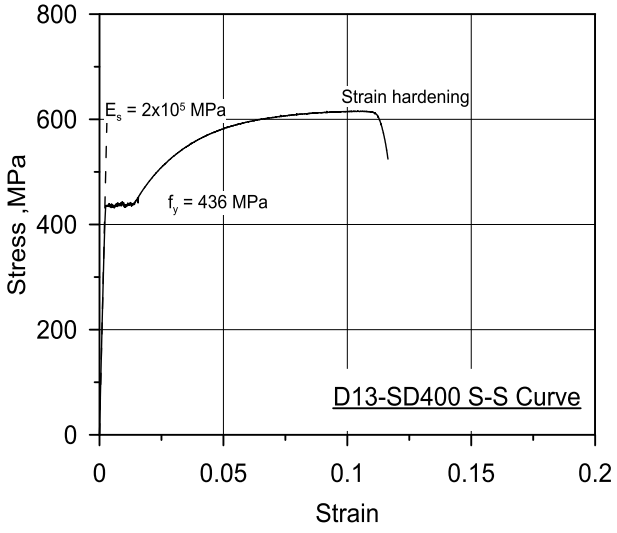
800
600
400
200
0
Stress ,MPa
$E_s$ = 2x10$^5$ MPa
Strain hardening
$f_y$ = 436 MPa
D13-SD400 S-S Curve
0
0.05
0.1
0.15
0.2
Strain

(b)

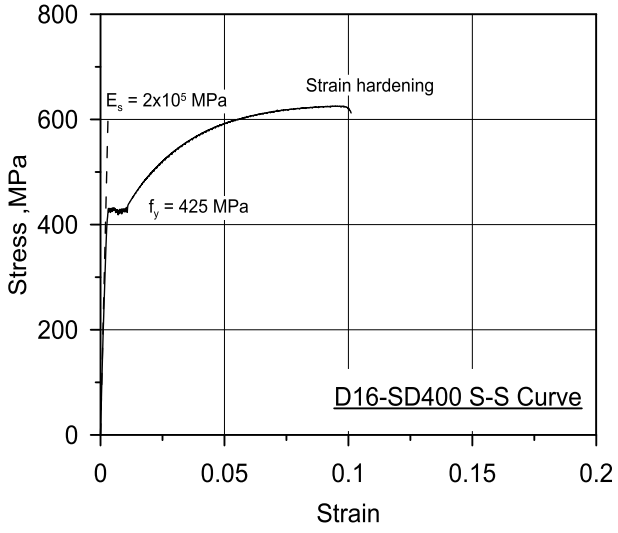


(c)

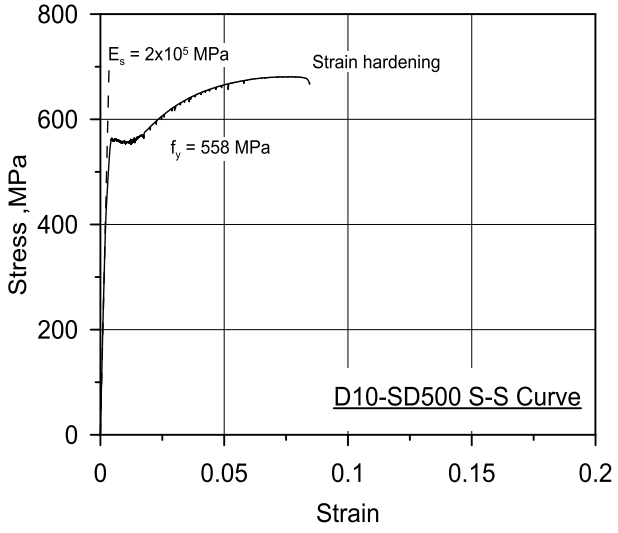


(d)

Figure 4.7 Stress-strain curve for deformed reinforcing steel bar: (a) D10-SD400; (b) D13-SD400; (c) D16-SD400; (d) D10-SD500

### 4.2.5. Manufacture of Specimens

Scaled-model specimens (total of 3) for the target structures were manufactured with rebar details designed according to the proposed STM design guidelines. The construction of the specimens was performed in three stages in accordance with the following sequence.

1. Rebar assembly of basements and columns and placement of basement
2. Concrete placement of columns
3. Rebar assembly and concrete placement of pier caps

In order to minimize damage to the gauge attached to rebars during concrete pouring, it was poured at the edges of the molds, and the use of vibrator for concrete compaction was also paid utmost attention.

*4.2.5.1 Reinforcement detail in specimens*

The specimens were constructed in a separate fabrication area with the details of the arrangement shown in Figure 4.8, Figure 4.9, and Figure 4.10. In Case 1 of Figure 4.8 (a), the horizontal shear reinforcement was not assigned through the width of pier cap, but only as much as is required for the assembly at each face of pier caps.

Under the current design of the bridge pier cap, the development length of the longitudinal reinforcement of the column is extended to the top of pier cap. In addition, in the current existing designs, the lateral ties in columns is also placed to the top of pier caps, causing inefficient designs due to interference

with the reinforcement of the column and the shear rebar in the pier caps. Park et al. (2013) verified that the development length of the column rebar does not significantly affect structural behaviors until ULS even if the minimum development length required in design codes for minimizing interference with the column rebar and shear reinforcement of the pier cap was used. In this study, for minimizing interference, the minimum amount of the development length of the longitudinal rebar and the lateral ties in the column was used. According to KDS 14 20 50:4.4.2 (3), the placement of the top end tie in the column is completed 40 mm below the compressive reinforcement in the pier cap. In addition, the longitudinal reinforcement of the column was positioned such that it would be end at 500 mm above from the position where the column and the pier cap would be in contact with each other to satisfy KDS 14 20 52: 4.1.2 (2). Details of the placement of these column rebars are given in Figure 4.8 and Figure 4.10.

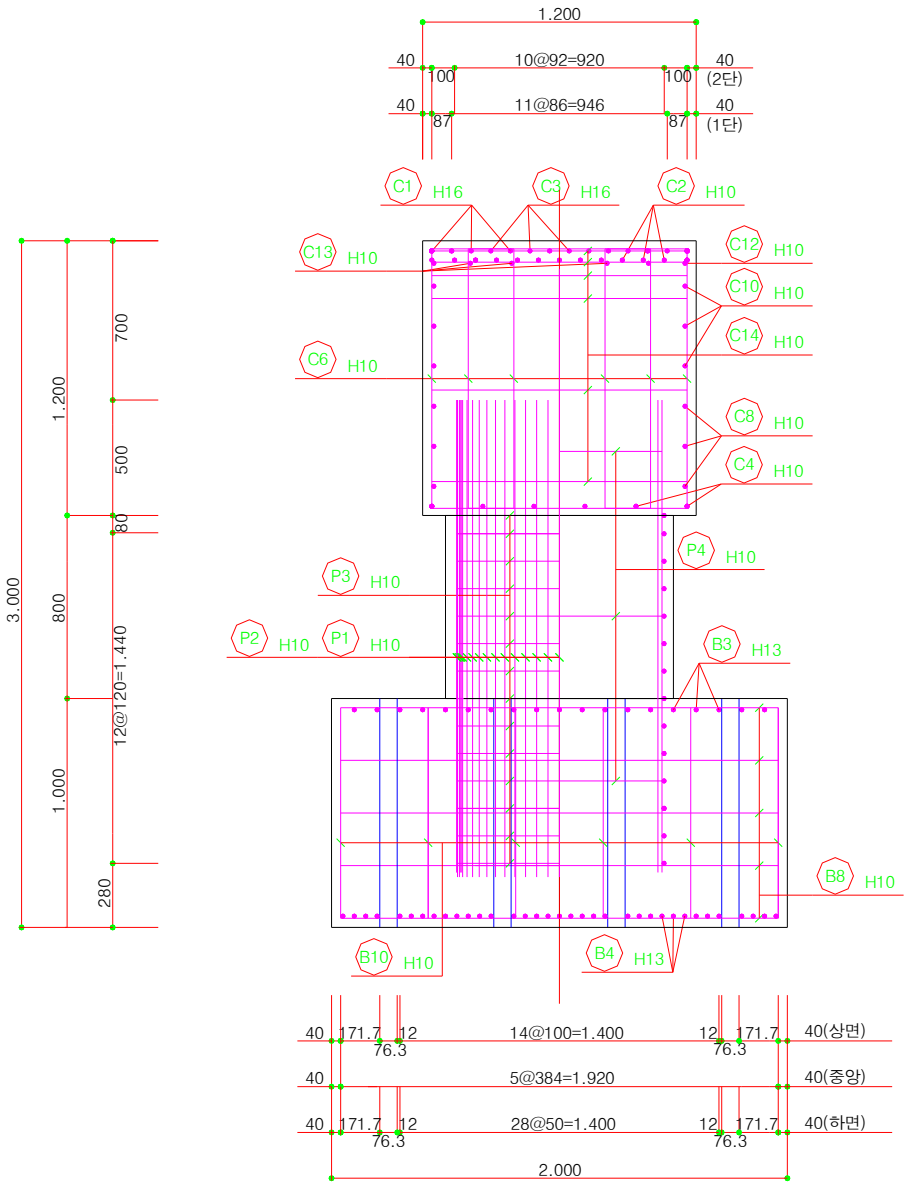
1.200
40
10@92=920
40
100
100
(2단)
40
11@86=946
40
87
87
(1단)
C1 H16
C3 H16
C2 H10
C13 H10
C12 H10
C10 H10
C14 H10
C6 H10
C8 H10
C4 H10
P4 H10
P3 H10
P2 H10
P1 H10
B3 H13
B8 H10
B10 H10
B4 H13
3.000
1.200
800
1.000
700
500
80
12@120=1.440
280
40 171.7 12 14@100=1.400 12 171.7 40(상면)
76.3
76.3
40 5@384=1.920 40(중앙)
40 171.7 12 28@50=1.400 12 171.7 40(하면)
76.3
76.3
2.000

(a)

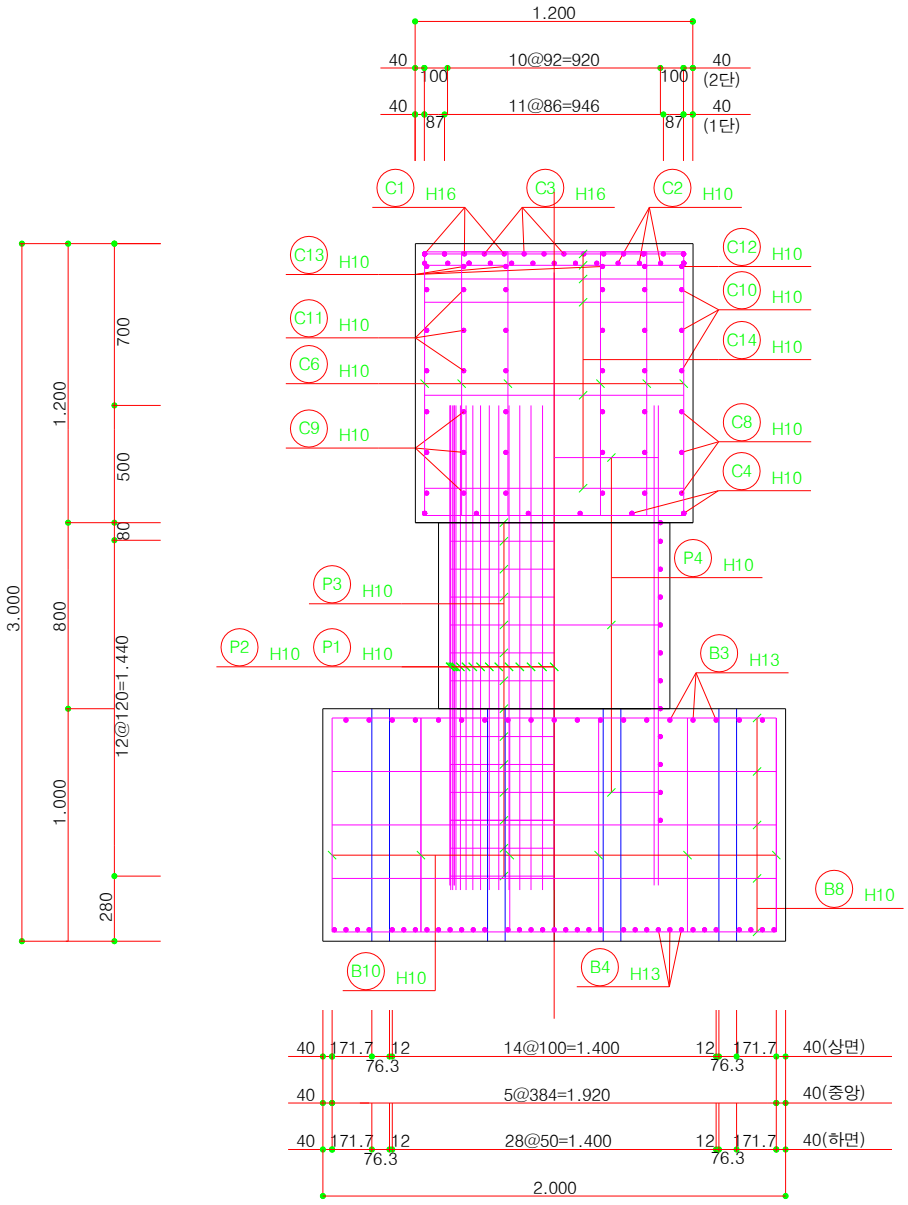
1.200
40
10@92=920
40
(2단)
100
100
40
11@86=946
40
(1단)
87
87
C1 H16
C3 H16
C2 H10
C13 H10
C12 H10
C10 H10
C11 H10
C14 H10
C6 H10
C9 H10
C8 H10
C4 H10
P4 H10
P3 H10
P2 H10
P1 H10
B3 H13
B8 H10
B10 H10
B4 H13
3.000
1.200
800
1.000
700
500
80
12@120=1.440
280
40 171.7 12
76.3
14@100=1.400
12 171.7 40(상면)
76.3
40
5@384=1.920
40(중앙)
40 171.7 12
76.3
28@50=1.400
12 171.7 40(하면)
76.3
2.000

(b)

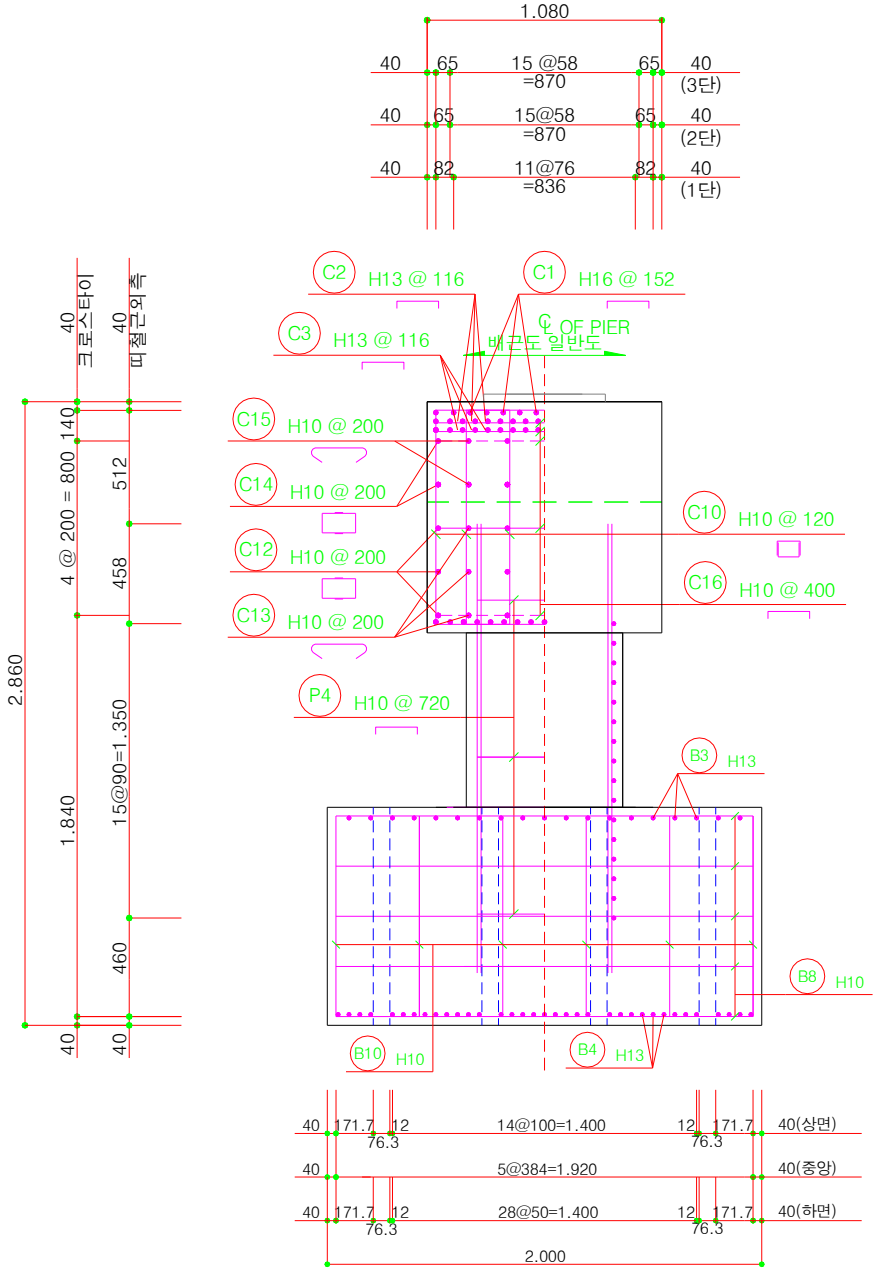


(c)

Figure 4.8 Sectional view of specimens: (a) Case 1; (b) Case 2; (c) Case 3

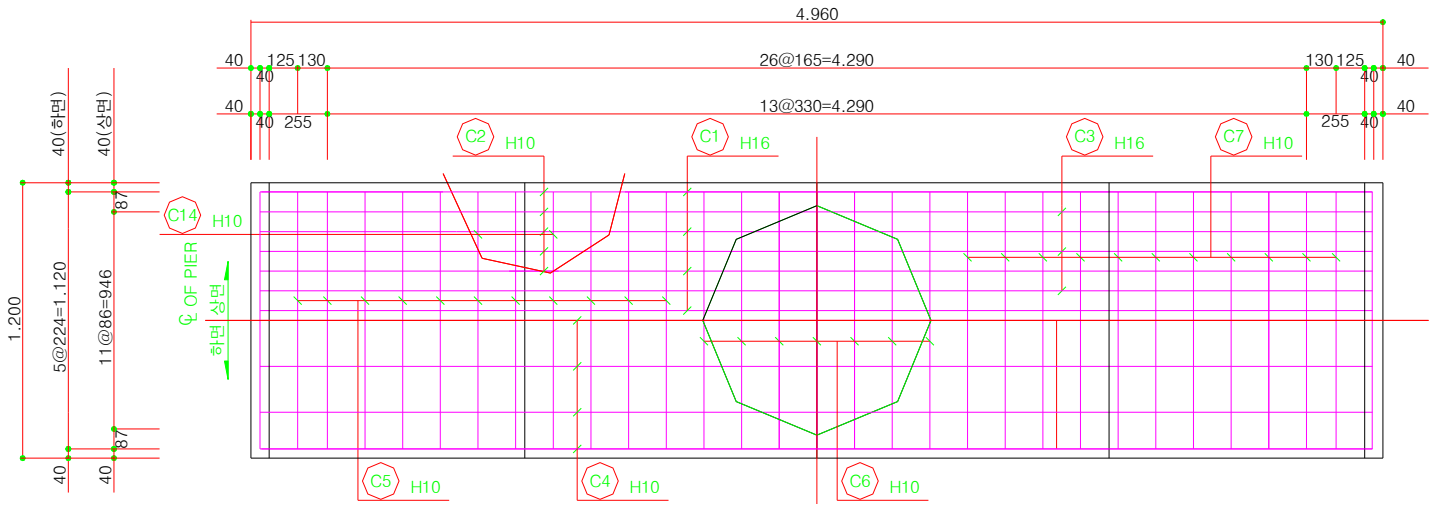
4.960
40
125 130
40
26@165=4.290
130 125
40
40
40
13@330=4.290
40
40
255
255
40
C2 H10
C1 H16
C3 H16
C7 H10
C14 H10
℄ OF PIER
하면 상면
C5 H10
C4 H10
C6 H10
1.200
40(하면)
40(상면)
87
5@224=1.120
11@86=946
87
40
40

(a)

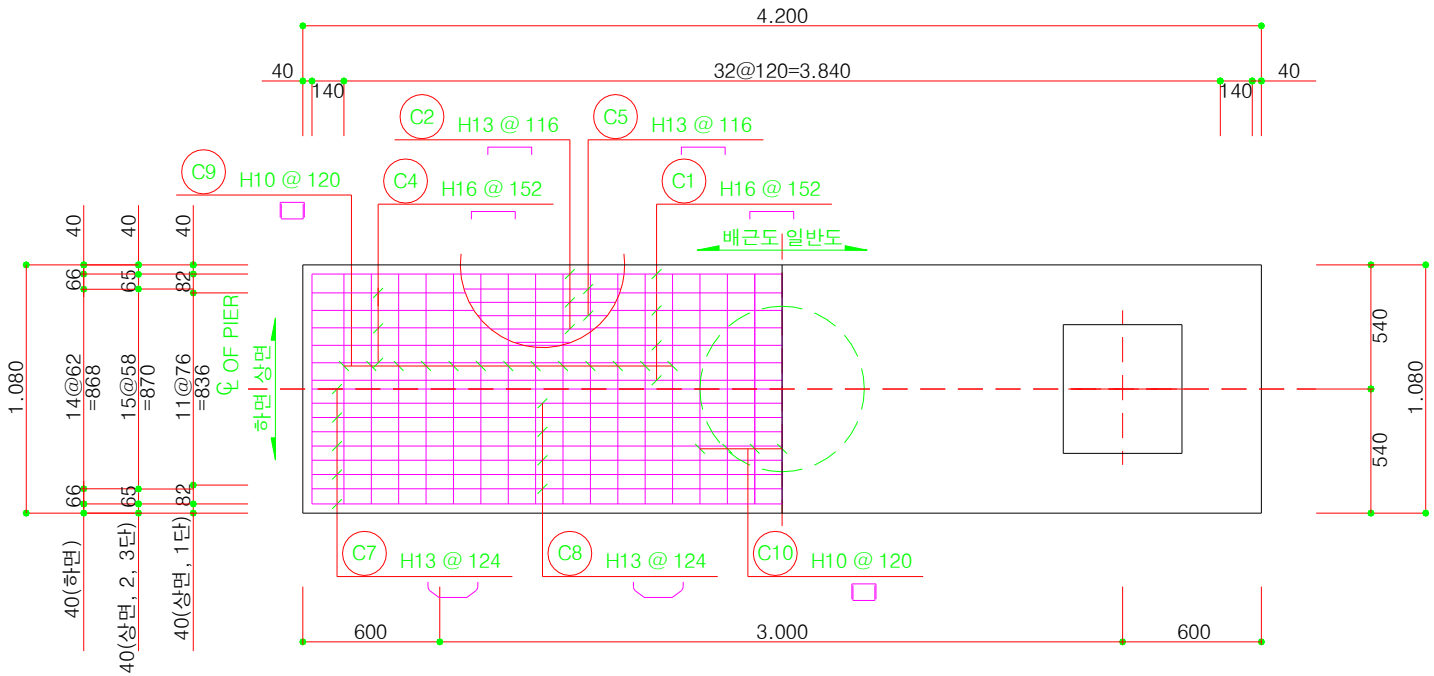


(b)

Figure 4.9 Plane view of specimens: (a) Case 1 and Case 2; (b) Case 3

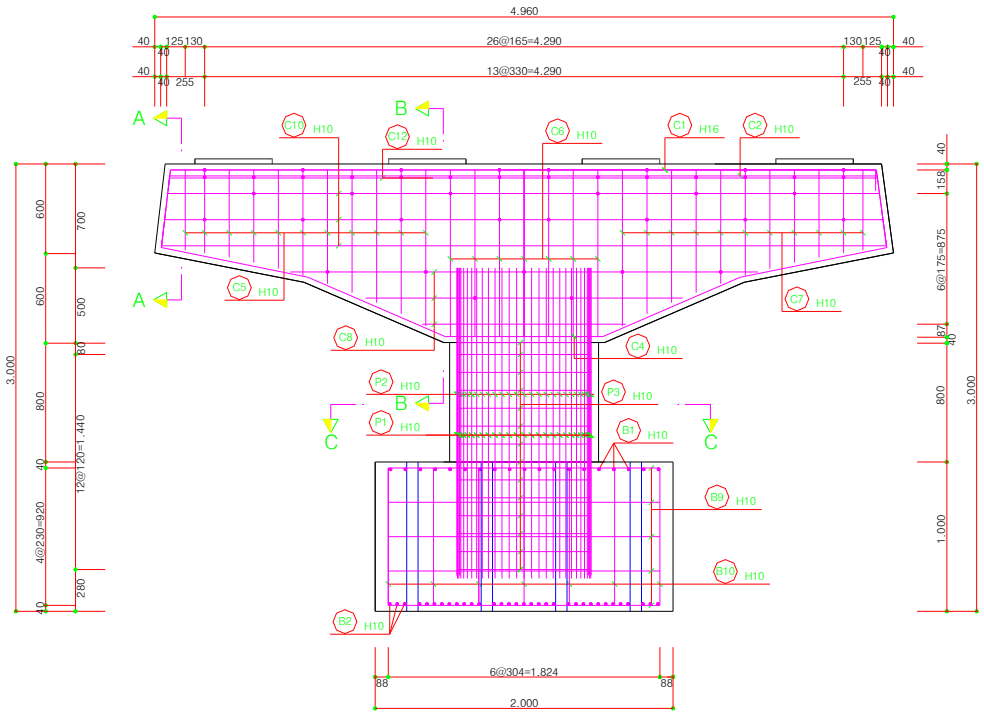
4.960
26@165=4.290
13@330=4.290
A
B
C
C10 H10
C12 H10
C6 H10
C1 H16
C2 H10
C5 H10
C7 H10
C8 H10
C4 H10
P2 H10
P3 H10
P1 H10
B1 H10
B9 H10
B10 H10
B2 H10
6@304=1.824
2.000
3.000
12@120=1.440
4@230=920
6@175=875
1.000

(a)

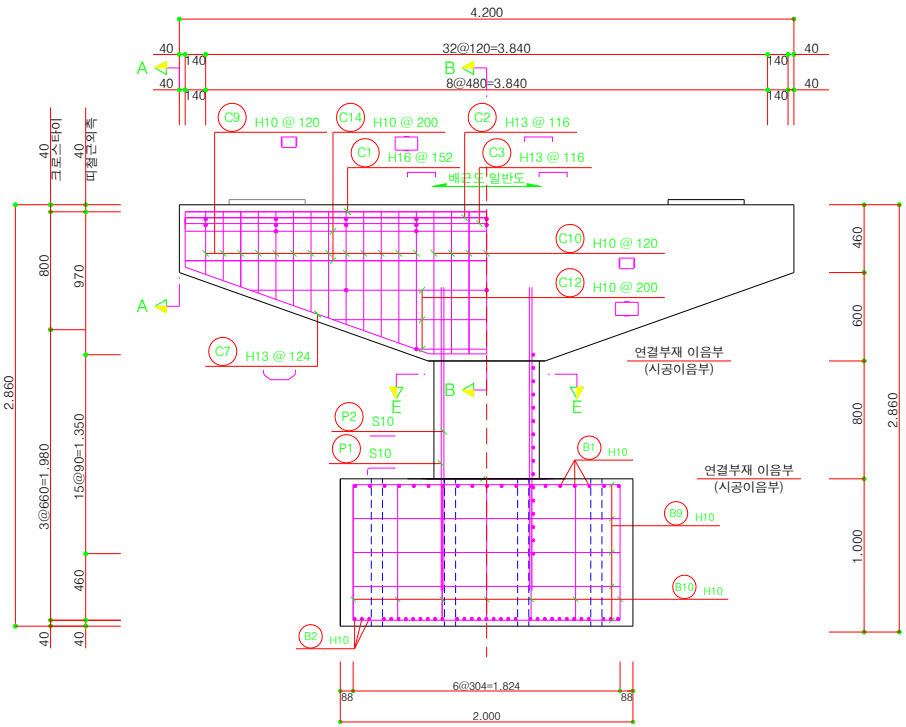


(b)

Figure 4.10 Front view of specimens: (a) Case 1 and Case 2; (b) Case 3

*4.2.5.2 Fabrication of basement*

Figure 4.11 shows the fabrication process of the basement. Rebars for basement and column were assembled together, and the assembly was installed in a mold. The specifications, lengths, and quantities of each rebar were inspected. The effects of lifting lug's position on the pier caps during the transport and test were excluded by installing the lifting lugs on top of the four corners of the basement.

After setting of rebars on the molds, total three cases of the basement were poured with one batch per case. Vibration was conducted for the concrete compaction and finished the surface of concrete after casting. Least 3 concrete cylinders were fabricated for each batch.

(a) (b)

(c) (d)

(e) (f)

Figure 4.11 Procedure of basement fabrication: (a) Assembly of basement rebar and column rebar; (b) Placement of rebar on the mold; (c) Set up of lifting lug; (d) Placing basement concrete and compaction; (e) Surface finishing; (f) Fabrication of cylinder specimens

*4.2.5.3 Fabrication of column*

As shown in Figure 4.12, a total of eight gauges were attached to the longitudinal reinforcement of each column, at the interface where the column and the pier cap meet and at the top of the rebar. After the installation of the molds, the entire columns of three cases were casted in a single batch. The surfaces of columns were finished rough to increase the friction of the interface with the pier caps. Similarly, concrete cylinders were manufactured.

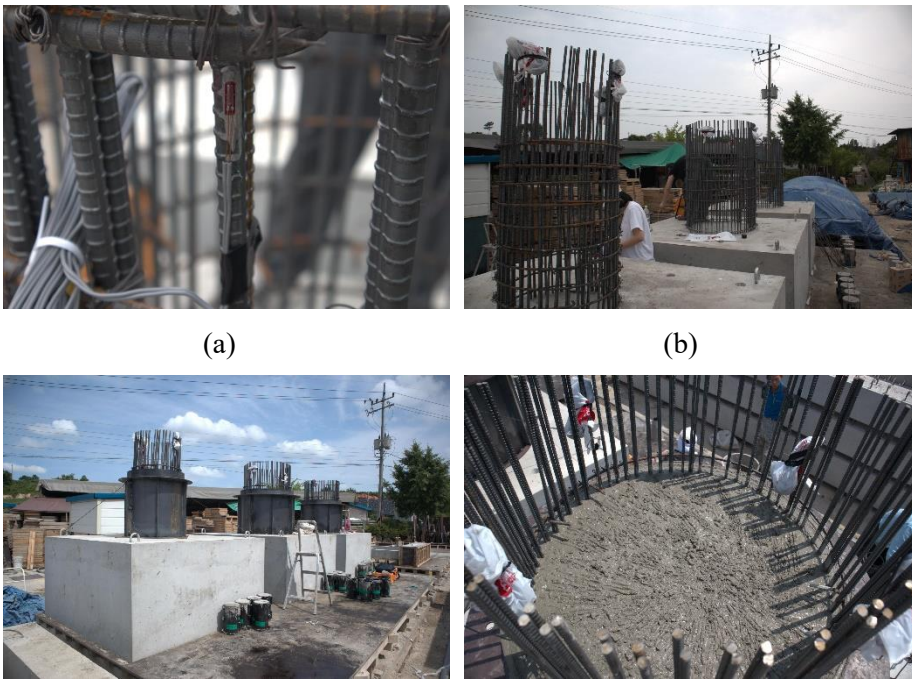

(a) (b)

(c) (d)

Figure 4.12 Procedure of column fabrication: (a) Installation of gauges; (b) Sorting and waterproofing of gauges; (c) Installation of molds; (d) Placing and finishing

*4.2.5.4 Fabrication of pier cap*

Reinforcement of the pier cap was assembled separately. The length, specifications, and quantity of each rebar in the pier cap were checked to see if it was assigned according to the drawings. After that, a total of 78 gauges were attached to each case of the pier cap. The gauge lines were moved along the reinforcement to the end of the wings of pier caps to prevent interference with the support bearing plates during loading procedure.

After the gauge installation, the bottom molds for pier cap were installed on the top of the column. A spacer was installed on the surface rebar to secure the depth of concrete cover, and then the side molds were installed. A total of three batches were casted, one batch per pier cap. The compaction was conducted with care to prevent damage to the gauges. Pier caps and their test cylinders were air-cured at the fabrication site.

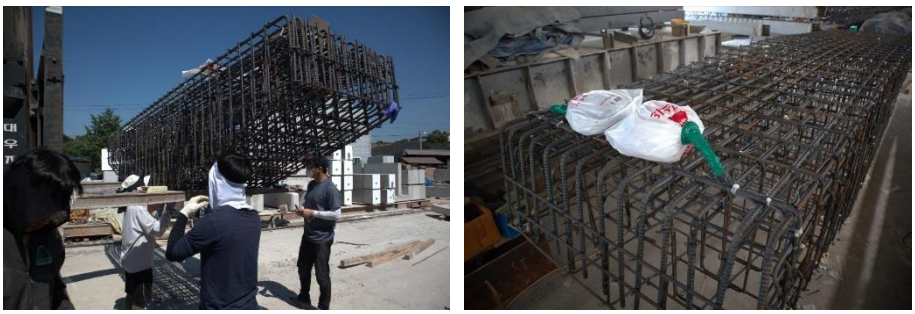

(a) (b)

Figure 4.13 Gauges in pier caps: (a) Installation of steel gauge; (b) Sorting and waterproofing of gauges

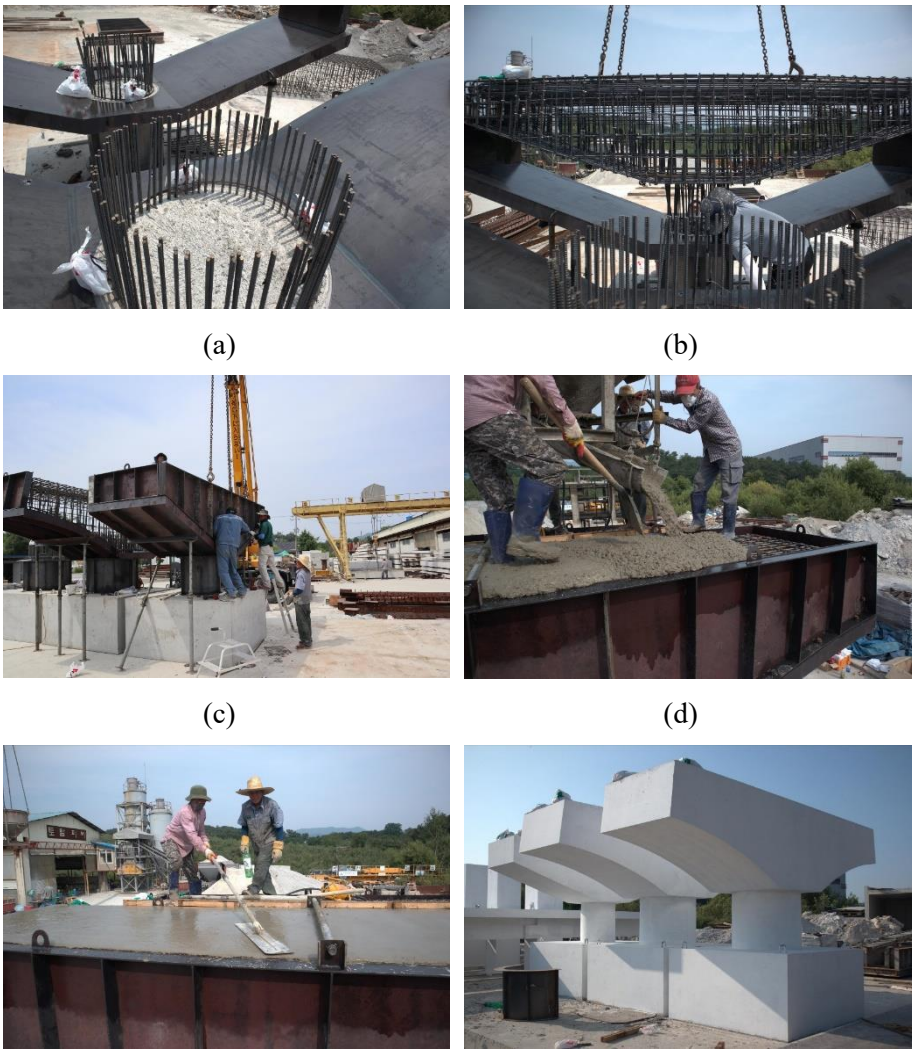

(a) (b)

(c) (d)

(e) (f)

Figure 4.14 Procedure of pier cap fabrication: (a) Installation of floor molds; (b) Disposition of pier cap rebars; (c) Installation of lateral molds; (d) Placing concrete; (e) Surface finishing; (f) Curing and painting

### 4.2.6. Test Setup

The test specimens, whose weight is 25 Ton per unit, were transported to the Hybrid Structural Testing Center in Myongji University by trucks as shown in Figure 4.15. To eliminate the effect of the self-weight of the specimens on the wings of pier caps and interference between the lifting lugs and the support bearings, a total of 4 lifting lugs were installed on the top corners of the basement and the specimens were lifted with the crane.

To observe the crack patterns well, grid work was performed on the surfaces of the specimens as shown in Figure 4.16. The spacing of grid was set to 200 mm for both horizontal and vertical directions. The grid work was conducted on both the front and back of the pier caps to more precisely identify the cracks on both sides.

(a) (b)

Figure 4.15 Conveyance of specimens: (a) Loading specimens; (b) Lifting lug

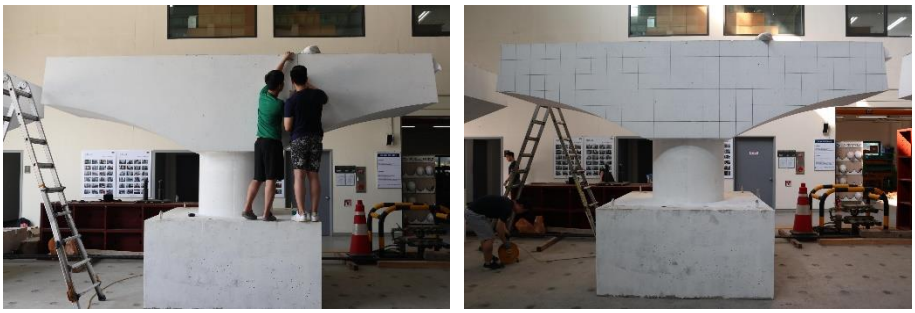

(a) (b)

Figure 4.16 Grid on surface of specimens: (a) Grid work; (b) View of grid

The static loading test of the specimens was conducted in the Hybrid Structural Testing Center of Myongji University. Up to three hydraulic actuators with 5,000 kN capacity per unit, shown in Figure 4.17, were used for the test. Structural frame was installed considering the load capacity and the dimension of the specimens and the actuators. The setting drawings for the scaled model test are shown in Figure 4.19 and Figure 4.20. Due to the limited frame size and bolt spacing, a horizontal gap of approximately 50 mm between the center of the jigs at the bottom of the actuator on the outer part and the center of the outer support bearings occurred.

(a)

(c)

(b)

Figure 4.17 Equipment settings: (a) Conveying actuators; (b) Install of structural frame; (c) Install actuators

Using a crane, the specimens were moved to the loading position inside the structural frame. The sidewalls of the basement were fastened by jigs with jacking machines connected to the floor, as shown in Figure 4.18 (c), to restrain the movement of the specimens in the lateral direction. After fixing the specimens, the steel and rubber plates in Figure 4.18 (b) were located at the loading position of the specimen and the load was applied through the plates. The rubber plate between the steel plate and the specimen serves to minimize the eccentricity of the load. Steel jigs were installed at the bottom of the

actuators, as shown in Figure 4.18 (c), in order to cover the entire plates through the actuators. Since Case 1 and Case 2 have four loading positions, the center actuator has a wide jig installed to simultaneously cover two support plates adjacent to the column with one actuator.

(a)

(b)

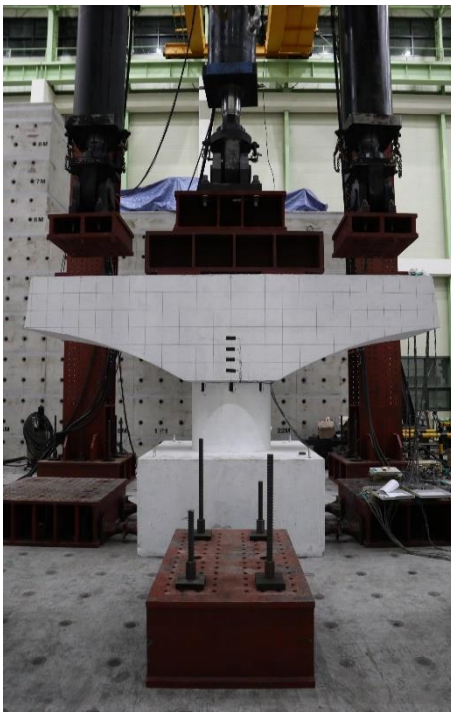

(c)

Figure 4.18 Specimen setting: (a) Lifting specimens; (b) Support jigs and plates with steel and rubber; (c) Install of jigs and plates

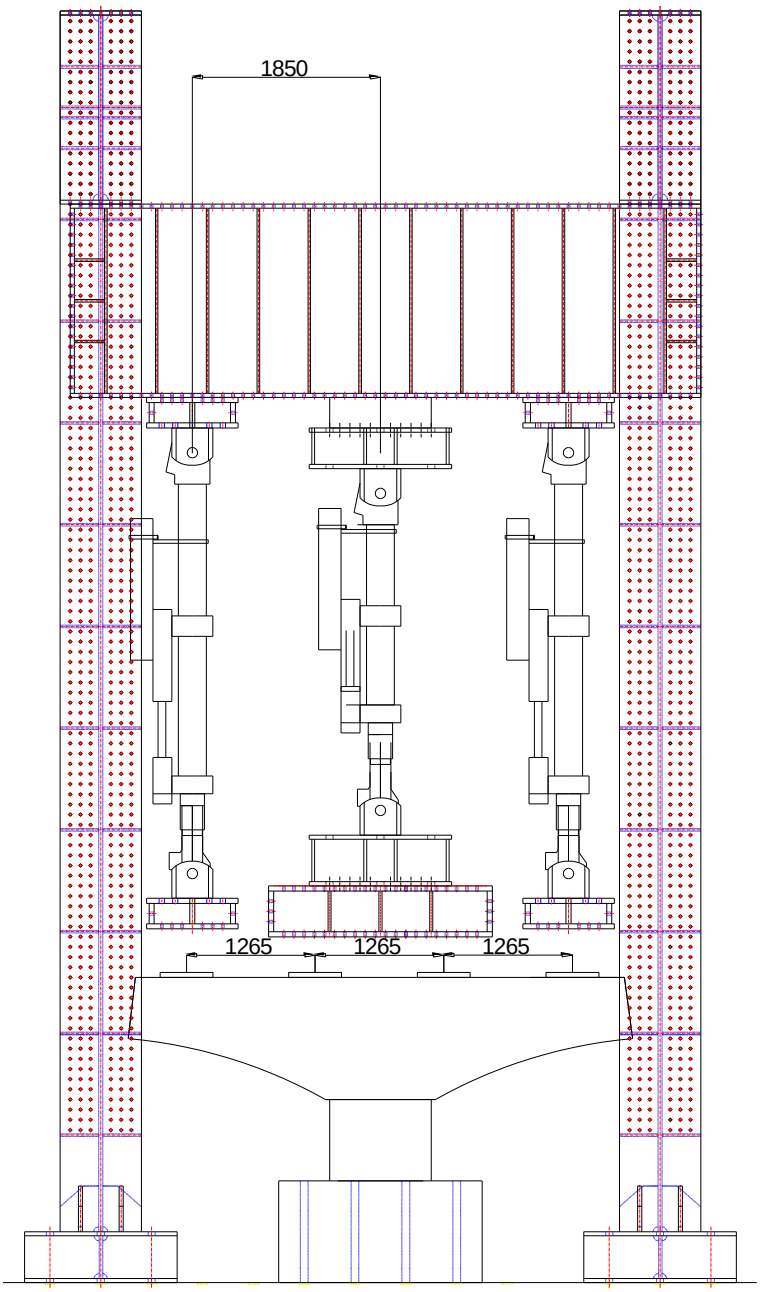


Figure 4.19 Set-up of scaled model test (Case 1 and Case 2)

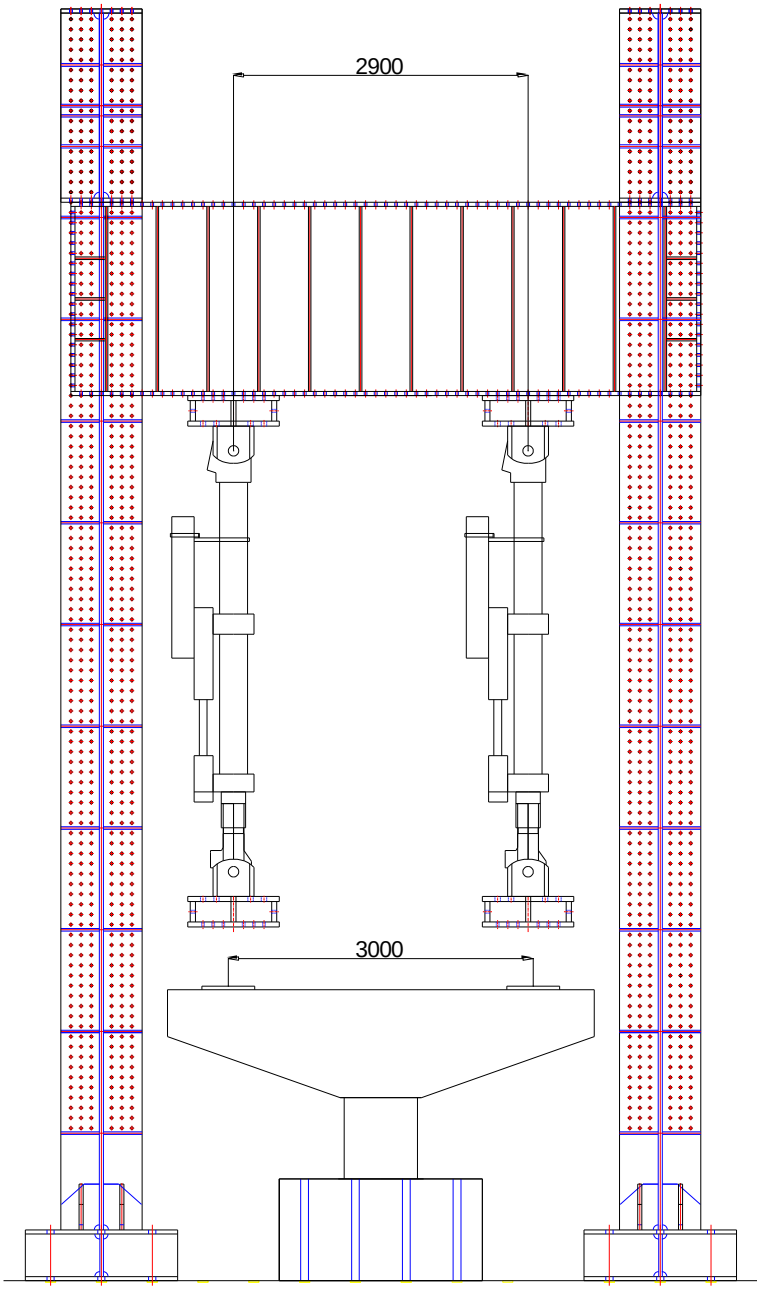


Figure 4.20 Set-up of scaled model test (Case 3)

### 4.2.7. Instrumentation

Four instruments of load cell, steel gauge, concrete gauge, and displacement transducer were used to measure the load, deflection at the end of pier cap, and the strain of the rebar and concrete. For each actuator, the load acting on the actuator and the displacement of the stroke were measured through the internal load cell and the displacement transducer. A maximum of 86 ERSGs steel gauges per specimen were used to identify the strains acting on rebars, and a total of 24 ERSGs concrete gauges were used for determining the concrete strain of the specimen. In order to prevent data loss due to loss of the gauge and measurement error, the gauges were attached to the specimens symmetrically in the direction of the thickness of the member. Two LVDTs were also used to measure deflections at both ends of the pier cap. Measurement were conducted with data loggers once every 6 seconds.

*4.2.7.1 Load cell*

Load data was collected from the load cell of 500 Ton capacity built into each actuator to measure the force applied to the actuators.

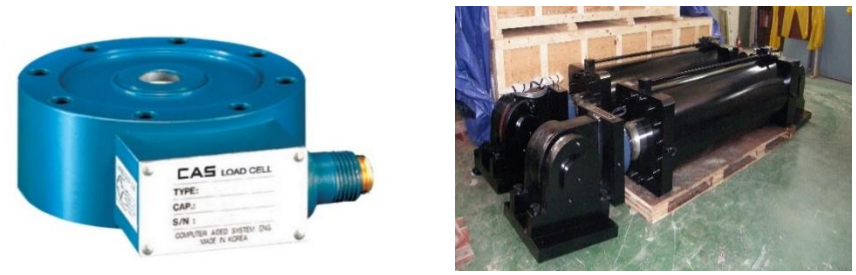


(a) (b)

Figure 4.21 Load cell properties: (a) LSU-500T(CAS); (b) 5,000 kN actuator

*4.2.7.2 ERSGs for reinforcing steel bars*

A total of 86 5 mm ERSGs steel gauges were attached to Case 1 and Case 2, respectively, for the measurement of rebar strain on members, and 99 for Case 3. The steel gauges were attached to the flexural reinforcement, compressive reinforcement, horizontal shear reinforcement, vertical shear reinforcement, and column longitudinal reinforcement, respectively. The locations of attachment were selected by reviewing the FEA result for each case, where relatively high strains were captured. The designation of ERSGs for rebar is shown in Figure 4.22. The detailed diagram of the locations of steel gauges is shown in Figure 4.23.

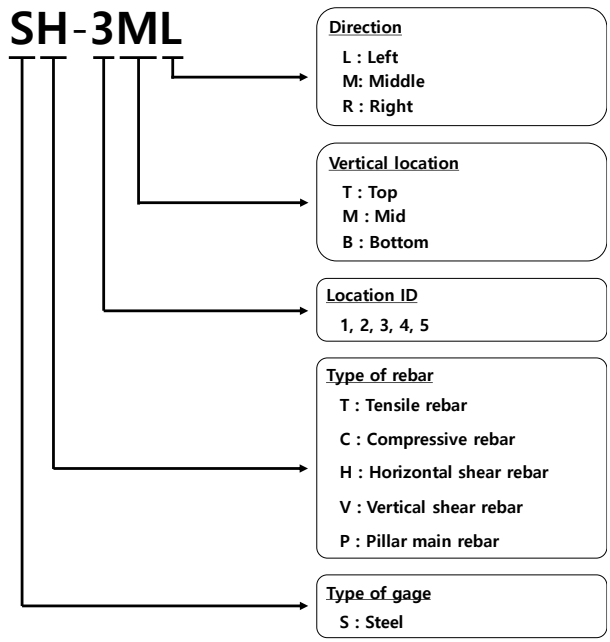


Figure 4.22 Designation of the ERSGs' location for rebars

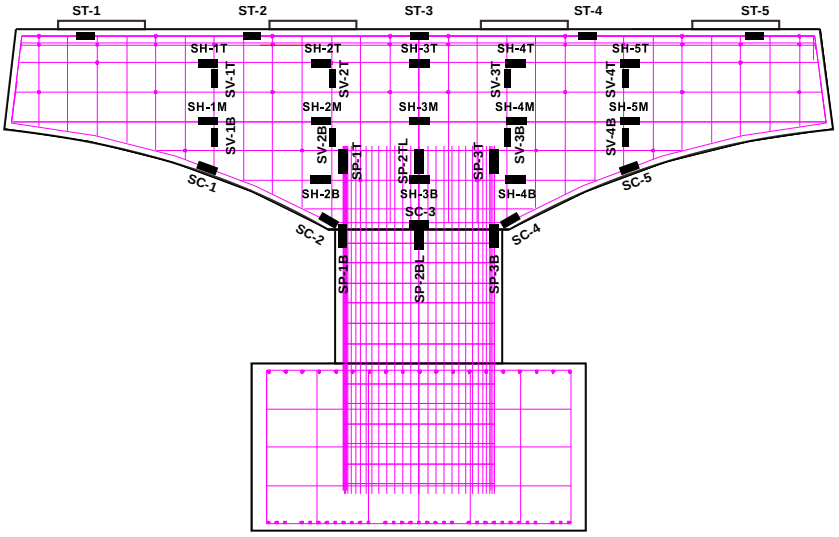
ST-1
ST-2
ST-3
ST-4
ST-5
SH-1T
SH-2T
SH-3T
SH-4T
SH-5T
SV-1T
SV-2T
SV-3T
SV-4T
SH-1M
SH-2M
SH-3M
SH-4M
SH-5M
SV-1B
SV-2B
SP-1T
SP-2TL
SP-3T
SV-3B
SV-4B
SC-1
SH-2B
SH-3B
SH-4B
SC-5
SC-3
SC-2
SC-4
SP-1B
SP-2BL
SP-3B

(a)

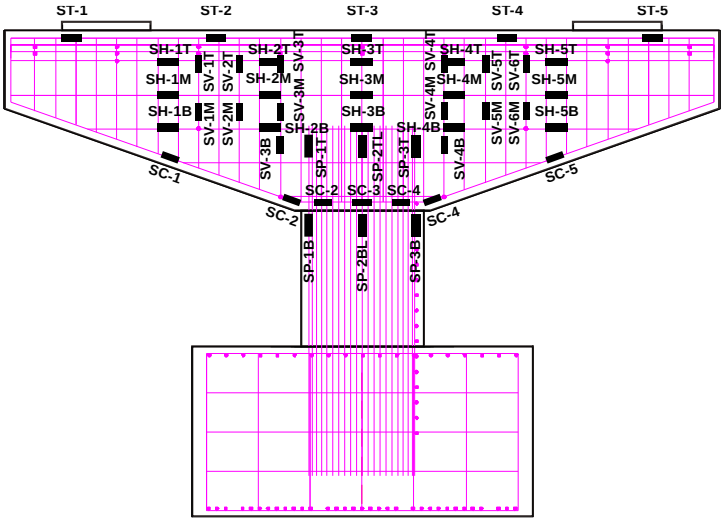
ST-1
ST-2
ST-3
ST-4
ST-5
SH-1T
SH-2T
SH-3T
SH-4T
SH-5T
SV-1T
SV-2T
SV-3T
SV-4T
SV-5T
SV-6T
SH-1M
SH-2M
SH-3M
SH-4M
SH-5M
SV-1M
SV-2M
SV-3M
SV-4M
SV-5M
SV-6M
SH-1B
SH-2B
SH-3B
SH-4B
SH-5B
SV-1B
SV-2B
SV-3B
SV-4B
SP-1T
SP-2TL
SP-3T
SC-1
SC-2
SC-3
SC-4
SC-5
SP-1B
SP-2BL
SP-3B

(b)

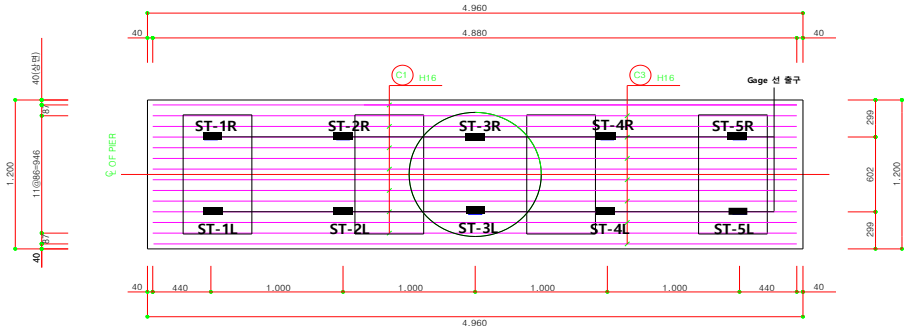
4.960
40
4.880
40
C1 H16
C3 H16
Gage 선 출구
ST-1R
ST-2R
ST-3R
ST-4R
ST-5R
ST-1L
ST-2L
ST-3L
ST-4L
ST-5L
℄ OF PIER
1,200
11@86=946
40(보강)
40
299
602
299
1,200
40
440
1,000
1,000
1,000
1,000
440
40
4.960

(c)

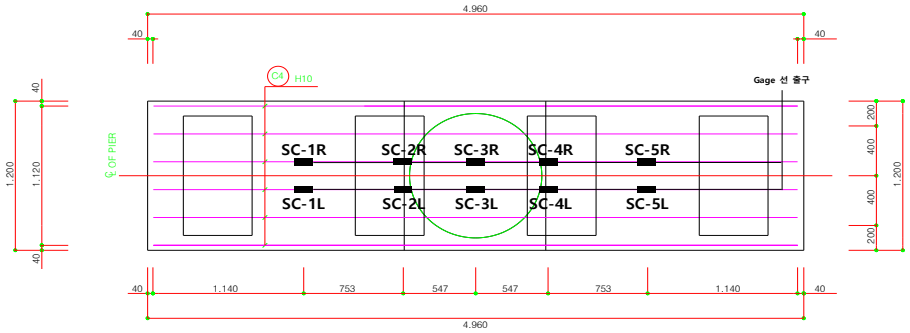
4.960
40
40
C4 H10
Gage 선 출구
SC-1R
SC-2R
SC-3R
SC-4R
SC-5R
SC-1L
SC-2L
SC-3L
SC-4L
SC-5L
℄ OF PIER
1,200
40
1,120
40
200
400
400
200
1,200
40
1,140
753
547
547
753
1,140
40
4.960

(d)

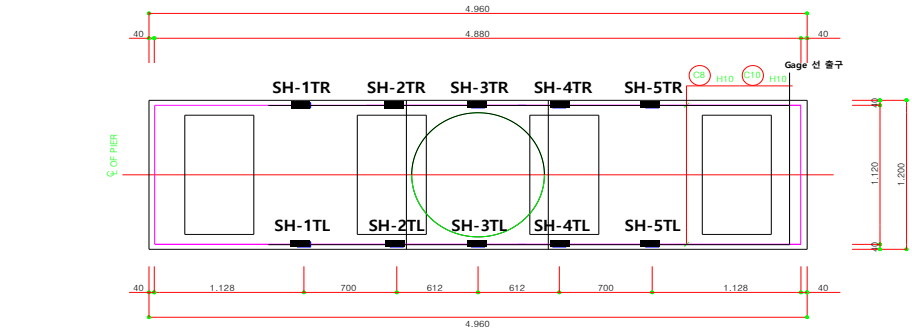
4.960
40
4.880
40
Gage 선 출구
C8 H10
C10 H10
SH-1TR
SH-2TR
SH-3TR
SH-4TR
SH-5TR
SH-1TL
SH-2TL
SH-3TL
SH-4TL
SH-5TL
℄ OF PIER
1,120
1,200
40
1,128
700
612
612
700
1,128
40
4.960

(e)

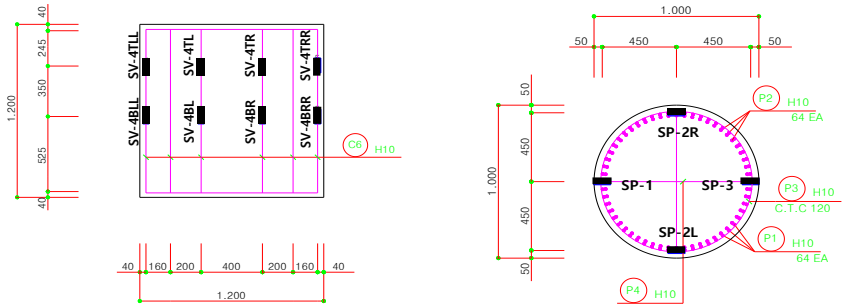


(f) (g)

Figure 4.23 Location of ERSGs for rebar: (a) Case 1 and Case 2; (b) Case 3; (c) Tensile rebar; (d) Compressive rebar; (e) Horizontal shear rebar; (f) Vertical shear rebar; (g) Pillar main rebar

*4.2.7.3 ERSGs for concrete*

Concrete strains were measured by a total of 24 60 mm ERSGs concrete gauges at each specimen in order to identify concrete strain on the surface of the pier cap and the column. Designation of concrete gauge is shown in Figure 4.24. The location and the detailed diagram of concrete gauges are shown in Figure 4.25 and Figure 4.26.

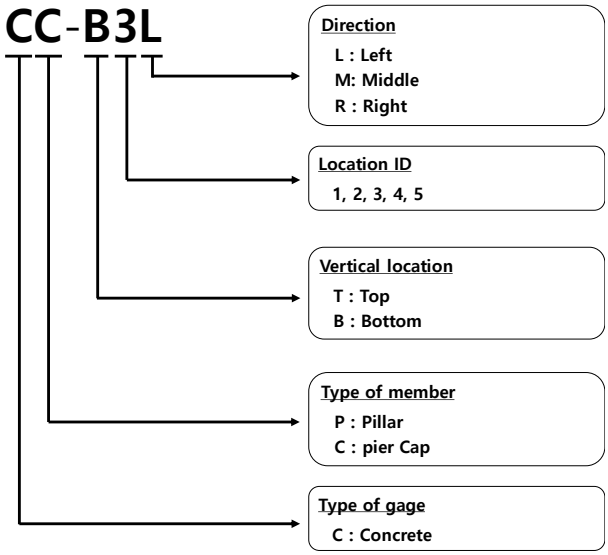


Figure 4.24 Designation of the ERSGs' location for concrete


Figure 4.25 ERSGs for concrete in Case 1

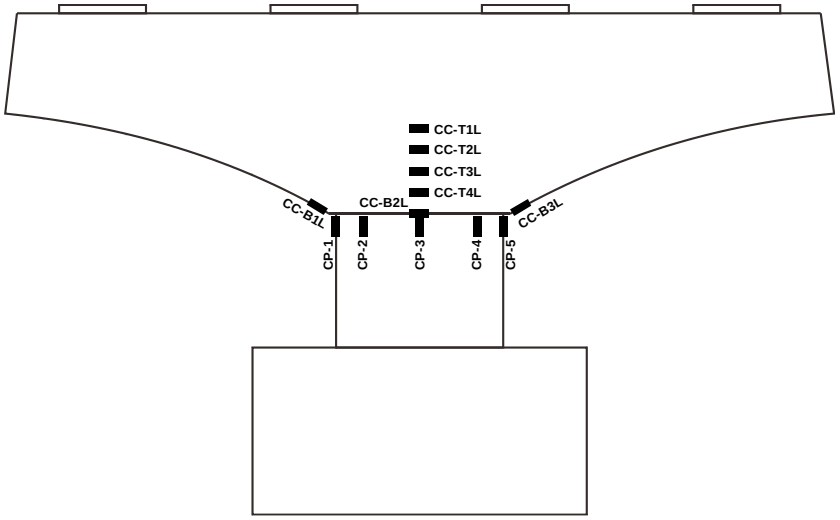
CC-T1L
CC-T2L
CC-T3L
CC-T4L
CC-B1L
CC-B2L
CC-B3L
CP-1
CP-2
CP-3
CP-4
CP-5

(a)

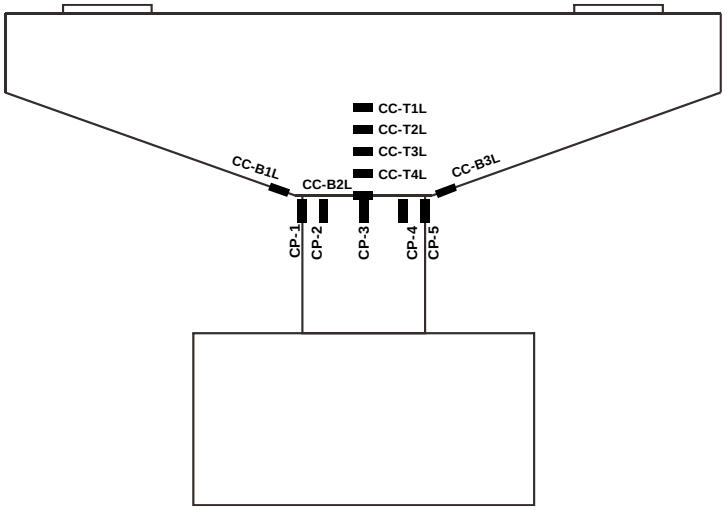
CC-T1L
CC-T2L
CC-T3L
CC-T4L
CC-B1L
CC-B2L
CC-B3L
CP-1
CP-2
CP-3
CP-4
CP-5

(b)

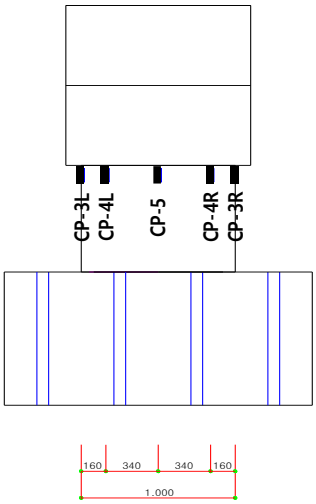


(c)

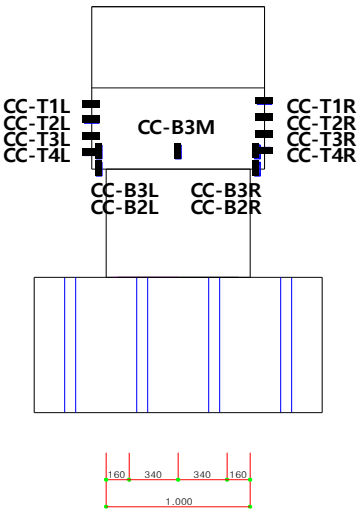


(d)

Figure 4.26 Location of ERSGs for concrete: (a) Case 1 and Case 2; (b) Case 3; (c) ERSG at pillar; (d) ERSG at pier cap

*4.2.7.4 LVDTs*

To measure the deflection of both ends of pier cap, a Linear Variables Differential Transformer (LVDT) of 100mm stroke was placed on the bottom of the both ends of pier cap using a frame as shown in Figure 4.27.

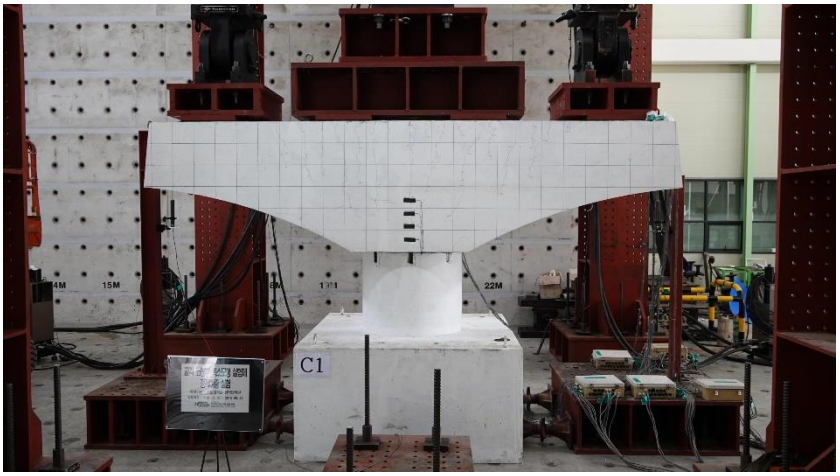


Figure 4.27 Setting of LVDT in the test

### 4.2.8. Test Loads

The load acting on the target structure for each limit state was derived according to the type of load in order to evaluate the specimens for the load at serviceability limit state and ultimate limit state.

The minimum design grade of reinforced concrete members provided by the KHBDC (2015) is Class E, and the assessment of Class E members requires the serviceability limit state load combination-V. Therefore, the total load of serviceability limit state load combination-V for Case A and B are shown in Table 4.9 and Table 4.10. The maximum load among each load at various load positions was applied evenly to all load positions, and the square of length scale factor of 2/5 was applied in order to fit the load size to the scaled models, as shown in Table 4.11.

Total load of the ultimate limit state load combination-I for Case A and B, which generates the greatest moment and shear force in the member, is shown in Table 4.12 and Table 4.13. The maximum load among each load at various load positions was applied evenly to all load positions, and the square of length scale factor of 2/5 was applied in order to fit the load size to the scaled models, as shown in Table 4.14.

Table 4.9 Applied loads for pier cap A at SLS load combination-V

| Type of load | Load factor | Applied load (kN) | | | |
|---|---|---|---|---|---|
| | | Left support | | Right support | |
| | | Outer | Inner | Inner | Outer |
| DC | 1.0 | 2,195 | 1,752 | 1,768 | 2,066 |
| DW | 1.0 | 117 | 163 | 165 | 99 |
| Total | | 2,312 | 1,915 | 1,933 | 2,165 |

Table 4.10 Applied loads for pier cap B at SLS load combination-V

| Type of load | Load factor | Applied load (kN) | |
|---|---|---|---|
| | | Left support | Right support |
| DC | 1.0 | 5,499 | 5,293 |
| DW | 1.0 | 751 | 767 |
| Total | | 6,250 | 6,060 |

Table 4.11 Applied loads for the specimens (scaled models) at SLS

| Load case | Design class | Case | Total load (kN) | Applied load (kN) | | | |
|---|---|---|---|---|---|---|---|
| | | | | Left support | | Right support | |
| | | | | Outer | Inner | Inner | Outer |
| Serviceability limit state load combination -V | E | 1, 2 | 1,480 | 370 | 370 | 370 | 370 |
| | | 3 | 2,000 | 1,000 | | 1,000 | |

Table 4.12 Applied loads for pier cap A at ULS load combination-I

| Type of load | Load factor | Applied load (kN) | | | |
|---|---|---|---|---|---|
| | | Left support | | Right support | |
| | | Outer | Inner | Inner | Outer |
| DC | 1.25 | 2,744 | 2,190 | 2,210 | 2,583 |
| DW | 1.50 | 176 | 245 | 248 | 149 |
| LL | 1.80 | 1,696 | 2,027 | 1,985 | 1,789 |
| Total | | 4,616 | 4,462 | 4,443 | 4,521 |

Table 4.13 Applied loads for pier cap B at ULS load combination-I

| Type of load | Load factor | Applied load (kN) | |
|---|---|---|---|
| | | Left support | Right support |
| DC | 1.25 | 6,874 | 6,616 |
| DW | 1.50 | 1,127 | 1,151 |
| LL | 1.80 | 3,762 | 1,051 |
| Total | | 11,763 | 8,818 |

Table 4.14 Applied loads for the specimens (scaled models) at ULS

| Load case | Design class | Case | Total load (kN) | Applied load (kN) | | | |
|---|---|---|---|---|---|---|---|
| | | | | Left support | | Right support | |
| | | | | Outer | Inner | Inner | Outer |
| Ultimate limit state load combination -I | E | 1, 2 | 2,956 | 739 | 739 | 739 | 739 |
| | | 3 | 3,764 | 1,882 | | 1,882 | |

A preliminary analysis for the scaled model specimens was performed as shown in Figure 4.28, Figure 4.29, and Figure 4.30. Before the material tests, material strengths with the increasement of design strengths by 10 percent were used at the analysis in order to consider the material strengths obtained from the material tests. As a result, the maximum load that the specimen can resist was obtained, and the maximum load was applied step by step considering the SLS and ULS load. In Case 1 and Case 2, a total of three hydraulic actuator were used. And the load at the center actuator was twice the load at each actuator on sides in order to apply equal loads on all 4 loading points. For Case 3, a total of two hydraulic actuators were used to equally apply the loads on the two loading points. Although the loading was intended to be carried out under load control in order to maintain the ratio of loads at the hydraulic actuators, the load control method may cause oscillations between the hydraulic actuators when adjusting the load, leading to a significant risk in the experiment. Therefore, the loading process was conducted by manually adjusting the rate of the displacement of the center actuator based on displacement control of the hydraulic actuators on both sides.

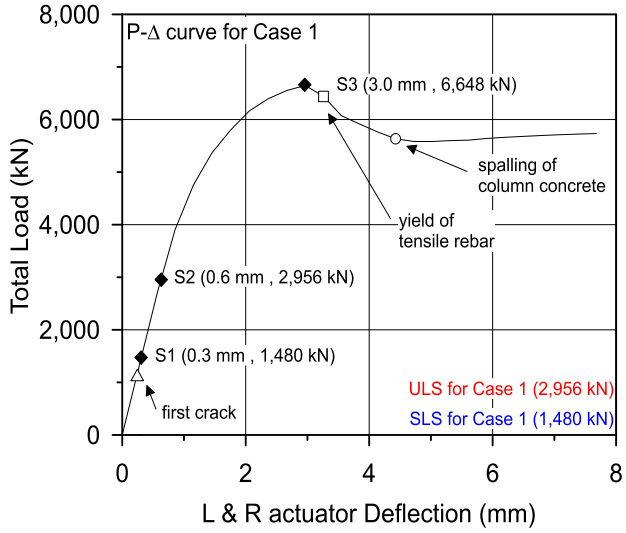


(a)

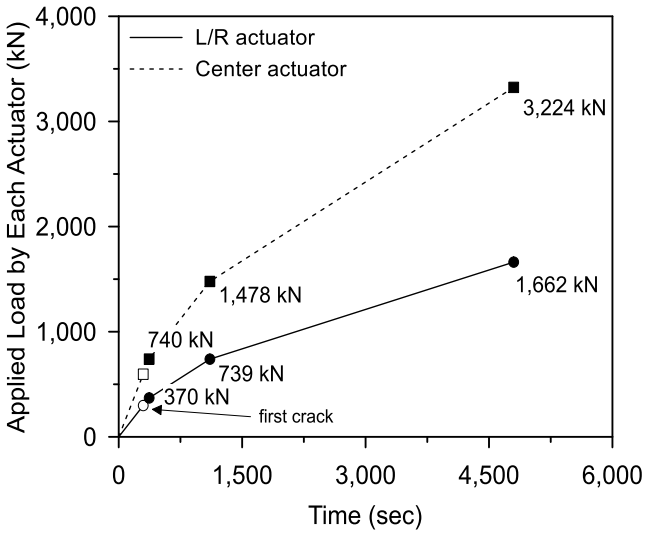


(b)

Figure 4.28 Loading procedure for Case 1: (a) Preliminary analysis result; (b) Applied load by each actuator

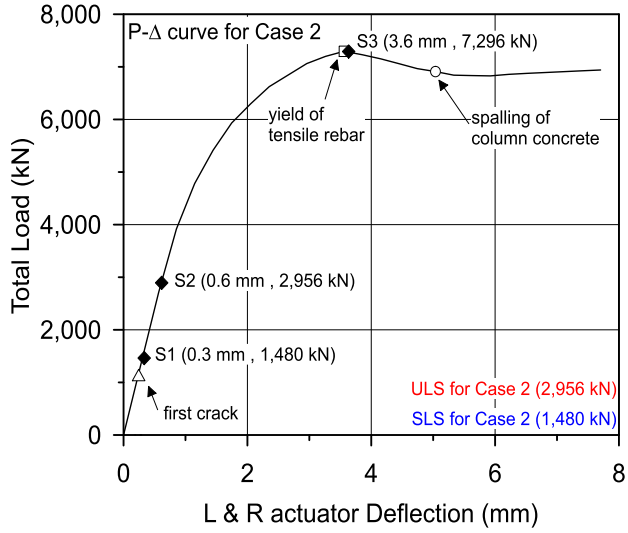


(a)

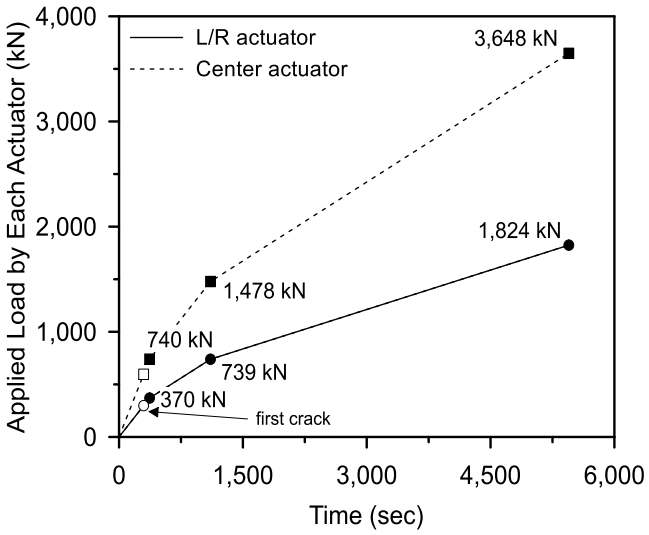


(b)

Figure 4.29 Loading procedure for Case 2: (a) Preliminary analysis result; (b) Applied load by each actuator

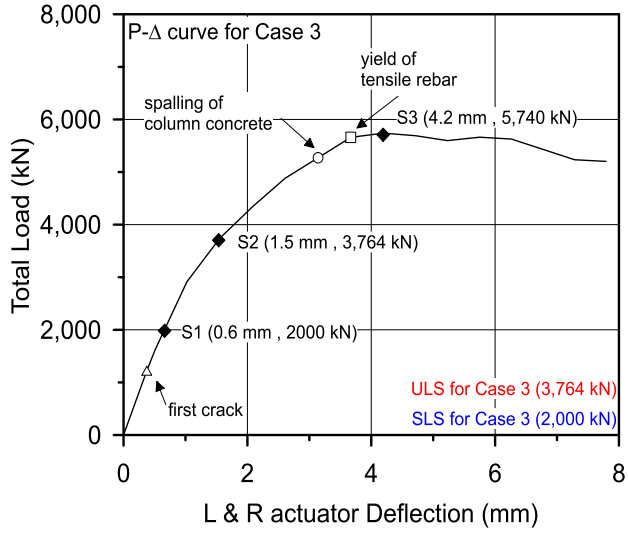


(a)

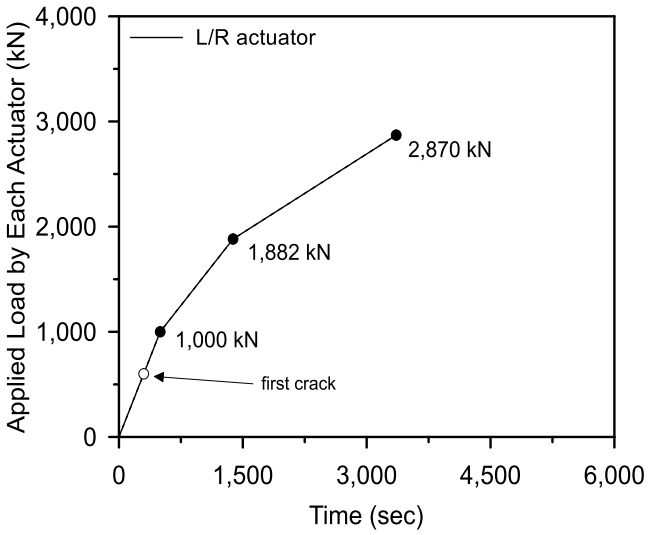


(b)

Figure 4.30 Loading procedure for Case 3: (a) Preliminary analysis result; (b) Applied load by each actuator

## 4.3. Test Results and Discussion

### 4.3.1. Load-deflection Relationship

The deflection at both ends of the pier cap was measured by increasing the load size until the specimen is in failure. The loading procedure was terminated when the total load begins to decrease as no longer increases. Test results showed flexural failures in all cases designed with the proposed STM design guidelines. In the load-deflection relationships of pier caps, the stiffness of the member decreases after the first crack occurrence. And the flexural reinforcement begins to yield, resulting in the significant decrease in stiffness. The member showed plastic behavior until the maximum load is reached. It showed ductile behavior that did not result in sudden shear failure near areas where diagonal cracks occurred.

In designing strut-and-tie models for each specimen, material factors of concrete and rebars were applied. Thus, ULS load shall be compared to the design load for which the material factor is taken into account. However, the maximum load obtained from the scaled model test is the resistance capability at the actual strength of each material according to the actual material test. Therefore, the design load shall be derived by reducing the maximum load from the test to the ratio of the design strength to the actual strength of each material in order to indicate the resistance capability at the design strength of each material.

Table 4.15 shows the design strengths and actual strengths for materials. The design strength of each material was used as described in KHBDC (2015).

The flexural strengths at actual strengths and the design strengths are able to be approximated from the Equation 4.2 and Equation 4.3. And the ratio of both flexural strengths in Equation 4.4 is intended to express the load reduction factor, $\psi_p$. With the load reduction factor for each case, design loads from the maximum loads were obtained as shown in Table 4.16.

$$M_n = A_s f_y d\left(1 - \frac{\rho f_y}{0.85 f_{ck}}\right) \tag{4.1}$$

$$M_{act} = A_s f_{y,\,act} d\left(1 - \frac{\rho f_{y,\,act}}{0.85 f_{c,\,act}}\right) \tag{4.2}$$

$$M_d = A_s f_{yd} d\left(1 - \frac{\rho f_{yd}}{0.85 f_{cd}}\right) \tag{4.3}$$

Table 4.15 Design strength and actual strength of steel rebar and concrete

| | Reinforcement | | | | Concrete | | |
|---|---|---|---|---|---|---|---|
| | Case 1 | Case 2 | Case 3 | | Case 1 | Case 2 | Case 3 |
| $f_y$ (MPa) | 400 | 400 | 400 | $f_{ck}$ (MPa) | 40 | 40 | 40 |
| $\phi_s$ | 0.9 | 0.9 | 0.9 | $\phi_c$ | 0.65 | 0.65 | 0.65 |
| | | | | $\alpha_{cc}$ | 0.85 | 0.85 | 0.85 |
| $f_{yd}$ (MPa) | 360 | 360 | 360 | $f_{cd}$ (MPa) | 22 | 22 | 22 |
| $f_{y,\,act}$* (MPa) | 432 | 432 | 431 | $f_{c,\,act}$ (MPa) | 35 | 32 | 36 |

* Case 1 & 2: Average of D16 and D10; Case 3: Average of D16 and D13

Table 4.16 Load reduction factor and corresponding design loads

| | Total load (kN) | | |
|---|---|---|---|
| | Case 1 | Case 2 | Case 3 |
| $\psi_p$ | 0.82 | 0.83 | 0.80 |
| $P_{\max}$ | 6,086 | 7,490 | 5,125 |
| $P_d$ | 5,008 | 6,186 | 4,120 |

$$\psi_p = \frac{M_d}{M_{act}} \tag{4.4}$$

$$P_d = \psi_p P_{\max} \tag{4.5}$$

*4.3.1.1 Case 1*

The load-deflection relationship of Case 1 is shown in Figure 4.31 and Table 4.17. The initial crack occurred at the load of 1,190 kN before reaching the SLS load of 1,480 kN. After the initial crack, the flexural rebar of the pier cap did not yield until the ULS load. And then, the member showed ductile behavior after the yield of flexural reinforcement. Maximum load of 6,086 kN was reached as the load was increased and then failed by flexure. The design load was derived by applying the load reduction factor to the maximum load of 6,086 kN to determine the design safety factor of Case 1 at ULS. With the load reduction factor of 0.82, the design load of Case 1 is 5,008 kN, 1.7 times the ULS load, significantly exceeding the ultimate limit state (ULS). In addition, sufficient shear capability was found in Case 1 even if only the minimum

horizontal shear reinforcement was assigned for assembly. In other words, sufficient load resistance and shear capability were exerted even in the absence of horizontal shear reinforcement not required in STM, which was basically based on the proposed efficient STM design guidelines, to induce flexural failure.

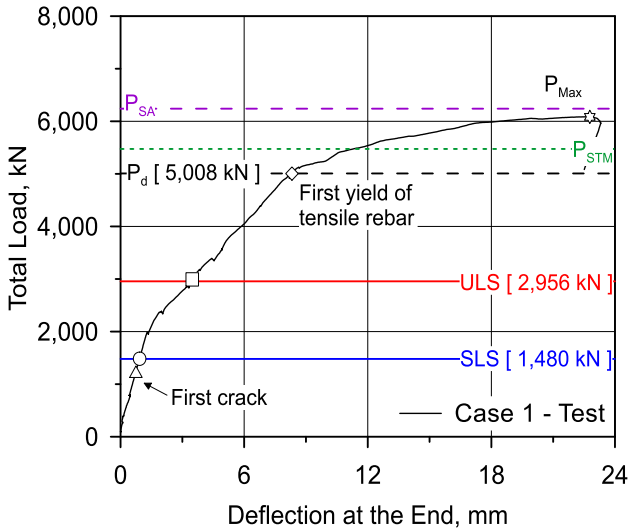


Figure 4.31 Measured load-deflection curve for Case 1

Table 4.17 Load and deflection at each state of Case 1

| | Initial crack | SLS | ULS | Design load | Yield of rebar | Maximum load |
|---|---|---|---|---|---|---|
| Load (kN) | 1,190 | 1,480 | 2,956 | 5,008 | 5,050 | 6,086 |
| Deflection (mm) | 0.7 | 1.0 | 3.5 | - | 8.4 | 22.6 |

*4.3.1.2 Case 2*

Figure 4.32 and Table 4.18 indicate the load-deflection relationship of Case 2. At the load of 1,192 kN before reaching SLS load of 1,480 kN, the initial crack occurred. After the initial crack, the yield of the flexural tensile rebar did not occur until ULS was reached, and the member showed ductile behavior after the yield of the flexural reinforcement. As the load increased, the maximum load of 7,490 kN was reached and flexural failure mode occurred.

To determine the design safety factor of Case 2 at ULS, the design load was determined by multiplying the load reduction factor to the maximum load of 7,490 kN. The design load of Case 2 is 6,186 kN with the load reduction factor of 0.83. In other words, it is conservatively 2.1 times the ULS load. The 0.2% of the horizontal shear reinforcement assigned for serviceability was found to serve as a complement for flexural reinforcement, increasing the bending capacity of the member. And the additional shear rebar in Case 2 secured the increased shear capability to exert sufficient shear performance until the failure. That is to say, sufficient load resistance and shear capability on the member designed in accordance with the proposed efficient STM design guidelines induced flexural failure.

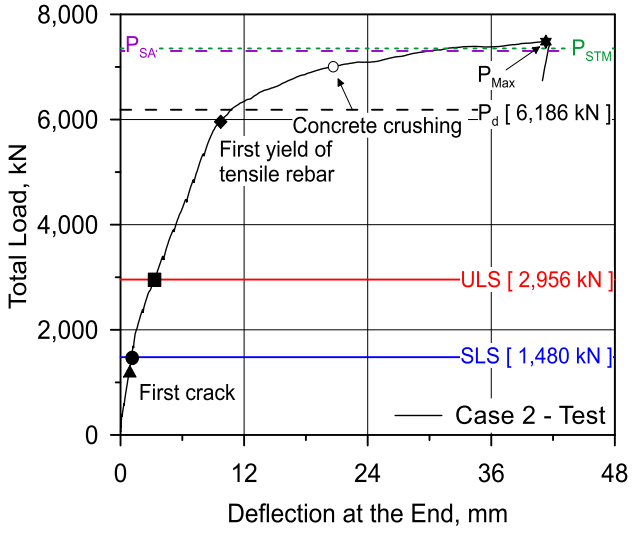


Figure 4.32 Measured load-deflection curve for Case 2

Table 4.18 Load and deflection at each state of Case 2

| | Initial crack | SLS | ULS | Yield of rebar | Design load | Maximum load |
|---|---|---|---|---|---|---|
| Load (kN) | 1,192 | 1,480 | 2,956 | 5,943 | 6,186 | 7,490 |
| Deflection (mm) | 0.9 | 1.0 | 3.5 | 9.5 | - | 41.6 |

*4.3.1.3 Case 3*

Figure 4.31 and Table 4.19 indicate the load and deflection at each state of Case 3. Unlike Case 1 and Case 2, in Case 3, an initial crack occurred at the load of 1,200 kN, which is far below the SLS load of 2,000 kN. This is because, different with the loads at Case 1 and Case 2 some of which directly transfers from inner support bearings to the column, the majority of the load is carried by the bending through the both wings of pier cap in Case 3. Case 3 failed after reaching the maximum load of 5,125 kN. At the load reduction factor of 0.80, the design load is 4,120 kN, ensuring the design safety factor of 1.1. Though, it is found to be significantly lower than that of Case 1 and Case 2. With the biased loading, Case 3 also secured load resistance and shear capability at the proposed guidelines, leading to failure in bending. However, in the absence of proper sectional depth of the pier cap at the large moment due to the biased loading, Case 3 may cause problems in the serviceability of cracks at SLS since the initial crack occurs at a relatively small total load. Similarly, large discrepancy in design safety factors of Case 2 and Case 3 is also due to the improper selection of sectional depth without any consideration of load positions according to the superstructure prior to the STM design.

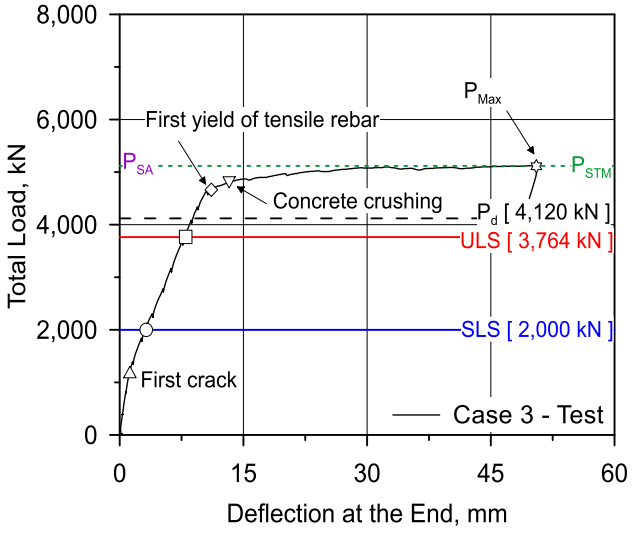


Figure 4.33 Measured load-deflection curve for Case 3

Table 4.19 Load and deflection at each state of Case 3

| | Initial crack | SLS | ULS | Design load | Yield of rebar | Maximum load |
|---|---|---|---|---|---|---|
| Load (kN) | 1,200 | 2,000 | 3,764 | 4,120 | 4,680 | 5,125 |
| Deflection (mm) | 1.2 | 3.2 | 8.0 | - | 11.2 | 50.6 |

*4.3.1.4 Comparison of test results*

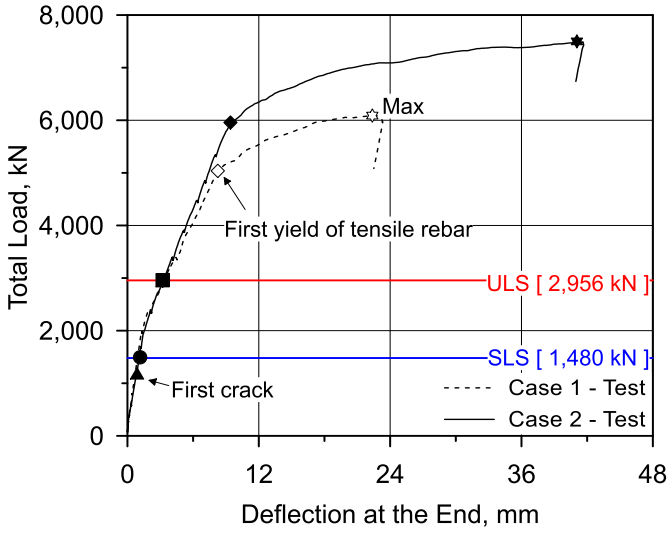


Figure 4.34 Comparison of measured load-deflection

Table 4.20 Comparison of load and deflection at each state

| | | Initial crack | SLS | ULS | Yield of rebar | Maximum load |
|---|---|---|---|---|---|---|
| Load (kN) | Case 1 | 1,190 | 1,480 | 2,956 | 5,050 | 6,086 |
| | Case 2 | 1,192 | 1,480 | 2,956 | 5,943 | 7,490 |
| | Ratio (C2/C1) | 1.00 | - | - | 1.18 | 1.23 |
| Deflection (mm) | Case 1 | 0.7 | 1.0 | 3.5 | 8.4 | 22.6 |
| | Case 2 | 0.9 | 1.0 | 3.5 | 9.5 | 41.6 |
| | Ratio (C2/C1) | 1.29 | 1.00 | 1.00 | 1.13 | 1.84 |

The load-deflection relationships of Case 1 and Case 2 were compared in Figure 4.34 to see the effect of the arrangement of horizontal shear rebar, and the comparison confirmed that the both cases showed very similar structural behavior up to ULS. As shown in Table 4.20, Case 2 shows that the horizontal shear reinforcement of 0.2% assists the flexural reinforcement, resulting in an 18% greater load at the initial yielding of flexural rebar than the load in Case 1, and a 23% increase in maximum load due to increased flexural capacity. The failure modes of both cases were flexural failure, and sufficient shear capabilities were also confirmed. Consequently, the comparison results confirmed that the horizontal shear reinforcement of 0.2% in the STM design of the pier caps does not significantly affect the shear performance, and that sufficient shear performance and structural safety are secured even at the less amount of shear reinforcement in accordance with the proposed STM design guidelines.

### 4.3.2. Crack Propagation

The crack propagation was measured by drawing cracks directly on the surface of the specimens at several loading stages. In the absence of direct crack width measurement, the crack width check for serviceability was conducted with indirect prediction of crack width in design codes and test results. The results of the measurements and their analysis are presented in this chapter.

*4.3.2.1 Case 1*

Figure 4.35 shows the propagation of cracks for Case 1 at each load state. In serviceability limit state (SLS), flexural cracks begin to occur at the top of the inner support areas, as shown in Figure 4.35 (a). The crack widths at the SLS moment are 0.08 mm and 0.13 mm, respectively, for the predictions in KHBDC (2015) and in the test result. The computations are addressed in the Appendix. The width of the crack is less than 0.3 mm, the limit value of allowable crack width at SLS in KHBDC (2015). Therefore, Case 1 satisfies the serviceability for the cracks.

After SLS, additional flexural cracks occur in the inner support area and these flexural cracks propagate to the column until ULS. In Figure 4.35 (b), there is no web shear cracks in Case 1, which means that the shear reinforcement does not play a structural role until ULS.

After the load at ULS, increased load causes web shear cracks in the direction of 45˚ at the area between inner support and outer support where the bending moment is relatively small. The web shear cracks do not make much

progress until the maximum load after propagating to some degree, and the flexural failure occurs without any sudden shear failure.

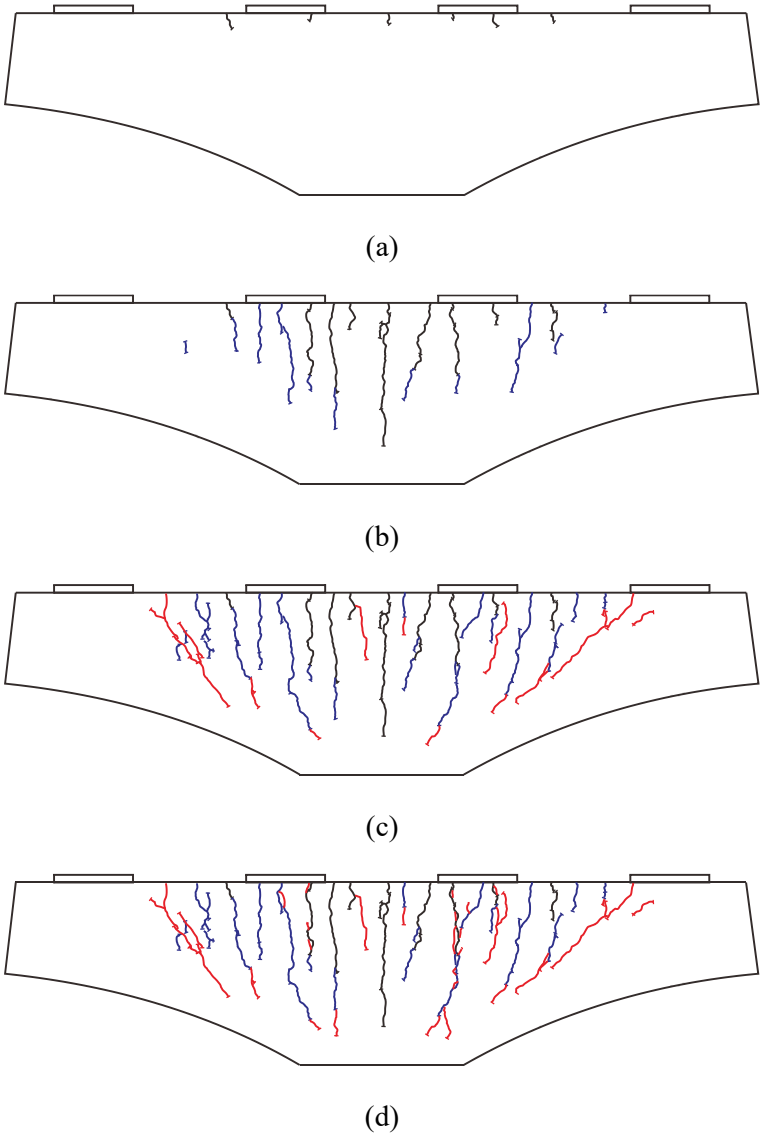

(a)

(b)

(c)

(d)

Figure 4.35 Crack propagation for Case 1: (a) SLS state; (b) ULS state; (c) At 5,000 kN; (d) At maximum load

*4.3.2.2 Case 2*

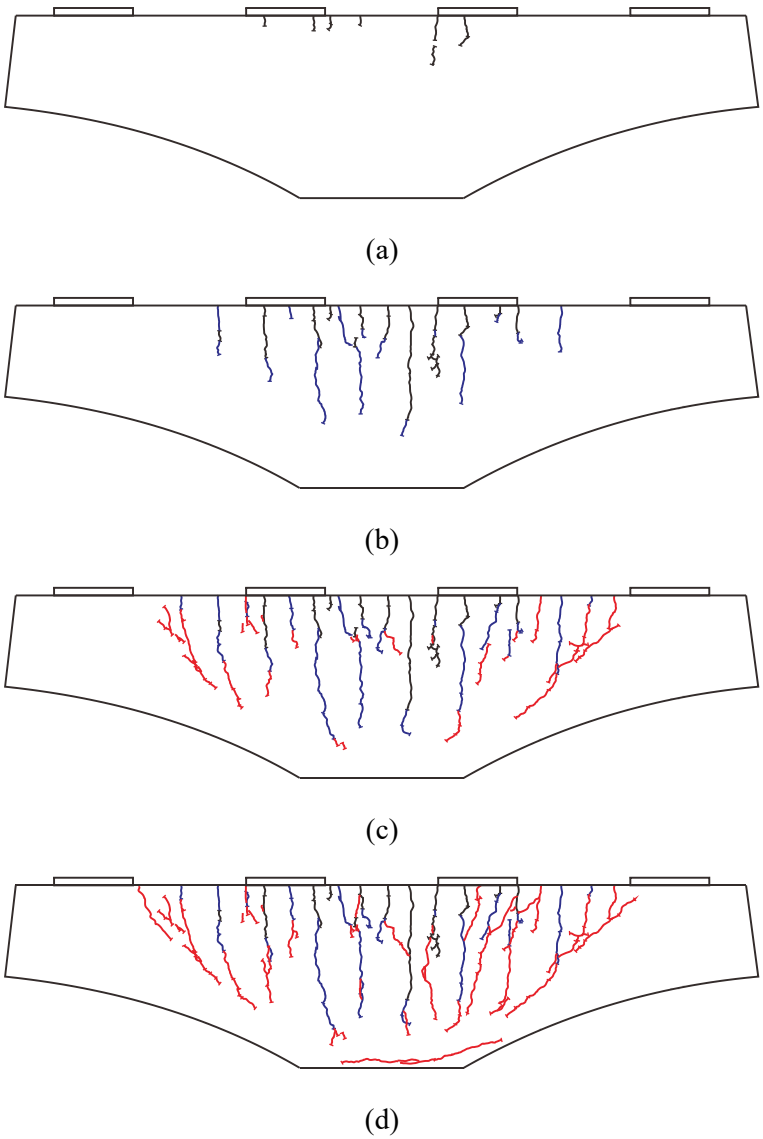


Figure 4.36 Crack propagation for Case 2: (a) SLS state; (b) ULS state; (c) At 5,352 kN; (d) At maximum load

Figure 4.36 indicates the crack propagation in each load stage for Case 2. The pattern of crack propagation in Case 2 is similar to that in Case 1 regardless of horizontal shear reinforcement. Same as in Case 1, cracks also begin to appear as flexural cracks in the area of the inner support at SLS load. At SLS, the predicted crack widths are 0.09 mm and 0.06 mm for the design code and the test result, satisfying the crack width limit of 0.3 mm in KHBDC (2015). Additional flexural cracks occur until ULS, and these flexural cracks progress along the compressive struts to the column. After the ultimate limit state (ULS), diagonal tension cracks are developed and propagate in the direction of 45° at the area between the inner and outer supports until the maximum load. As in Case 1, there is no sudden shear failure and there is a pattern of deep beam behaviors.

The increased flexural resistance capacity by horizontal shear reinforcement results in the ability to resist a larger load. Consequently, as shown in Figure 4.36 (d), the cracks at the bottom of the pier cap advance to the horizontal, resulting in compressive failure of concrete at the bottom of the pier cap.

*4.3.2.3 Case 3*

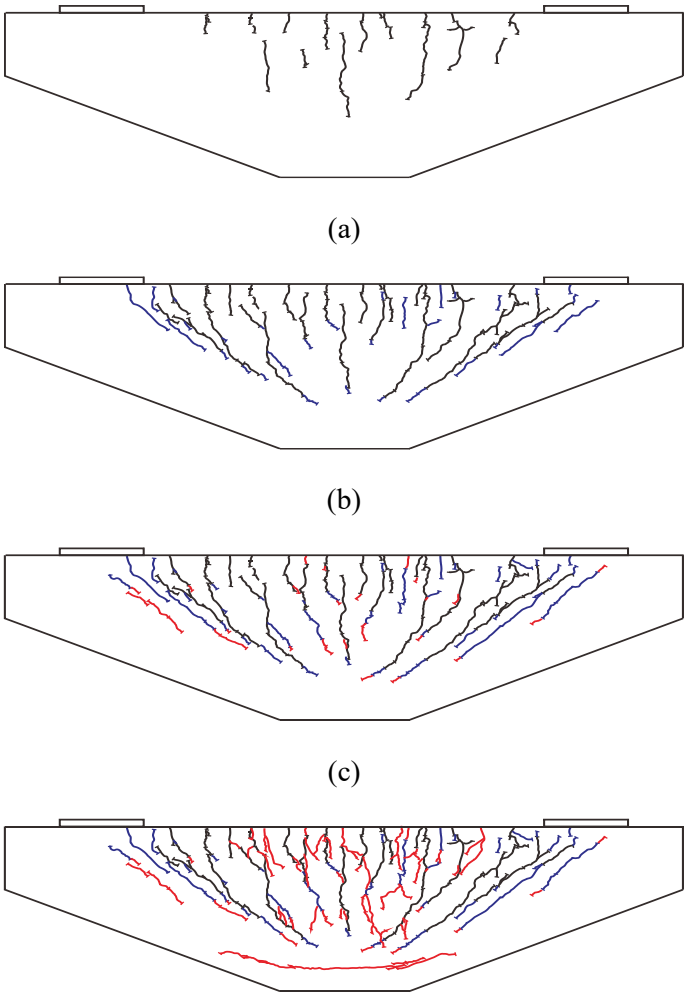

Figure 4.37 Crack propagation for Case 3: (a) SLS state; (b) ULS state; (c) At 4,630 kN; (d) At maximum load

The propagation of cracks for Case 3 is shown in Figure 4.37. The pattern of crack propagation at each load state in Case 3 differs from those of Case 1 and Case 2. Initial cracks begin to appear as flexural cracks in the center of the pier cap. After the initial cracks, these transverse tension cracks propagate vertically to about one-half or more of the sectional depth of the pier cap, causing esthetic issue in serviceability for the cracks. This is because the load is biased, resulting in a larger bending moment at the same total load and earlier flexural cracks. However, in the prospect of crack width, the serviceability is satisfied with the crack widths predicted indirectly in design codes and test. Crack widths are 0.11 mm and 0.30 mm for KHBDC (2015) and the test.

For Case 3, the load transfer from the supports to the column is delivered in full along the compressive struts within the wings of pier cap. Thus, the diagonal tension crack occurs earlier than Case 1 and Case 2 because a larger load is transferred from the wings, even under the same total load. These web shear cracks occur and propagate from the supports to the column until ultimate limit state (ULS) load.

In the loads larger than ULS load, the cracks progress somewhat, but the existing cracks stop making progress as the load increases. There was no sudden shear failure in Case 3 until the maximum load was reached, with a pattern of deep beam behavior. In Case 3, the flexure capacity is high because a large amount of flexural reinforcement corresponding to the biased load is laid out. Thus, the cracks in the horizontal direction at the bottom of the pier cap propagate, resulting in crushing of the bottom part of pier cap concrete.

### 4.3.3. Load-strain Relationship

The measurement results of the strain at the measuring locations representing the behavior of the members were presented for each case. The overall strain histories in all cases correspond to the crack patterns and the load-deflection relationship. The locations of the measured strains are in accordance with Figure 4.23 and Figure 4.24. The measurement results for the entire locations are shown in Appendix C.

*4.3.3.1 Flexural reinforcement*

The relationships of load-strain at the center of the flexural reinforcement of the pier caps, measured in ST-3, are shown in Figure 4.38. The load at the point where the slope of the graph starts to change is the point at which the first crack occurs at the ST-3 position, and the flexural reinforcement at this position is fully under tension force, which increases the strain as the load increases. After the crack at ST-3, the strain increases linearly with increasing load until the rebars begin to yield.

The strains of flexural reinforcement at ULS is approximately 0.0010 for Case 1 and Case 2, about half of the yield strain of 0.0021 obtained from uniaxial tension test of rebar. This means that the flexural reinforcement does not yield until ULS, and the member can sufficiently resistant to the load exceeding ULS load. In Case 3, the strain of flexural rebar at ULS is about 0.0022 because the larger moment occurs in the same total load, and the flexural rebar theoretically yields, although the slope on the graph does not decrease rapidly at the very position.

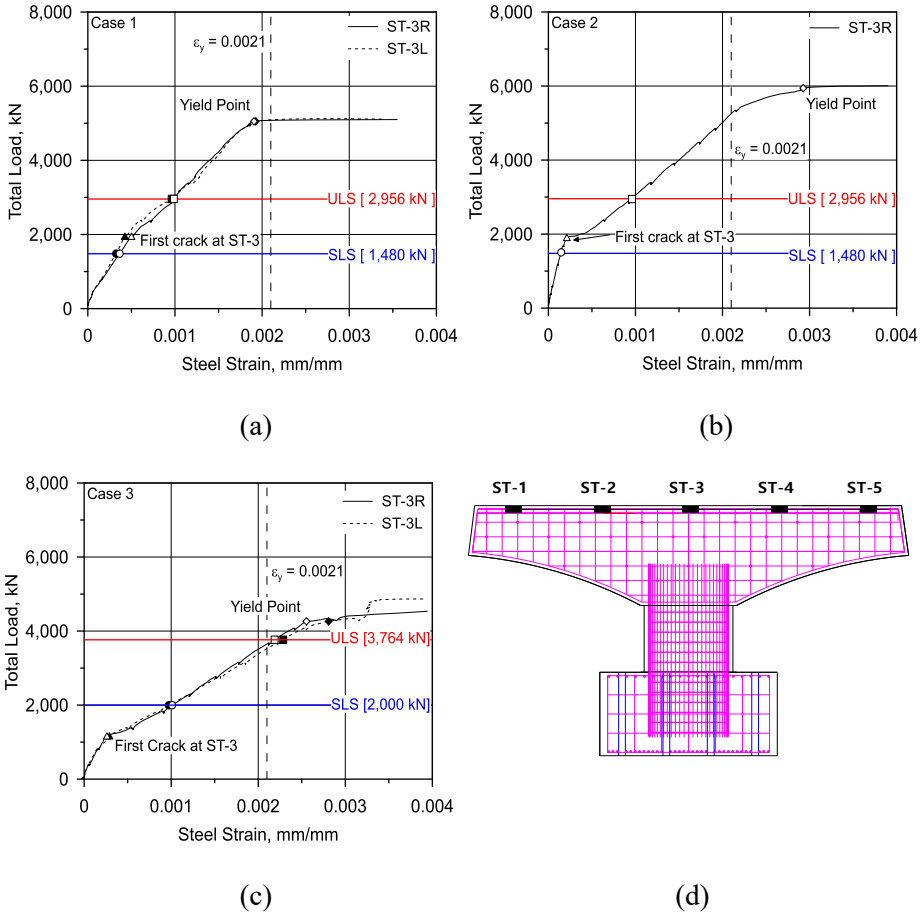


Figure 4.38 Load-strain relationship for flexural reinforcement (ST-3 series):

(a) Case 1; (b) Case 2; (c) Case 3; (d) Location of ST series

*4.3.3.2 Compressive reinforcement*

The load-strain relationship of compressive reinforcement at the bottom of the pier cap, measured at SC-4, is shown in Figure 4.39. SC-2 and SC-4 are the locations where the greatest compressive strain is expected in the finite element analysis results.

The strain of the compressive reinforcement at the center of the pier cap, SC-3, is approximately 0.0001 even for the maximum load, not significantly affected by the structural behavior. In the load-strain curve of the compressive reinforcement, the slope decreases after the first crack and then the slope decreases again at the load where the flexural reinforcement first yields, increasing the rate of compressive strain due to the increase of the load.

In Case 2 and Case 3, the slope tends to decrease significantly depending on the very large increase in compressive strain near the maximum load. However, the magnitude of the compressive strain at this point is far short of the yield strain of the reinforcement, and the cause of rapid increase of compression strain is that the length of plastic hinge with the yield of flexural rebar reaches the location of SC-4, resulting in a large rotational deformation at the location.

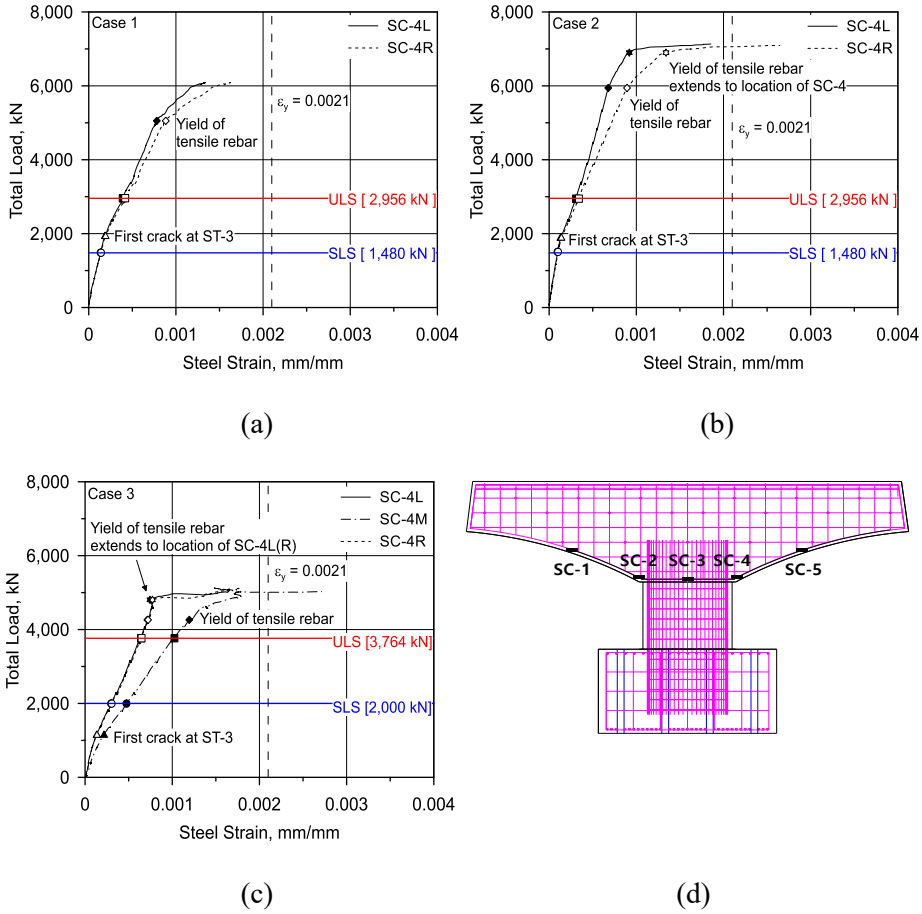


Figure 4.39 Load-strain relationship for compressive reinforcement (SC-4 series): (a) Case 1; (b) Case 2; (c) Case 3; (d) Location of SC series

*4.3.3.3 Column longitudinal reinforcement*

As predicted by the finite element analysis results, the largest compressive strain occurred at SP-1B and SP-3B, the bottom of the area where the pier cap and column meet, as shown in Fig. 4.40. In the location of strain measurement of the column rebar other than SP-1B and SP-3B, little strain occurred.

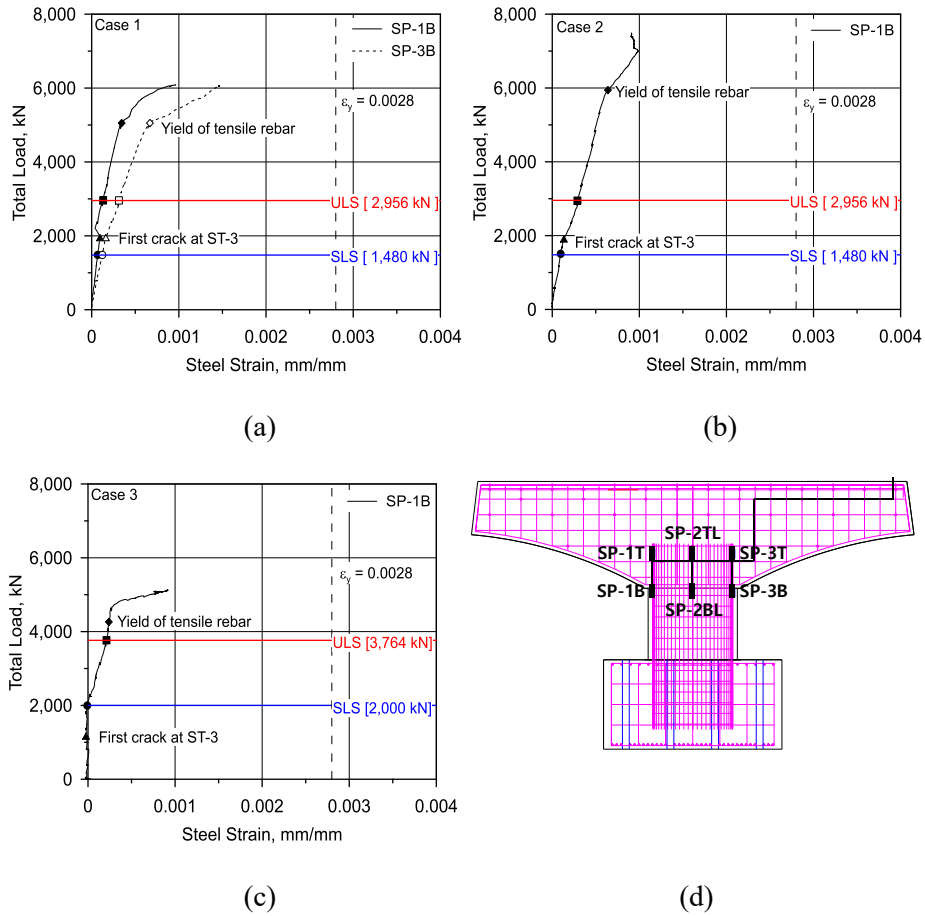


Figure 4.40 Load-strain relationship for column longitudinal reinforcement (SP-1B and SP-3B): (a) Case 1; (b) Case 2; (c) Case 3; (d) Location of SP series

The strain of the column reinforcement to reach the maximum load is up to 0.0015, far below the yield strain of the column reinforcement, 0.0028. This suggests that the compression in the column member is mainly transferred by concrete, so the direct role of the longitudinal reinforcement of the column is relatively small.

*4.3.3.4 Vertical shear reinforcement*

The load-strain relationship of rebar corresponding to the location of web shear cracks among vertical shear reinforcement is shown in Figure 4.41.

In Case 1 and Case 2, no web shear crack was found up to ULS load through the crack patterns. This phenomenon corresponds to the increase of strain at SV-1T after the stagnated increase of strain until ULS, which means that the load mechanism changes to be transferred to the vertical shear reinforcement after the occurrence of the diagonal cracks. The maximum strain of the vertical shear reinforcement at the failure, which is about half of the yield strain, is verified of its sufficient shear capacity of the vertical shear reinforcement designed with the proposed STM guidelines.

In Case 3, web shear cracks occur after SLS, and therefore, the strain of vertical shear reinforcement at the SV-2 shown in Fig. 4.41 (c) rarely occurs until SLS. From then on, the strain takes place, showing a strain of about 0.0005 or more when reaching ULS. Sufficient amount of vertical shear reinforcement is also arranged in Case 3 to prevent shear failure at ULS.

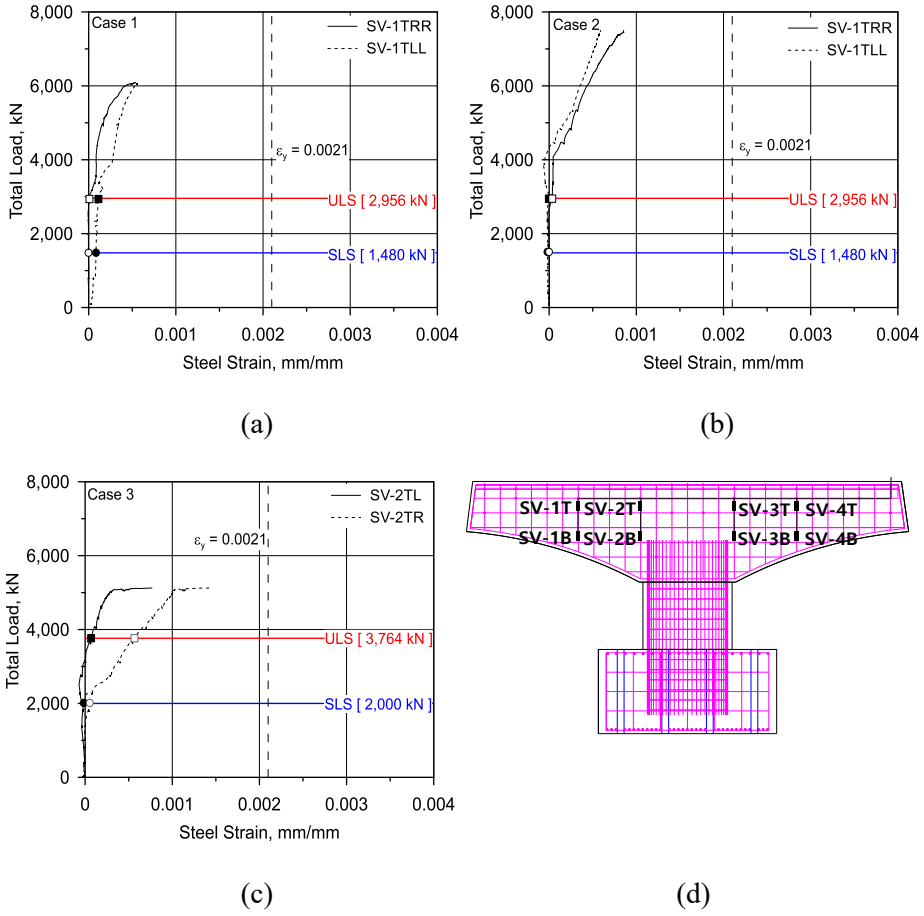


Figure 4.41 Load-strain relationship for vertical shear reinforcement (SV series): (a) Case 1; (b) Case 2; (c) Case 3; (d) Location of SV series

*4.3.3.5 Horizontal shear reinforcement*

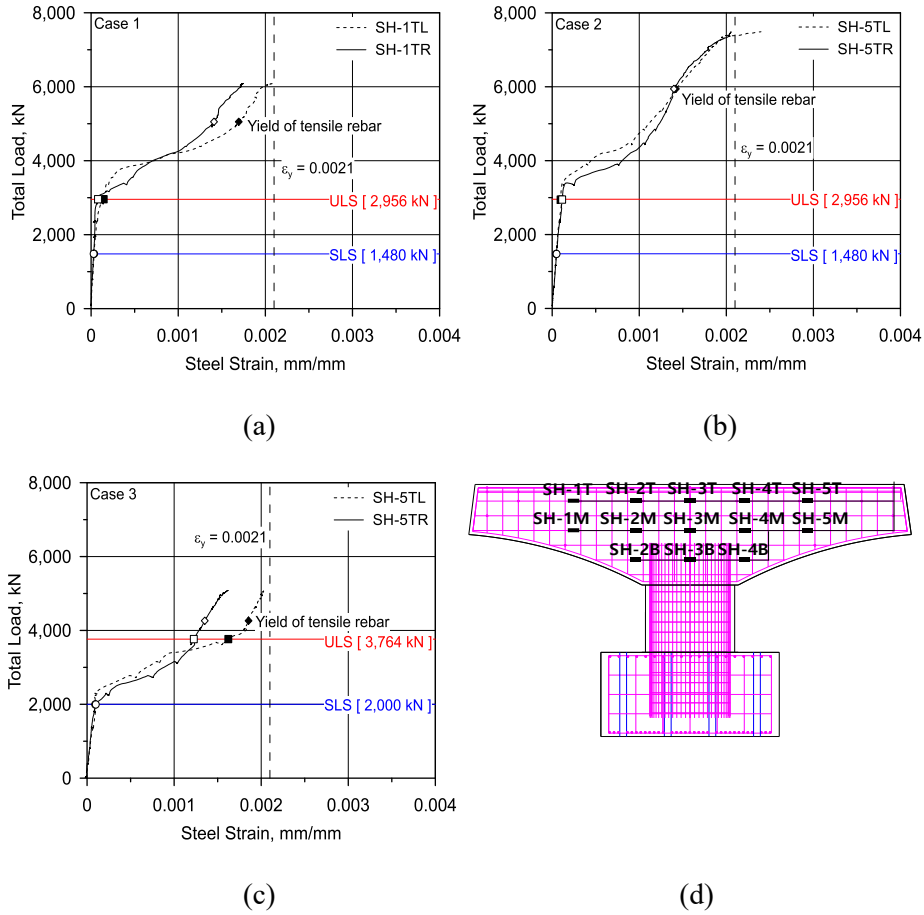


Figure 4.42 Load-strain relationship for horizontal shear reinforcement (SH series): (a) Case 1; (b) Case 2; (c) Case 3; (d) Location of SH series

The results of the measurement of the strain at SH-1T and SH-5T, the locations where diagonal crack occurs, are shown in Fig. 4.42.

The load-strain relationship of horizontal shear reinforcement is similar to that of flexural reinforcement. After the first crack, strain rarely occurs until a flexural crack additionally occurs in the area of the shear critical section, and then the strain increases after the occurrence of additional flexural cracks. The horizontal shear reinforcement of the upper part complements the flexural rebar to resist the bending moment and starts to yield when it approaches the maximum load after the first yield of the flexural reinforcement. In other words, the horizontal shear reinforcement improves flexural resistance and thus resists to a greater load. For the increased horizontal shear reinforcement in Case 2, the strain shows smaller than Case 1 at the same load state.

*4.3.3.6 Column concrete*

Fig. 4.43 shows the results of measurement of concrete compressive strain at CP-1 and CP-5 where the greatest compressive stress occurs among the column concrete. At CP-3 locations, concrete compression strain seldom occurred. However, at the location under large compressive stress where the pier cap and the column meet, there was a trend of column concrete strain similar to the compressive strain of the longitudinal reinforcement of the column. In all cases, the maximum compressive strain does not exceed 0.0018, the compressive strain at the maximum compressive strength obtained from the compressive strength test of the concrete, so no crushing in column concrete occurred until failure.

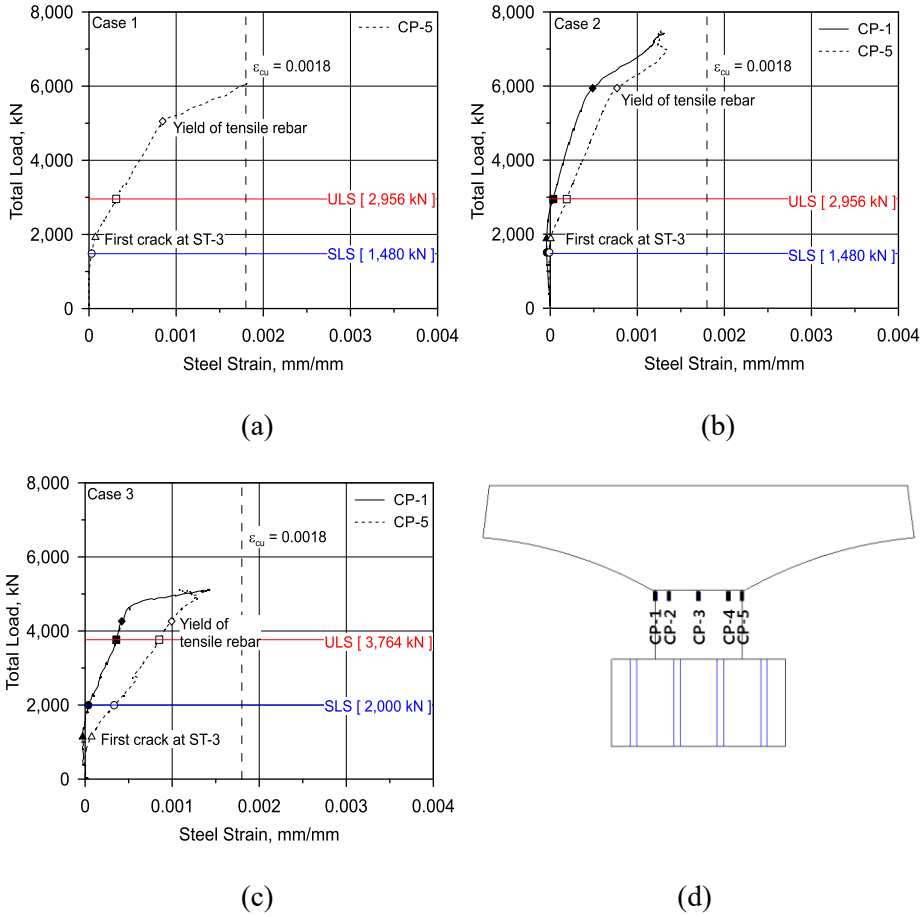


Figure 4.43 Load-strain relationship for column concrete (CP series): (a) Case 1; (b) Case 2; (c) Case 3; (d) Location of CP series

*4.3.3.7 Pier cap concrete*

Fig. 4.44 presents the measurement results of the concrete compressive strain at the central location of the pier cap width showing the largest compressive strain among CC-B1 and CC-B3, a position corresponding to the corner of the pier cap bottom.

Until ULS, the compressive strain is below 0.0005 and it is confirmed that the compression in concrete is sufficiently resistant to the ULS load. The strain is then increased as the load increases, and the compressive strain at the maximum load is shown of 0.0018 or so, the compressive strain at the compressive strength according to the cylinder test. In Case 2 and Case 3, cracks in horizontal direction occurred and advanced at the bottom of the pier cap concrete prior to the failure. Therefore, concrete in the cracked area was not able to transfer the compression properly, and even the strains of the graphs went back again.

As such, it was possible to identify the load-strain relationship of rebar and concrete at each location of the members, and the evaluation verified that they have sufficient load resistance capacities exceeding the ultimate limit state (ULS) loads in all cases.

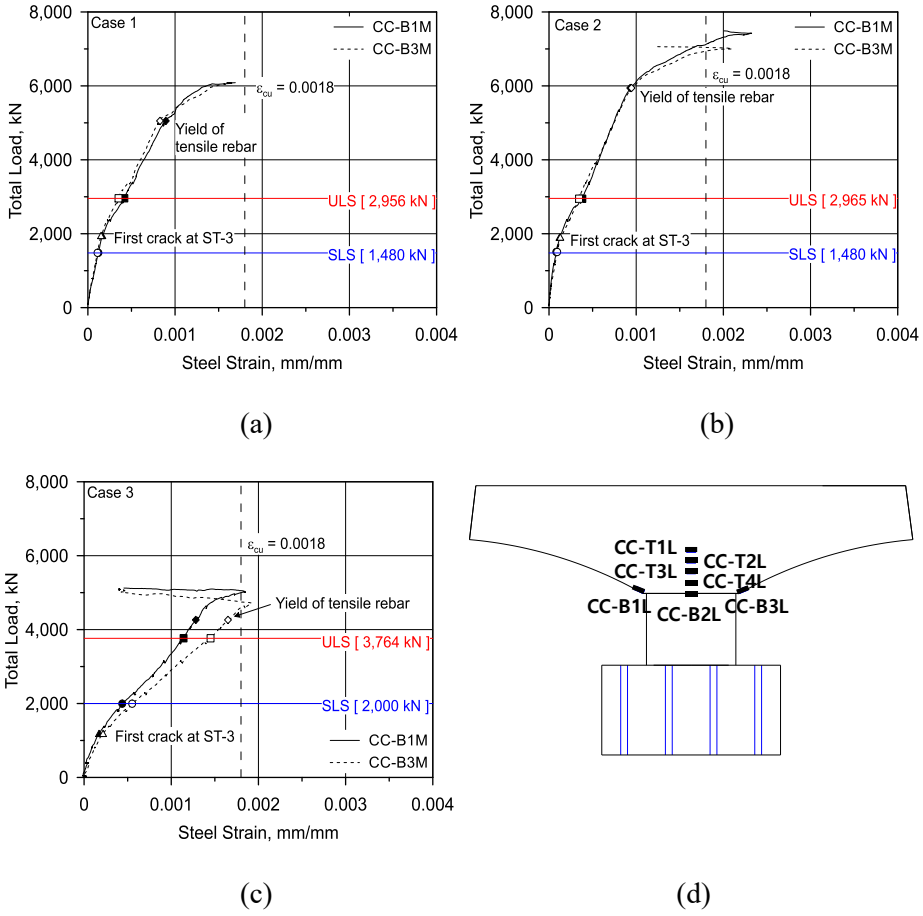


Figure 4.44 Load-strain relationship for pier cap concrete (CC series): (a) Case 1; (b) Case 2; (c) Case 3; (d) Location of CC series

### 4.3.4. STM Predictions

The load resistance capacities for experimental cases were compared with the predictions in the STMs. For the STM predictions, ACI 318-19 was considered. It is noted that the strength reduction factor was not considered when the capacities were evaluated by the design code. Also, the material strengths obtained from the tests were used to evaluate the loads at the predictions.

As presented in Table 4.21, the capacities of the cases from the STM were governed by the yielding of the vertical tie, not the yielding of the tensile tie. Consequently, the predictions in the STMs show failures in shear for three cases. However, the actual failures were dominated by flexure in the test results, corresponding to the flexural strengths from the sectional analyses. The STM predictions for tensile ties, also, well correspond to the maximum loads from the test with the errors below 11 percent, rather than the predictions for vertical ties. This phenomenon occurred because the STMs under-estimate the shear strength of pier caps. For shear strength of RC member, the contribution of concrete cannot be ignored. The STM design concept in the pier caps, however, does not consider the role of concrete in shear, assuming that all shear is resisted by vertical ties in truss mechanism.

In the test, the shear strengths of the pier caps could not be captured because of the dominant flexural failure mode. For the understanding of shear in pier cap, additional parametric analyses with FE analysis shall be conducted.

Table 4.21 Comparison of the test with STM predictions

| Case | $P_{Max}$ (kN) | $P_{SA}$ (kN) | STM predictions (kN) | | | $\frac{P_{Tensile\ tie}}{P_{Max}}$ | $\frac{P_{Vertical\ tie}}{P_{Max}}$ | Failure mode |
|---|---|---|---|---|---|---|---|---|
| | | | $P_{Tensile\ tie}$ | $P_{Strut}$ | $P_{Vertical\ tie}$ | | | |
| 1 | 6,086 | 6,240 | 5,474 | 15,868 | 4,815 | 0.90 | 0.79 | Flexure |
| 2 | 7,490 | 7,304 | 6,883 | 14,509 | 4,815 | 0.92 | 0.64 | Flexure |
| 3 | 5,125 | 5,133 | 5,684 | 10,381 | 4,765 | 1.11 | 0.93 | Flexure |

## 4.4. Concluding Remarks

In this chapter, the static loading test of scaled-model specimens with a length scale factor of 2/5 was performed to verify the validity of the STM design guidelines for efficient rebar arrangement of bridge pier cap. Through the experiment, structural behaviors such as load-deflection relationship, crack propagation patterns, and strains at the elements were measured and analyzed. Summary of the test results is as follows.

1. Through the load-deflection relationships in all cases, it was confirmed that the flexural failure mode with ductile behavior was secured, not the sudden brittle shear failure, in members with shear reinforcement satisfying the proposed design guidelines. All cases designed with the guidelines exert load resistance capacities exceeding ULS load. However, in the absence of the selection of proper sectional depth in pier cap dimension considering the superstructure and their loading position before STM design, the design safety factor of each case showed a large discrepancy.

2. For all cases, serviceability for the crack width at SLS was satisfied. Although, Case 3 failed to properly select the sectional depth taking the loading position into account prior to the STM design, leading to the premature cracks. And these flexural cracks considerably propagate until SLS. The propagation pattern of the crack at each limit state was different depending on the loading position, but the proper amount of shear reinforcement resulted in no sudden brittle failure after diagonal shear cracks and reached flexural failure.

3. The strains of rebar and concrete at the monitoring locations of the members were measured and the behaviors of the member were analyzed more closely. The analysis results confirmed that the shear performance of the shear rebar arranged based on the guidelines is sufficient until ULS without the occurrence of shear failure.

4. The load resistance capacities from test results were compared with the STM predictions. The STMs do not consider the effect of concrete in shear because of their design concept. Thus, the STM predictions under-estimate the shear strengths of the pier caps, causing a wrong predictions of failure mode and the member's strength. The STM prediction results confirmed that the shear performance of the pier cap shall be appropriately evaluated to find out the proper failure in the member.

In conclusion, the pier caps designed with the proposed STM design guidelines ensure structural safety and can induce more efficient reinforcement so as to prevent problems such as low constructability and economical degradation due to the excessive arrangement of rebars in the pier caps. However, prior to the STM design, it is necessary to ensure consistent design safety factor. This limit is able to be cleared through the selection of appropriate pier cap section depth. Proper way to figure out the failure of pier cap in STM prediction is also needed.

# V. Analytical Study

## 5.1. Introduction

Scaled-model test in Chapter 4 confirmed the structural feasibility of the proposed STM design guidelines for efficient reinforcement in bridge pier cap. Through the experiment, structural feasibility such as shear performance and load resistance capacity in the design of pier caps with the guidelines was secured. However, it was also confirmed that variables such as sectional depth and loading positions may affect design safety factors, crack serviceability in SLS, and in some cases may be problematic in design. Parametric studies understanding the shear strength of pier cap are also required. Thus, further analysis of these variables is required. Due to the constraints in the test, there is a limit to the analysis of variables with the test alone. To overcome the constraints of experiment and verify the validity of the test results, verification of the experiment and parametric analysis were performed through the commercial finite element analysis programs, DIANA and VECTOR 2.

First, FE models were selected to simulate the scaled-model specimens. The validity of the FE model was verified by comparing with the test results. Subsequently, analyses of additional variables such as sectional depth of pier cap and the amount of reinforcement were conducted using verified FE models. Chapter 5.2 introduced verification of the FE model, and Chapter 5.3 proposed revised design guidelines that allow appropriate sectional depth based on the analysis of variables and results with respect to sectional depth. Also, proper way to predict shear strength of pier cap in STM design was guided.

## 5.2. FE Analysis for Verification of FE Model

### 5.2.1 Geometry Model

A total of three cases of bridge pier caps were used in the test on scaled models in Chapter 4. 3-D analyses were performed in DIANA, a commercial finite element analysis program, for verification of scaled model test. Additional verification with 2-D analyses by VECTOR 2 was conducted for increased analytical reliability and ease of parametric analyses.

To simulate the experiment, specimens of bridge pier cap and steel support bearings were modelled in FE modeling. In DIANA, concrete members and steel plates were modeled as 8-node solid elements in 3-D, simulating details such as rebar arrangement intervals to the thickness direction of the pier cap. In VECTOR 2, the 4-point plane stress rectangle and the 3-point constant strain triangle in 2-D were modelled and the total amount of rebar to the thickness direction was assigned in the models. DIANA used the embedded bar element to simulate separate rebar. Similarly, in VECTOR 2, the 2-node truss bar element was used to simulate each rebar. Full composite behavior between concrete and rebar is assumed in all FE models. For DIANA, the specimens were modeled as quarter models shown in Figure 5.1 (a), considering the symmetry of pier cap, since the analysis is relatively more time-consuming with the 3-D higher powered elements. For VECTOR 2, the entire specimens were fully modelled because the analysis was relatively less time-consuming with a 2-D low powered element. Based on the results of DIANA analysis, the

basements were not modeled, but were imitated by attaching boundary conditions at the bottom edge of the column.

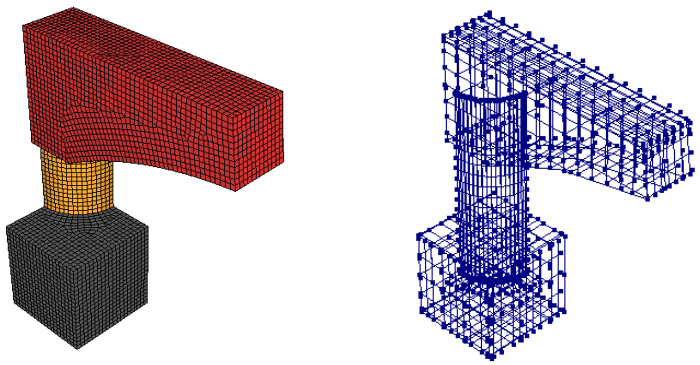

(a)

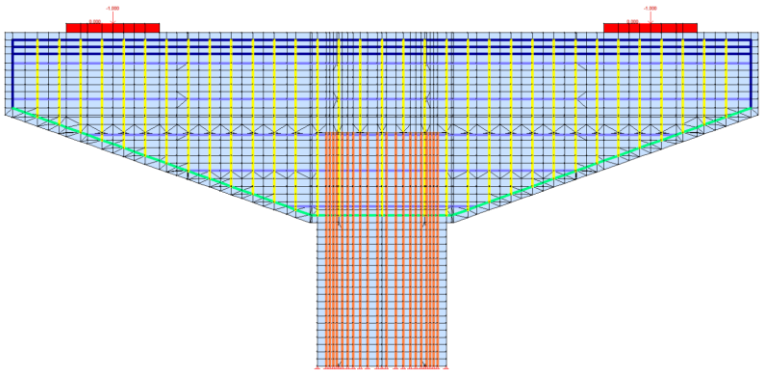

(b)

Figure 5.1 Geometry model of the finite element analysis: (a) DIANA; (b) VECTOR 2

### 5.2.2 Material Model

*5.2.2.1 Concrete*

For material model of concrete, smeared crack model and rotating crack model were selected because it is difficult to predict and model cracks in advance by simulating the heterogeneity of concrete and cracking patterns caused by rebar. And total strain-based crack model was used for stable analysis of three-dimensional solid elements. In VECTOR 2, crack widths were calculated in the basis of DSFM for the cracked concrete, using a post-processing program called Augustus.

The compressive model of concrete used the Thorenfeldt model given in Equation 5.2 that can be simulated with given material properties, and the tensile model used the linear-ultimate crack strain model considering the effect of tension stiffening, which is the tensile resistance capability of concrete after tensile strength. In the case of the compressive model, the coefficients in the model were adjusted to fit in the s-s curve obtained from the compressive strength test of concrete. Since concrete tensile strength was not tested separately, the average tensile strength of concrete presented in KHBDC (2015) Equation 5.5.6, given in Equation 5.1, was approximated using the concrete compressive strength obtained with the cylinder tests. The ultimate strain in tension stiffening model of 0.0002 was obtained from the iterative attempts for better predicting the initial stiffness and the initial crack in the tests.

$$f_{ct} = 0.30\left(f_{cu}\right)^{2/3} \tag{5.1}$$

$$\frac{f_c}{f_c'} = \frac{n\left(\frac{\varepsilon_c}{\varepsilon_{co}}\right)}{(n-1)+\left(\frac{\varepsilon_c}{\varepsilon_{co}}\right)^{nk}} \tag{5.2}$$

Table 5.1 Coefficients in Thorenfeldt model to fit into the test results

| Class | Case | $f_{cu}$ (MPa) | $f_{ct}$ (MPa) | $n$ | $k$ | $\varepsilon_{co}$ (x$10^{-3}$) |
|---|---|---|---|---|---|---|
| Pier cap | 1 | 35 | 3.21 | 3.15 | 1.32 | 2.10 |
| | 2 | 32 | 3.02 | 3.10 | 1.30 | 2.00 |
| | 3 | 36 | 3.27 | 3.15 | 1.32 | 2.05 |

*5.2.2.2 Reinforcement*

In order to verify the strains of rebar at each location of components in the test, each rebar was simulated using the discrete reinforcement element in FE model. To model rebar, the embedded reinforcement bar type was used in DIANA. In VECTOR 2, each bar was modeled using truss bar type. For all rebar models in FE analysis, a fully composite behavior of concrete and rebar is assumed. In DIANA, the stress-strain relationships of rebar obtained from the test were directly represented in Von Mises plasticity model, simulating the constitutive behavior of elastoplastic material model with hardening. In VECTOR 2, Elastic Hardening (Curvilinear) model with the test results of stress-strain relationship was used to simulate the yield and hardening behaviors.

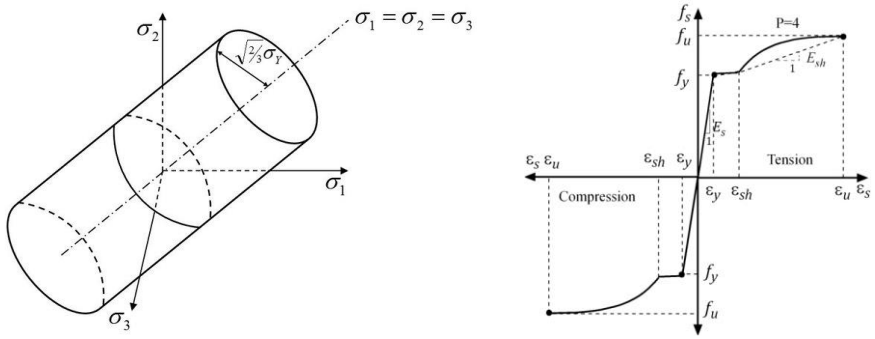


(a) (b)

Figure 5.2 Plasticity model for reinforcement: (a) Von mises plasticity model; (b) Elastic hardening(Curvilinear) model (Wong et al. 2013)

*5.2.2.3 Steel Plate*

In DIANA, the load was applied directly onto the top of the pier cap without modeling the steel plate, separately. On the other hand, VECTOR 2 simulates a steel plate using a structural steel model to take into account the thickness of the steel plate in a two-dimensional analysis.

### 5.2.3 Boundary Conditions

Boundary conditions were assigned to simulate the test environment. In the case of DIANA, the bottom face of the basement was constrained in all directions to constraint horizontal and vertical movement. In addition, the quarter models also imposed constraints in each direction on the boundaries of the quarter models. For VECTOR 2, the basement was not modeled separately, so the bottom edge of the column was similarly restrained in all directions to limit horizontal and vertical movement.

### 5.2.4 Analysis Results

The load-deflection relationship, crack propagation, and rebar strain for each case measured in the experiment were compared with the results obtained from the FE analysis.

*5.2.4.1 Load-deflection relationship*

The load-deflection relationship in the FE analysis, comparing with the experimental results, is shown in Figure 5.3, Table 5.2, Table 5.3 and Table 5.4. Both results from DIANA and VECTOR 2 tended to be larger in initial stiffness than experimental results, and generally well predicted the behaviors in the experiment. Both FE analyses also showed quite similar behavior before the yield of tensile rebar. In DIANA, the load tends to decrease rapidly without properly simulating the ductile behavior of the member after the yield of flexural reinforcement. Due to differences in initial stiffness, the deflection of the members in the FE analysis varies somewhat from the experimental results, but the load in each state varies within 10 percent of the test results. Through the comparisons, the feasibility of the FE analysis results to verify the structural safety and serviceability of the pier caps was validated.

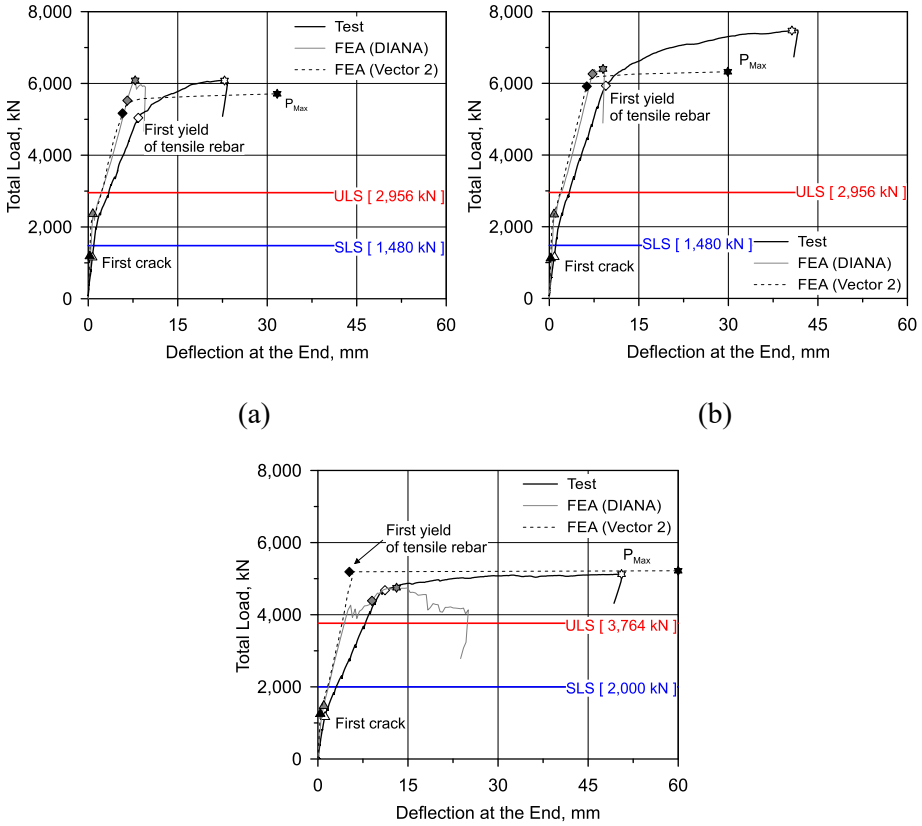


Figure 5.3 Load-deflection curve of the FE analyses: (a) Case 1; (b) Case 2; (c) Case 3

Table 5.2 Compassion of the test and FE analysis (Case 1)

| State | Total load (kN) | | | | | Deflection (mm) | | | | |
|---|---|---|---|---|---|---|---|---|---|---|
| | DIANA | VEC.2 | Test | FEA / Test | | DIANA | VEC.2 | Test | FEA / Test | |
| | | | | DIANA | VEC.2 | | | | DIANA | VEC.2 |
| First crack | 2,400 | 1,224 | 1,190 | 2.02 | 1.03 | 0.8 | 0.2 | 0.7 | 1.14 | 0.29 |
| SLS | 1,480 | | | - | | 0.5 | 0.3 | 1.0 | 0.50 | 0.30 |
| ULS | 2,956 | | | - | | 2.2 | 2.1 | 3.5 | 0.63 | 0.60 |
| First yield | 5,525 | 5,168 | 5,050 | 1.09 | 1.02 | 6.6 | 5.7 | 8.4 | 0.79 | 0.68 |
| Max. load | 6,086 | 5,712 | 6,086 | 1.00 | 0.94 | 7.6 | 31.7 | 22.6 | 0.34 | 1.40 |

Table 5.3 Compassion of the test and FE analysis (Case 2)

| State | Total load (kN) | | | | | Deflection (mm) | | | | |
|---|---|---|---|---|---|---|---|---|---|---|
| | DIANA | VEC.2 | Test | FEA / Test | | DIANA | VEC.2 | Test | FEA / Test | |
| | | | | DIANA | VEC.2 | | | | DIANA | VEC.2 |
| First crack | 2,383 | 1,156 | 1,192 | 2.00 | 0.97 | 0.8 | 0.2 | 0.7 | 1.14 | 0.29 |
| SLS | 1,480 | | | - | | 0.5 | 0.3 | 1.0 | 0.50 | 0.30 |
| ULS | 2,956 | | | - | | 2.2 | 1.8 | 3.5 | 0.63 | 0.52 |
| First yield | 6,263 | 5,916 | 5,943 | 1.05 | 1.00 | 7.2 | 6.3 | 9.5 | 0.76 | 0.66 |
| Max. load | 6,402 | 6,324 | 7,490 | 0.85 | 0.84 | 9.0 | 29.9 | 41.6 | 0.22 | 0.72 |

Table 5.4 Compassion of the test and FE analysis (Case 3)

| State | Total load (kN) | | | | | Deflection (mm) | | | | |
|---|---|---|---|---|---|---|---|---|---|---|
| | DIANA | VEC.2 | Test | FEA / Test | | DIANA | VEC.2 | Test | FEA / Test | |
| | | | | DIANA | VEC.2 | | | | DIANA | VEC.2 |
| First crack | 1,500 | 1,290 | 1,200 | 1.25 | 1.08 | 1.0 | 0.4 | 1.2 | 0.83 | 0.33 |
| SLS | 2,000 | | | - | | 1.9 | 1.6 | 3.2 | 0.59 | 0.50 |
| ULS | 3,764 | | | - | | 4.5 | 4.0 | 8.0 | 0.56 | 0.50 |
| First yield | 4,390 | 5,190 | 4,680 | 0.94 | 1.11 | 9.0 | 5.2 | 11.2 | 0.80 | 0.46 |
| Max. load | 4,750 | 5,219 | 5,125 | 0.93 | 1.02 | 13.1 | 60.0 | 50.6 | 0.26 | 1.19 |

*5.2.4.2 Crack propagation*

Propagation in cracks obtained from FE analysis was compared with experimental results. Figure 5.4, Figure 5.5, and Figure 5.6 overlaps the crack patterns of DIANA and VECTOR 2 to the patterns from the experiment. Cracks marked with black solid lines are cracks measured in the experiment. The left half is crack in VECTOR 2 and the right half is crack in DIANA.

Comparing the crack patterns at SLS, ULS, and maximum load in all cases, FE analyses confirmed that the progress of the crack pattern measured in the experiment was well predicted. The comparison results ensured the validity of the FE analyses as verification methods for assessing the serviceability of cracks.

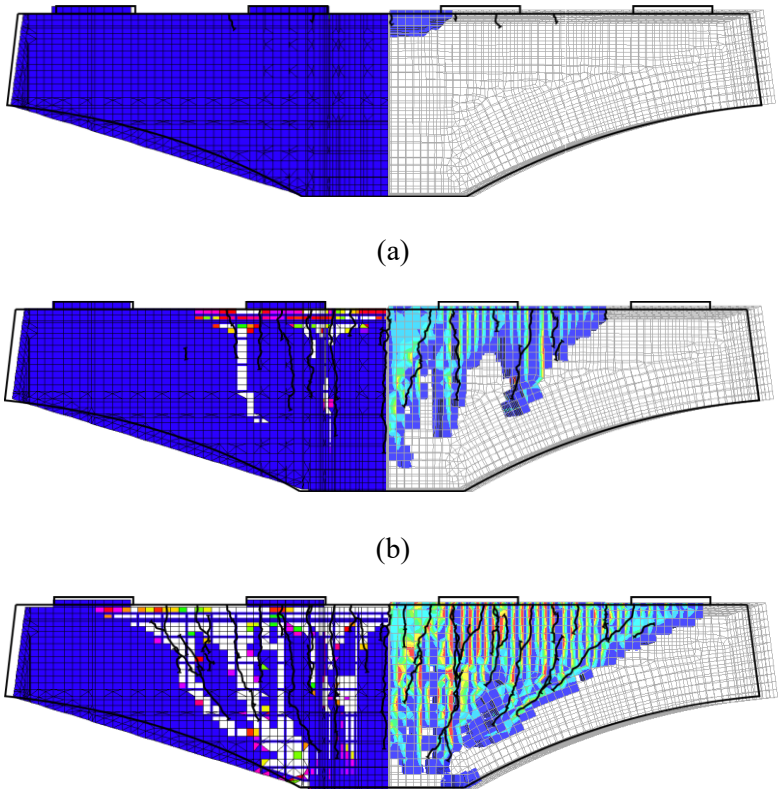

(a)

(b)

(c)

Figure 5.4 Crack in FEA(DIANA) for Case 1: (a) SLS state; (b) ULS state; (c) At maximum load

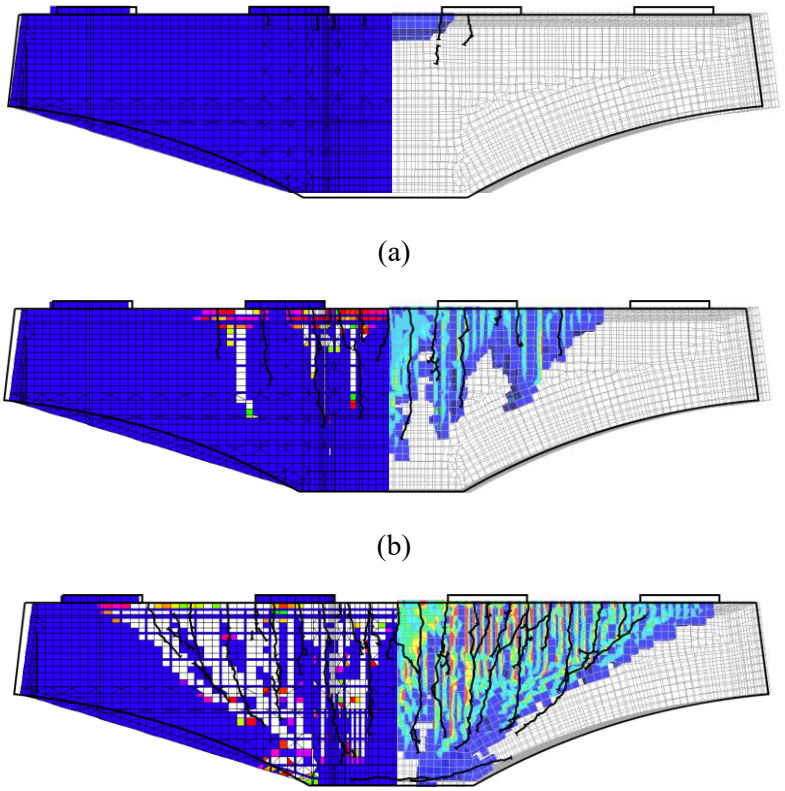

(a)

(b)

(c)

Figure 5.5 Crack in FEA(DIANA) for Case 2: (a) SLS state; (b) ULS state; (c) At maximum load

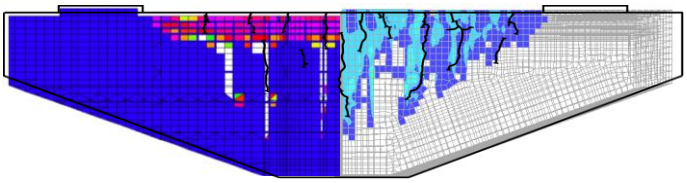

(a)

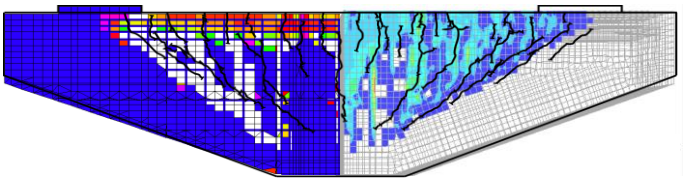

(b)

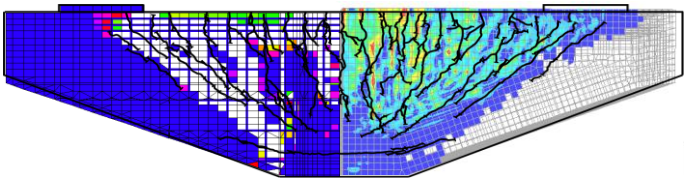

(c)

Figure 5.6 Crack in FEA(DIANA) for Case 3: (a) SLS state; (b) ULS state; (c) At maximum load

*5.2.4.3 Strain of reinforcing steel bar and concrete*

The load-strain relationship of each location of rebar according to the DIANA is shown together with the experimental results as follows. As shown in Figure 5.7, in the case of ST-3, center of tensile reinforcement, FE analysis results show greater initial stiffness than that of the experimental results. As in the test, the strain from DIANA shows decrease in the slope after initial crack, increasing the strain only without increasing the load after yielding.

For SC-4 with the largest compressive strain at the compressive rebar of the pier cap, the analysis results well illustrate the strain increase tendency in the experiment shown in Figure 5.8. The concrete strain at the bottom of the pier cap shown in Figure 5.13 is also good at predicting the test results, and the compressive strains of rebar and concrete in the adjacent locations such as SC-4 and CC-B3M show quite similar tendencies, showing composite behavior.

In Figure 5.10 and 5.11, strains of the vertical and horizontal shear rebar near diagonal cracks, as in the results of experiment, starts to produce tensile strain after ULS in Case 1 and Case 2, and for Case 3, the strain occurs after SLS load.

The strain of column longitudinal rebar and column concrete from FE analysis shown in Figure 5.9 and Figure 5.12, respectively, is similar to the experimental value. The strains of rebar and concrete in adjacent locations designated as SP-3B and CP-5 are very similar because of composite behavior.

Consequently, structural safety of specimen was also verified through the comparison of test and FE analysis results of steel and concrete strains at the major locations.

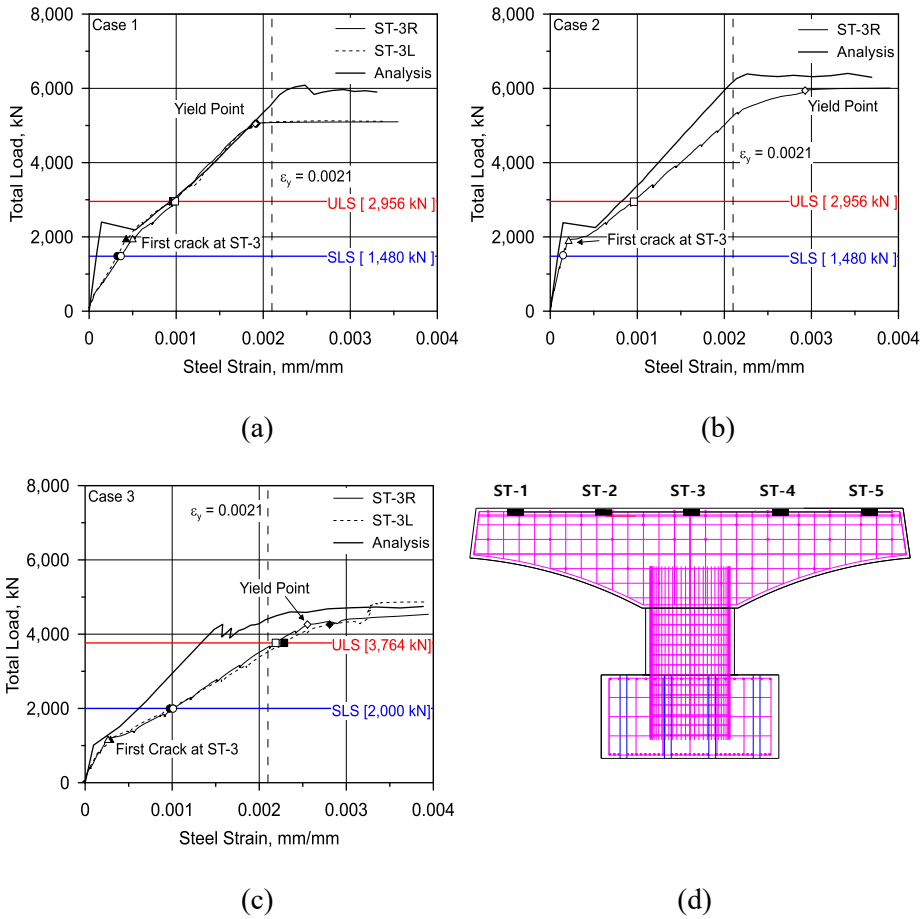


Figure 5.7 Load-strain relationship for flexural reinforcement (ST-3 series): (a) Case 1; (b) Case 2; (c) Case 3; (d) Location of ST series

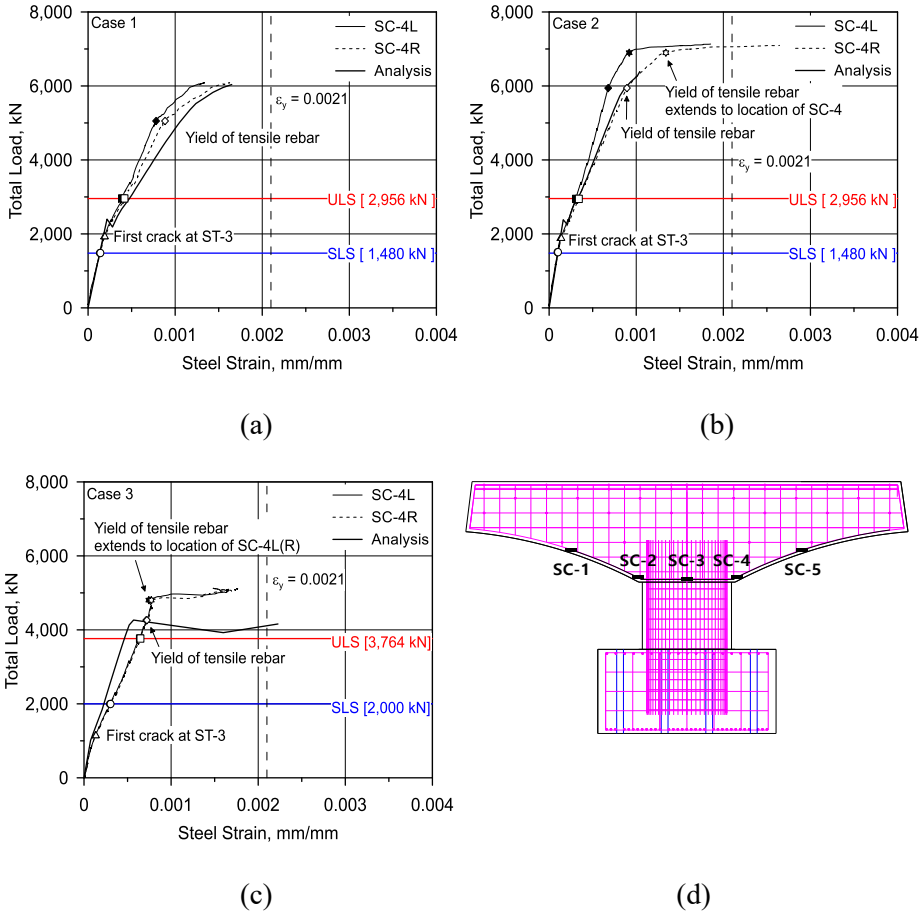


Figure 5.8 Load-strain relationship for compressive reinforcement (SC-4 series): (a) Case 1; (b) Case 2; (c) Case 3; (d) Location of SC series

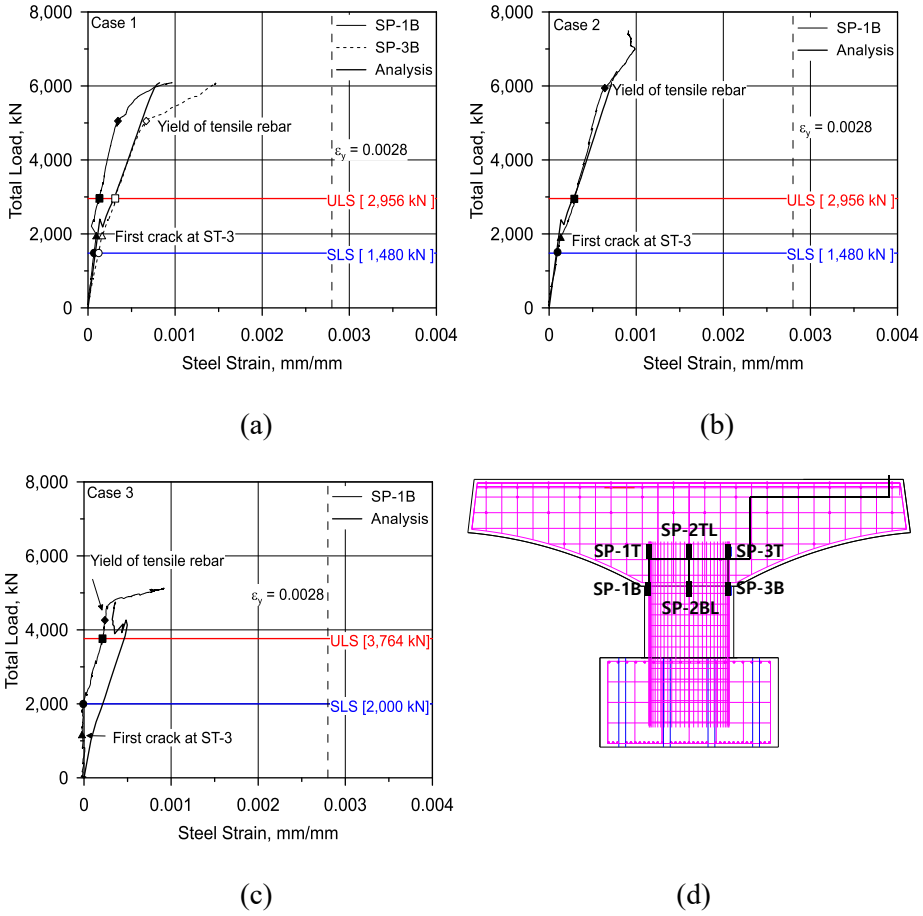


Figure 5.9 Load-strain relationship for column longitudinal reinforcement (SP-1B and SP-3B): (a) Case 1; (b) Case 2; (c) Case 3; (d) Location of SP series

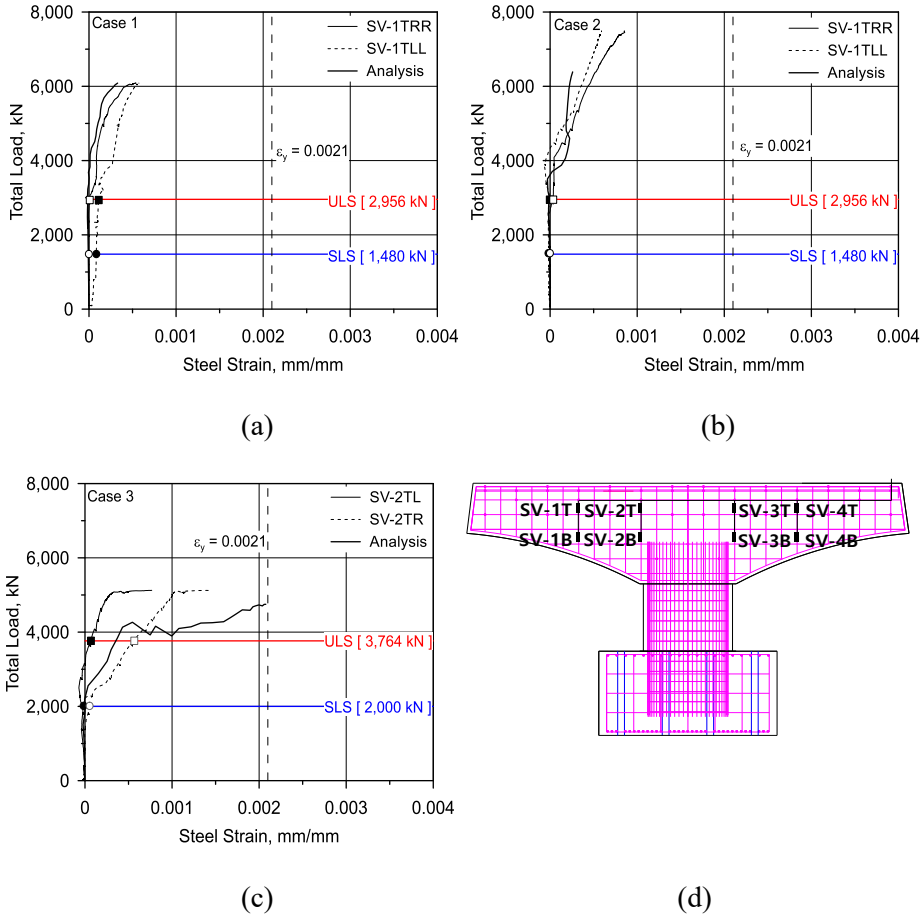


Figure 5.10 Load-strain relationship for vertical shear reinforcement (SV series): (a) Case 1; (b) Case 2; (c) Case 3; (d) Location of SV series

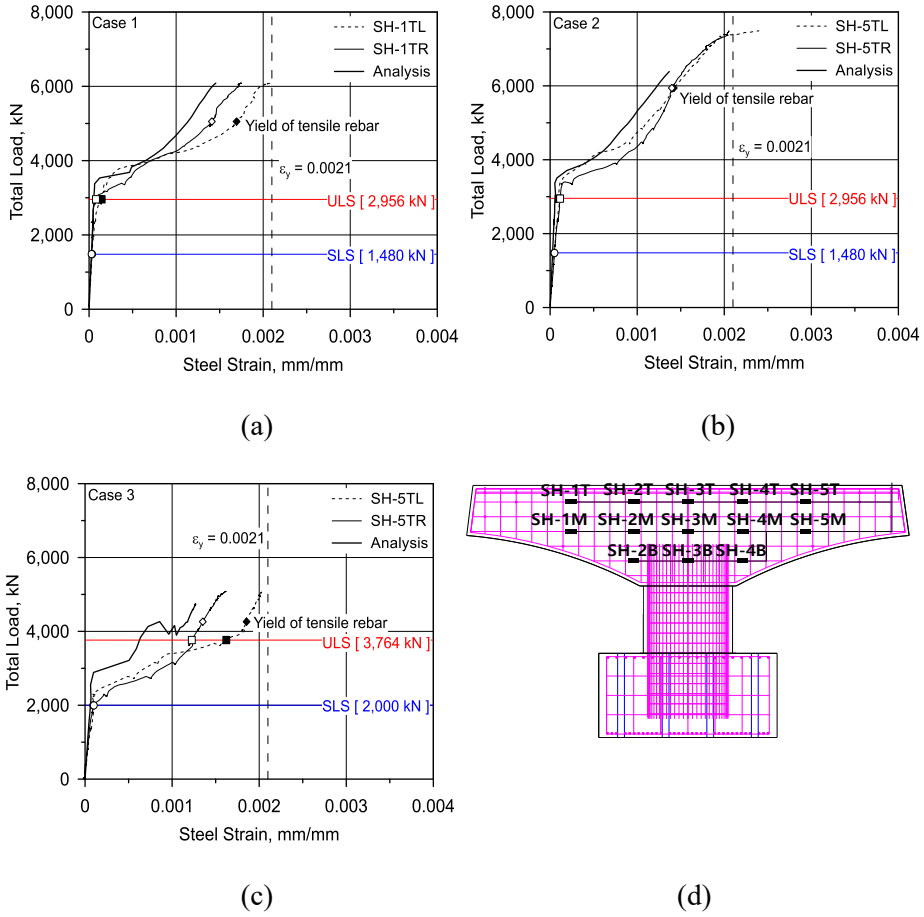


Figure 5.11 Load-strain relationship for horizontal shear reinforcement (SH series): (a) Case 1; (b) Case 2; (c) Case 3; (d) Location of SH series

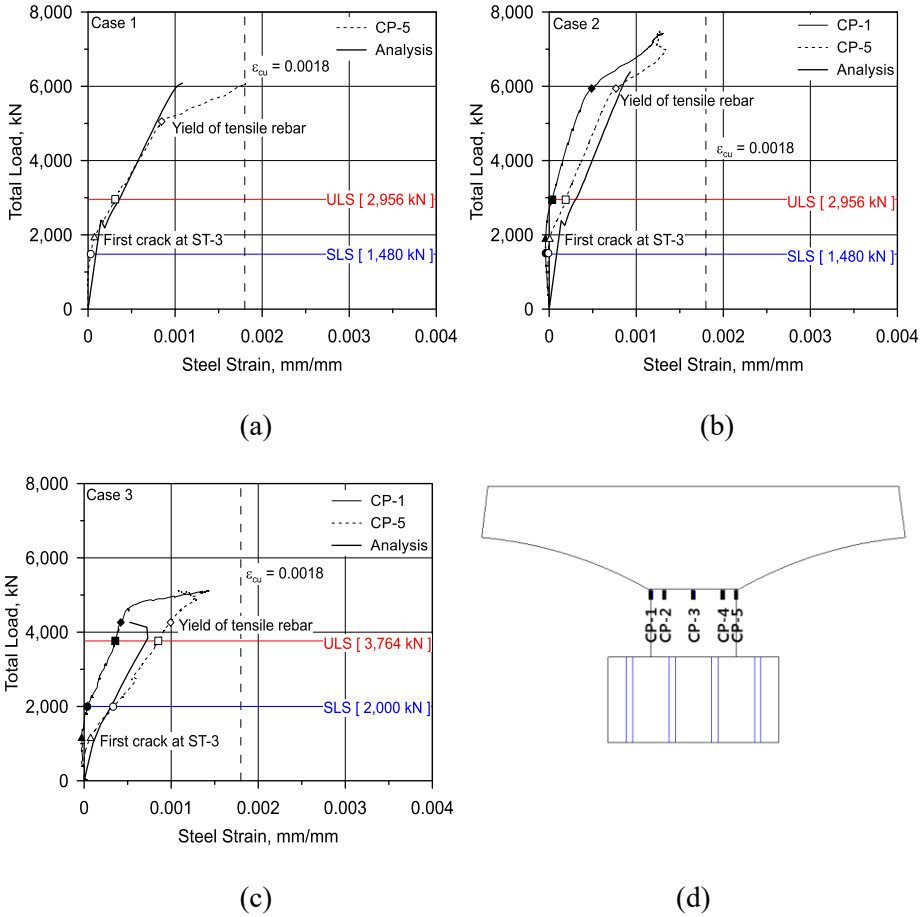


Figure 5.12 Load-strain relationship for column concrete (CP series): (a) Case 1; (b) Case 2; (c) Case 3; (d) Location of CP series

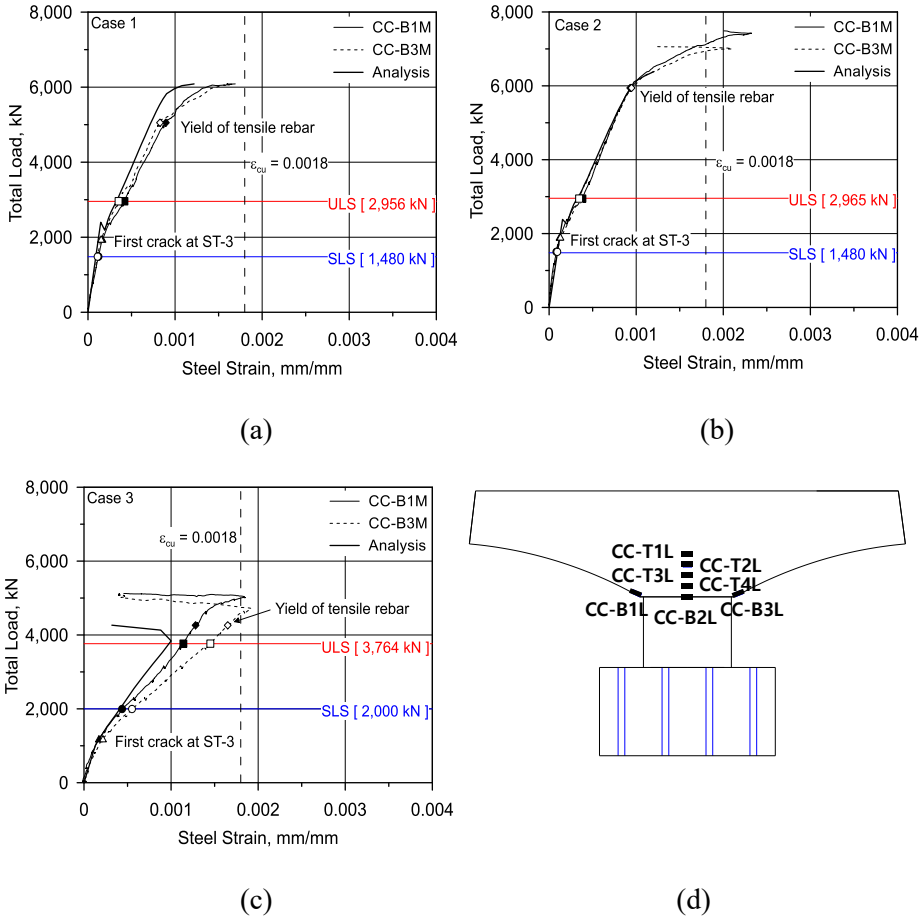


Figure 5.13 Load-strain relationship for pier cap concrete (CC series): (a) Case 1; (b) Case 2; (c) Case 3; (d) Location of CC series

## 5.3. Analysis for Parametric Study

The experiments and analyses confirmed that the pier caps designed with the proposed STM design guidelines for bridge pier caps to place more efficient reinforcement ensure structural safety and prevent problems such as low constructability and economic degradation due to the over-reinforcement in the pier cap. However, if an appropriate sectional size is not selected prior to the STM design, drawbacks may arise in the area of consistency in design safety factors and the serviceability of cracks at SLS.

In this chapter, the effects of sectional depth on the STM design and structural behavior of bridge pier caps were identified. Based on these effects of sectional depth on bridge pier caps, the design method for the appropriate sectional depth in bridge pier cap was presented and the verification of this proposal was carried out.

### 5.3.1 Effect of Sectional Depth

*5.3.1.1 Required amount of reinforcement in STM design*

With variation of sectional depths for bridge number 5 and 7, rebar for the STM designed with the proposed guidelines was analyzed to understand the effect of the sectional depth on the reinforcement of the pier cap. Table 5.5 and 5.6 show the required rebar ratios in bridge number 5 and 7 according to several sectional depths, as required in the proposed guidelines. Trends of rebar ratios with regard to sectional depths are shown in Figure 5.14.

As sectional depth decreases, moment arm that resists moment in the STM of pier cap decreases, and the element force acting on the tensile tie increases to resist the equivalent moment. Therefore, as shown in Figure 5.14, the required flexural rebar ratio increases as the sectional depth decreases. The vertical tie force, however, is not significantly affected by changes in the depth, and the required shear rebar ratio is barely affected by the sectional depth.

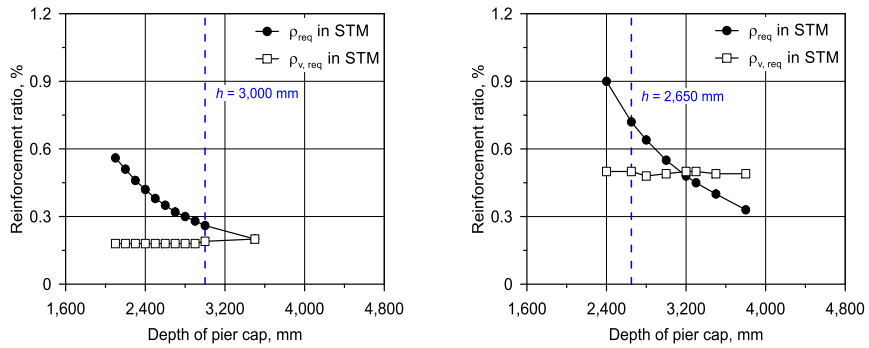


Figure 5.14 Required reinforcement ratio in STM for various sectional depth: (a) Bridge number 5; (b) Bridge number 7

Table 5.5 Required rebar ratio for various sectional depth (Bridge # 5)

| $h$ (mm) | Flexural reinforcement | | | | Vertical shear reinforcement | | | |
|---|---|---|---|---|---|---|---|---|
| | $A_{st}$ ($mm^2$) | $d$ (mm) | $b_w$ (mm) | $\rho_{req}$ | $A_v$ ($mm^2$) | $\eta_{req}$ (NA) | $s_{req}$ (mm) | $\rho_{v,\,req}$ |
| 3,500 | 20,304 | 3,384 | 3,000 | **0.0020** | 9,003 | 3.94 | 395 | **0.0020** |
| 3,000 | 22,229 | 2,884 | 3,000 | **0.0026** | 8,903 | 3.83 | 418 | **0.0019** |
| 2,900 | 23,062 | 2,784 | 3,000 | **0.0028** | 8,833 | 3.80 | 421 | **0.0018** |
| 2,800 | 23,997 | 2,684 | 3,000 | **0.0030** | 8,833 | 3.80 | 421 | **0.0018** |
| 2,700 | 25,010 | 2,584 | 3,000 | **0.0032** | 8,833 | 3.80 | 421 | **0.0018** |
| 2,600 | 26,113 | 2,484 | 3,000 | **0.0035** | 8,833 | 3.80 | 421 | **0.0018** |
| 2,500 | 27,317 | 2,384 | 3,000 | **0.0038** | 8,822 | 3.80 | 421 | **0.0018** |
| 2,400 | 28,638 | 2,284 | 3,000 | **0.0042** | 8,834 | 3.80 | 421 | **0.0018** |
| 2,300 | 30,093 | 2,184 | 3,000 | **0.0046** | 8,821 | 3.80 | 421 | **0.0018** |
| 2,200 | 31,704 | 2,084 | 3,000 | **0.0051** | 8,834 | 3.80 | 421 | **0.0018** |
| 2,100 | 33,498 | 1,984 | 3,000 | **0.0056** | 8,834 | 3.80 | 421 | **0.0018** |
| 2,000 | 35,506 | 1,884 | 3,000 | **0.0063** | 8,835 | 3.80 | 421 | **0.0018** |

Table 5.6 Required rebar ratio for various sectional depth (Bridge # 7)

| $h$ (mm) | Flexural reinforcement | | | | Vertical shear reinforcement | | | |
|---|---|---|---|---|---|---|---|---|
| | $A_{st}$ ($mm^2$) | $d$ (mm) | $b_w$ (mm) | $\rho_{req}$ | $A_v$ ($mm^2$) | $\eta_{req}$ (NA) | $s_{req}$ (mm) | $\rho_{v,\,req}$ |
| 3,800 | 32,968 | 3,680 | 2,700 | **0.0033** | 25,556 | 11.00 | 171 | **0.0050** |
| 3,500 | 36,082 | 3,380 | 2,700 | **0.0040** | 25,556 | 11.00 | 171 | **0.0050** |
| 3,300 | 38,507 | 3,180 | 2,700 | **0.0045** | 25,556 | 11.00 | 171 | **0.0050** |
| 3,200 | 39,846 | 3,080 | 2,700 | **0.0048** | 25,556 | 11.00 | 171 | **0.0050** |
| 3,000 | 42,824 | 2,880 | 2,700 | **0.0055** | 25,556 | 11.00 | 171 | **0.0050** |
| 2,800 | 46,283 | 2,680 | 2,700 | **0.0064** | 25,556 | 11.00 | 171 | **0.0050** |
| 2,650 | 49,267 | 2,530 | 2,700 | **0.0072** | 25,556 | 11.00 | 171 | **0.0050** |
| 2,400 | 55,201 | 2,280 | 2,700 | **0.0090** | 25,556 | 11.00 | 171 | **0.0050** |

Meanwhile, KCI (Korea Concrete Institute(KCI) 2012a), KHBDC (Korea Road Association 2015), and ACI 318 (ACI Committee 318 2014) stipulate that the minimum flexural reinforcement in general flexural members shall be used for ductile behavior with the larger value of following Equation 5.3 and 5.4. For the pier caps with $f_{ck} = 40$ MPa and $f_y = 400$ MPa, minimum flexural reinforcement ratio, $\rho_{\min}$, is 0.0040 based on the codes.

$$A_{s,\min} = \frac{0.25\sqrt{f_{ck}}}{f_y} b_w d \tag{5.3}$$

$$A_{s,\min} = \frac{1.4}{f_y} b_w d \tag{5.4}$$

However, according to Seguirant et al. (2010) and Kim et al. (2018), these rules for minimum flexural reinforcement are derived from the flexural strength and crack moment at the cross section of the member where the Bernoulli's assumption is satisfied. Thus, the relationship does not fit in bridge pier caps where the Bernoulli's assumption is not applicable. In addition, Kim et al. (2018) indicated that the coefficient of 0.25 in Equation 5.3 is 1.42 to 1.85 times the value of the coefficient derived from the actual rectangular cross section, and the ratio of nominal flexural strength and crack moment showed the results of 1.31 to 2.71. Also, the ratios of the loads at first yield of tensile rebar and at first crack for bridge number 5 and 7 with STM design guidelines are 5.12 and 3.25 in VECTOR 2. These factors imply that the design code provides quite a conservative value of minimum flexural rebar. Therefore, it is not necessary to apply the rule of minimum flexural rebar to the design of pier caps.

*5.3.1.2 Design safety factor*

In order to determine the load resistance capacities according to the sectional depth of pier cap, Lee (2020) analyzed the design safety factor of the pier caps, bridge number 5 and 7, designed with the proposed STM design guidelines presented in this study, according to the sectional depth.

For Lee (2020), members designed with the proposed STM guidelines show structural safeties, with load resistance capacities above the ULS loads, regardless of sectional depth. As shown in Figure 5.15, the FE analyses demonstrated the higher design safety factor as the depth of pier cap increases.

Since the STM design is a lower bound solution, the design ensures structural safety independent to the sectional depth. However, an appropriate selection of sectional depth must be preceded before the STM design to ensure more consistent design safety factors regardless of the type of pier cap.

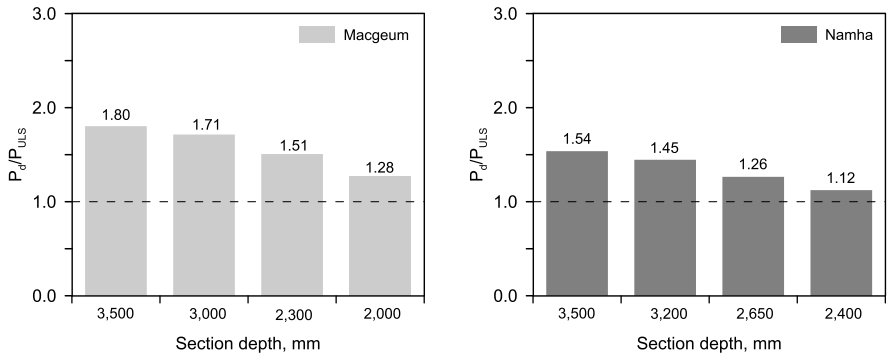


Figure 5.15 Design safety factor with various sectional depth in the proposed STM guidelines: (a) Bridge number 5; (b) Bridge number 7 (Lee, 2020)

*5.3.1.3 Serviceability in cracks*

Crack moment in typical flexural concrete members is as Equation 5.5. The equation is derived from a rectangular section, where $z$ is a section modulus and $f_r$ is a modulus of rupture for concrete. $C$ is a coefficient for sectional configuration such as T-type section. In the equation, sectional depth, $h$, is a parameter that greatly affects the moment where crack occurs. Though reinforcement in the member affects the crack propagation, the most dominant factor for the initial crack is the sectional depth of concrete. Therefore, it is necessary to increase the crack moment by securing the appropriate sectional depth in order to prevent crack generation at SLS.

$$M_{cr} = f_r \cdot z = 0.625\sqrt{f_{ck}} \cdot C\frac{b_w h^2}{6} \tag{5.5}$$

To identify the influence of sectional depth on serviceability for cracks, the FE analysis was conducted on Case 2-1 and Case 3-1, redesigned with the STM guidelines by adjusting the sectional depths of Case 2 and Case 3. The design characteristics of each case are shown in Table 5.7. The results of FE analysis shown in Figure 5.16 and Figure 5.17 found that different crack propagation was captured at SLS in the pier caps with the difference in sectional depth, even in the pier caps designed according to the same design guidelines. In other words, cracks are less propagated until SLS because of the increased crack moment as the depth of the section increases.

Lee (2020) similarly suggested that an increase in sectional depth could improve serviceability for cracks through the FE analyses.

Table 5.7 Reinforcement detail of FE cases

| Case | Rebar ratio (%) | | | $h$ (mm) | Note |
|---|---|---|---|---|---|
| | $\rho$ | $\rho_v$ | $\rho_h$ | | |
| 2 | 0.26 | 0.20 | 0.20 | 1,200 | Satisfy proposed STM guidelines for bridge # 5 |
| 2-1 | 0.49 | 0.20 | 0.20 | 920 | Satisfy proposed STM guidelines for bridge # 5 |
| 3 | 0.67 | 0.32 | 0.20 | 1,060 | Satisfy proposed STM guidelines for bridge # 7 |
| 3-1 | 0.48 | 0.50 | 0.20 | 1,320 | Satisfy proposed STM guidelines for bridge # 7 |

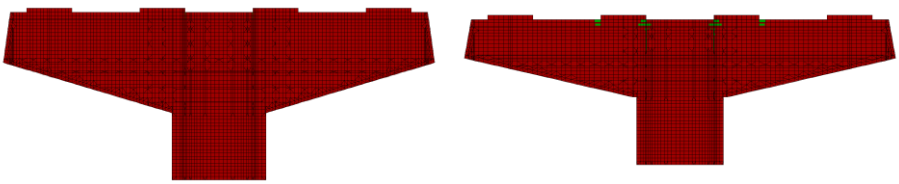

(a) (b)

Figure 5.16 Crack state at Serviceability Limit State(SLS) for bridge # 5: (a) Case 2; (b) Case 2-1

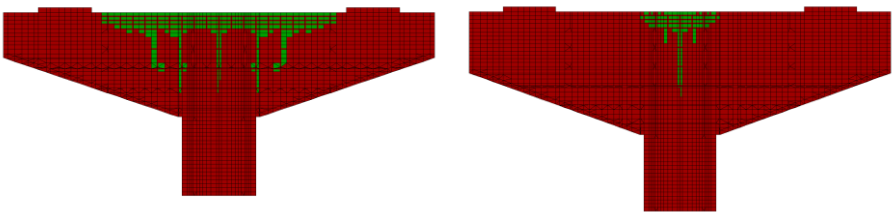

(a) (b)

Figure 5.17 Crack state at Serviceability Limit State(SLS) for bridge # 7: (a) Case 3; (b) Case 3-1

### 5.3.2 Shear Strength of Pier Caps

The experiments confirmed that flexural failure is dominated in the proposed STM designs for pier caps. It is because STM does not consider the contribution of concrete in shear strength of pier cap, under-estimating the shear strength of pier cap. To figure out the shear strengths of the experimental cases, numerical analyses using VECTOR 2 were conducted as follows.

*5.3.2.1 Contribution of concrete*

In the experimental cases, flexural failure stands out because the flexural strength is lesser than the shear strength. To capture the shear strengths, the amount of flexural tensile reinforcement shall be increased. With this concept, four analytical cases were selected as shown in Table 5.8. Case 2-$V_c$ and Case 3-$V_c$ are the cases which have no shear rebars and have increased flexural reinforcement, representing the shear strength of concrete in the experimental cases. Case 2-$V_n$ and Case 3-$V_n$ are the cases which have same shear rebars as the experiment with design guidelines and have increased flexural reinforcement, representing the entire shear strength of the experimental cases.

The analysis results for the cases with no shear reinforcement are shown in Figure 5.18 and 5.19. Due to the increased flexural rebar, shear failure was dominated in both cases. Shown in Figure 5.18, yielding of tensile rebar did not occurred until failure and diagonal concrete strut was crushed causing the shear failure. The maximum load at the failure can be treated as the contribution of concrete in shear strength. Shown in Figure 5. 19, the shear contribution of concrete is large enough to be similar to or above the flexural strength.

Table 5.8 Reinforcement detail of FE cases with shear failure

| Case | Rebar ratio (%) | | | $h$ (mm) | Note |
|---|---|---|---|---|---|
| | $\rho$ | $\rho_v$ | $\rho_h$ | | |
| 2 | 0.26 | 0.20 | 0.20 | 1,200 | Satisfy proposed STM guidelines for bridge # 5 |
| 2-$V_c$ | 1.04 | - | - | 1,200 | No shear rebars<br>Increased flexural rebar (4 times) |
| 2-$V_n$ | 1.04 | 0.20 | 0.20 | 1,200 | Increased flexural rebar (4 times) |
| 3 | 0.67 | 0.32 | 0.20 | 1,060 | Satisfy proposed STM guidelines for bridge # 7 |
| 3-$V_c$ | 2.01 | - | - | 1,060 | No shear rebars<br>Increased flexural rebar (3 times) |
| 3-$V_n$ | 2.01 | 0.32 | 0.20 | 1,060 | Increased flexural rebar (3 times) |

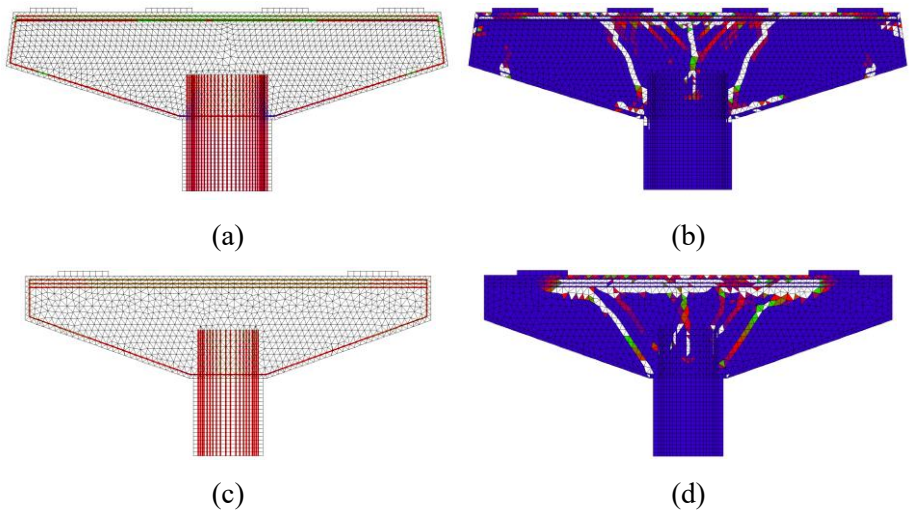


Figure 5.18 Rebar stress and crack state at failure: (a) Rebar stress in Case 2-$V_c$; (b) Crack state in Case 2- $V_c$; (c) Rebar stress in Case 3-$V_c$; (d) Crack state in Case 3- $V_c$

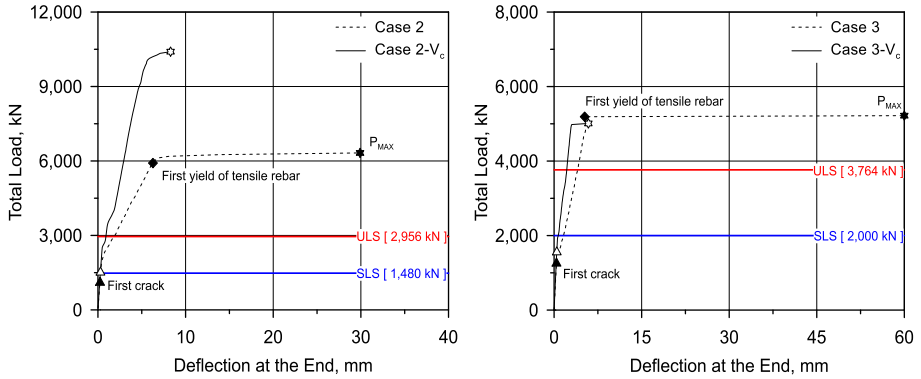


(a) (b)

Figure 5.19 Load-deflection curve of the FEA: (a) Case 2-$V_c$; (b) Case 3-$V_c$

$$V_n = V_c + V_s \tag{5.6}$$

$$V_c = \left[ 0.85\kappa\left(\rho f_{ck}\right)^{1/3}\left(\frac{2d}{x}\right) + 0.15 f_n \right] b_w d \tag{5.7}$$

$$V_s = f_{vy} A_v \sin\alpha \tag{5.8}$$

KHBDC (2015), shown in Equation 5.6 to 5.8, presents a shear strength of deep component classified into concrete contribution and reinforcement contribution. In the calculation, the material factors are ruled out in order to compare with analytical results. For the contribution of concrete shown in Equation 5.7, the shear strength of concrete is affected by flexural reinforcement ratio. The analytical results for the cases with increased flexural rebar, thus, do not represent the concrete shear strength of experimental cases having lower flexural rebar. Analytical prediction of shear strength for the experimental cases is impossible without increasement in flexural rebar. In this

basis, shear strengths of concrete in experimental cases were predicted with the equation presented in KHBDC. The ratios of concrete shear strength from design code to that from FEA, shown in Table 5.9, verified the validity of Equation 5.7.

*5.3.2.2 Contribution of reinforcement*

As shown in Table 5.8, Case 2-$V_n$ and Case 3-$V_n$ represent the shear strength of the member with shear reinforcement. The analysis results for the cases with shear reinforcement are shown in Figure 5.20 and 5.21. Shear failure was dominated in both cases. Until the shear failure, shear reinforcement yielded and diagonal concrete strut was crushed before the yielding of tensile rebar, as shown in Figure 5.20. The maximum loads at the failure in the cases can be treated as the complex contribution of concrete and reinforcement in shear strength. Shown in Figure 5. 21, the shear strengths of the cases with shear rebars are increased compared to the cases without shear reinforcement. The gap between maximum loads of the cases with shear rebars and that without shear rebars can be treated as the contribution of reinforcement in shear strength.

Equation 5.8 in KHBDC (2015) presents a contribution of shear reinforcement in the shear strength of deep component. It is not affected by flexural reinforcement ratio. Therefore, the analytical results for the cases with increased flexural rebar can represent the contribution of shear reinforcement in shear strength of experimental cases. Shear strengths of reinforcement in experimental cases were predicted with the equation presented in KHBDC. The ratios of the rebar strength from design code to that from FEA, shown in Table 5.9, verified the validity of Equation 5.8.

With the FE analyses, shear strength of pier cap could be determined. In practical design procedure, however, it is difficult to conduct FE analysis. As a practical alternative, shear strength of deep component in design code can be used to figure out the shear performance of pier caps. As shown in Table 5.9, nominal shear strengths of pier caps are well predicted with the equation in the design code, compared to VECTOR 2 analysis results. With the verified prediction in the design code, shear strengths of experimental cases can also be estimated. In the basis of the verified prediction, the total load capacities in shear for Case 2 and Case 3 is 8,364 kN and 5,644 kN, respectively.

The prediction results in both design code and FEA show that contribution of concrete in shear strength of pier cap cannot be ignored because their proportion in shear strength is quite large. However, the STM predictions do not consider the contribution of concrete, resulting in underestimation of shear strength. In STM prediction, the underestimation of shear strength may cause the wrong prediction of the failure mode where flexural failure is dominant.

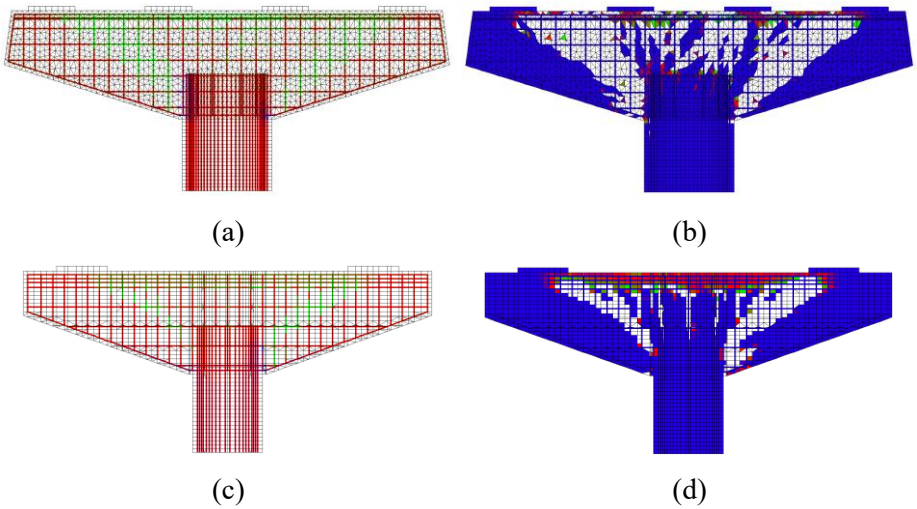

(a) (b) (c) (d)

Figure 5.20 Rebar stress and crack state at failure: (a) Rebar stress in Case 2-$V_n$; (b) Crack state in Case 2- $V_n$; (c) Rebar stress in Case 3-$V_n$; (d) Crack state in Case 3- $V_n$

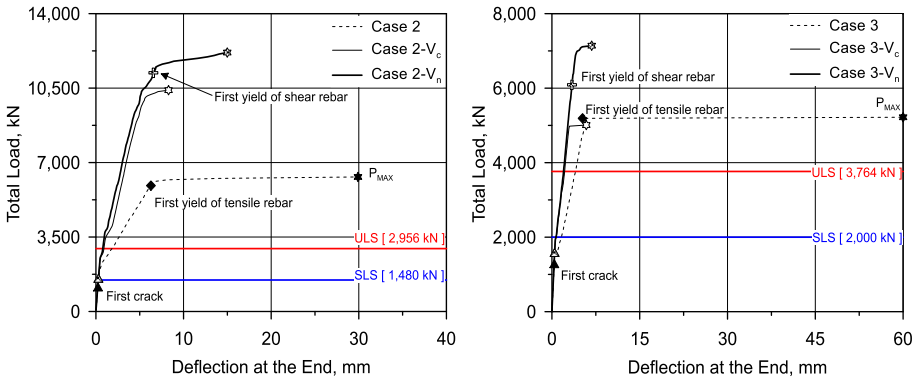


(a) (b)

Figure 5.21 Load-deflection curve of the FEA: (a) Case 2-$V_n$; (b) Case 3-$V_n$

Table 5.9 Prediction of shear strength in pier cap with design code

| Case | $\rho$ (%) | $V_{c,KHBDC}$ (kN) | $V_{c,VEC2}$ (kN) | $\frac{V_{c,KHBDC}}{V_{c,VEC2}}$ | $V_{s,KHBDC}$ (kN) | $V_{s,VEC2}$ (kN) | $\frac{V_{s,KHBDC}}{V_{s,VEC2}}$ | $V_{n,KHBDC}$ (kN) | $V_{n,VEC2}$ (kN) | $\frac{V_{n,KHBDC}}{V_{n,VEC2}}$ |
|---|---|---|---|---|---|---|---|---|---|---|
| 2 | 0.26 | 1,531 | Flexural failure | - | 560 | 442 | **1.27** | **2,091** | Flexural failure | - |
| 2-$V_c$ | 1.04 | 2,362 | 2,601 | **0.91** | - | - | - | 2,362 | 2,601 | **0.91** |
| 2-$V_n$ | 1.04 | 2,362 | 2,601 | **0.91** | 560 | 442 | **1.27** | 2,922 | 3,043 | **0.96** |
| 3 | 0.67 | 1,702 | Flexural failure | - | 1,120 | 1,065 | **1.05** | **2,822** | Flexural failure | - |
| 3-$V_c$ | 2.01 | 2,455 | 2,505 | **0.98** | - | - | - | 2,455 | 2,505 | **0.98** |
| 3-$V_n$ | 2.01 | 2,455 | 2,505 | **0.98** | 1,120 | 1,065 | **1.05** | 3,575 | 3,570 | **1.00** |

*5.3.2.3 Parametric analysis with sectional depth*

To find out shear behavior of pier cap with various shear span to depth ratio, the experimental cases following the design guidelines with different sectional depths were selected as shown in Table 5.10 and Table 5.11. Total 8 groups are selected with different sectional depth and loading points. Each group has three analytical cases with same sectional depth: one represents the member designed with STM design guidelines; another is to find out the contribution of concrete in shear; the other shows the shear strength of the member. Group 1 to 4 are based on Case 2 with the 4-point loading, and group 5 to 8 are based on Case 3 with 2-point loading. The sectional depths were chosen to represent the range of the shear span to depth ratio from 0.5 to 2.0.

Total load to deflection relationships from the analyses results are shown in Figure 5.22 and Figure 5.23. The loading capacities of the members, the shear contribution of concrete in Equation 5.5 and failure modes are shown in Table 5.12 and Table 5.13. The results show that there is little change in flexural strength of the member as the sectional depth increases. In contrast with flexural strength, shear strength of the member increases with the increase of the sectional depth. This is because shear reinforcement corresponding to the STM design guidelines does not be affected by sectional depth, which is differ to the effect on concrete section resisting to shear. The graphs also show that the contribution of concrete is dominant for shear resistance in the condition of low amount of shear reinforcement with the basis of STM design guidelines. For the members with shear failure, the shear strengths by FEA are guaranteed to be greater than the KHBDC prediction of shear. In this shear condition, if the

section is designed so that the shear prediction in KHBDC is greater than the shear at ULS load, the shear strength exceeding the ULS load is guaranteed in the pier caps designed with the STM design guidelines. In other words, more efficient sectional design is possible if the shear strength in KHBDC is designed close to the shear force at ULS.

The STM predictions for the analytical cases are shown in Table 5.12 and Table 5.13. The determinant STM was used in the thesis for the convenience of design. As mentioned above in 5.3.1.1, the change in sectional depth does not affect the force of vertical tie in STM, resulting in same vertical tie strength regardless of sectional depth. In determinant strut-and-tie models, the failure of vertical tie means the failure of the pier cap itself. However, the truss mechanism alone in determinant STM does not consider the arch mechanism and the contribution of concrete in shear capacity. Because of these drawbacks, failures in vertical ties at the STM may underestimate the strengths of the members as shown in Table 5.12 and Table 5.13 representing $P_{STM} / P_{FEA}$. In shear prediction of deep component in KHBDC shown in Equation 5.4, the contribution of concrete and sectional size in shear is reflected. In evaluating the strength of vertical ties, the underestimation of STM can be complemented by presenting the shear strength in KHBDC as the minimum value of the tie's strength. In Table 5.12 and Table 5.13 shown as $P_{Guide} / P_{FEA}$, the vertical ties' strengths are evaluated considering the shear strength of KHBDC as the minimum value of the strength. With this evaluation concept, the failure modes and strengths of pier caps can be evaluated more reasonably.

Table 5.10 Analytical cases for shear strength check (Case 2 based)

| Group | Case | $b_w$ (mm) | $h$ (mm) | $a/d$ | Reinforcement ratio (%) | | |
|---|---|---|---|---|---|---|---|
| | | | | | $\rho$ | $\rho_v$ | $\rho_h$ |
| 1 | C2-1400-4P | 1,200 | 1,400 | 1.05 | 0.20 | 0.20 | 0.20 |
| | C2-1400-4P-$V_c$ | | | | 1.20 | - | - |
| | C2-1400-4P-$V_n$ | | | | 1.20 | 0.20 | 0.20 |
| 2 | C2-1200-4P | | 1,200 | 1.21 | 0.26 | 0.20 | 0.20 |
| | C2-1200-4P-$V_c$ | | | | 1.56 | - | - |
| | C2-1200-4P-$V_n$ | | | | 1.56 | 0.20 | 0.20 |
| 3 | C2-920-4P | | 920 | 1.60 | 0.49 | 0.20 | 0.20 |
| | C2-920-4P-$V_c$ | | | | 2.94 | - | - |
| | C2-920-4P-$V_n$ | | | | 2.94 | 0.20 | 0.20 |
| 4 | C2-800-4P | | 800 | 1.85 | 0.67 | 0.21 | 0.20 |
| | C2-800-4P-$V_c$ | | | | 4.02 | - | - |
| | C2-800-4P-$V_n$ | | | | 4.02 | 0.21 | 0.20 |

Table 5.11 Analytical cases for shear strength check (Case 3 based)

| Group | Case | $b_w$ (mm) | $h$ (mm) | $a/d$ | Reinforcement ratio (%) | | |
|---|---|---|---|---|---|---|---|
| | | | | | $\rho$ | $\rho_v$ | $\rho_h$ |
| 5 | C3-1400-2P | 1,080 | 1,400 | 0.81 | 0.40 | 0.50 | 0.20 |
| | C3-1400-2P-$V_c$ | | | | 1.20 | - | - |
| | C3-1400-2P-$V_n$ | | | | 1.20 | 0.50 | 0.20 |
| 6 | C3-1280-2P | | 1,280 | 0.87 | 0.48 | 0.50 | 0.20 |
| | C3-1280-2P-$V_c$ | | | | 1.44 | - | - |
| | C3-1280-2P-$V_n$ | | | | 1.44 | 0.50 | 0.20 |
| 7 | C3-1060-2P | | 1,060 | 1.09 | 0.67 | 0.50 | 0.20 |
| | C3-1060-2P-$V_c$ | | | | 2.01 | - | - |
| | C3-1060-2P-$V_n$ | | | | 2.01 | 0.50 | 0.20 |
| 8 | C3-960-2P | | 960 | 1.21 | 0.90 | 0.50 | 0.20 |
| | C3-960-2P-$V_c$ | | | | 2.70 | - | - |
| | C3-960-2P-$V_n$ | | | | 2.70 | 0.50 | 0.20 |

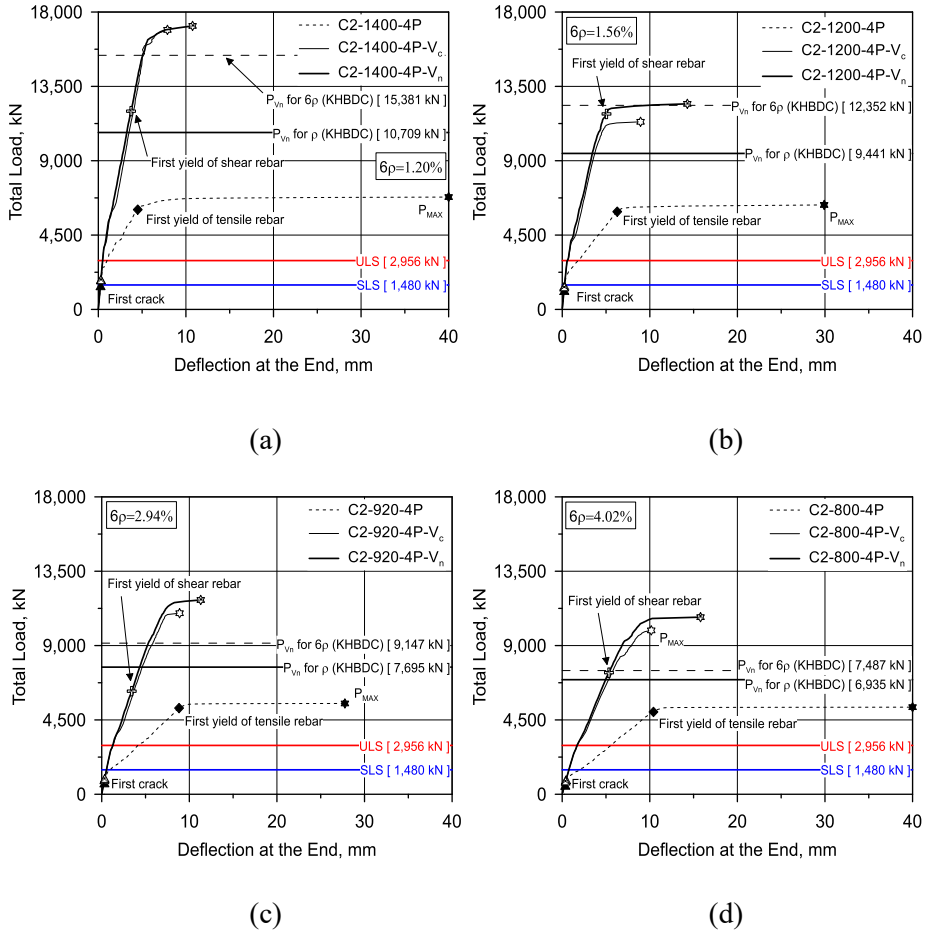


Figure 5.22 Load-deflection curve of the FEA with various sectional depth (Case 2): (a) Group 1; (b) Group 2; (c) Group 3; (d) Group 4;

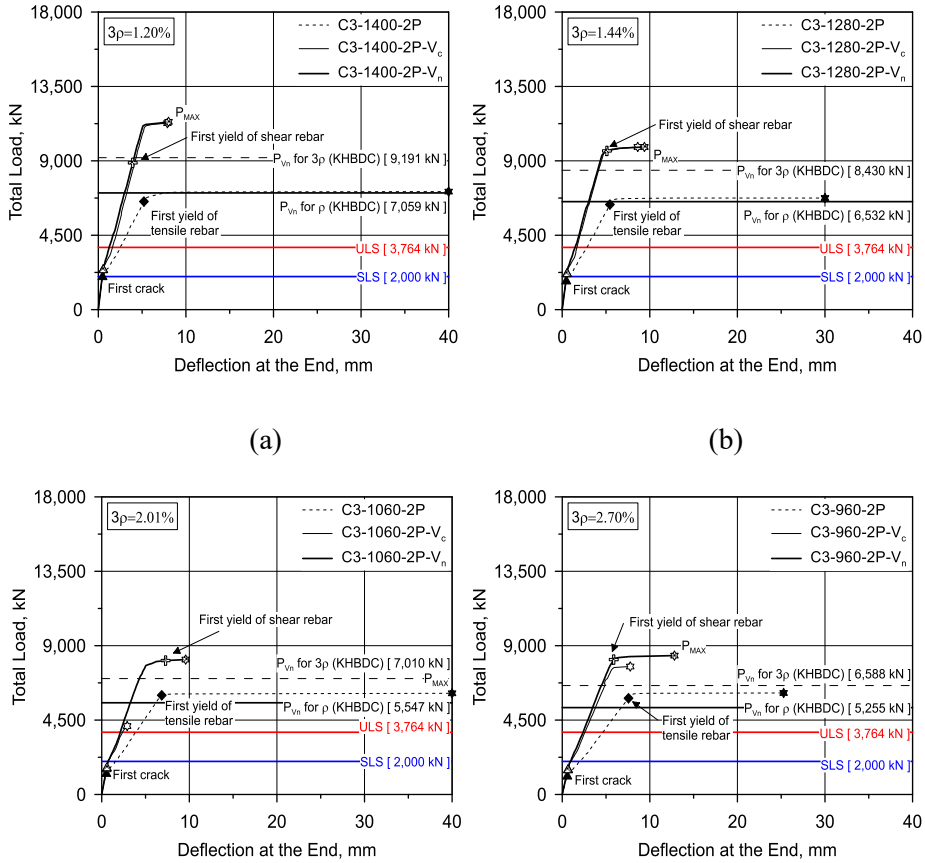


Figure 5.23 Load-deflection curve of the FEA with various sectional depth (Case 3): (a) Group 5; (b) Group 6; (c) Group 7; (d) Group 8;

Table 5.12 Shear strength check results (Case 2 based)

| Case | $h$ (mm) | $a/d$ | Reinforcement ratio (%) | | | STM strength prediction (kN) | | | $P_{FEA}$ (kN) | $M_n$ (kN) | $V_{n,\,KHBDC}$ (kN) | $\frac{P_{STM}}{P_{FEA}}$ | $\frac{P_{Guide}}{P_{FEA}}$ | Failure mode |
|---|---|---|---|---|---|---|---|---|---|---|---|---|---|---|
| | | | $\rho$ | $\rho_v$ | $\rho_h$ | $P_{Tensile\ tie}$ | $P_{Strut}$ | $P_{Vertical\ tie}$ | | | | | | |
| C2-1400-4P | 1,400 | 1.05 | 0.20 | 0.20 | 0.20 | **7,137** | 15,107 | 4,816 | **6,800** | 7,641 | 10,709 | 0.71 | **1.05** | Flexure |
| C2-1400-4P-$V_c$ | | | 1.20 | - | - | 42,822 | 15,107 | 0 | 16,920 | 31,649 | 13,142 | - | - | Shear |
| C2-1400-4P-$V_n$ | | | 1.20 | 0.20 | 0.20 | 42,822 | **15,107** | 4,816 | **17,160** | 31,649 | 15,381 | 0.28 | **0.88** | Shear |
| C2-1200-4P | 1,200 | 1.21 | 0.26 | 0.20 | 0.20 | **6,883** | 14,509 | 4,815 | **6,324** | 7,161 | 9,441 | 0.76 | **1.09** | Flexure |
| C2-1200-4P-$V_c$ | | | 1.56 | - | - | 41,298 | 14,509 | 0 | 11,356 | 30,310 | 10,613 | - | - | Shear |
| C2-1200-4P-$V_n$ | | | 1.56 | 0.20 | 0.20 | 41,298 | 14,509 | 4,815 | **13,002** | 30,310 | **12,852** | 0.37 | **0.99** | Shear |
| C2-920-4P | 920 | 1.60 | 0.49 | 0.20 | 0.20 | **5,409** | 11,446 | 4,816 | **5,496** | 6,296 | 7,695 | 0.88 | **0.98** | Flexure |
| C2-920-4P-$V_c$ | | | 2.94 | - | - | 32,454 | 11,446 | 0 | 11,040 | 26,453 | 6,908 | - | - | Shear |
| C2-920-4P-$V_n$ | | | 2.94 | 0.20 | 0.20 | 32,454 | 11,446 | 4,816 | **11,760** | 26,453 | **9,147** | 0.41 | **0.78** | Shear |
| C2-800-4P | 800 | 1.85 | 0.67 | 0.21 | 0.20 | **5,290** | 9,424 | 4,816 | **5,264** | 6,141 | 6,935 | 0.91 | **1.00** | Flexure |
| C2-800-4P-$V_c$ | | | 4.02 | - | - | 31,740 | 9,424 | 0 | 9,920 | 23,491 | 5,247 | - | - | Shear |
| C2-800-4P-$V_n$ | | | 4.02 | 0.21 | 0.20 | 31,740 | 9,424 | 4,816 | **10,720** | 23,491 | **7,487** | 0.45 | **0.70** | Shear |

Table 5.13 Shear strength check results (Case 3 based)

| Case | $h$ (mm) | $a/d$ | Reinforcement ratio (%) | | | STM strength prediction (kN) | | | $P_{FEA}$ (kN) | $M_n$ (kN) | $V_{n,\,KHBDC}$ (kN) | $\frac{P_{STM}}{P_{FEA}}$ | $\frac{P_{Guide}}{P_{FEA}}$ | Failure mode |
|---|---|---|---|---|---|---|---|---|---|---|---|---|---|---|
| | | | $\rho$ | $\rho_v$ | $\rho_h$ | $P_{Tensile\ tie}$ | $P_{Strut}$ | $P_{Vertical\ tie}$ | | | | | | |
| C3-1400-2P | 1,400 | 0.81 | 0.40 | 0.50 | 0.20 | **6,823** | 11,833 | 4,765 | **7,140** | 7,223 | 7,059 | 0.67 | **0.96** | Flexure |
| C3-1400-2P-$V_c$ | | | 1.20 | - | - | 20,469 | 11,833 | 0 | 11,040 | 17,899 | 6,952 | - | - | Shear |
| C3-1400-2P-$V_n$ | | | 1.20 | 0.50 | 0.20 | 20,469 | 11,833 | 4,765 | **11,120** | 17,899 | **9,191** | 0.43 | **0.83** | Shear |
| C3-1280-2P | 1,280 | 0.87 | 0.48 | 0.50 | 0.20 | 6,601 | 11,206 | 4,765 | **6,750** | 6,978 | **6,532** | 0.71 | **0.97** | Flexure |
| C3-1280-2P-$V_c$ | | | 1.44 | - | - | 19,803 | 11,206 | 0 | 9,840 | 17,371 | 6,191 | - | - | Shear |
| C3-1280-2P-$V_n$ | | | 1.44 | 0.50 | 0.20 | 19,803 | 11,206 | 4,765 | **9,840** | 17,371 | **8,430** | 0.48 | **0.86** | Shear |
| C3-1060-2P | 1,060 | 1.09 | 0.67 | 0.50 | 0.20 | 5,684 | 10,381 | 4,765 | **6,120** | 6,512 | **5,547** | 0.78 | **0.91** | Flexure |
| C3-1060-2P-$V_c$ | | | 2.01 | - | - | 17,052 | 10,381 | 0 | 4,140 | 16,280 | 4,771 | - | - | Shear |
| C3-1060-2P-$V_n$ | | | 2.01 | 0.50 | 0.20 | 17,052 | 10,381 | 4,765 | **8,160** | 16,280 | **7,010** | 0.58 | **0.86** | Shear |
| C3-960-2P | 960 | 1.21 | 0.90 | 0.50 | 0.20 | 5,465 | 8,604 | 4,765 | **6,120** | 6,241 | **5,255** | 0.78 | **0.86** | Flexure |
| C3-960-2P-$V_c$ | | | 2.70 | - | - | 16,395 | 8,604 | 0 | 7,740 | 15,473 | 4,349 | - | - | Shear |
| C3-960-2P-$V_n$ | | | 2.70 | 0.50 | 0.20 | 16,395 | 8,604 | 4,765 | **8,400** | 15,473 | **6,588** | 0.57 | **0.78** | Shear |

### 5.3.3 Revised Design Guidelines for Efficient Pier Cap Designs

With the analytical studies, the effects of sectional depth in pier cap behavior designed with STM and the shear properties of pier cap following the STM guidelines were analyzed.

Based on the analyses results, following revised design guidelines for efficient pier cap designs considering shear properties are proposed.

1. Avoid vertical ties between column and adjacent load point to prevent excessive design of vertical shear reinforcement.

2. Reinforcement required in STM is structurally enough because STM design is kind of lower-bound solution.

3. It is enough for horizontal shear rebar to follow the rules of minimum distributed rebar mesh in deep components.

4. Design the STM of pier caps considering the elastic stress distribution.

5. When determining sectional size of pier cap in STM, it is efficient to design the section so that shear strength of deep component in design code is close to the shear force at ULS.

6. When evaluating the strength of pier cap in STM design, the strength of vertical tie need not be less than the shear strength of deep component from KHBDC 5.7.2.3 (5). It can compensate for the underestimation of the pier cap strength in determinant STM.

### 5.3.4 Validation of Revised Design Guidelines

*5.3.4.1 Re-design of bridge pier caps*

The reinforcement ratio for 7 design cases of domestic pier caps, which were redesigned in accordance with the revised guidelines for pier caps, is shown in Table 5.14.

Table 5.14 Comparison of designs b/w existing design and revised design

| Bridge number | Type | $b_w$ (mm) | $h$ (mm) | | Reinforcement ratio | | |
|---|---|---|---|---|---|---|---|
| | | | Existing | Revised | Rebar type | Existing | Revised |
| 1 | T | 2,500 | 2,800 | 2,700 | $\rho$ | 0.0049 | 0.0043 |
| | | | | | $\rho_v$ | 0.0037 | 0.0020 |
| | | | | | $\rho_h$ | 0.0045 | 0.0020 |
| 2 | Π | 3,000 | 2,800 | 2,500 | $\rho$ | 0.0046 | 0.0042 |
| | | | | | $\rho_v$ | 0.0051 | 0.0038 |
| | | | | | $\rho_h$ | 0.0041 | 0.0020 |
| 3 | T | 2,500 | 3,000 | 3,000 | $\rho$ | 0.0080 | 0.0046 |
| | | | | | $\rho_v$ | 0.0127 | 0.0020 |
| | | | | | $\rho_h$ | 0.0095 | 0.0020 |
| 4 | Π | 2,500 | 3,000 | 2,500 | $\rho$ | 0.0066 | 0.0044 |
| | | | | | $\rho_v$ | 0.0103 | 0.0020 |
| | | | | | $\rho_h$ | 0.0077 | 0.0020 |
| 5 | T | 3,000 | 3,000 | 2,000 | $\rho$ | 0.0028 | 0.0067 |
| | | | | | $\rho_v$ | 0.0031 | 0.0021 |
| | | | | | $\rho_h$ | 0.0023 | 0.0020 |
| 6 | T | 2,900 | 3,000 | 2,750 | $\rho$ | 0.0039 | 0.0040 |
| | | | | | $\rho_v$ | 0.0084 | 0.0020 |
| | | | | | $\rho_h$ | 0.0032 | 0.0020 |
| 7 | T | 2,700 | 2,650 | 2,400 | $\rho$ | 0.0076 | 0.0090 |
| | | | | | $\rho_v$ | 0.0034 | 0.0050 |
| | | | | | $\rho_h$ | 0.0026 | 0.0020 |

*5.3.4.2 Reinforcement ratio distribution change*

The changes in the distribution of reinforcement ratio of design cases for the pier caps in Korea according to the re-design with the revised STM design guidelines are shown in Figure 5.24. As a result of the revised design following the proposed STM design guidelines for pier cap, the required shear reinforcement ratio was designed to be less than 0.6% to prevent excessive shear rebar design in the existing design. In addition, the clause for proper sectional depth in the guidelines resulted in the reduced sectional depths, as shown in Figure 5.24 (b). In other words, if the bridge pier cap is designed in accordance with the proposed design guidelines, unnecessary additional sectional depths in pier cap can be prevented.

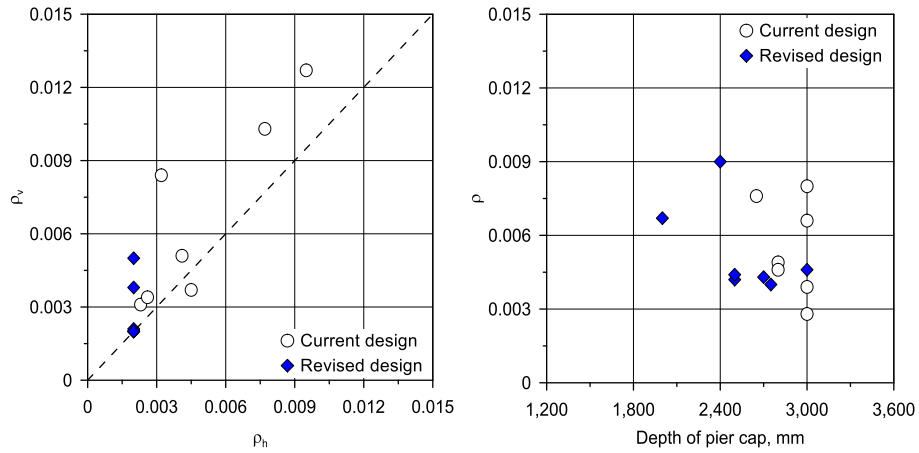


Figure 5.24 Reinforcement ratio distribution change in revised STM design cases of domestic pier cap: (a) Shear rebar ratio; (b) Sectional depth

*5.3.4.3 Consistency of design safety*

For target structures designed with effective STMs according to the revised design guidelines, design safety factors representing the load resistance capacity of the members were analyzed with FE models and were summarized in Table 5.15 and Figure 5.25.

Design safety factors in existing designs of domestic bridge pier caps, where sections were set without any mechanical basis and rebars were placed at the discretion of the designer, are inconsistent. And a higher average design safety factor of 2.16 confirmed that they were too conservatively designed than is necessary for the ULS loads. For members re-designed in accordance with the proposed design guidelines, the deviation of the design safety factor is not greater than that of the existing design, and a more efficient design safety factor of 1.60 on average is achieved. That is, the proposed design guidelines provide the direction to ensure more consistent and efficient load resistance capacities in pier caps regardless of the type of bridge.

Table 5.15 Comparison of safety b/w existing design and revised design

| Bridge number | $\psi_p$ | $P_{ULS}$ (kN) | $P_d$ (kN) | | Safety Factor | |
|---|---|---|---|---|---|---|
| | | | Existing | Revised | Existing | Revised |
| 1 | 0.88 | 18,101 | 39,460 | 28,705 | 2.18 | 1.59 |
| 2 | 0.87 | 37,990 | 104,010 | 71,459 | 2.74 | 1.88 |
| 3 | 0.87 | 25,990 | 55,014 | 36,084 | 2.12 | 1.39 |
| 4 | 0.88 | 35,298 | 106,778 | 49,751 | 3.03 | 1.41 |
| 5 | 0.88 | 18,475 | 36,682 | 32,900 | 1.99 | 1.78 |
| 6 | 0.88 | 23,103 | 43,440 | 35,250 | 1.88 | 1.53 |
| 7 | 0.87 | 23,525 | 28,816 | 38,250 | 1.22 | 1.63 |

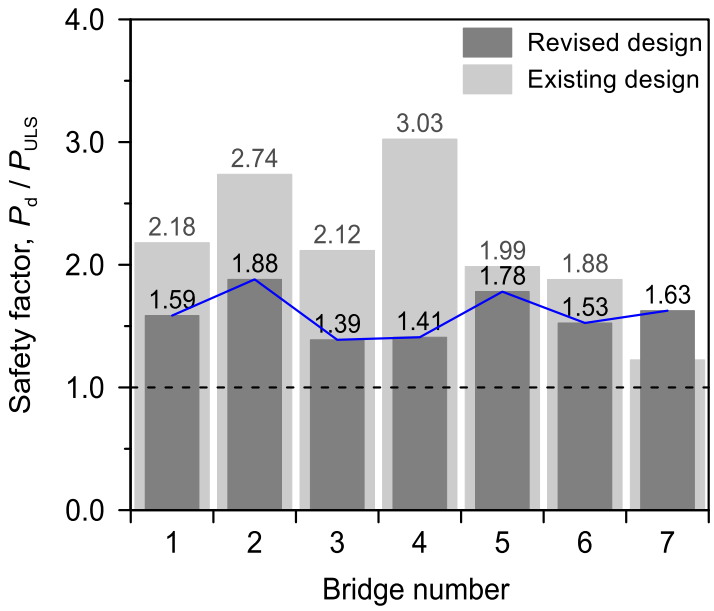


Figure 5.25 Comparison of design safeties for consistency

## 5.4. Concluding Remarks

In this chapter, the effects of sectional depth on both STM design and structural behaviors of bridge pier cap were identified. Based on the effects of sectional depth on shear, the design guide for appropriate sectional depths in bridge pier cap was presented and the verification of the proposal was carried out. Also, the shear properties in pier cap behavior were understood and more efficient way to predict the shear strength in STM was presented. In summary, the results are as follows.

1. For verification of the FE models presented in this study, scaled models in the test were simulated using DIANA and VECTOR 2. The FE analysis results well predicted load-deflection behavior, crack propagation patterns, and strains at the major locations of the specimens to verify the validity of the FE model as a means for parametric analysis.

2. In the STM design of pier cap, reinforcement ratios, design safety factors and serviceability in cracks according to the sectional depth were analyzed to determine the influence of the sectional depth on amount of reinforcement and structural behavior of pier cap prior to STM design. The analysis found that the change in sectional depth primarily affects the flexural reinforcement ratio in the proposed STM design guidelines and that adequate sectional depth shall be determined to satisfy consistent design safety factors and serviceability in cracks.

3. The shear capacities of experimental cases not captured in the test were analyzed with FEA. With the numerical analysis for shear capacity of pier

cap, it is confirmed that STM does not consider the contribution of concrete in shear strength of pier cap, under-estimating the shear strength of pier cap. The effects of sectional depth in shear are also not properly considered in STM prediction. Prior to the STM design of pier cap, proper sectional depth can be chosen using the concept of sectional design in shear. Also, the weakness of determinant STM in the shear capacity prediction of pier cap can be improved using the shear strength of deep component in KHBDC.

4. In order to verify the validity of the revised design guidelines, the design features and structural behaviors of 7 domestic design cases satisfying the revised design guidelines were analyzed. In the cases of designing pier caps in accordance with the proposed design guidelines, additional layouts of unnecessary rebars could be avoided so that reinforcement be placed more efficiently. In addition, designs with the proposed guidelines provide more consistent and efficient design safety factors, guiding the designers to determine proper sectional depth of pier caps prior to the STM design.

# VI. Conclusion

The final goal of this study is to ensure the more rational design with efficient arrangement of reinforcement at bridge pier cap. To this end, STM design guidelines for bridge pier cap were proposed to enable efficient arrangement of reinforcement, based on the identification of current status and limitations of bridge pier cap designs. In addition, a scaled model test and FE analyses were conducted to verify the feasibility of the proposed design guidelines in structural safety. With the analytical bases, the proposed design guidelines were revised to overcome the limits of the guidelines.

## 6.1. STM for Efficient Rebar Arrangement in Pier Cap

When designing the pier cap with STM, it is confirmed that additional unnecessary vertical shear ties at the location of the shear critical section, an area adjacent to the column, would result in excessive design of vertical shear reinforcement.

The STM-based design is a lower-bound solution, which ensures a structural safety of the STM design. However, in the current design of pier cap, designers usually design pier caps with more conservative amount of reinforcement than is required in the STM.

General STM design of bridge pier cap excludes the structural role of horizontal shear reinforcement in truss and tied-arch behaviors assumed in the behavior of pier cap. However, the majority of designs with STM have a

horizontal shear reinforcement correspondent to the vertical shear rebar. This may result in excessive horizontal shear reinforcement than is necessary.

When forming a strut-and-tie model, it is advantageous to locate each element according to the stress distribution acting on the pier cap. If the spacing between the location of bottom strut and cover of the pier cap is closer than that corresponding to the line of action in the compressive stress distribution, the vertical shear reinforcement will slightly increase. The spacing between the location of column strut and cover of the column influences the amount of vertical shear rebar in the same manner.

Through the above analyses, following efficient STM design guidelines for bridge pier cap were proposed.

1. Avoid vertical ties between column and adjacent load point to prevent excessive design of vertical shear reinforcement.

2. Reinforcement required in STM is structurally enough because STM design is kind of lower-bound solution.

3. It is enough for horizontal shear rebar to follow the rules of minimum distributed rebar mesh in deep components.

4. Design the strut-and-tie model of pier caps considering the elastic stress distribution.

## 6.2. Verification of the Proposed STM Guidelines

Structural safety and serviceability of pier caps designed with the proposed STM guidelines, inducing efficient rebar arrangement, were evaluated through a static loading test of scaled models of the pier caps with a length scale factor of 2/5 and nonlinear finite element analyses of the specimens. The results of the study through a scaled model test and FE analyses are as follows.

1. It was confirmed that all members with shear reinforcement satisfying the proposed STM guidelines showed flexural failures with ductile behavior, not the brittle shear failure. Furthermore, sufficient load resistance capacities were achieved in all cases designed with the STM guidelines, exceeding the ULS loads. However, with the inappropriate sectional sizes, the design safety factors were inconsistent.

2. For the improper sectional depth, where not taking the loading position into account as shown in Case 3, prior to the STM design, premature cracks were generated and these flexural cracks significantly propagated at SLS. Even in the improper sectional depth, Case 3 failed in flexure with ductile behavior after the occurrence of diagonal shear cracks because of the appropriate amount of shear rebar.

3. In the STM prediction of shear capacity, the contribution of concrete in shear is not properly considered. With this determinant STM design concept, the shear capacity of pier cap can be underestimated. The analytical study showed that shear prediction for deep component in design code can be used as a complementary for shear prediction in STM.

## 6.3. Improved Guidelines Considering Shear Properties

The influence of sectional depth on both the design features and the structural behaviors, especially shear behavior, of bridge pier cap was analyzed by FE analysis. Based on this, design guidelines were revised to allow proper sectional depths and shear capacities in bridge pier cap designs considering shear properties and verification of the revised design guidelines was conducted.

1. Changes in sectional depth mostly affect the flexural rebars required in STM designs, and adequate sectional depth shall be secured to satisfy consistent design safety and prevent critical crack propagation.

2. Based on the analytical studies for shear capacity, determination of sectional size using the concept of sectional analysis before STM design is efficient in sectional design of pier cap.

3. For the better prediction of pier cap's capacity in simple determinant STM, shear prediction for deep component in design code can be used as a minimum value of vertical tie's strength when determining the strength of pier cap in the STM.

4. 7 design cases of bridge pier cap were designed with the revised guidelines and the FE analyses were conducted. For the guidelines, unnecessary reinforcement could be prevented so that rebars be placed more efficiently. In addition, the cases following the guidelines with reduced sectional depths provide more consistent and efficient structural safeties, and the guidelines make the pier caps prevent too conservative shear resistance.

# References

ACI Committee 318 (2014). “Building Code Requirements for Structural Concrete (ACI 318M-14) and Commentary (ACI 318RM-14)”, American Concrete Institute, Farmington Hills, MI, 520 pp.

AASHTO. (2014). “AASHTO LRFD Bridge Design Specifications,” 7th edition, American Association of State Highway and Transportation Officials, Washington, D.C., 1632 pp.

Anderson, N. S. and Ramirez, J. A. (1989). “Detailing of Stirrup Reinforcement,” *ACI Structural Journal*, Vol. 86, No.5, pp.507-515.

Birrcher, D., Tuchscherer, R., Huizinga, M., and Bayrak, O. (2013). “Minimum Web Reinforcement in Deep Beams,” *ACI Structural Journal*, Vol. 110, No. 2, pp. 297-306.

Cho. J. Y. (2019). “Study on rational bridge pier cap reinforcement designs for detail design of Limit State Design, Final Report,” Korea Expressway Corporation, Gimcheon, Korea, 402 pp. (in Korean)

CSA A23.3 (2014). “Design of Concrete Structures (CSA A23.3-14)”, Canadian Standard Association, Mississauga, Ont., Canada, 290 pp.

EI-Metwally, S. E-D. E. and Chen, W-F. (2017). *Structural Concrete Strut-and-Tie Models for Unified Design*, CRC Press, Boca Raton, 246 pp.

European Committee for Standardization. (2004). “Eurocode 2: Design of Concrete Structures-Part 1-1: General Rules and Rules for Buildings”, Brussel, Belgium, 230 pp.

Hsuing, W. and Frantz, G. C. (1985). “Transverse Stirrup Spacing in RC Beam,” *Journal of Structural Engineering*, Vol. 11, No.2, pp.353-362.

Kim, M. Y., Cho, J. Y., and Lee, H. J. (2018). “Minimum Reinforcement Specifications for Flexural Reinforced Concrete Members,” *Journal of the Korea Concrete Institute*, Vol. 30, No. 2, pp.179-187. (in Korean)

Kim, T. H., Lee, H. M., Kim, Y. J., and Shin, H. M. (2010). “Performance assessment of precast concrete segmental bridge columns with a shear resistant connecting structure,” *Engineering Structures*, Vol. 32, No. 5, pp. 1292-1303.

Korea Concrete Institute. (2012). “Design Code and Commentary of Concrete Structures”, Seoul, Korea, 548 pp. (in Korean)

Korean Road Association. (2015). “Korean Highway Bridge Design Code (Limit State Design)”, Sejong, Korea, 811 pp. (in Korean)

Lee, C. J. (2020). *Effect of STM Design on Structural Behavior of Bridge Pier Cap according to Depth and Load Distribution*, Master’s thesis, Seoul National University, Seoul, Korea, 71 pp.

Lim, E. and Hwang, S-J. (2016). “Modeling of the strut-and-tie parameters of deep beams for shear strength prediction,” *Engineering Structures*, Vol. 108, pp.104-112.

Muttoni, A., Schwartz, J., and Thurlimann, B. (1997) *Design of Concrete Structures with Stress Fields*, Birkhäuser Verlag, Basel, 146 pp.

Nielsen, M. P. (1998). *Limit Analysis and Concrete Plasticity: Second Edition*, CRC Press, Boca Raton, 936 pp.

Park, B. S., Park, S. H., and Cho, J. Y. (2013) “A pre-assembly method of steel reinforcement to improve the constructability of pier coping,” *Engineering Structures*, Vol. 48, pp.166–175.

Wight, J. K. and Parra-Montesinos, G. J. (2003), “Strut-and-Tie Models for Deep Beam Design,” *Concrete International*, Vol. 25, No. 5, pp. 63-70.

Rogowsky, D. M., MacGregor, J. G., and Ong, S. Y. (1986). “Tests of Reinforced Concrete Deep Beams,” *ACI Journal*, Vol. 83, No. 55, pp. 614-623.

Saatci, S. and Vecchio, F.J. (2009). “Effects of Shear Mechanisms on Impact Behavior of Reinforced Concrete Beams,” *ACI structural Journal*, Vol. 106, No. 1, pp. 78-86.

Schlaich, J., Schafer, K., and Jennewein, M. (1987). “Toward a Consistent Design of Structural Concrete,” *PCI Journal*, Vol. 32, No. 3, pp. 74-150.

Schlaich, J. and Schafer, K. (1991). “Design and Detailing of Structural Concrete Using Strut-and-Tie Models,” *The Structural Engineer*, Vol. 69, No. 6, pp. 113-125.

Seguirant, S. J., Brice, R., and Khaleghi, B. (2010) “Making Sense of Minimum Flexural Reinforcement Requirements for Reinforced Concrete Members,” *PCI Journal*, Vol. 55, No. 3, pp.61-85.

Tan, K. H. and Cheng, G. H. (2006). “Size Effect on Shear Strength of Deep Beams: Investigating with Strut-and-Tie Model,” *Journal of Structural Engineering*, Vol. 132, No.5, pp.673-685.

Thorenfeldt, E., Tomaszewicz, A., and Jensen, J. J. (1987). *Mechanical properties of high strength concrete and application in design*, Proceedings of international symposium on utilization of high strength concrete, Stavanger, Norway, pp. 149-159.

Tuchscherer, R., Birrcher, D., and Bayrak, O. (2011). “Strut-and-Tie Model Design Provisions,” *PCI Journal*, Vol. 56, No. 1, pp. 155-170.

Tuchscherer, R., Birrcher, D., Huizinga, M., and Bayrak, O. (2011). “Distribution of Stirrups across Web of Deep Beams,” *ACI Structural Journal*, Vol. 108, No. 6, pp. 779-781.

Vecchio, F. J. and Collins, M. P. (1986). “The modified compression-field theory for reinforced concrete elements subjected to shear,” *ACI Journal*, Vol. 83, No. 2, pp.219-231.

Wight, J. K. and MacGregor, J. G. (2011). *Reinforced Concrete: Mechanics and Design: 6th Edition*, Prentice-Hall, Inc., New-Jersey, 1176 pp.

Williams, C., Deschenes, D., and Bayrak, O. (2011). "Strut-and-Tie Model Design Examples for Bridges: Final Report," CTR Technical Report, p. 276.

Wong, P. S., Vecchio, F. J., and Trommels, H. (2013). "VECTOR2 & FORMWORKS USER'S MANUAL: SECOND EDITION," VECTOR2 Manual, p. 318.

Zhong, J. T., Wang, L., Deng, P., Zhou, M. (2017). "A new evaluation procedure for the strut-and-tie models of the disturbed regions of reinforced concrete structures," *Engineering Structures*, vol.148, pp.660-672.

# Appendix A

# Required reinforcement ratio in STM design guideline

# A.1. Element Force with Disposition of STM

## A.1.1 Bridge Number 5

*A.1.1.1 Positioning the STM depending on the stress distribution analysis*

Using DIANA FE program, the stress distribution acting on the 2-D model of the pier cap for the load combination applied to bridge number 5 was analyzed. Two-dimensional elastic finite element analysis was conducted at the pier cap with the specifications given in Figure A.1. According to the stress flow obtained from the elastic analysis, strut and tie elements were arranged as shown in Figure A.2.

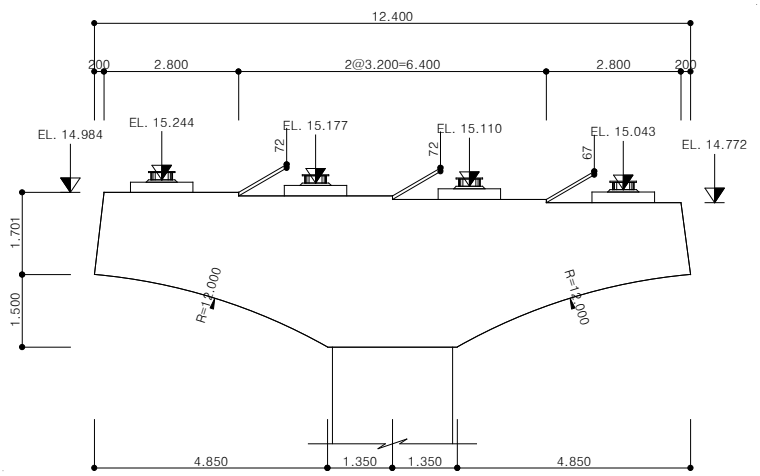


Figure A.1 Pier cap dimension and loading for bridge number 5

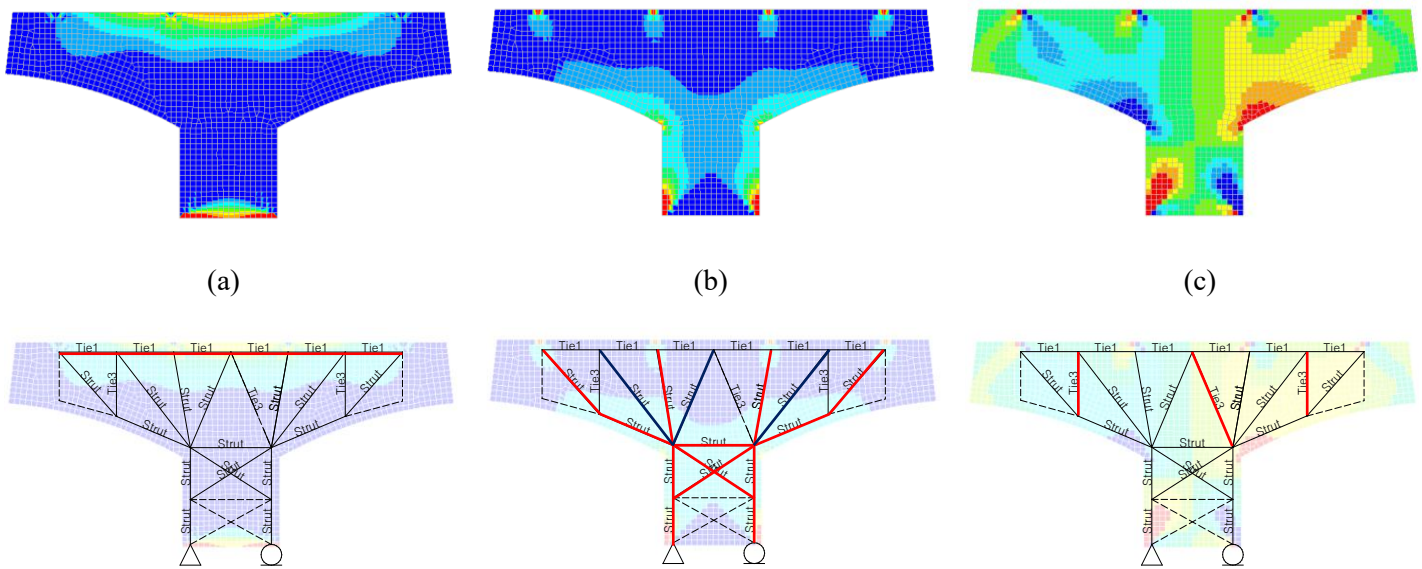


Figure A.2 Disposition of Strut-and-tie model considering elastic FE analysis: (a) S1: Principal stress for tension; (b) S2: Principal stress for compression; (c) SXY: Shear stress; (d) Tensile tie location with stress flow; (e) Compressive strut location with stress flow; (f) Shear tie location with stress flow

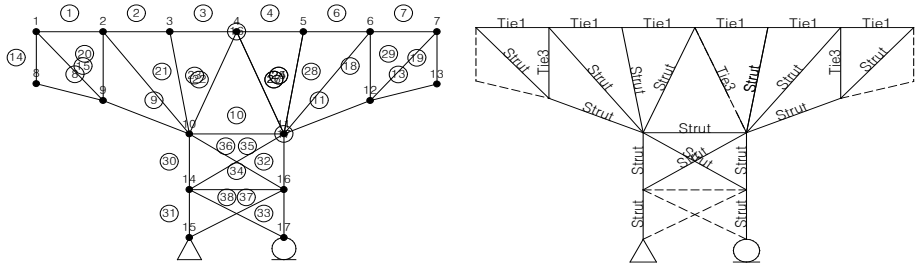


Figure A.3 Element of Strut-and-tie model considering elastic FE analysis

For the tensile ties, the ties were placed at the top of the member corresponding to the stress distribution, and the compressive struts were placed according to the principal compressive stress flow from the loading points to the column. As mentioned in main chapters, vertical shear ties were placed, not placing between the outer part of the column and the inner loading points.

*A.1.1.2 Element forces at strut-and-tie model*

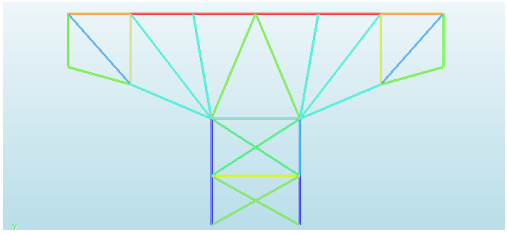

Figure A.4 Truss analysis for pier cap STM (DIANA)

Table A.1 Element forces of bridge number 5

| Type | Element number | Element force (kN) |
|---|---|---|
| Tensile tie | 1 | 4,584 |
| | 2 | 7,070 |
| | 3 | 8,003 |
| | 4 | 7,810 |
| | 6 | 6,884 |
| | 7 | 4,460 |
| Strut | 8 | 0 |
| | 9 | -4,974 |
| | 10 | -5,113 |
| | 11 | -4,839 |
| | 13 | 0 |
| Vertical tie | 15 | 3,205 |
| | 18 | 3,124 |

The element force acting on each STM element was determined by analyzing the STM with truss analysis. The analysis was based on the ultimate limit state load combination-I. As a result of the truss analysis, the element forces acting on each STM element are shown in the following Table A.1.

## A.1.2 Bridge Number 7

*A.1.2.1 Positioning the STM depending on the stress distribution analysis*

Using DIANA FE program, the stress distribution acting on the 2-D model of the pier cap for the load combination applied to bridge number 7 was analyzed. Two-dimensional elastic finite element analysis was conducted at the pier cap with the specifications given in Figure A.5. According to the stress flow obtained from the elastic analysis, strut and tie elements were arranged as shown in Figure A.6.

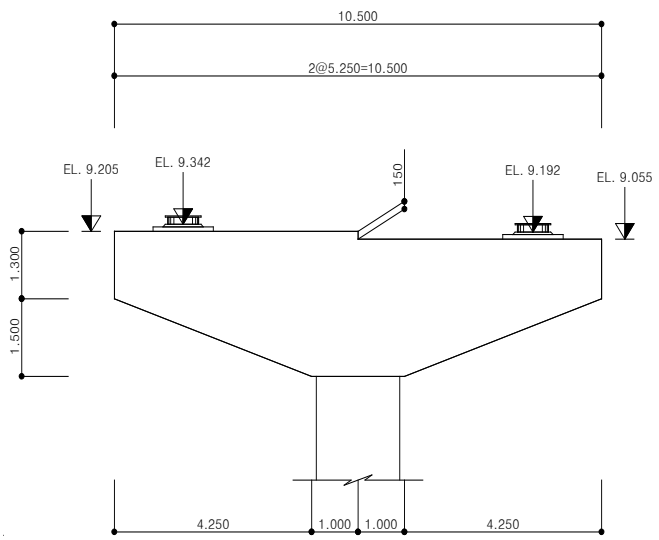


Figure A.5 Pier cap dimension and loading for bridge number 7

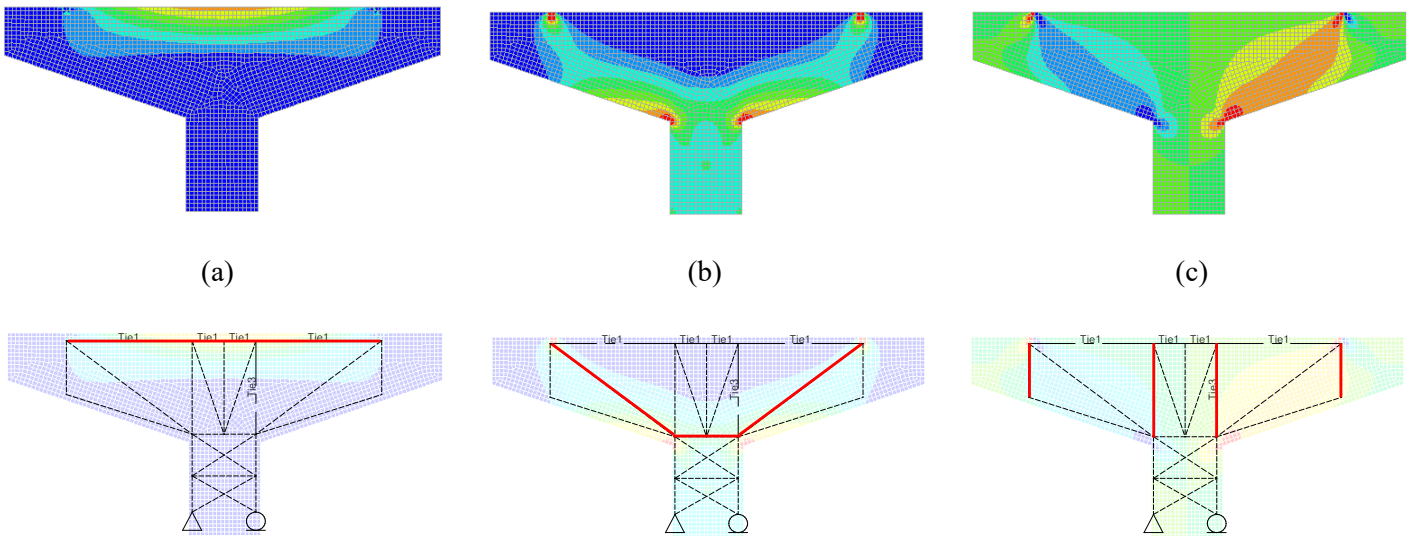


Figure A.6 Disposition of Strut-and-tie model considering elastic FE analysis: (a) S1: Principal stress for tension; (b) S2: Principal stress for compression; (c) SXY: Shear stress; (d) Tensile tie location with stress flow; (e) Compressive strut location with stress flow; (f) Shear tie location with stress flow

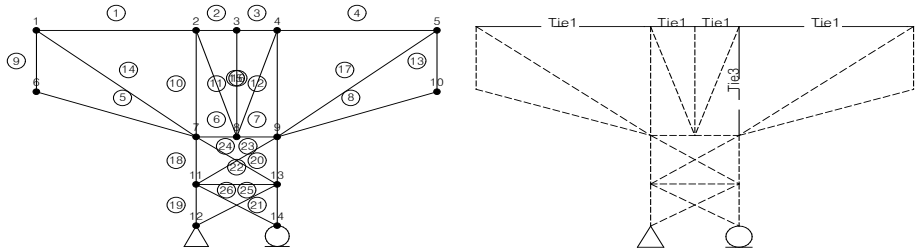


Figure A.7 Element of Strut-and-tie model considering elastic FE analysis

For the tensile ties, the ties were placed at the top of the member corresponding to the stress distribution, and the compressive struts were placed according to the principal compressive stress flow from the loading points to the column. As mentioned in main chapters, vertical shear ties were placed, not placing between the outer part of the column and the inner loading points.

*A.1.2.2 Element forces at strut-and-tie model*

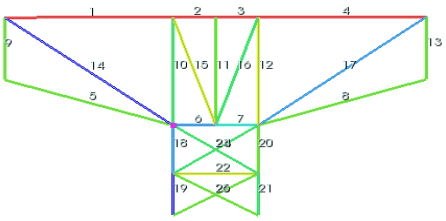


Figure A.8 Truss analysis for pier cap STM (DIANA)

Table A.2 Element forces for bridge number 7

| Type | Element number | Element force (kN) |
|---|---|---|
| Tensile tie | 1 | 16,466 |
| | 2 | 14,519 |
| | 3 | 14,519 |
| | 4 | 12,569 |
| Strut | 6 | 0 |
| | 7 | -12,428 |
| | 8 | -8,531 |
| | 9 | 0 |
| Vertical tie | 10 | 0 |
| | 11 | -5,943 |
| | 13 | 0 |
| | 15 | 5,943 |
| | 18 | 0 |

The element force acting on each STM element was determined by analyzing the STM with truss analysis. The analysis was based on the ultimate limit state load combination-I. As a result of the truss analysis, the element forces acting on each STM element are shown in the following Table A.2.

## A.2. Required Reinforcement in STM

### A.2.1 Bridge Number 5

*A.2.1.1 Calculation of flexural reinforcement*

Since the largest tension force occurred in element 3, the largest amount of rebar is required in element 3, and the required amount and ratio of rebar in the tension ties are as shown in Equation A.1 and Equation A.2.

$$A_{st} = \frac{F_t}{\phi f_y} = \frac{8,002,000}{0.9 \times 400} = 22,228 \text{ mm}^2 \quad \text{(A.1)}$$

$$\rho_{st} = \frac{A_{st}}{b_w d} = \frac{22,228}{3,000 \times 2,889} = 0.0026 \quad \text{(A.2)}$$

*A.2.1.2 Calculation of vertical shear reinforcement*

As the largest element force occurred in element 15, the largest amount of rebar is required in element 15, and therefore the required amount of rebar for vertical shear ties is shown in Equation A.3.

$$A_{st} = \frac{F_v}{\phi f_y} = \frac{3,205,000}{0.9 \times 400} = 8,903 \text{ mm}^2 \quad \text{(A.3)}$$

Equation A.5 shows the required spacing of vertical shear rebars when placing the H22-6EA closed bar (3 sets) within the maximum effective width of the vertical tie (1,600 mm).

$$\eta_{req} = \frac{A_v}{6A_{H22}} = \frac{8,903}{6 \times 387.1} = 3.83 \quad \text{(A.4)}$$

$$s_{req} = \frac{1,600}{\eta_{req}} = \frac{1,600}{3.83} = 418 \text{ mm} \quad \text{(A.5)}$$

Therefore, the vertical shear reinforcement ratio required in the STM of the member is shown in Equation A.6.

$$\rho_v = \frac{6A_{H22}}{b_w s_{req}} = \frac{6 \times 387.1}{3,000 \times 418} = 0.0019 \quad \text{(A.6)}$$

## A.2.2 Bridge Number 7

*A.2.2.1 Calculation of flexural reinforcement*

Since the largest tension force occurred in element 1, the largest amount of rebar is required in element 1, and the required amount and ratio of rebar in the tension ties are as shown in Equation A.7 and Equation A.8.

$$A_{st} = \frac{F_t}{\phi f_y} = \frac{16,465,000}{0.9 \times 400} = 45,736 \text{ mm}^2 \quad \text{(A.7)}$$

$$\rho_{st} = \frac{A_{st}}{b_w d} = \frac{45,736}{2,700 \times 2,530} = 0.0067 \quad \text{(A.8)}$$

*A.2.2.2 Calculation of vertical shear reinforcement*

As the largest element force occurred in element 12, the largest amount of rebar is required in element 12, and therefore the required amount of rebar for vertical shear ties is shown in Equation A.9.

$$A_{st} = \frac{F_v}{\phi f_y} = \frac{5,943,000}{0.9 \times 400} = 16,508 \text{ mm}^2 \quad \text{(A.9)}$$

Equation A.11 shows the required spacing of vertical shear rebars when placing the H22-6EA closed bar (3 sets) within the maximum effective width of the vertical tie (1,885 mm).

$$\eta_{req} = \frac{A_v}{6A_{H22}} = \frac{16,508}{6 \times 387.1} = 7.11 \quad \text{(A.10)}$$

$$s_{req} = \frac{1{,}885}{\eta_{req}} = \frac{1{,}885}{7.11} = 265 \text{ mm} \quad \text{(A.11)}$$

Therefore, the vertical shear reinforcement ratio required in the STM of the member is shown in Equation A.12.

$$\rho_v = \frac{6A_{H22}}{b_w s_{req}} = \frac{6 \times 387.1}{2{,}700 \times 265} = 0.0032 \quad \text{(A.12)}$$

## A.3. Details of Reinforcement in Scaled-Model Specimens

A total of three experimental cases of scaled-model specimens were selected, as shown in Table A.3 (same as Table 4.1), using the required reinforcement ratio for each bridge pier cap presented in A.1 and A.2.

Table A.3 Reinforcement detail of experimental cases

| Case | Rebar ratio (%) | | | Note |
|---|---|---|---|---|
| | $\rho$ | $\rho_v$ | $\rho_h$ | |
| A | 0.28 | 0.31 | 0.23 | Existing reinforcement detail of bridge # 5 (4-point load) |
| B | 0.76 | 0.34 | 0.26 | Existing reinforcement detail of bridge # 7 (2-point load) |
| 1 | 0.26 | 0.19 | 0.06 | Satisfying proposed STM design guidelines for bridge # 5 (No horizontal shear reinforcement) |
| 2 | 0.26 | 0.20 | 0.20 | Satisfying proposed STM design guidelines for bridge # 5 (Minimum horizontal shear rebar for serviceability) |
| 3 | 0.67 | 0.32 | 0.20 | Satisfying proposed STM design guidelines for bridge # 7 (Minimum horizontal shear rebar for serviceability) |

# Appendix B

# Results of unconfined compression test for cylinder specimens

Table B.1 Unconfined compression test results for cylinder of pier cap

(unit: MPa)

| Case | $t$ (days) | Specimen 1 | | Specimen 2 | | Specimen 3 | | Average | |
|---|---|---|---|---|---|---|---|---|---|
| | | $f_c(t)$ | $E_c(t)$ | $f_c(t)$ | $E_c(t)$ | $f_c(t)$ | $E_c(t)$ | $f_c(t)$ | $E_c(t)$ |
| 1 | 7 | 26.0 | - | 26.6 | - | 26.1 | - | 26.2 | - |
| | 41 | 35.9 | 25,056 | 34.0 | 25,575 | 36.3 | 25,996 | 35.4 | 25,542 |
| 2 | 7 | 25.9 | - | 26.1 | - | 26.6 | - | 26.2 | - |
| | 33 | 35.0 | 25,174 | 29.9 | 25,518 | 30.0 | 24,837 | 31.6 | 25,176 |
| 3 | 7 | 27.1 | - | 27.1 | - | 26.9 | - | 27.0 | - |
| | 41 | 36.9 | 25,026 | 36.2 | 24,992 | 35.3 | 24,955 | 36.2 | 24,991 |

Table B.2 Unconfined compression test results for cylinder of basement

(unit: MPa)

| Case | $t$ (days) | Specimen 1 | | Specimen 2 | | Specimen 3 | | Average | |
|---|---|---|---|---|---|---|---|---|---|
| | | $f_c(t)$ | $E_c(t)$ | $f_c(t)$ | $E_c(t)$ | $f_c(t)$ | $E_c(t)$ | $f_c(t)$ | $E_c(t)$ |
| 1 | 7 | 34.8 | - | 37.0 | - | 31.6 | - | 34.5 | - |
| | 55 | 53.6 | 35,484 | 52.7 | 34,765 | 53.8 | 33,788 | 53.4 | 34,679 |
| 2 | 7 | 38.7 | - | 39.5 | - | 40.4 | - | 39.5 | - |
| | 55 | 57.1 | 36,555 | 56.8 | 35,316 | 57.7 | 35,252 | 57.2 | 35,708 |
| 3 | 7 | 35.1 | - | 37.7 | - | 37.0 | - | 36.6 | - |
| | 55 | 55.9 | 35,802 | 55.3 | 36,904 | 59.4 | 35,644 | 56.9 | 36,117 |

Table B.3 Unconfined compression test results for cylinder of column

(unit: MPa)

| Case | $t$ (days) | Specimen 1 | | Specimen 2 | | Specimen 3 | | Average | |
|---|---|---|---|---|---|---|---|---|---|
| | | $f_c(t)$ | $E_c(t)$ | $f_c(t)$ | $E_c(t)$ | $f_c(t)$ | $E_c(t)$ | $f_c(t)$ | $E_c(t)$ |
| all | 7 | 43.7 | - | 41.2 | - | 42.4 | - | 42.4 | - |
| | 51 | 55.1 | 37,237 | 51.3 | 33,147 | 52.1 | 36,455 | 52.8 | 35,613 |

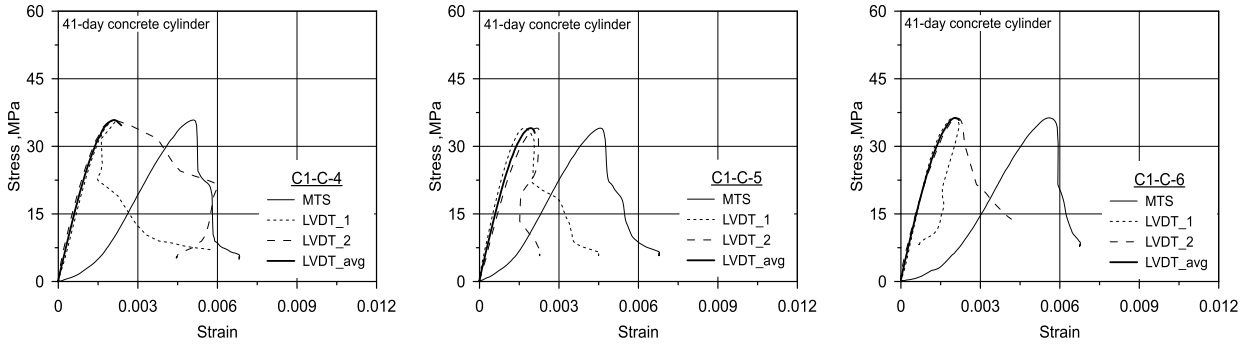
41-day concrete cylinder
C1-C-4
C1-C-5
C1-C-6
MTS
LVDT_1
LVDT_2
LVDT_avg
Stress ,MPa
Strain
0
15
30
45
60
0.003
0.006
0.009
0.012

(a)

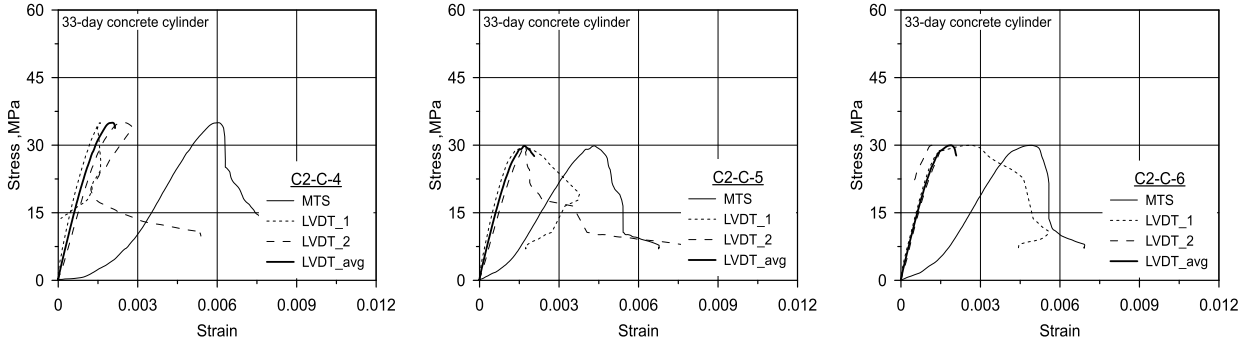
33-day concrete cylinder
C2-C-4
C2-C-5
C2-C-6
MTS
LVDT_1
LVDT_2
LVDT_avg
Stress ,MPa
Strain
0
15
30
45
60
0.003
0.006
0.009
0.012

(b)

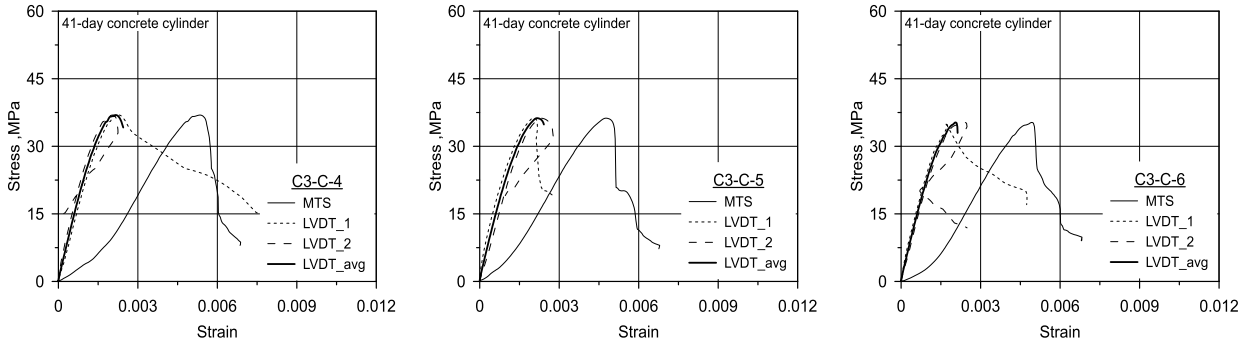


(c)

Figure B.1 Stress-strain curve for concrete cylinder of pier cap: (a) Case 1; (b) Case 2; (c) Case 3

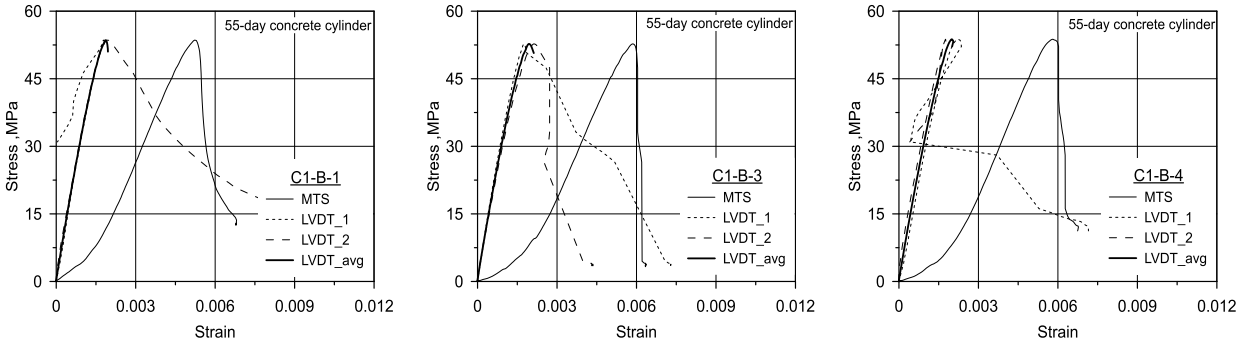
55-day concrete cylinder
Stress ,MPa
Strain
C1-B-1
C1-B-3
C1-B-4
MTS
LVDT_1
LVDT_2
LVDT_avg
0
15
30
45
60
0.003
0.006
0.009
0.012

(a)

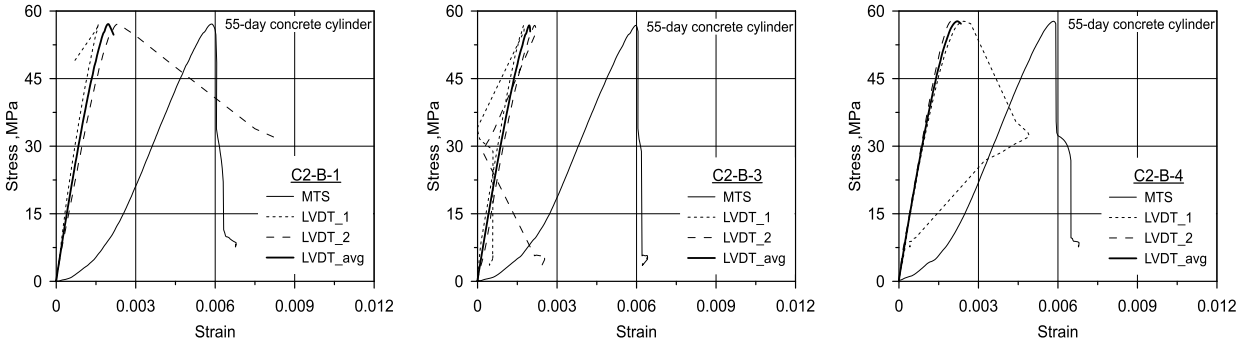
55-day concrete cylinder
Stress ,MPa
Strain
C2-B-1
C2-B-3
C2-B-4
MTS
LVDT_1
LVDT_2
LVDT_avg
0
15
30
45
60
0.003
0.006
0.009
0.012

(b)

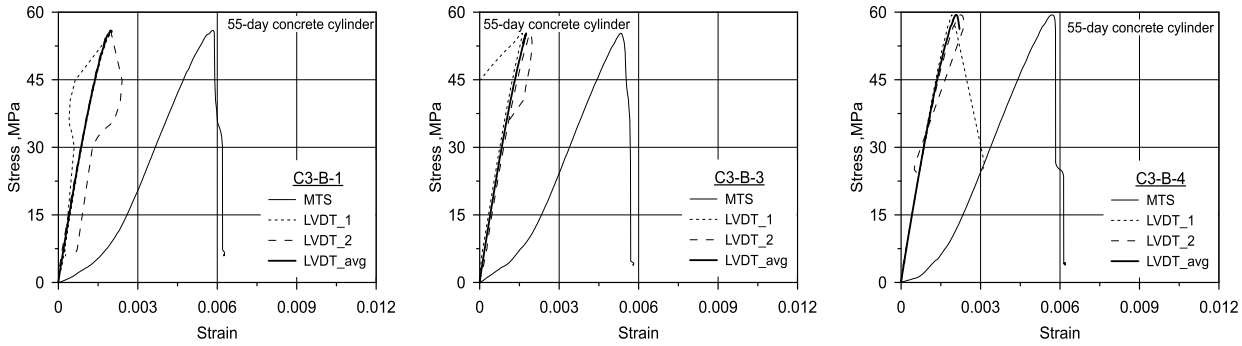


(c)

Figure B.2 Stress-strain curve for concrete cylinder of basement: (a) Case 1; (b) Case 2; (c) Case 3

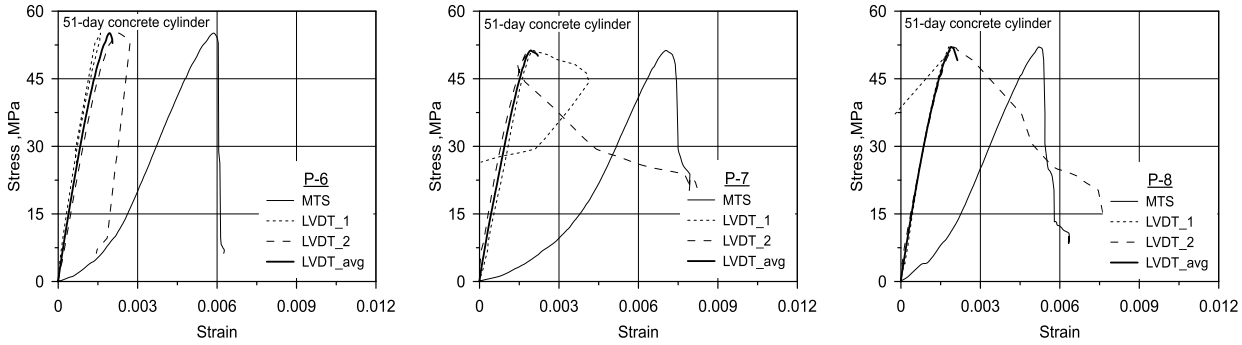


Figure B.3 Stress-strain curve for concrete cylinder of column

# Appendix C

# Load-strain relationship of scaled model test

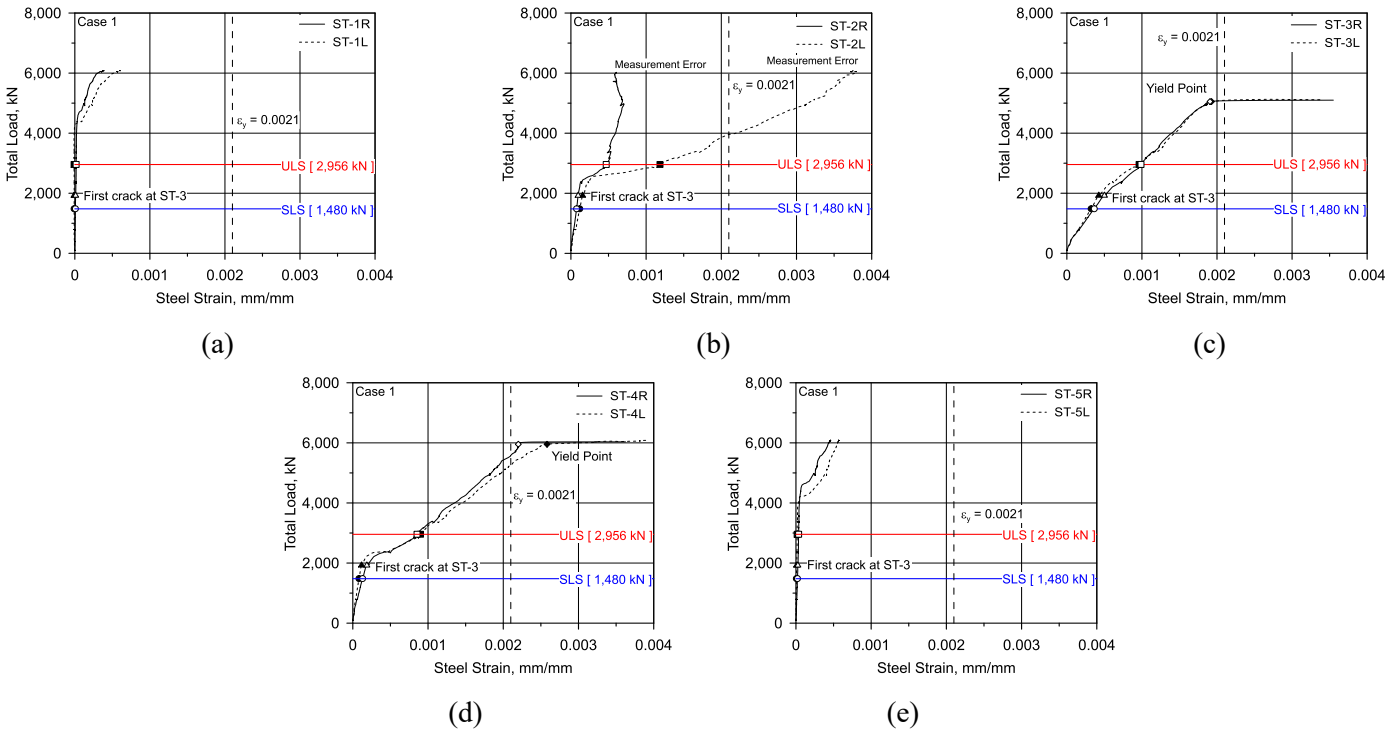


Figure C.1 Load-strain curve of flexural reinforcement for Case 1

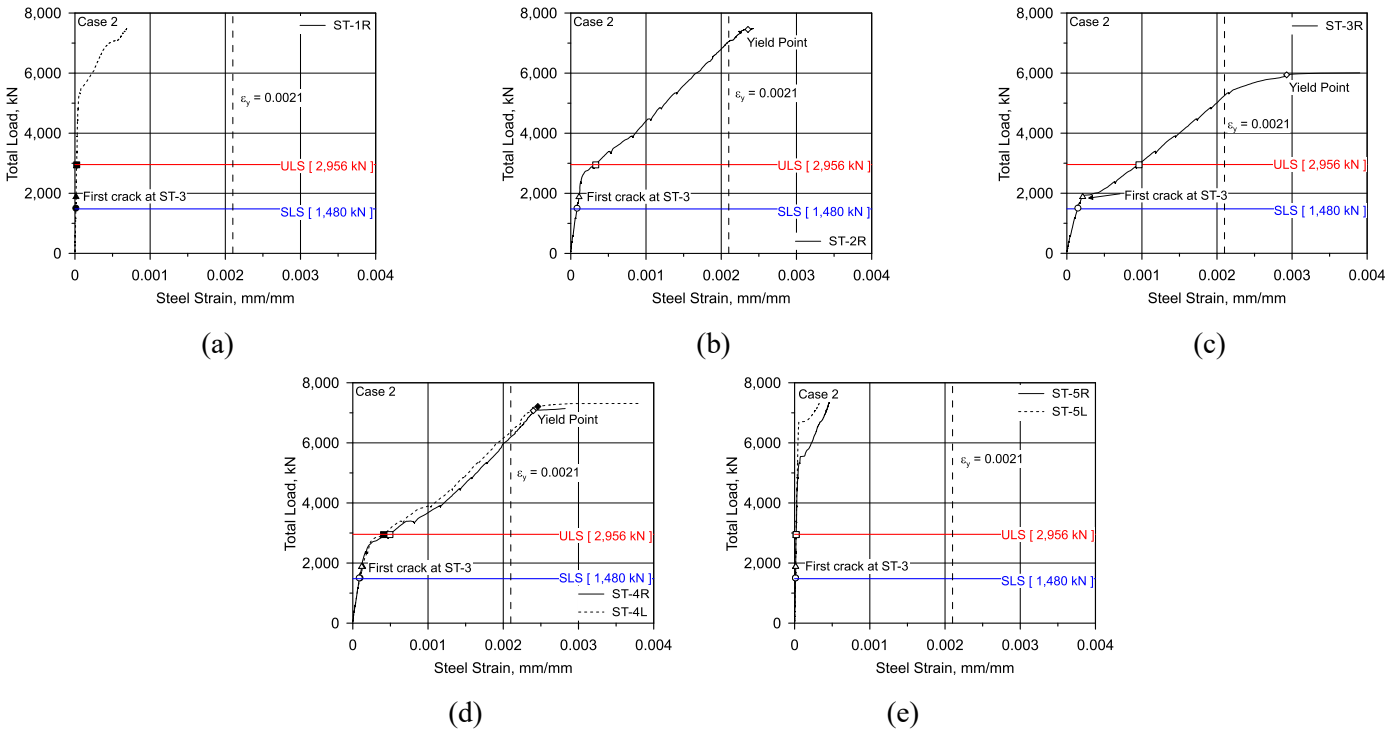


Figure C.2 Load-strain curve of flexural reinforcement for Case 2

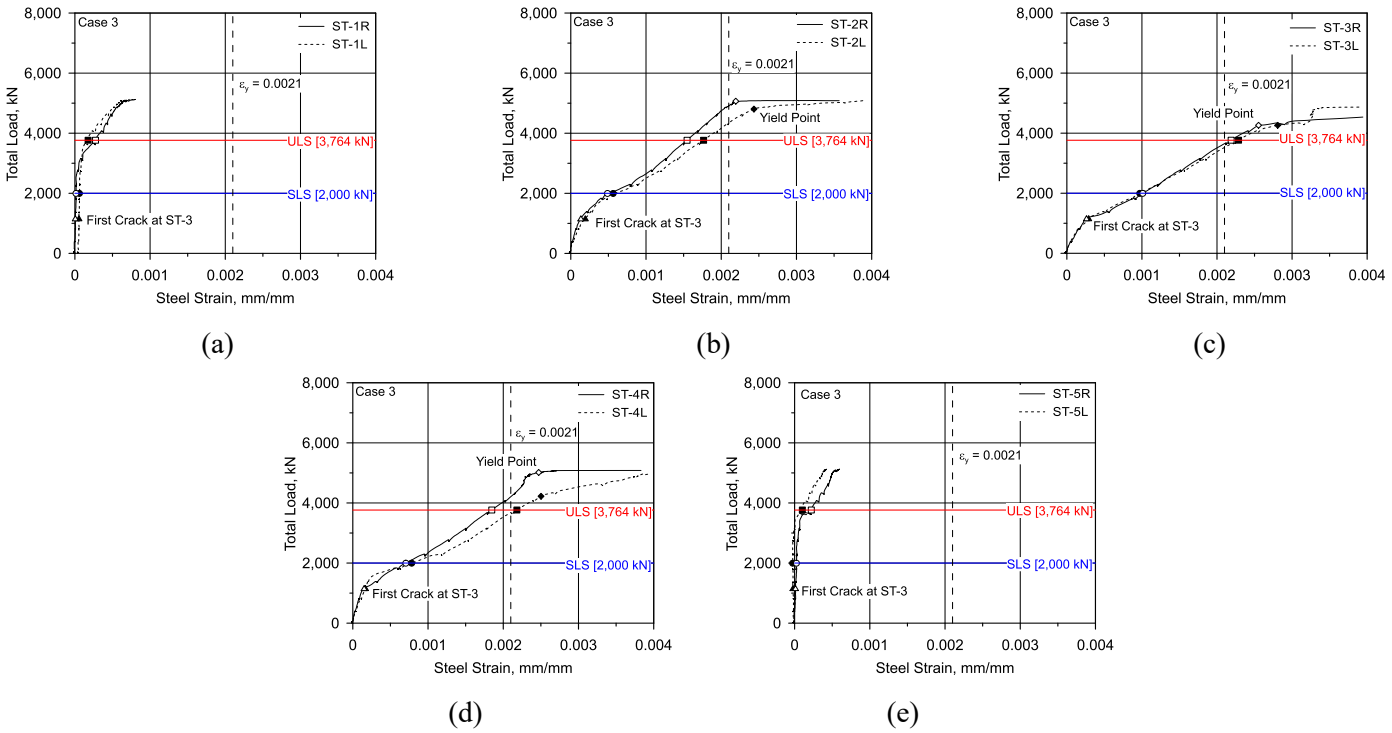


Figure C.3 Load-strain curve of flexural reinforcement for Case 3

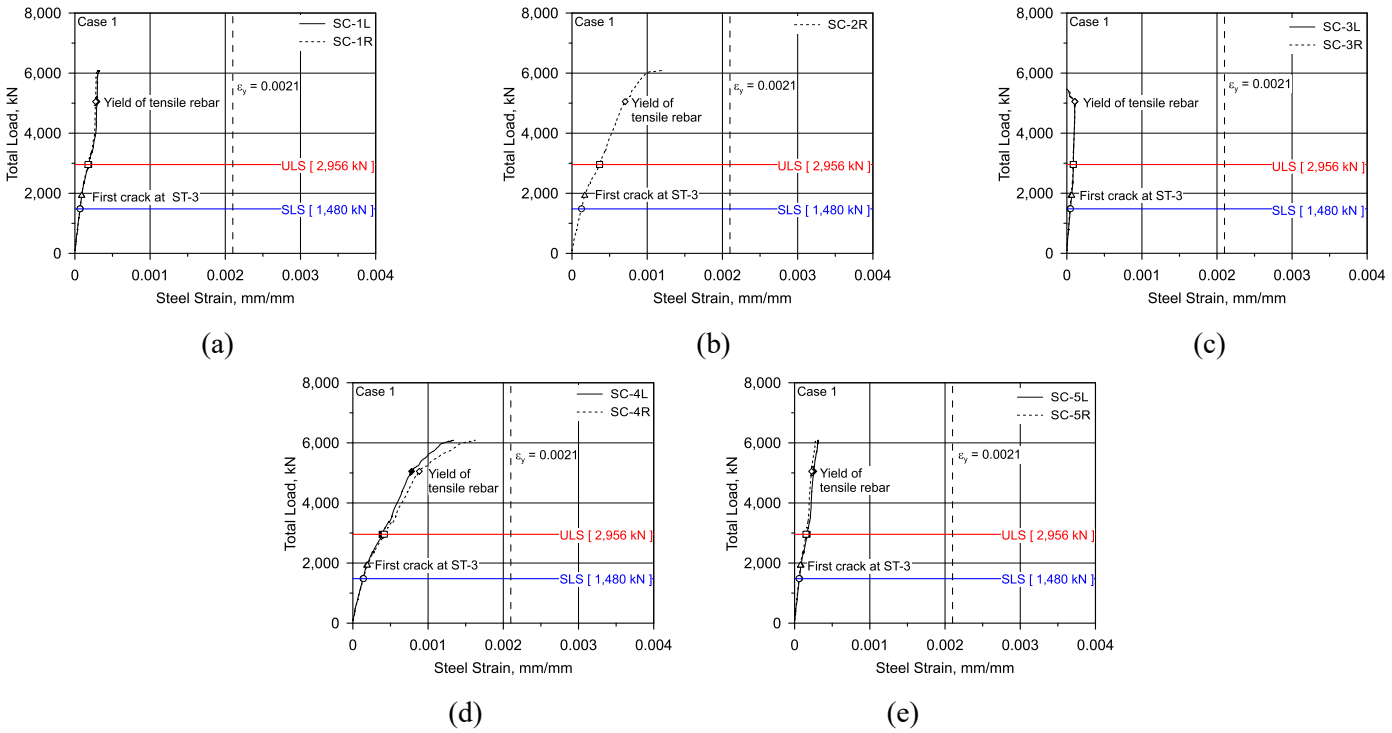


Figure C.4 Load-strain curve of compressive reinforcement for Case 1

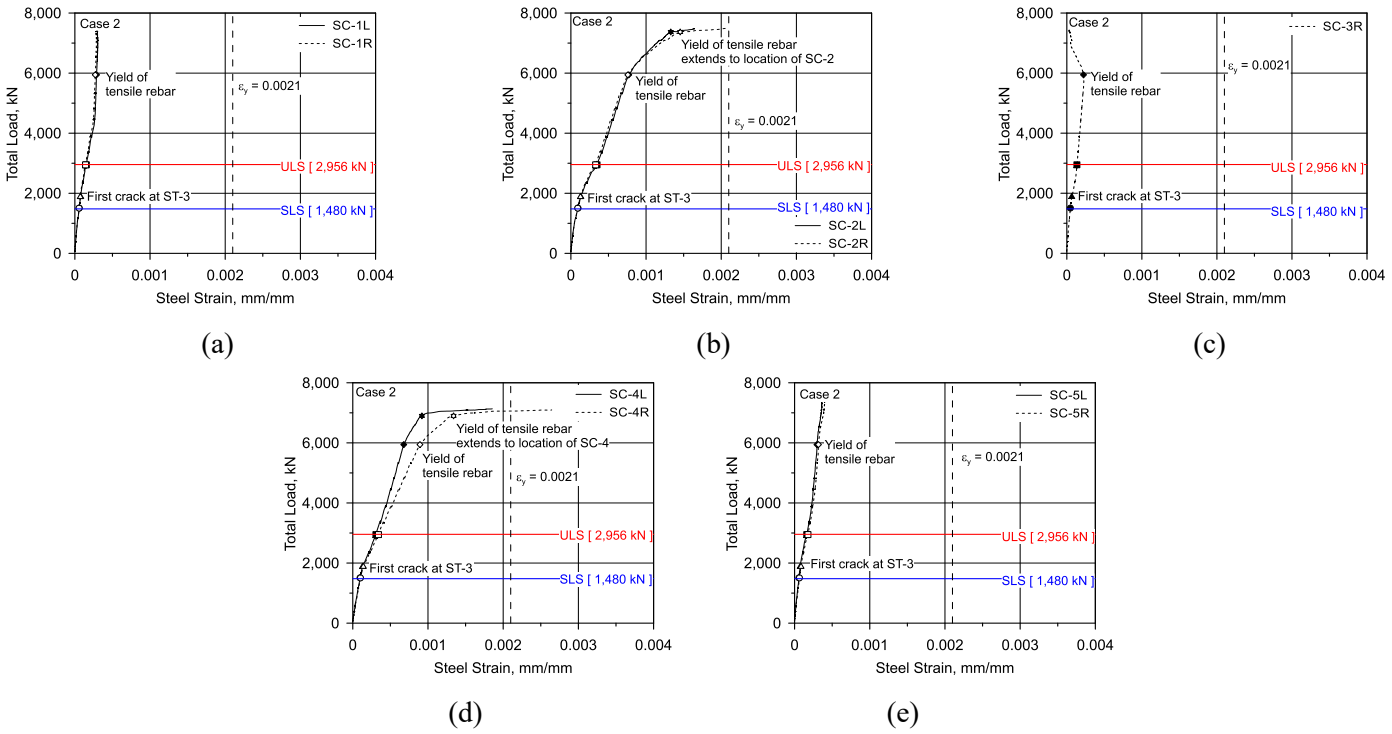


Figure C.5 Load-strain curve of compressive reinforcement for Case 2

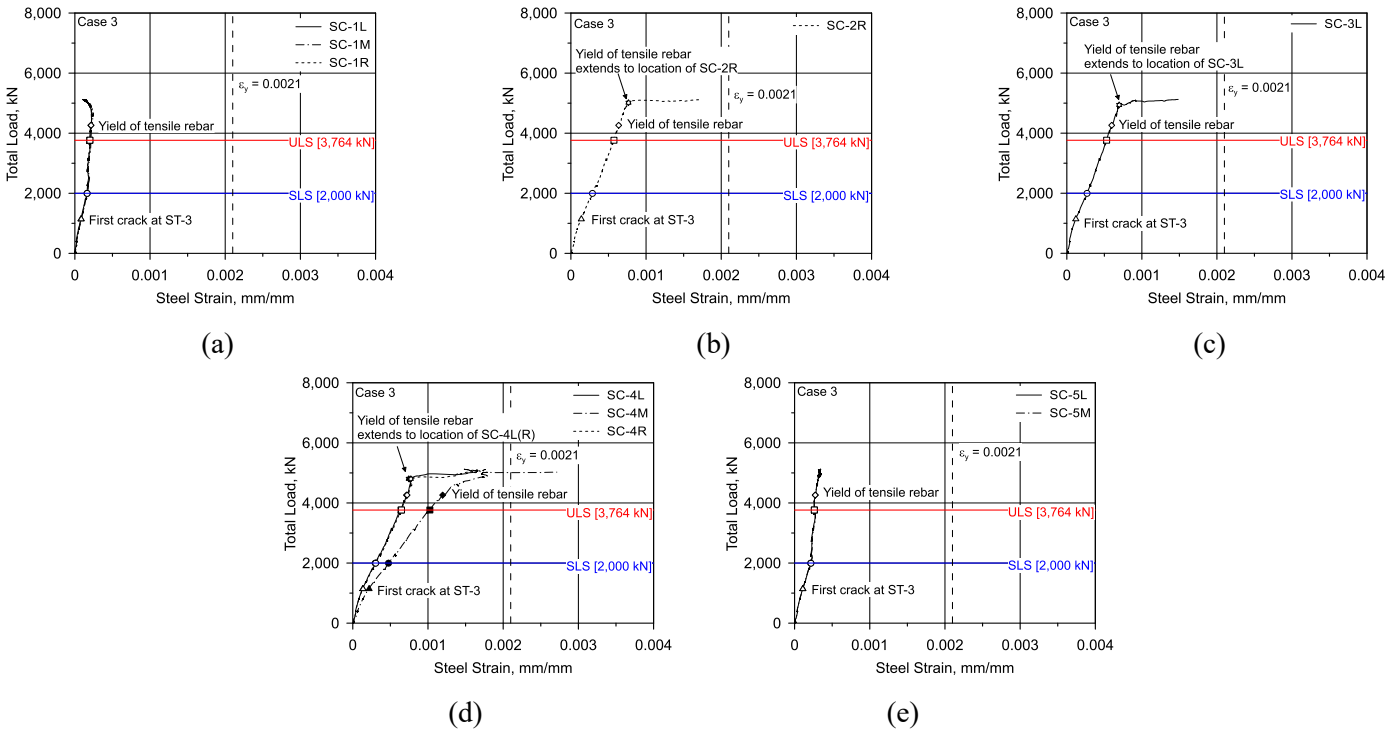


Figure C.6 Load-strain curve of compressive reinforcement for Case 3

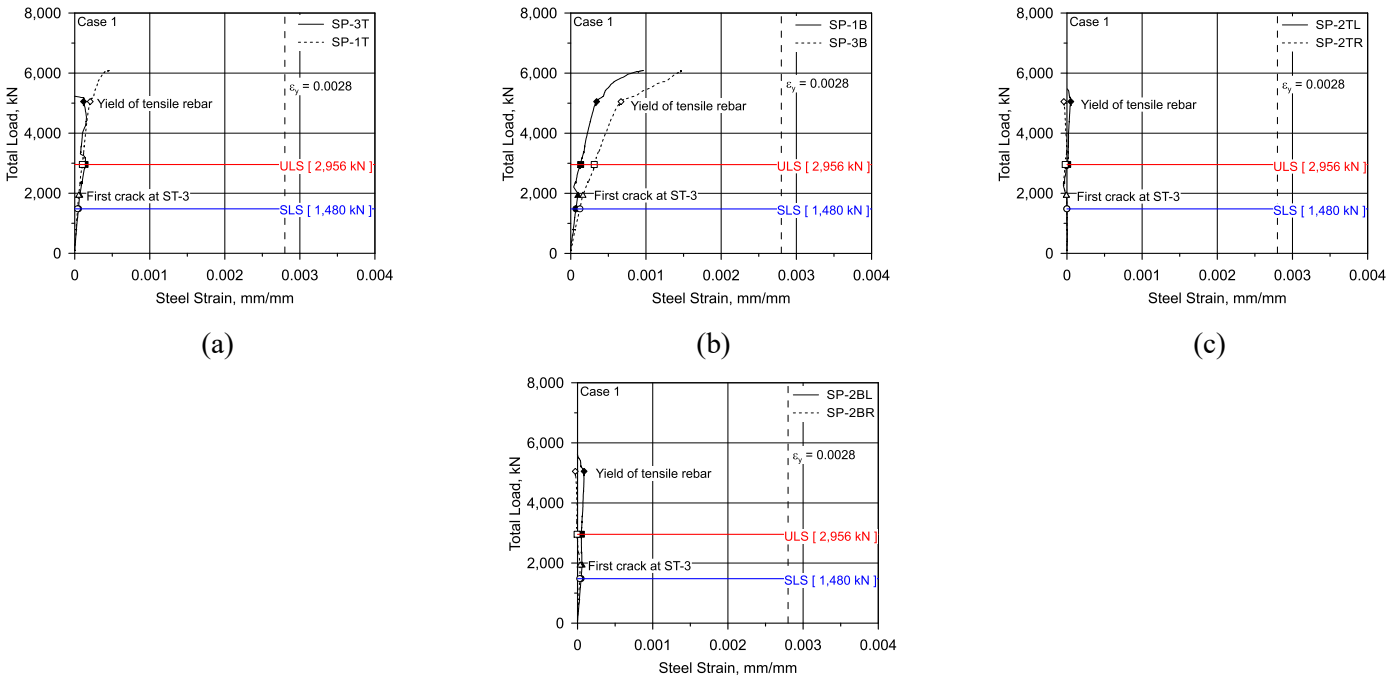


Figure C.7 Load-strain curve of column longitudinal rebar for Case 1

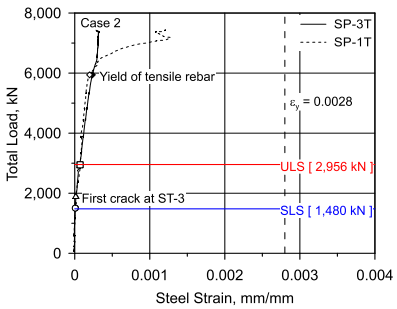


(a)

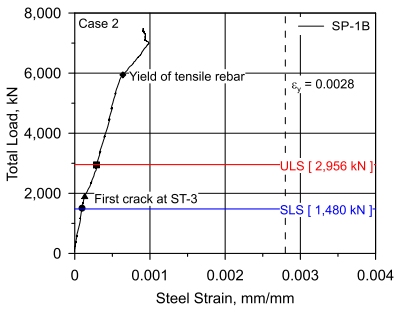


(b)

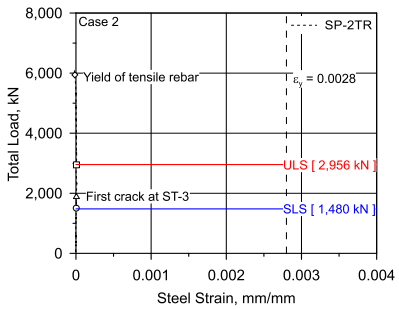


(c)

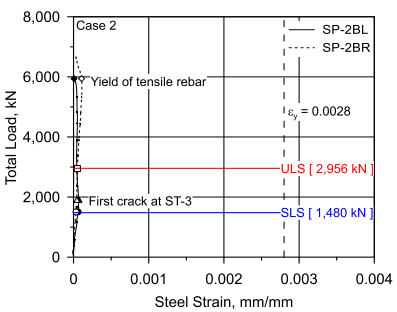


(d)

Figure C.8 Load-strain curve of column longitudinal rebar for Case 2

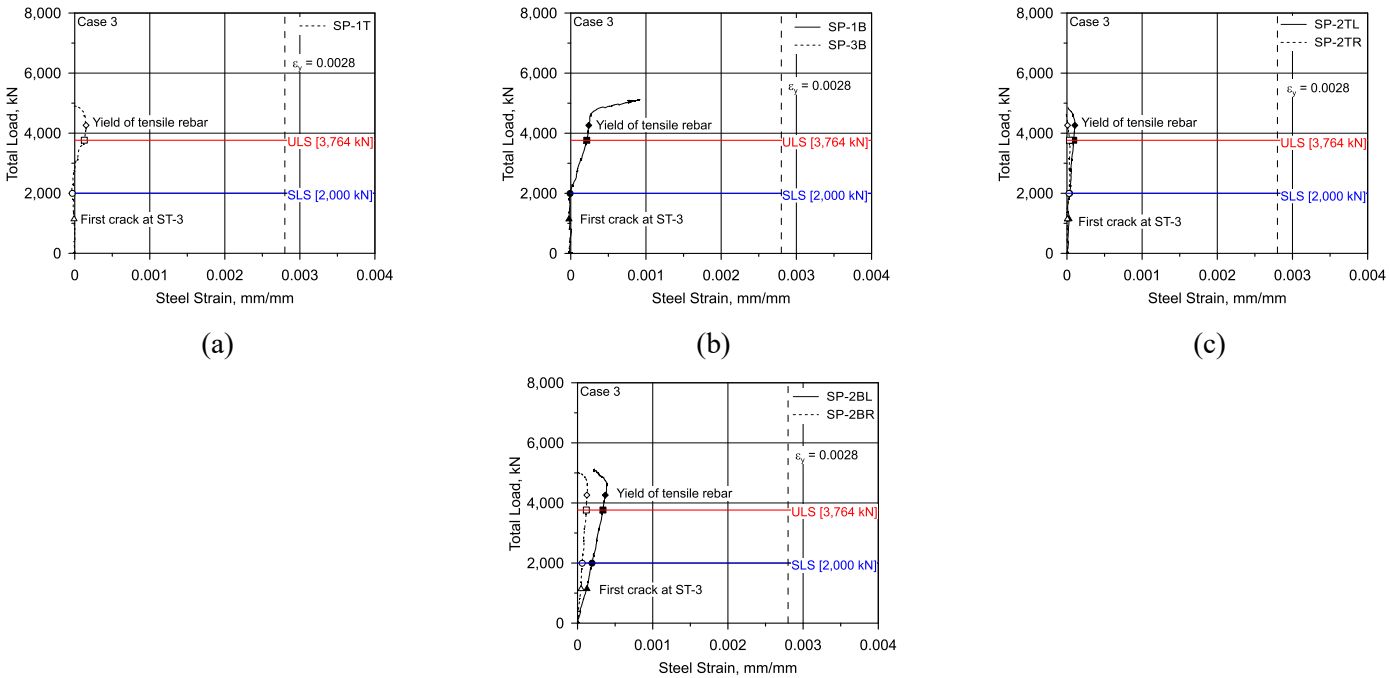


Figure C.9 Load-strain curve of column longitudinal rebar for Case 3

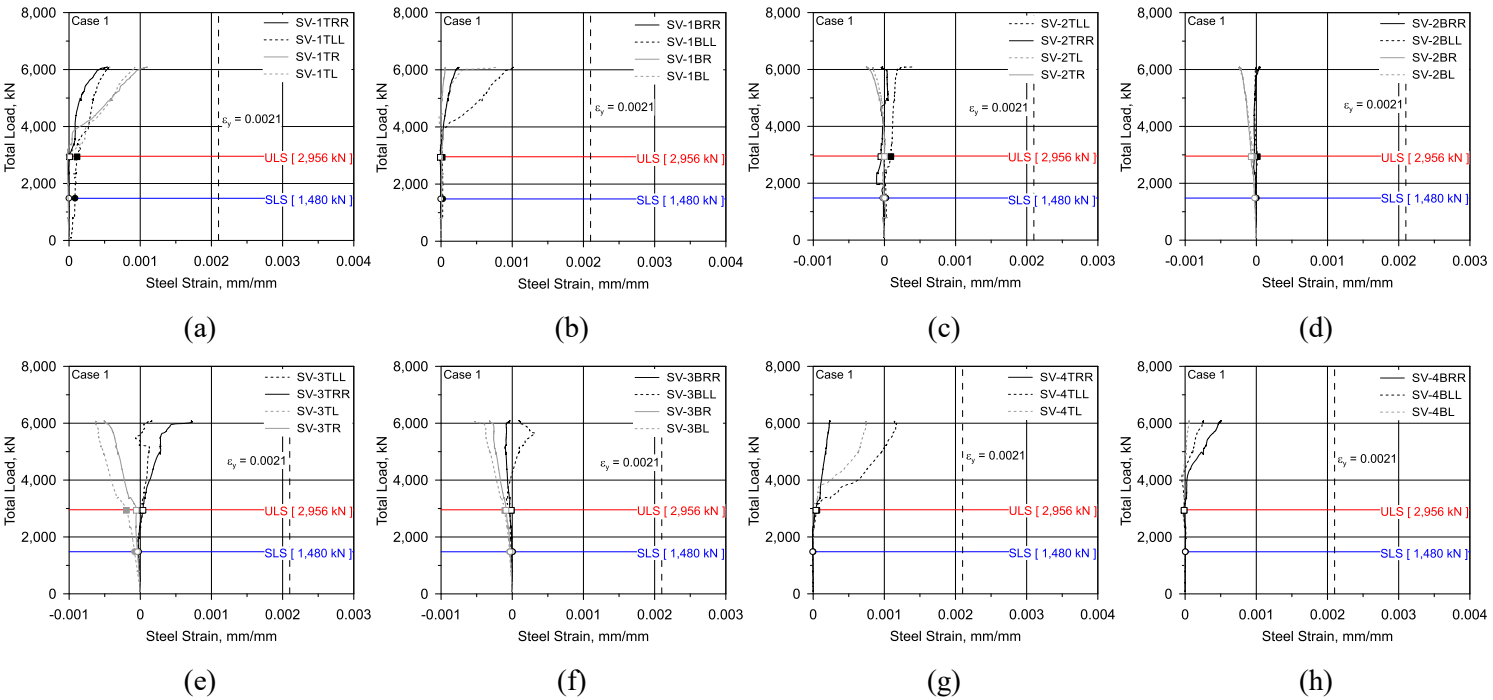


Figure C.10 Load-strain curve of vertical shear reinforcement for Case 1

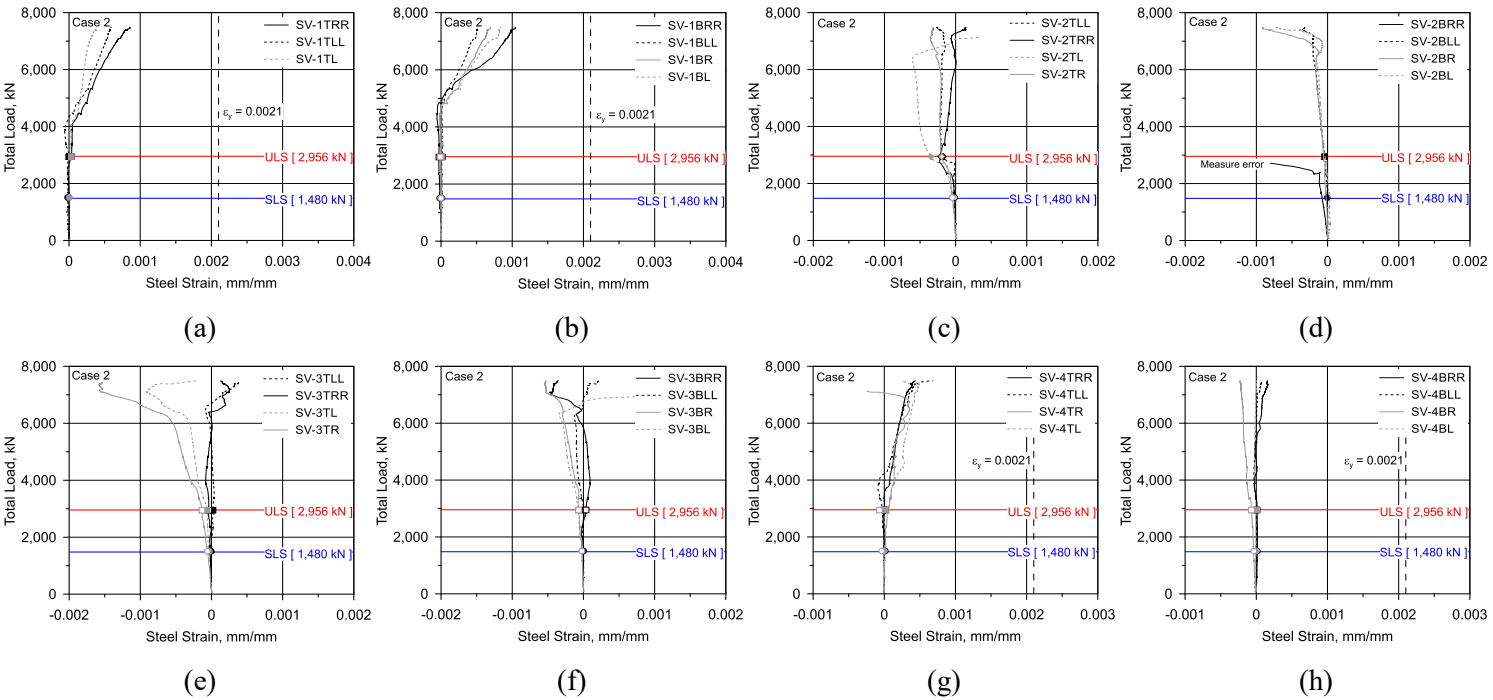


Figure C.11 Load-strain curve of vertical shear reinforcement for Case 2

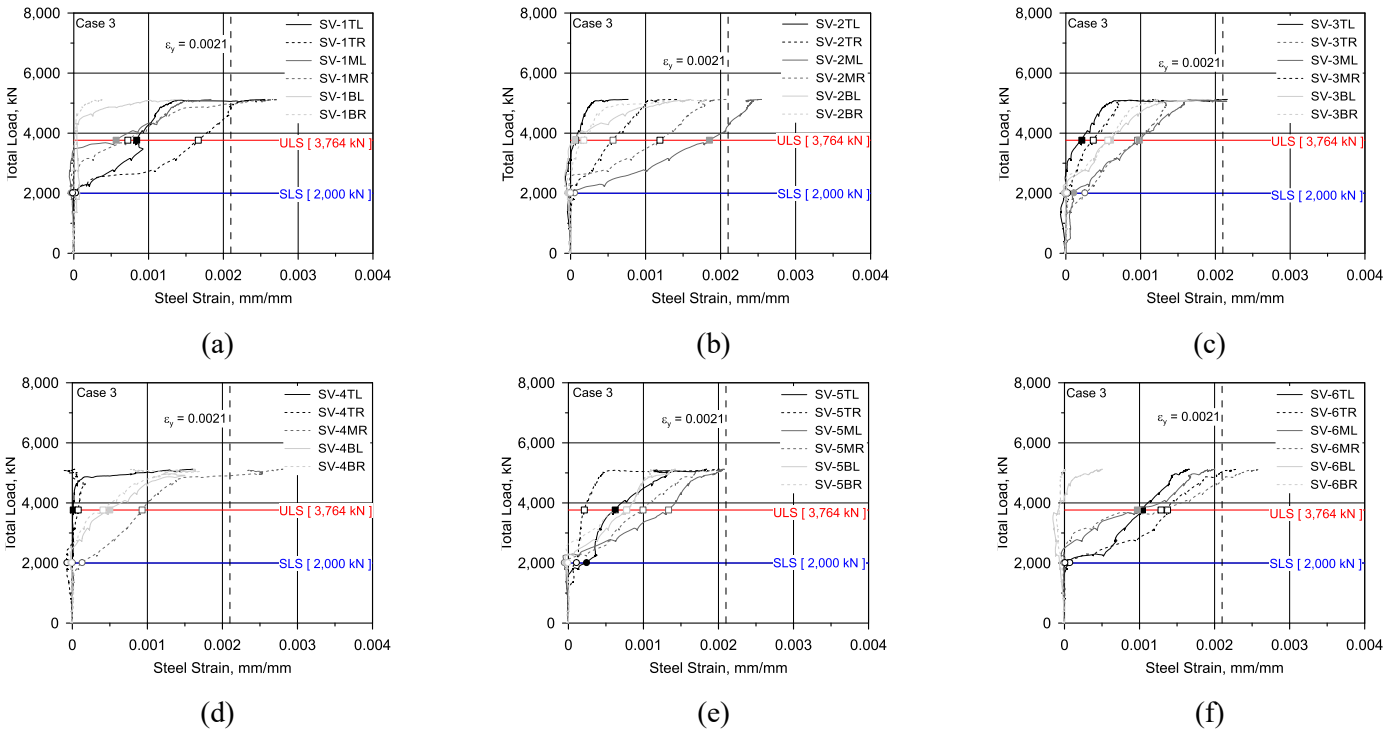


Figure C.12 Load-strain curve of vertical shear reinforcement for Case 3

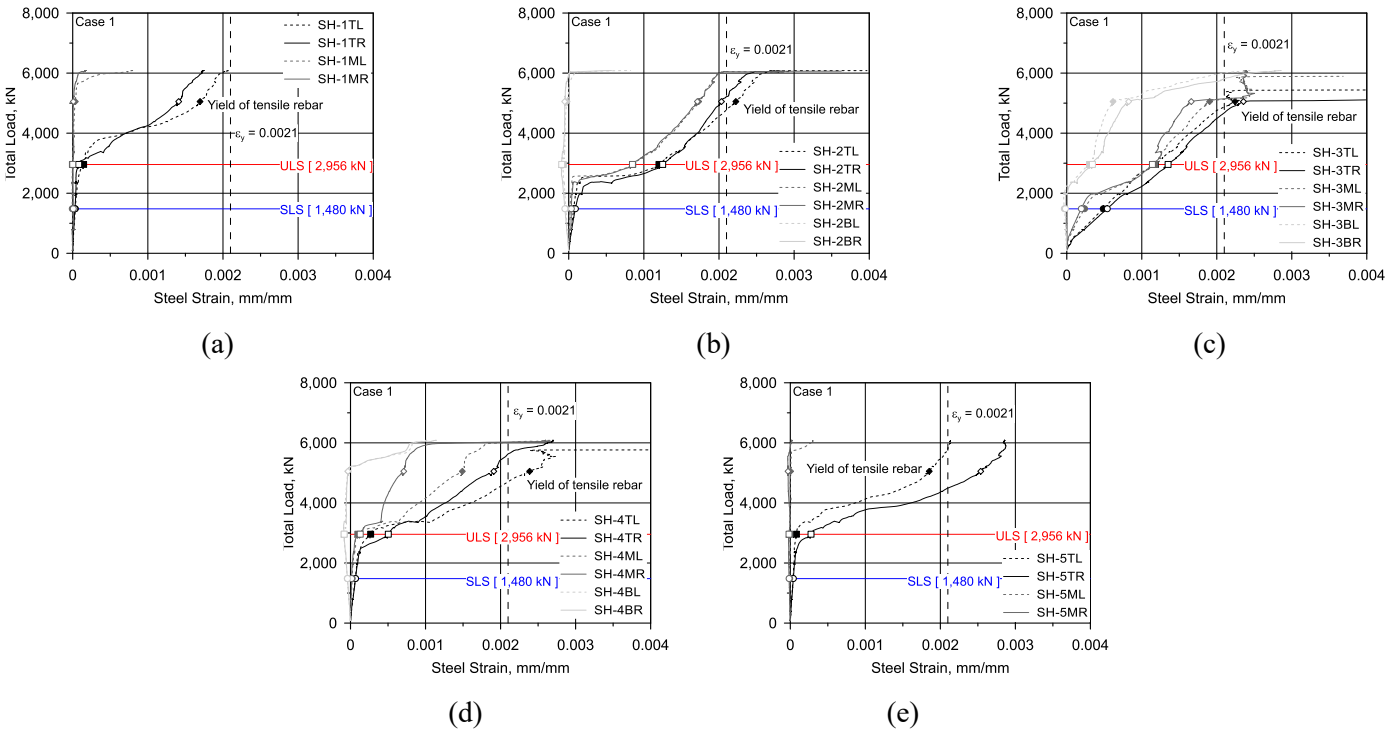


Figure C.13 Load-strain curve of horizontal shear rebar for Case 1

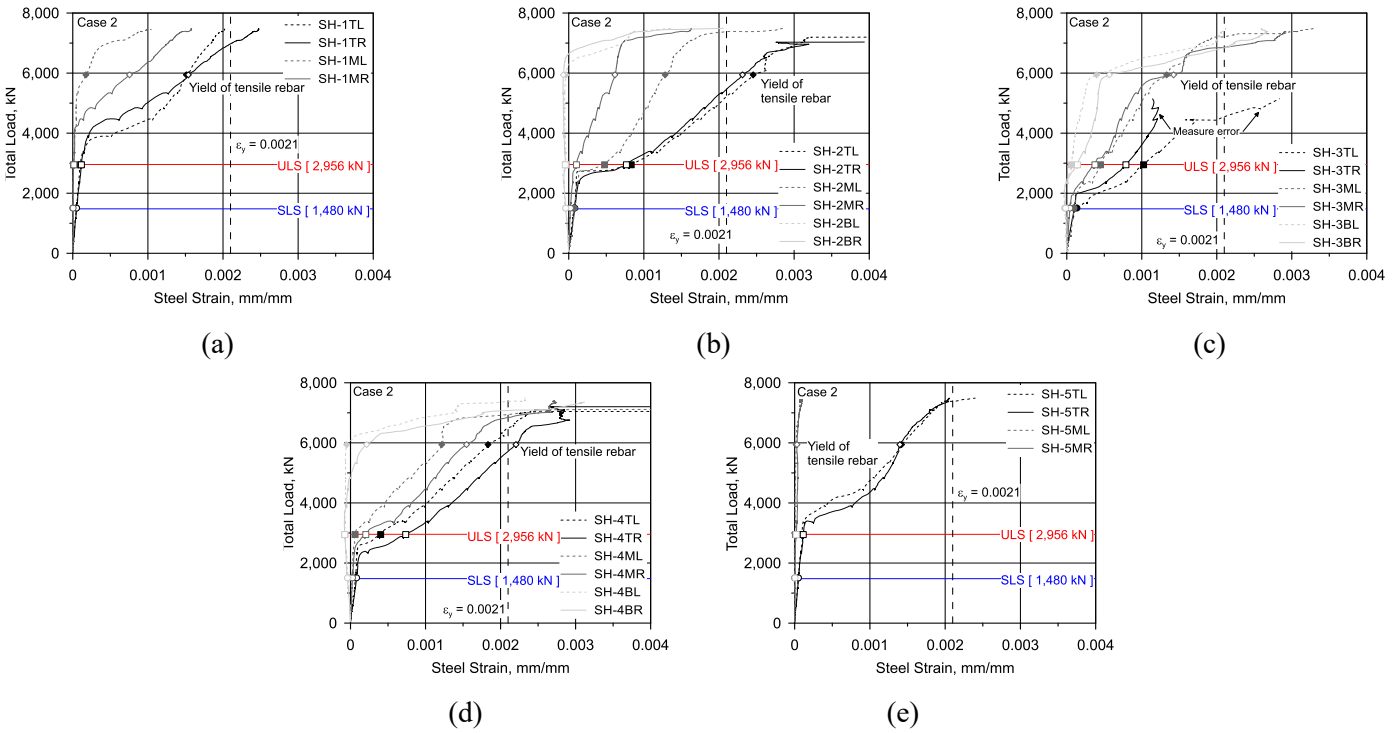


Figure C.14 Load-strain curve of horizontal shear rebar for Case 2

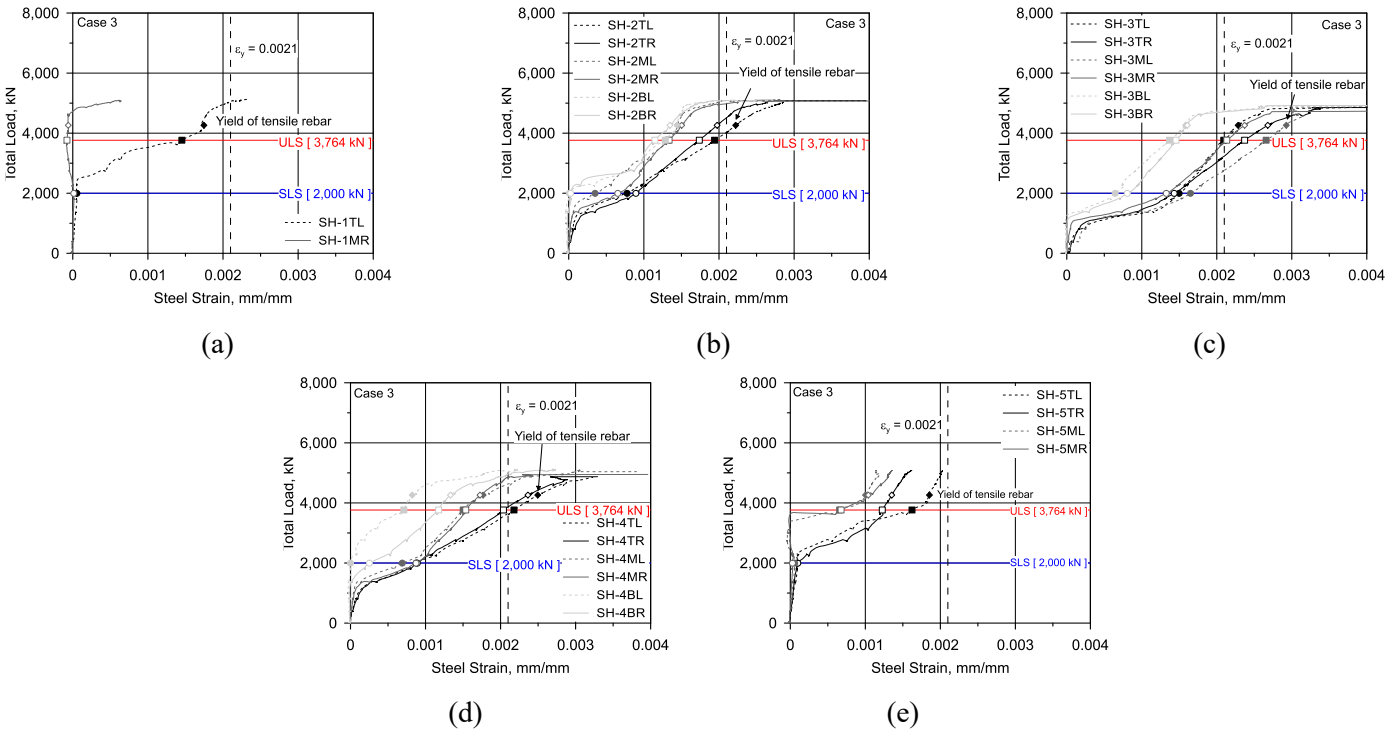


Figure C.15 Load-strain curve of horizontal shear rebar for Case 3

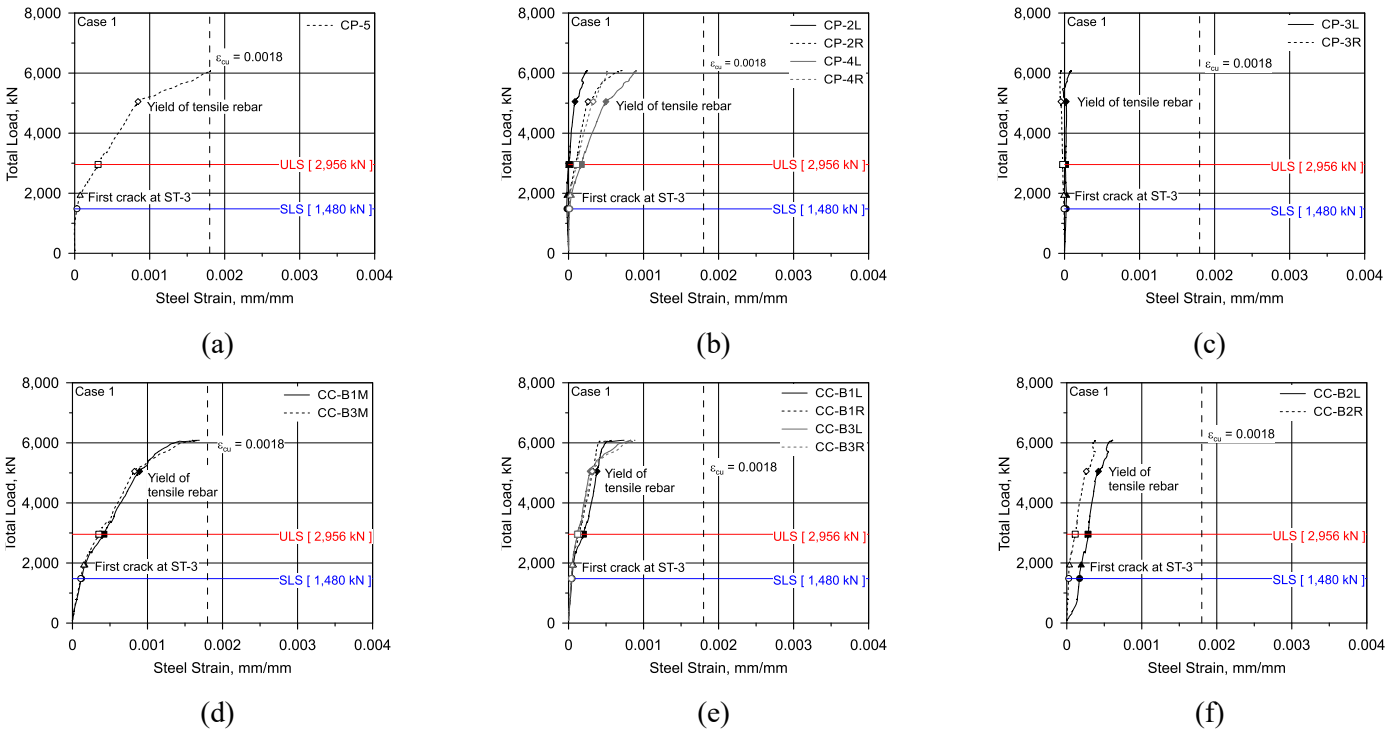


Figure C.16 Load-strain curve of concrete for Case 1

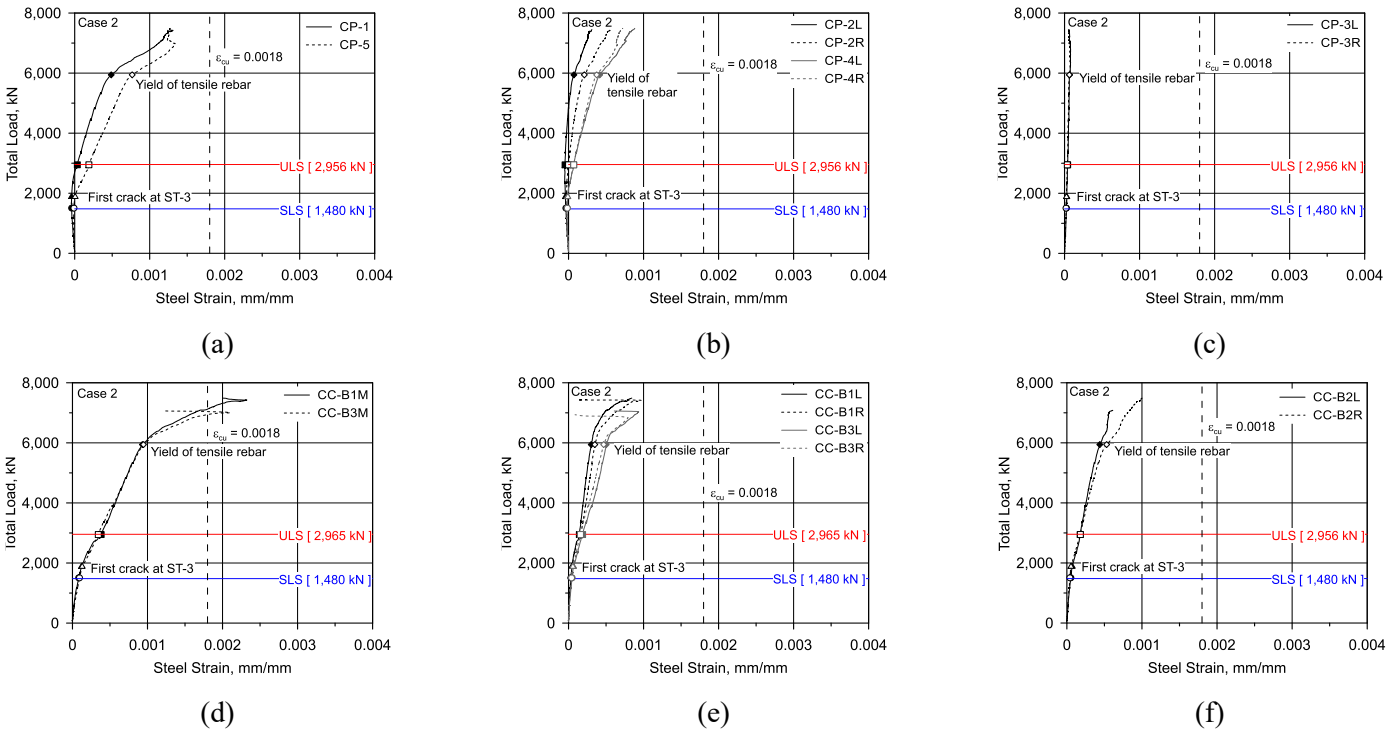


Figure C.17 Load-strain curve of concrete for Case 2

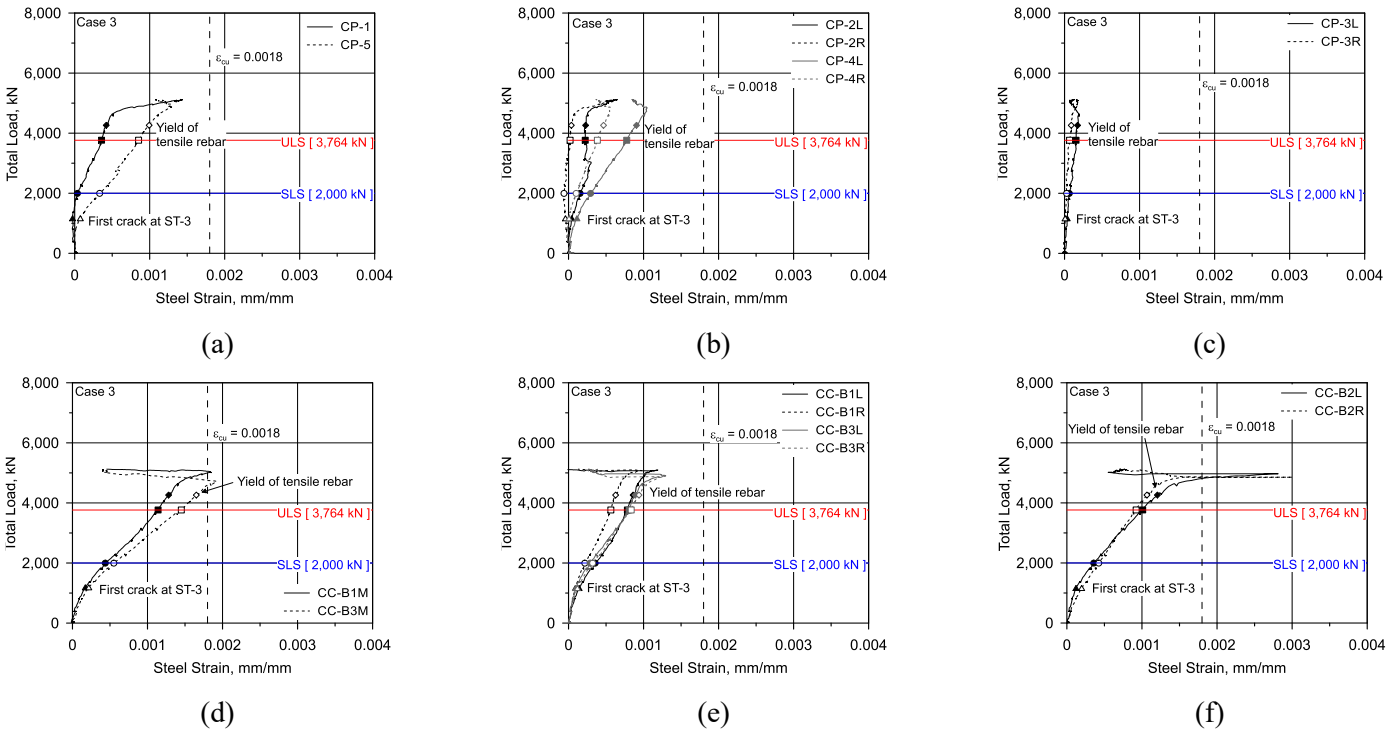


Figure C.18 Load-strain curve of concrete for Case 3

# Appendix D

# Crack width calculations

## D.1. Properties for crack width calculation

In design codes, crack width can be calculated by product of crack spacing and the difference of average strains for steel rebar and concrete between occurred cracks. In this concept, linear elastic stress distribution for the cross section where maximum moment is acting is assumed.

In linear elastic analysis, neutral axis shown in Equation D.2 can be addressed using the Equation D.3. With the loading properties of the experimental cases, maximum moments at SLS can also be calculated. Then, the tensile stress of rebar at the SLS moment can be calculated by Equation D.4 and tensile stress of rebar at first cracked state also can be addressed by Equation D.6. In calculation, all horizontal rebar is considered for flexural rebar.

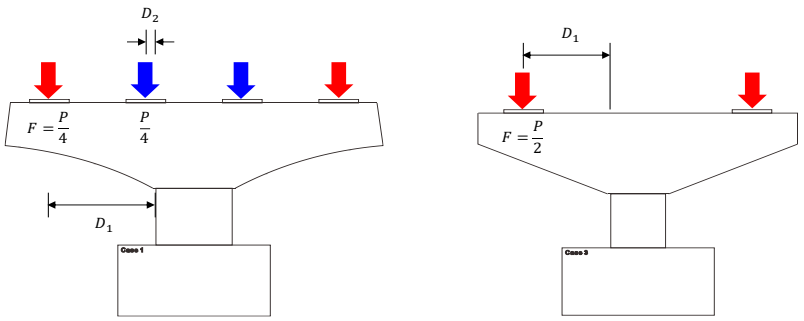


Figure D.1 Pier cap loading properties for experimental cases

$$M_{SLS} = F \cdot (D_1 + D_2) \tag{D.1}$$

$$c = kd \tag{D.2}$$

$$k = \sqrt{(n\rho)^2 + 2n\rho} - n\rho \tag{D.3}$$

$$f_{so} = \frac{M_{SLS}}{A_s(1-k/3)d} \tag{D.4}$$

$$f_{ctm} = 0.3(f_{ck} + 4)^{2/3} \tag{D.5}$$

$$f_{sr} = \frac{M_{cr}}{A_s(1-k/3)d} = \frac{0.625\sqrt{f_{ck}}C\frac{b_w h^2}{6}}{A_s(1-k/3)d} \tag{D.6}$$

The maximum moment at SLS for Case 1 to 3 is following. The moment in Case 1 and Case 2 are addressed in Equation D.7 and that of Case 3 is in D.8.

$$M_{SLS} = \left(\frac{1{,}480{,}000}{4}\right)(1{,}397.5 + 132.5) = 566{,}100{,}000 \text{ N}\cdot\text{mm} \tag{D.7}$$

$$M_{SLS} = \left(\frac{2{,}000{,}000}{2}\right)(1{,}140) = 1{,}140{,}000{,}000 \text{ N}\cdot\text{mm} \tag{D.8}$$

Then, the tensile stresses of rebar at the SLS moment were calculated by Equation D.9 for Case 1, D.10 for Case 2, and D.11 for Case 3.

$$f_{so} = \frac{M_{SLS}}{A_s(1-k/3)d} = \frac{566{,}100{,}000}{4{,}135(1-0.1957/3)(1{,}147)} = 128 \text{ MPa} \tag{D.9}$$

$$f_{so} = \frac{M_{SLS}}{A_s(1-k/3)d} = \frac{566{,}100{,}000}{6{,}703(1-0.2647/3)(924)} = 100 \text{ MPa} \tag{D.10}$$

$$f_{so} = \frac{M_{SLS}}{A_s(1-k/3)d} = \frac{1{,}140{,}000{,}000}{9{,}052(1-0.3239/3)(860)} = 164 \text{ MPa} \quad \text{(D.11)}$$

The tensile stresses of rebar at first cracked state were calculated by Equation D.12 for Case 1, D.13 for Case 2, and D.14 for Case 3.

$$f_{sr} = \frac{0.625\sqrt{f_{ck}}C\frac{b_w h^2}{6}}{A_s(1-k/3)d} = \frac{0.625\sqrt{35}\frac{1{,}200\times(1{,}200)^2}{6}}{4{,}135(1-0.1957/3)(1{,}147)} = 240 \text{ MPa} \quad \text{(D.12)}$$

$$f_{sr} = \frac{0.625\sqrt{f_{ck}}C\frac{b_w h^2}{6}}{A_s(1-k/3)d} = \frac{0.625\sqrt{32}\frac{1{,}200\times(1{,}200)^2}{6}}{6{,}703(1-0.2647/3)(924)} = 180 \text{ MPa} \quad \text{(D.13)}$$

$$f_{sr} = \frac{0.625\sqrt{f_{ck}}C\frac{b_w h^2}{6}}{A_s(1-k/3)d} = \frac{0.625\sqrt{36}\frac{1{,}080\times(1{,}010)^2}{6}}{9{,}052(1-0.3239/3)(860)} = 99 \text{ MPa} \quad \text{(D.14)}$$

The tensile strengths of concrete at first crack were calculated by Equation D.15 for Case 1, D.16 for Case 2, and D.17 for Case 3.

$$f_{ctm} = 0.3(35+4)^{2/3} = 3.45 \text{ MPa} \quad \text{(D.15)}$$

$$f_{ctm} = 0.3(32+4)^{2/3} = 3.27 \text{ MPa} \quad \text{(D.16)}$$

$$f_{ctm} = 0.3(36+4)^{2/3} = 3.51 \text{ MPa} \quad \text{(D.17)}$$

## D.2. Design crack width in KHBDC (2015)

### D.2.1 Case 1

*D.2.1.1 Calculation of difference of average strain for rebar and concrete*

In KHBDC 5.8.3.4, effective tension depth for concrete is following.

$$d_{cte} = \min\left[2.5(h-d),\ (h-c)/3,\ h/2\right] = 133 \text{ mm} \quad \text{(D.18)}$$

In KHBDC Equation 5.8.6, effective reinforcement ratio is following.

$$\rho_e = \left(A_s + \xi_1^2 A_p\right) / A_{cte} = A_s / \left(d_{cte} b_w\right) = 4{,}135 / \left(133 \times 1{,}200\right) = 0.0259 \quad \text{(D.19)}$$

The strain difference in KHBDC Equation 5.8.5 is shown in below.

$$\left(\varepsilon_{sm} - \varepsilon_{cm}\right) = \frac{f_{so}}{E_s} - 0.4\frac{f_{cte}}{E_s \rho_e}\left(1 + n\rho_e\right) = 0.00032 \geq 0.6\frac{f_{so}}{E_s} = 0.00038 \quad \text{(D.20)}$$

*D.2.1.2 Calculation of maximum crack spacing*

In KHBDC Equation 5.8.7a, maximum crack spacing is following.

$$l_{r,\max} = 3.4c_c + \frac{0.425 k_1 k_2 d_b}{\rho_e} = 213 \text{ mm} \quad \text{(D.21)}$$

*D.2.1.3 Design crack width*

Design crack width can be obtained by KHBDC Equation 5.8.4.

$$\omega_k = l_{r,\max}\left(\varepsilon_{sm} - \varepsilon_{cm}\right) = 213 \times 0.00038 = 0.08 \text{ mm} \quad \text{(D.22)}$$

## D.2.2 Case 2

*D.2.2.1 Calculation of difference of average strain for rebar and concrete*

In KHBDC 5.8.3.4, effective tension depth for concrete is following.

$$d_{cte} = \min\left[2.5(h-d),\ (h-c)/3,\ h/2\right] = 318 \text{ mm} \quad \text{(D.23)}$$

In KHBDC Equation 5.8.6, effective reinforcement ratio is following.

$$\rho_e = \frac{A_s + \xi_1^2 A_p}{A_{cte}} = \frac{A_s}{d_{cte} b_w} = \frac{5,419}{318 \times 1,200} = 0.0142 \quad \text{(D.24)}$$

The strain difference in KHBDC Equation 5.8.5 is shown in below.

$$\left(\varepsilon_{sm} - \varepsilon_{cm}\right) = \frac{f_{so}}{E_s} - 0.4\frac{f_{cte}}{E_s \rho_e}\left(1 + n\rho_e\right) = -0.00006 \geq 0.6\frac{f_{so}}{E_s} = 0.00030 \quad \text{(D.25)}$$

*D.2.2.2 Calculation of maximum crack spacing*

In KHBDC Equation 5.8.7a, maximum crack spacing is following.

$$l_{r,\max} = 3.4c_c + \frac{0.425 k_1 k_2 d_b}{\rho_e} = 299 \text{ mm} \quad \text{(D.26)}$$

*D.2.2.3 Design crack width*

With the maximum crack spacing and the strain difference calculated, design crack width can be obtained by KHBDC Equation 5.8.4 as following.

$$\omega_k = l_{r,\max}\left(\varepsilon_{sm} - \varepsilon_{cm}\right) = 299 \times 0.00030 = 0.09 \text{ mm} \quad \text{(D.27)}$$

## D.2.3 Case 3

*D.2.3.1 Calculation of difference of average strain for rebar and concrete*

In KHBDC 5.8.3.4, effective tension depth for concrete is following.

$$d_{cte} = \min\left[2.5(h-d),\ (h-c)/3,\ h/2\right] = 244 \text{ mm} \tag{D.28}$$

In KHBDC Equation 5.8.6, effective reinforcement ratio is following.

$$\rho_e = \frac{A_s + \xi_1^2 A_p}{A_{cte}} = \frac{A_s}{d_{cte} b_w} = \frac{8{,}196}{244 \times 1{,}080} = 0.0311 \tag{D.29}$$

The strain difference in KHBDC Equation 5.8.5 is shown in below.

$$\left(\varepsilon_{sm} - \varepsilon_{cm}\right) = \frac{f_{so}}{E_s} - 0.4\frac{f_{cte}}{E_s \rho_e}\left(1 + n\rho_e\right) = 0.00054 \geq 0.6\frac{f_{so}}{E_s} = 0.00049 \tag{D.30}$$

*D.2.3.2 Calculation of maximum crack spacing*

In KHBDC Equation 5.8.7a, maximum crack spacing is following.

$$l_{r,\max} = 3.4c_c + \frac{0.425 k_1 k_2 d_b}{\rho_e} = 196 \text{ mm} \tag{D.31}$$

*D.2.3.3 Design crack width*

With the maximum crack spacing and the strain difference calculated, design crack width can be obtained by KHBDC Equation 5.8.4 as following.

$$\omega_k = l_{r,\max}\left(\varepsilon_{sm} - \varepsilon_{cm}\right) = 196 \times 0.00054 = 0.11 \text{ mm} \tag{D.32}$$

## D.3. Design crack width in KCI (2017)

### D.3.1 Case 1

*D.3.1.1 Calculation of difference of average strain for rebar and concrete*

In KCI III.3.3, effective tension depth for concrete is following.

$$d_{cte} = \min\left[2.5(h-d),\ (h-c)/3\right] = 133 \text{ mm} \quad \text{(D.33)}$$

In KCI Equation III.3.5, effective reinforcement ratio is following.

$$\rho_e = \left(A_s + \xi_1^2 A_p\right)/A_{cte} = A_s/\left(d_{cte} b_w\right) = 4{,}135/\left(133\times 1{,}200\right) = 0.0259 \quad \text{(D.34)}$$

The strain difference in KCI Equation III.3.7 is shown in below.

$$\left(\varepsilon_{sm} - \varepsilon_{cm}\right) = \frac{f_{so}}{E_s}\left[1 - \beta_1\beta_2\left(1 + n_i\rho_e\right)\left(\frac{f_{sr}}{f_{so}}\right)^2\right] \geq 0.6\frac{f_{so}}{E_s} = 0.00038 \quad \text{(D.35)}$$

*D.3.1.2 Calculation of maximum crack spacing*

In KCI Equation III.3.3, average crack spacing is following.

$$l_s = 2c_c + \frac{0.25k_1k_2d_b}{\rho_e} = 125 \text{ mm} \quad \text{(D.36)}$$

*D.3.1.3 Design crack width*

Design crack width can be obtained by KCI Equation III.3.2.

$$\omega_d = \kappa_{st} l_s \left(\varepsilon_{sm} - \varepsilon_{cm}\right) = 1.7\times 125\times 0.00038 = 0.08 \text{ mm} \quad \text{(D.37)}$$

## D.3.2 Case 2

*D.3.2.1 Calculation of difference of average strain for rebar and concrete*

In KCI III.3.3, effective tension depth for concrete is following.

$$d_{cte} = \min\left[2.5(h-d),\ (h-c)/3,\ h/2\right] = 318 \text{ mm} \quad \text{(D.38)}$$

In KCI Equation III.3.5, effective reinforcement ratio is following.

$$\rho_e = \frac{A_s + \xi_1^2 A_p}{A_{cte}} = \frac{A_s}{d_{cte} b_w} = \frac{5,419}{318 \times 1,200} = 0.0142 \quad \text{(D.39)}$$

The strain difference in KCI Equation III.3.7 is shown in below.

$$(\varepsilon_{sm} - \varepsilon_{cm}) = \frac{f_{so}}{E_s}\left[1 - \beta_1\beta_2(1 + n_i\rho_e)\left(\frac{f_{sr}}{f_{so}}\right)^2\right] \geq 0.6\frac{f_{so}}{E_s} = 0.00030 \quad \text{(D.40)}$$

*D.3.2.2 Calculation of maximum crack spacing*

In KCI Equation III.3.3, average crack spacing is following.

$$l_s = 2c_c + \frac{0.25 k_1 k_2 d_b}{\rho_e} = 176 \text{ mm} \quad \text{(D.41)}$$

*D.3.2.3 Design crack width*

With the average crack spacing and the strain difference calculated, design crack width can be obtained by KCI Equation III.3.2.

$$\omega_d = \kappa_{st} l_s (\varepsilon_{sm} - \varepsilon_{cm}) = 1.7 \times 176 \times 0.00030 = 0.09 \text{ mm} \quad \text{(D.42)}$$

## D.3.3 Case 3

*D.3.3.1 Calculation of difference of average strain for rebar and concrete*

In KCI III.3.3, effective tension depth for concrete is following.

$$d_{cte} = \min\left[2.5(h-d),\ (h-c)/3,\ h/2\right] = 244 \text{ mm} \quad \text{(D.43)}$$

In KCI Equation III.3.5, effective reinforcement ratio is following.

$$\rho_e = \frac{A_s + \xi_1^2 A_p}{A_{cte}} = \frac{A_s}{d_{cte} b_w} = \frac{5,419}{318 \times 1,200} = 0.0311 \quad \text{(D.44)}$$

The strain difference in KCI Equation III.3.7 is shown in below.

$$(\varepsilon_{sm} - \varepsilon_{cm}) = \frac{f_{so}}{E_s}\left[1 - \beta_1\beta_2(1 + n_i\rho_e)\left(\frac{f_{sr}}{f_{so}}\right)^2\right] \geq 0.6\frac{f_{so}}{E_s} = 0.00049 \quad \text{(D.45)}$$

*D.3.3.2 Calculation of maximum crack spacing*

In KCI Equation III.3.3, average crack spacing is following.

$$l_s = 2c_c + \frac{0.25k_1k_2d_b}{\rho_e} = 115 \text{ mm} \quad \text{(D.46)}$$

*D.3.3.3 Design crack width*

With the average crack spacing and the strain difference calculated, design crack width can be obtained by KCI Equation III.3.2.

$$\omega_d = \kappa_{st} l_s (\varepsilon_{sm} - \varepsilon_{cm}) = 1.7 \times 115 \times 0.00049 = 0.10 \text{ mm} \quad \text{(D.47)}$$

## D.4. Crack width prediction from test results

Based on the concept of calculating crack width in design codes, crack widths were calculated with the test data. In actual, the continuous average strain between cracks occurred at SLS shall be measured to predict the crack width from the measured strains. However, it is difficult to measure the entire area during the structural test, the average strain values from the local steel gauges located between the outer cracks at SLS were assumed to be $\varepsilon_{sm}$. Then, $\varepsilon_{cm}$ can be ignored because it is relatively very small. The average crack spacing can be obtained from the actual crack data containing the length of cracks and the number of cracks at SLS.

The measured steel gauge strains belong to the area where cracks occurred at SLS are presented in Table D.1.

Table D.1 Average steel gauge from the test results

| Gauge label | Strain at SLS ($\times 10^{-3}$) | | | Note |
|---|---|---|---|---|
| | Case 1 | Case 2 | Case 3 | |
| ST-2L | 0.12 | - | 0.56 | The gauge locations are not within cracks at SLS for Case 2 |
| ST-2R | 0.08 | - | 0.49 | |
| ST-3L | 0.32 | - | 0.97 | ST-3L for Case 2 could not be measured |
| ST-3R | 0.36 | 0.14 | 1.01 | |
| ST-4L | 0.08 | - | 0.78 | The gauge locations are not within cracks at SLS for Case 2 |
| ST-4R | 0.13 | - | 0.70 | |
| $\varepsilon_{sm}$ | 0.18 | 0.14 | 0.75 | |

Table D.2 Average crack spacing from the test results

| Case | Crack properties at SLS | | |
|---|---|---|---|
| | Length between cracks (mm) | Number of cracks (EA) | $l_s$ (mm) |
| 1 | 2,140 | 6 | 428 |
| 2 | 1,340 | 6 | 268 |
| 3 | 1,900 | 9 | 238 |

Table D.3 Design crack width prediction from the test results

| Case | $\varepsilon_{sm}$ (mm/mm) | $l_s$ (mm) | $\kappa_{st}$ | $\omega_d$ (mm) |
|---|---|---|---|---|
| 1 | 0.00018 | 428 | 1.7 | 0.13 |
| 2 | 0.00014 | 268 | | 0.06 |
| 3 | 0.00075 | 238 | | 0.30 |

Table D.2 shows the details of calculating average crack spacing from the test. The average crack spacing can be obtained dividing length between cracks by the number of spacing from the number of cracks.

From the data, design crack width following the KCI (2017) can be calculated as shown in Table D.3.

# 국문초록

# 효율적인 교각 피어캡 설계를 위한 스트럿-타이 모델

박 재 현

교각 피어캡은 교량의 상부구조 및 차량하중을 교각 기둥부로 전달하는 부재로서 교량에서 매우 중요한 부재이다. 부재의 구조적 역할의 중요성에 의해 피어캡은 보수적인 설계가 이루어지는 경우가 많아 철근이 과다하게 배근 되어왔다. 그러나 피어캡 철근의 과다 배근은 교각 상부에 위치한 작업 환경 및 기둥 철근과의 간섭 등을 고려할 때 시공성을 크게 저하시키며, 필요 이상의 배근으로 인해 비경제적인 설계 결과를 초래한다.

한편, 하중 및 기하학적 조건에 따라 응력교란영역에 해당하는 교각 피어캡은 강도설계법에서 한계상태설계법으로의 설계 방법 전환에 따라 설계기준에서 제시하고 있는 스트럿-타이 모델 설계를 기반으로 철근을 배근하고 있다. 교각 피어캡의 스트럿-타이 모델 설계에서는 설계자의 재량에 따라 다양한 스트럿-타이 모델을 선정하여 부재를 설계할 수 있다. 그러나 설계자의 역량에 따라 설계 자유도가 보장된 스트럿-타이 모델 설계는 비효율적인 모델

선정에 따른 과도한 철근 배근의 가능성을 내재하고 있다. 이와 같은 보수적인 피어캡 설계를 지양하기 위해서는 합리적으로 교각 피어캡을 설계할 수 있는 설계가이드라인이 제시될 필요가 있으며, 이는 교각 피어캡의 설계 현황에 대한 분석 및 제시된 가이드라인의 구조적 안전성 평가를 통해 가능하다.

본 연구에서는 과도한 철근 배근에 따른 보수적인 설계를 방지할 수 있는 교각 피어캡의 보다 합리적인 설계 가이드라인을 제시하고자 한다. 이를 위해 설계기준에서의 교각 피어캡 설계 현황에 대한 분석, 축소모형을 통한 정적압축실험, 실험의 검증 및 매개변수연구를 위한 유한요소해석을 통한 해석 연구가 수행되었다.

한계상태설계법에 기반한 여러 설계기준에서 제시하는 교각 피어캡 설계 규정의 비교·분석 및 실제 스트럿-타이 모델을 사용한 교각 피어캡 설계 사례 분석을 통해 현행 교각 피어캡의 설계 현황을 파악하였다. 이를 토대로 보다 합리적인 철근 배근이 가능한 교각 피어캡의 스트럿-타이 모델 설계 가이드라인을 정립하였다.

제시된 교각 피어캡에 대한 설계 가이드라인의 구조적 안전성 평가를 위해 축소모형실험체를 제작하여 정적압축시험을 수행하고 비선형 유한요소해석을 수행하여 결과를 검증하였다. 실험은 제시된

설계 가이드라인에 따라 배근된 교각 피어캡 3 개소에 대하여 수평 전단철근량과 상부구조에 따른 하중 재하 분포를 고려하여 수행되었다. 실험을 통해 재하 하중, 처짐, 철근 및 콘크리트의 변형률, 균열 양상과 같은 구조 거동이 측정되었다. 실험 수행 결과, 제안된 설계 가이드라인에 따라 설계된 교각 피어캡은 극한한계상태(ULS)를 초과하는 하중 저항 능력을 보여 설계 가이드라인의 구조적 타당성을 검증하였다. 그러나 하중 분포 및 단면 크기에 따라 사용한계상태에서의 균열 진전 및 일관되지 못한 설계 안전율과 같은 한계가 발생하였다.

실험의 제한적인 변수 범위의 한계를 극복하여 다양한 단면 크기에서의 전단을 포함한 피어캡의 구조 거동을 관측하기 위해 유한요소해석 방법을 이용한 매개변수연구가 추가적으로 수행되었다. 그 결과 스트럿-타이 모델에 따른 철근 배근 이전에 전단강도에 대한 설계기준 식을 활용한 적절한 단면 크기를 선정하면 적절하게 단면을 선정할 수 있다는 것을 확인하였다. 또한 정정 스트럿-타이 모델 설계 시 수직 타이에 의해 부재 강도가 과소평가 되는 것을 전단강도에 대한 설계기준 식을 부재 강도의 하한으로 두어 보완할 수 있었다. 이를 통해 기존 제시되었던 설계 가이드라인의 한계를 보완한 개선된 설계 가이드라인을 제시하였다.

본 연구를 통해 교각 피어캡의 설계에서 구조적 안전성 및 사용성에 대한 평가가 수행되었으며, 보다 합리적인 설계가 가능하도록 교각 피어캡 설계 가이드라인이 제안되었다. 제시된 가이드라인은 설계 실무에서 교각 피어캡의 비효율적인 설계에 따른 과도한 철근 배근 및 과도한 단면 선정을 방지하여 사회 인프라 구조물의 시공성 및 경제성을 증진시킬 수 있을 것으로 기대된다.

**주요어:** 피어캡, 스트럿-타이 모델, 전단 철근비, 축소모형실험, 한계상태설계법, 설계기준, 비선형 유한요소해석

**학 번:** 2015-31057